

2021

ANTI-INFLAMMATORY EFFECTS OF POLYPHENOL-ENRICHED EXTRACTS

Chang Liu
University of Rhode Island, hichang813@uri.edu

Follow this and additional works at: https://digitalcommons.uri.edu/oa_diss

Terms of Use

All rights reserved under copyright.

Recommended Citation

Liu, Chang, "ANTI-INFLAMMATORY EFFECTS OF POLYPHENOL-ENRICHED EXTRACTS" (2021). *Open Access Dissertations*. Paper 1266.
https://digitalcommons.uri.edu/oa_diss/1266

This Dissertation is brought to you by the University of Rhode Island. It has been accepted for inclusion in Open Access Dissertations by an authorized administrator of DigitalCommons@URI. For more information, please contact digitalcommons-group@uri.edu. For permission to reuse copyrighted content, contact the author directly.

ANTI-INFLAMMATORY EFFECTS OF POLYPHENOL-ENRICHED
EXTRACTS
BY
CHANG LIU

A DISSERTATION SUBMITTED IN PARTIAL FULFILLMENT OF THE
REQUIREMENTS FOR THE DEGREE OF
DOCTOR OF PHILOSOPHY
IN
PHARMACEUTICAL SCIENCES

UNIVERSITY OF RHODE ISLAND

2020

DOCTOR OF PHILOSOPHY DISSERTATION

OF

CHANG LIU

APPROVED:

Dissertation Committee:

Major Professor Navindra P. Seeram

Angela L. Slitt

Xinyuan Chen

Daniel Roxbury

Brenton DeBoef
DEAN OF THE GRADUATE SCHOOL

UNIVERSITY OF RHODE ISLAND
2020

ABSTRACT

Our laboratory initiated a comprehensive research program to investigate the phytochemical composition and biological effects of several botanical based natural products including pomegranate (*Punica granatum*), red maple (*Acer rubrum*), polyphenol-enriched maple (*Acer saccharum*) syrup extract, and various phytocannabinoids (*Cannabis sp.*). We hypothesize that these bioactive natural products can exert beneficial biological effects via their antioxidant and anti-inflammatory effects.

In **Manuscript 1-4**, we identified a series of phytochemicals from botanical extracts including pomegranate, red maple, phenolic-enriched maple syrup extract (MSX) and evaluated their biological activities for potential cosmeceutical and/or dermatological applications. In **Manuscript 1** (published in *Journal of Functional Foods*; 2019, 54, 559-567), we evaluated the skin protective and antioxidative effects of pomegranate phenolics [(i.e. punicalagin (PA) and ellagic acid (EA)] and their gut microbial metabolite (i.e. urolithin A; UA) against oxidative stress induced by hydrogen peroxide (H₂O₂) in human keratinocytes. In this study, we reported that a chemically standardized and commercial available pomegranate extract (PE; Pomella[®]) and its phenolics including PA, EA, and UA exerted protective effects against oxidative stress and cytotoxicity in human keratinocytes. In **Manuscript 2** (Published in *Food and Function*; 2020, 11, 5105-5114), we investigated the antioxidative and cytoprotective effects of a proprietary red maple leaves extract (commercially available as Maplifa[™]) and its major phenolic compound, ginnalin A (GA), in human skin cells exposed to oxidative stress inducers including H₂O₂ and methylglyoxal (MGO). In this study, we reported that Maplifa[™] and GA exerted skin protective effects by down-regulation of reactive oxygen species and apoptosis-associated caspase family proteins. In **Manuscript 3** (Published in *Dermatologic Therapy*; 2020, e13426), we reported that phenolic-enriched maple syrup extract (MSX) showed protective effects on human keratinocytes against H₂O₂ and MGO induced cytotoxicity and DNA damage. In **Manuscript 4** (Published in *Journal of Functional Foods*; 2020, 75, 104208), we assessed the anti-elastase activity, skin permeability, and cytoprotective effects of glucitol-core containing gallotannins (GCGs) from red maple using biochemical-, computational-, and cell culture-based assays. This study reported that GCGs from red maple are skin permeable elastase inhibitors with antioxidant and cytoprotective activities, which supported potential cosmeceutical applications of Maplifa[™].

In **Manuscript 5-7**, we investigated the anti-inflammatory effects of two inflammasome inhibitors, namely, cannabidiol (CBD) and punicalagin (PA), and explored their mechanisms of action. In **Manuscript 5** (Published in *Journal of Natural Products*, 2020, 83, 2025-2029), we reported that CBD's suppressive effect on the activation of NLRP3 inflammasome is associated with its modulation of P2X7 receptor. In **Manuscript 6** (Published in *Cannabis and Cannabinoid Research*, 2020, Online ahead of print), we used network-based pharmacology analysis and computational docking approach to study CBD's molecular targets and signaling pathways that involved in the anti-inflammatory activity. We reported that CBD's anti-inflammatory effect can be associated with a series of molecular targets including proteins and signaling pathways, which supported the utilization of CBD as a promising anti-inflammatory natural product. In **Manuscript 7** (To be submitted to *Journal of Natural Products*), we evaluated the inhibitory effects of PA on NLRP3 inflammasome activation and its effects on inflammasome activation related receptor (i.e. P2X7) with a cellular based model using human monocytes. In addition, we evaluated the anti-inflammatory effects of PA in two different mouse models of peritonitis. Our findings supported that PA's overall anti-inflammatory effects may be attributed to its inhibitory effects on the activation of NLRP3 inflammasome.

ACKNOWLEDGMENTS

I would like to express my deep and sincere gratitude to my co-major professors, Drs. Navindra Seeram and Angela Slitt. Thank you both for providing me the invaluable guidance and challenging me to be a better scientist. To my committee members, Drs. Xinyuan Chen and Daniel Roxbury, for providing expertise and consistently pushing my research to be better. To College of Pharmacy, for offering a teaching assistantship and consistently support. To my lab mates, Dr. Hang Ma, and other lab members for your continued guidance, support, and laughter that have been instrumental. To my family, thank you for your constant support.

PREFACE

This dissertation was written according to the University of Rhode Island “Guidelines for the Format of Theses and Dissertations” standards for manuscript format. The dissertation comprises of six major chapters. The publication status of each manuscript is as follows:

Manuscript 1: **Liu Chang**, Guo Hao, Dasilva Nick, Li Dongli, Zhang Kun, Wan Yinsheng, Gao Xinhua, Chen Hongduo, Seeram Navindra, Ma Hang (2019) Pomegranate (*Punica granatum*) Phenolics Ameliorate Hydrogen Peroxide-Induced Oxidative Stress and Cytotoxicity in Human Keratinocytes. Published in *Journal of Functional Foods*, 54, 559-567.

Manuscript 2: **Liu Chang**, Guo Hao, Dain Joel, Wan Yinsheng, Gao Xinghua, Chen Hongduo, Seeram Navindra, Ma Hang (2020) Cytoprotective Effects of A Proprietary Red Maple Leaves Extract and Its Major Polyphenol, Ginnalin A, against Hydrogen Peroxide and Methylglyoxal Induced Oxidative Stress in Human Keratinocytes. Published in *Food & Function*, 11, 5105-5114.

Manuscript 3: Sheng Jie, **Liu Chang**, Petrovas Sophia, Wan Yinsheng, Chen Hongduo, Seeram Navindra, Ma Hang (2020) Phenolic-Enriched Maple Syrup Extract Protects Human Keratinocytes against Hydrogen Peroxide and Methylglyoxal Induced Cytotoxicity. Published in *Dermatological Therapy*, e13426.

Manuscript 4: **Liu Chang**, Xu Yiming, Kirk Riley, Li Huifang, Li Dongli, DaSilva Nicholas, Bertin Matthew, Seeram Navindra, Ma Hang (2020) Inhibitory effects of skin permeable glucitol-core containing gallotannins from red maple leaves on elastase and their protective effects on human keratinocytes. Published in *Journal of Functional Foods*, 75, 104208

Manuscript 5: **Liu Chang**, Ma Hang, Slitt Angela, Seeram Navindra (2020) Inhibitory Effect of Cannabidiol on the Activation of NLRP3 Inflammasome is Associated with Its Modulation of P2X7 Receptor in Human Monocytes. Published in *Journal of Natural Products*, 83, 2025-2029

Manuscript 6: Ma Hang, Xu Feng, **Liu Chang**, Seeram Navindra (2020) A Network Pharmacology Approach to Identify Potential Molecular Targets for Cannabidiol’s Anti-Inflammatory Activity. Published in *Cannabis and Cannabinoid Research*, Online ahead of print.

Manuscript 7: Liu Chang, Ma Hang, Slitt Angela, Seeram Navindra (2020) Punicalagin, the major polyphenol in pomegranate (*Punica granatum*), is an NLRP3 inflammasome inhibitor in vitro and in vivo, to be submitted to *Journal of Natural Products*

TABLE OF CONTENTS

ABSTRACT.....	ii
ACKNOWLEDGMENTS.....	iv
PREFACE.....	v
TABLE OF CONTENTS	vii
LIST OF TABLES	viii
LIST OF FIGURES	ix
MANUSCRIPT 1	1
MANUSCRIPT 2	27
MANUSCRIPT 3	50
MANUSCRIPT 4	66
MANUSCRIPT 5	99
MANUSCRIPT 6	120
MANUSCRIPT 7	148

LIST OF TABLES

MANUSCRIPT 4:

Table 1. Inhibitory effects of GTs on elastase activity.....	94
--	----

MANUSCRIPT 6:

Table 1. Topological parameters of potential targets for CBD's anti-inflammatory activity in the "Compound-Target-Disease" network.....	139
--	-----

Table 2. Interactions between CBD and target proteins. Free energy of binding and inhibition constant predicted by computational docking	140
---	-----

Table 3. The functional analysis of identified compound-related targets by gene ontology (GO) analysis and KEGG signaling pathway analysis.....	141
--	-----

Table S1. Total Analysis of Topological Parameters of Potential Targets in "Compound-Target-Disease" Network.....	147
--	-----

LIST OF FIGURES

MANUSCRIPT 1:

Figure 1. Effects of H ₂ O ₂ on viability of HaCaT cells and ROS production in HaCaT cells.....	20
Figure 2. Effects of PE and pomegranate phenolics on viability of HaCaT cells.....	21
Figure 3. Effects of PE and pomegranate phenolics on ROS production in HaCaT cells exposed to H ₂ O ₂	22
Figure 4. Effects of PE and pomegranate phenolics on cell viability of HaCaT cells exposed to H ₂ O ₂	23
Figure 5. Effects of PE and pomegranate phenolics on apoptosis of HaCaT cells induced by H ₂ O ₂	24
Figure 6. Effects of PE and pomegranate phenolics on necrosis of HaCaT cells induced by H ₂ O ₂	25
Figure 7. Effects of PE and pomegranate phenolics on cellular caspase 3/7 (A), caspase 8 (B) and caspase 9 (C) in HaCaT cells exposed to H ₂ O ₂	26

MANUSCRIPT 2:

Figure 1. Effect of Maplifa TM and GA on viability of HaCaT cells.....	43
Figure 2. Effects of Maplifa TM and GA on the viability of HaCaT cells insulted with H ₂ O ₂ or MGO...	44
Figure 3. Effects of Maplifa TM and GA on the H ₂ O ₂ - and MGO-induced ROS production.....	45

Figure 4. Effects of Maplifa™ and GA on H₂O₂-induced apoptosis in HaCaT cells..... 46

Figure 5. Effects of Maplifa™ and GA on (A) cellular caspase-3/7, (B) caspase-8, and (C) caspase-9 in HaCaT cells exposed to H₂O₂ 47

Figure 6. Effects of Maplifa™ and GA on MGO-induced production of mitochondria-derived ROS .. 48

Figure 7. Effects of Maplifa™ and GA on MGO-induced production of mitochondria-derived ROS .. 49

MANUSCRIPT 3:

Figure 1. Effects of MSX on the cell viability of H₂O₂ and MGO challenged HaCaT cells. MSX (6.25-100 µg/mL) were nontoxic to HaCaT cells..... 63

Figure 2. Effects of MSX on the production of ROS in HaCaT cells in the DCFDA assay. HaCaT cells were pretreated with MSX (12.5, 25, and 50 µg/mL) for 2 hours and then treated with DCFDA reagent (20 µM) followed by incubation with H₂O₂ (200 µM) for 1 hour. 64

Figure 3. Effects of MSX (50 µM) on the integrity of DNA in MGO- and H₂O₂-challenged HaCaT cells. 65

MANUSCRIPT 4:

Figure 1. Chemical structures of GTs including GCGs (ginnalins A-C and maplexins F-J), pentagalloyl glucose (PGG), and tannic acid (TA), as well as their structural building moiety gallic acid (GLA) and microbial metabolite pyrogallol (PYG), as well as their inhibitory effects on elastase enzyme. 89

Figure 2. Kinetic assay to determine the inhibition mode of GCGs including GA and MJ on elastase enzyme by plotting the Lineweaver–Burk plots.	90
Figure 3. Molecular docking of elastase protein (A) and ligands including GLA, GA, MJ, and PGG. The free binding energy between protein and ligand was estimated (B). Top potential ligand binding sites for GLA (C), GA (D), MJ (E), and PGG (F) and the binding molecular forces were obtained via Site Finder module with MOE.....	91
Figure 4. Skin permeability of GTs predicted by the SwissADME tool based on their physico-chemical properties including Log Kp, Log Po/w, Log S(ESOL), and Log S(Ali) (A). The skin permeability of GA verified by biochemical experimental assays including PAMPA (B and C) and cellular uptake assay with human keratinocyte HaCaT cells (D). Degradation of GA in various conditions (E).....	92
Figure 5. Cytotoxicity of GTs (at concentrations of 10, 1000, and 1000 μ M) including GA, GB, GC, MF, MJ, PGG, and TA, along with their chemical structure unit, GLA, and gut microbial metabolite, PYG, was evaluated in human keratinocytes HaCaT cells by the MTS assay	93
Figure 6. Cytoprotective effects of red maple GTs against H ₂ O ₂ -induced oxidative stress in HaCaT cells.	94
Figure 7. Effects of Maplifa™ and GA on MGO-induced production of mitochondria-derived ROS ..	95
Figure S1. Inhibitory effects of Maplifa® on elastase enzyme. Inhibition values are shown as mean \pm standard deviation (SD) from three independent experiments	96
Figure S2. Evaluation of the skin permeability of Maplifa® by the PAMPA assay.	97

Figure S3. HPLC-DAD profiles of GA in various conditions including basic and acidic environment, UV radiation and heat.	98
---	----

MANUSCRIPT 5:

Figure 1. Effects of CBD on the LPS-induced secretion of cytokines IL-1 β (A) and TNF- α (B) in THP-1 monocytes	113
---	-----

Figure 2. CBD's specific inhibition of NLRP3 inflammasome	114
---	-----

Figure 3. Effects of CBD and nigericin on intracellular potassium in THP-1 monocytes.	115
--	-----

Figure 4. Effects of CBD on LPS-nigericin stimulated intracellular potassium in THP-1 monocytes.	116
---	-----

Figure 5. Interactions between CBD and the P2X7 receptor predicted by molecular docking.	117
---	-----

Chart 1. Chemical structure of CBD, oridonin, and MCC950 (A); Chemical structures shown in 3D model (B)	112
--	-----

Figure S1. Effect of CBD on the viability of THP-1 monocytes.	118
--	-----

Figure S2. Effect of CBD on the intracellular calcium in THP-1 monocytes.	119
--	-----

MANUSCRIPT 6:

Figure 1. Cannabidiol-target-inflammation network created by software Cytoscape	135
---	-----

Figure 2. Computational docking for interactions between CBD and potential target proteins for CBD's anti-inflammatory activity.	136
--	-----

Figure 3. Interaction network (created by software Cytoscape) of potential target proteins for CBD's anti-inflammatory activity.....	137
Figure 4. Interaction network (created by software Cytoscape) of protein core subnetwork of target proteins for CBD's anti-inflammatory activity. Darker color indicates greater number of degrees.....	138
Figure 5. Network diagram (created by software Cytoscape) of putative signaling pathways that are involved in CBD's anti-inflammatory activity and related diseases.....	139
Figure S1. Divided view of Figure 1 'cannabidiol-target-inflammation network'.....	140
Figure S2. Enlarged view (i) of Figure 1 'cannabidiol-target-inflammation network'.....	141
Figure S3. Enlarged view (ii) of Figure 1 'cannabidiol-target-inflammation network'.....	142
Figure S4. Enlarged view (iii) of Figure 1 'cannabidiol-target-inflammation network'.....	143
Figure S5. Enlarged view (iv) of Figure 1 'cannabidiol-target-inflammation network'.....	144
 MANUSCRIPT 7:	
Figure 1. (A) Cytokines IL-1 β and TNF- α changes in LPS-primed (100 ng/mL, 4 h) THP-1 cells after incubation of compound library followed by induction of nigericin (10 μ M, 1 h). (B) Analysis of IL-1 β and TNF- α release in the PA-pretreated or treated LPS-primed THP-1 cells followed by the induction of nigericin. IL-1 β release in the supernatant (C) and cell lysate (D) from the PA-treated LPS-primed THP-1 cells followed by the induction of nigericin	165

Figure 2. Analysis of cellular active-caspase 1 (A) and extracellular active caspase-1 (B) in the PA-treated LPS-primed (100 ng/mL, 4 h) THP-1 cells followed by the induction of Nigericin (10 μ M, 1 h). (C) LDH release in the PA-treated LPS-primed (100 ng/mL, 4 h) THP-1 cells followed by the induction of nigericin (10 μ M, 1 h). THP-1 cells were stimulated and treated with PA as indicated, mRNA levels of il-1 β (D), caspase-1 (E), and nlrp3 (F) and protein levels of caspase-1, and nlrp3 (G) were determined using qRT-PCR and western blotting, respectively 166

Figure 3. (A-C) THP-1 cells were stimulated and treated with PA as indicated, mito-SOX intensity was determined using Flow cytometry and confocal microscopy, respectively. The results were qualified by FlowJo. (D) Mito-Tracker staining was apply to analyze cellular mitochondrial distribution in the PA-treated LPS-primed (100 ng/mL, 4 h) THP-1 cells followed by the induction of nigericin (10 μ M, 1 h). 167

Figure 4. Interactions between PA and the P2X7 receptor predicted by molecular docking. (A) PA binds to the P2X7 receptor at a site located at the head and left flipper of the P2X7 receptor's upper body and enlarged view of PA showed at the binding site in the P2X7 receptor. (B) Surface plasmon resonance (SPR) analysis of PA interaction with P2X7. (C) Illustration of types of interactions between CBD and the P2X7 receptor..... 168

Figure 5. Effects of PA on the genes involved in the inflammasome activation. 169

Figure 6. (A) The mice were intraperitoneally injected with PA (50 mg/kg) or oridonin (20 mg/kg). Next, the mice were intraperitoneally injected with LPS (10 mg/kg) or MSU (1 mg/mouse). The serum and peritoneal fluid were collected and IL-1 β and TNF- α in the serum or peritoneal cavity were determined. Treatment of PA inhibited serum IL-1 β (B) and TNF- α (C) and peritoneal fluid IL-1 β (D) but didn't affect peritoneal fluid TNF- α (E). Besides, treatment of PA also inhibited serum IL-1 β (F) but didn't affect serum TNF- α (G) 170

..... 170

CHAPTER 1

MANUSCRIPT 1

Published: 6 February 2019

Journal of Functional Foods 54 (2019) 559-567

Pomegranate (*Punica granatum*) Phenolics Ameliorate Hydrogen Peroxide-Induced Oxidative Stress and Cytotoxicity in Human Keratinocytes

Chang Liu^b, Hao Guo^{b,c,d}, Nicholas A. DaSilva^b, Dongli Li^a, Kun Zhang^a, Yinsheng Wan^d, Xing-Hua Gao^c, Hong-Duo Chen^c, Navindra P. Seeram^{b,*}, Hang Ma^{a,b*}

^a School of Biotechnology and Health Sciences, Wuyi University; International Healthcare Innovation Institute (Jiangmen), Jiangmen 529020, Guangdong, China

^b Bioactive Botanical Research Laboratory, Department of Biomedical and Pharmaceutical Sciences, College of Pharmacy, University of Rhode Island, Kingston, RI 02881, USA

^c Department of Dermatology, Key Laboratory of Immunodermatology, No.1 Hospital of China Medical University, Shenyang 110001, China

^d Department of Biology, Providence College, Providence, RI 02918, USA

*Corresponding authors

Tel.: +1 401 874 9367; E-mail address: nseeram@uri.edu (N.P.S.)

Tel.: +1 401 874 7654; E-mail address: hang_ma@uri.edu (H.M.)

Bioactive Botanical Research Laboratory, Dept. of Biomedical & Pharmaceutical Sciences

College of Pharmacy, The University of Rhode Island, Avedisian Hall Lab 440,

7 Greenhouse Road, Kingston, RI 02881USA

Abstract

Pomegranate phenolics have been reported to exert skin beneficial effects but their mechanisms of action remain unclear. Herein, we investigated a standardized commercial pomegranate extract (PE; Pomella[®]) and its phenolics including punicalagin (PA), ellagic acid (EA), and urolithin A (UA) for their protective effects against hydrogen peroxide (H₂O₂)-induced oxidative stress and cytotoxicity in human keratinocyte HaCaT cells. PE, PA, and EA reduced the production of H₂O₂-induced ROS in HaCaT cells by 1.03-, 1.37-, and 2.67-fold, respectively. PE, PA, and UA increased the viability of H₂O₂-stimulated HaCaT cells by 89.9, 94.9, and 90.0%, respectively. PE, PA, and UA reduced apoptotic cell populations by 3.39, 7.11, and 8.26%, respectively. In addition, PE, PA and UA decreased H₂O₂-stimulated caspase-3 level by 2.31-, 2.06-, and 2.68-fold, respectively. The ameliorative effects of this PE and its phenolics against the H₂O₂-induced oxidative stress and cytotoxicity in keratinocytes support their utilization as natural cosmeceuticals for skin health.

Keywords: Pomegranate, phenolics, keratinocytes, oxidative stress, cytotoxicity, skin protection

1. Introduction

Epidermis, the outermost layer and protective barrier of skin, is mainly composed of keratinocytes (80-95%) (Baroni et al., 2012; Feingold, 2007). Keratinocytes are constantly exposed to many harmful stimuli including extrinsic insults (e.g. UV-exposure, smoking, and pollutants) (D'Orazio, Jarrett, Amaro-Ortiz, & Scott, 2013; Rinnerthaler, Bischof, Streubel, Trost, & Richter, 2015) and intrinsic stresses (e.g. toxins, oxidation, and glycation) (Gkogkolou & Bohm, 2012). Both extrinsic and intrinsic factors can lead to cellular oxidative stress through the formation of reactive oxygen species (ROS) including superoxide anion radical ($O_2^{\cdot-}$), and hydroxyl radical (OH^{\cdot}) in keratinocytes (Farage, Miller, Elsner, & Maibach, 2008; Poljsak, Dahmane, & Godic, 2012). Although the generation of ROS is a biologically inevitable process and cells have developed complex antioxidant mechanisms, oxidative stress occurs when ROS levels exceed the antioxidant capacity of cells. Excessive production of ROS can impair the integrity of the structure of keratinocytes, which further leads to the loss of cellular functions and eventually causes cell death. Compromised keratinocytes are directly associated with the skin aging process and many aging-related skin symptoms including dehydration (Sengupta et al., 2010), irritation (Lawrence, Dickson, & Benford, 1997), laxity (Yaar & Gilchrest, 2001), and the formation of wrinkles (Blume-Peytavi et al., 2016). Therefore, the use of natural product antioxidant interventions, including dietary phenolics, to counteract ROS-induced oxidative stress in keratinocytes has attracted research interest for cosmeceutical and/or dermatological applications (Filip et al., 2011; Rahman, Biswas, & Kirkham, 2006).

Previous published studies using *in vitro* and *in vivo* models support the skin protective effects of bioactive compounds from pomegranate (*Punica granatum*) fruit. A pomegranate fruit extract was reported to show antioxidant effects in immortalized human keratinocytes by decreasing UVB-induced cytotoxicity and intracellular glutathione content (Zaid, Afaq, Syed, Dreher, & Mukhtar, 2007). Similarly, a pomegranate fruit extract [standardized to 30% punicalagins (PA), a characteristic ellagitannin in pomegranate] showed protective effects against UVA- and UVB-induced damage in human fibroblasts by reducing inflammatory and oxidative stresses (Pacheco-Palencia, Mertens-Talcott, & Talcott, 2008). A pomegranate fruit extract was also reported to show photochemopreventive effects

in normal human keratinocytes against UVA-mediated activation of transcription factor (signal transducer and activator of transcription 3; STAT3), protein kinase B (Akt), and extracellular signal-regulated kinase and the UVB-mediated activation of mitogen-activated protein kinase (MAPK) and nuclear factor kappa-light-chain-enhancer of activated B (NF-κB) pathways (Syed et al., 2006). The photochemopreventive effects of that pomegranate extract were further supported by an *in vivo* study wherein its oral delivery (by dissolving pomegranate extract in drinking water; 0.2%, wt/vol) protected mouse skin from UVB radiation by mediating the UVB-induced signaling pathways (Khan, Syed, Pal, Mukhtar, & Afaq, 2012). Moreover, the skin protective effects of pomegranate phenolics are supported by a double-blind and placebo-controlled human clinical trial (Kasai, Yoshimura, Koga, Arii, & Kawasaki, 2006), in which the oral consumption of an ellagic acid (EA) - enriched pomegranate extract showed ameliorative effect against UV radiation-induced sun burn at a dosage of 100 mg/day. In addition, this pomegranate extract also showed inhibitory effects of pigmentation in human skin cells (Kasai et al., 2006). Interestingly, the gut microbial metabolites of pomegranate ellagitannins, namely, urolithins, have also been reported to show skin lightening effects by reducing the melanin production in murine melanoma cells (Wang, Chang, Hsu, & Su, 2017). However, the protective effects of pomegranate fruit extracts, their constituent phenolics (such as punicalagins and ellagic acid), and their gut microbial metabolites (such as urolithin A; UA) against hydrogen peroxide (H₂O₂)-induced oxidative stress in human keratinocytes HaCaT cells and their mechanisms of action remain unclear.

Our laboratory has initiated a program to systematically investigate the phytochemical composition of pomegranate and has identified over 100 phenolic compounds from various aerial parts of pomegranate (Liu & Seeram, 2018; Yuan et al., 2012; Yuan, Wan, Ma, & Seeram, 2013). In addition, our group has investigated a standardized pomegranate fruit extract (PE; Pomella[®]) and its phenolics, PA, EA and urolithins, for their neuroprotective effects against Alzheimer's disease (Yuan et al., 2016) and their anti-neuroinflammatory (DaSilva et al., 2017) and anti-glycation (Liu et al., 2014) effects. Herein, using human HaCaT keratinocytes, we investigated the skin protective effects of this PE and its phenolics (PE, EA and UA) by evaluating their capacity to reduce H₂O₂-induced ROS production and toxicity, as well as their potential mechanisms of action by investigating their anti-apoptosis and -necrosis effects, and effects on caspases-3/7, -8, and -9 enzymes. The ameliorative effects of the

pomegranate phenolics in human keratinocytes support their utilization as natural cosmeceuticals for skin health.

2. Materials and Methods

2.1 Chemicals and reagents

Pomegranate fruit extract (PE; Pomella[®]) was kindly provided by Verdure Sciences (Noblesville, IN, USA). The PE was standardized to punicalagins (PA; c.a. 30%) and ellagic acid (EA; c.a. 2.3%) and has been extensively chemically characterized by our laboratory (Yuan et al., 2012; Yuan, Wan, Ma, & Seeram, 2013; Ahmed et al., 2014; Yuan et al., 2016). PE contains a total polyphenol content (as gallic acid equivalents) of 61.5% (Ahmed et al., 2014). PA and EA were purchased from Sigma Chemical Co. (St. Louis, MO, USA). Urolithin A (3,8-dihydroxy-6H-dibenzo [b, d] pyran-6-one; UA) was synthesized in our laboratory using a reported protocol (Yuan et al., 2013). Hoechst 33342, crystal violet, propidium iodide (PI), dimethyl sulfoxide (DMSO), hydrogen peroxide (H₂O₂), and 2',7'-dichlorouorescein diacetate (DCFDA) were purchased from Sigma Chemical Co. (St. Louis, MO, USA). CellTiter-Glo[®] (CTG) 2.0 assay kit was purchased from Promega (Fitchburg, WI, USA). Alexa Fluor[®] 488 Annexin V/Dead cell apoptosis kit was purchased from Thermo Fisher Scientific (Waltham, MA, USA). Caspase-Glo[®] assay kits for caspase- 3/7, -8, and -9 were purchased from Promega (Fitchburg, WI, USA).

2.2. Cell culture and sample preparation

Human keratinocyte HaCaT cells were purchased from the American Type Culture Collection (ATCC, Rockville, USA) and maintained in Dulbecco's modified Eagle's medium (DMEM) (Life Technologies, Gaithersburg, MD, USA) supplemented with 10% fetal bovine serum (FBS) (Life Technologies, Gaithersburg, MD, USA) at 37 °C in the presence of 5% CO₂ at constant humidity. Test samples were dissolved in DMSO as stock solution and then diluted with cell culture medium to the desired concentrations (6.25-100 µg/mL for PE and 6.25-100 µM for the purified compounds; DMSO% < 0.1%).

2.3. Measurement of reactive oxygen species (ROS)

HaCaT cells were seeded in 96-well plates at 5×10^3 cells per well for 12 h and then incubated with test samples (at aforementioned concentrations) for 12 h. Next, medium was removed and cells were washed twice with phosphate-buffered saline (PBS). Medium containing fluorescent probe (DCFDA; 20 μ M) was then added to the cells and incubated for 20 min. Cells were then treated with 100 μ L H_2O_2 (at concentrations of 50, 100, 200, 400, and 800 μ M) for 1 h followed by measuring fluorescence intensity of each well with excitation and emission wavelengths of 485 and 525 nm, respectively, using a Spectramax M2 plate reader (Molecular Devices, Sunnyvale, CA, USA).

2.4 Measurement of H_2O_2 -induced cytotoxicity in HaCaT cells

The viability of H_2O_2 -treated HaCaT cells was measured by a CTG 2.0 assay using a previously reported method (Ma et al., 2016; Ma et al., 2018). HaCaT cells were seeded in 96-well plates at 5×10^3 cells per well and allowed to attach for 12 h. Media was then removed and 100 μ L of H_2O_2 (at concentrations of 50, 100, 200, 400, and 800 μ M) was added and incubated for 24 h. Next, CTG 2.0 reagent (100 μ L) was added in each well and shaken at 200 rpm for 2 min on an orbital shaker. The plate was then kept at room temperature for 10 min after which luminescence intensity was recorded using a Spectramax M2 plate reader. Morphological analysis was conducted to evaluate cell damage with crystal violet staining method. Cells were fixed in 70% ethanol for 15 min after which medium was removed. Staining solution (0.05% w/v) was added to each well and incubated for 20 min. Then the staining solution was removed and cells were washed with PBS for three times. The morphological changes of cells were observed by an EVOS Cell Imaging System (Invitrogen, Waltham, MA, USA).

2.5. Detection of apoptosis and necrosis (flow cytometry assay)

HaCaT cells were seeded in 6-well plates at 0.3×10^6 cells per well and allowed to attach for 12 h followed by treatment of test samples (at aforementioned concentrations) for 6 h. The medium was then removed and cells were washed twice with PBS. Next, cells were treated with H_2O_2 (at 200 μ M) and incubated for 24 h. Detection of apoptosis was performed according to the previously reported method (Zhang et al., 2017). Cells were then harvested and suspended in 500 μ L of binding buffer containing 5

μL of FITC-labeled Annexin-V and 5 μL of propidium iodide (PI) followed by incubation in the dark for 15 min. Then the population of apoptotic and necrotic cells were measured by flow cytometry (BD FACSCalibur, San Jose, CA, USA) and data were analyzed using software FlowJo (LLC, Ashland, Oregon, USA).

2.6. Hoechst 33342 and propidium iodide PI double staining

HaCaT cells were seeded in 24 well plates at 0.5×10^5 cells per well and allowed to attach for 12 h followed by treatment of test samples (at aforementioned concentrations) for 6 h. Medium were then removed and cells were washed twice with PBS. Next, 300 μL of fresh medium containing H_2O_2 (200 μM) were added to cells and incubated for 24 h. Medium were then removed and cells were washed twice with PBS. Hoechst 33342 staining buffer (300 μL) was added to the cells and incubated for 30 min in darkness. Next, PI staining buffer (300 μL) was added to the cells and incubated for 30 min in darkness. The morphological changes of the nucleus of the cells were observed by an EVOS Cell Imaging System with a fluorescence microscope (Invitrogen, Waltham, MA, USA).

2.7. Measurements of caspases -3/7, -8, and -9 levels

HaCaT cells were seeded in 96-well plates at 5×10^3 cells per well and allowed to attach for 12h. Cells were then treated with test samples (at aforementioned concentrations) for 6 h. Media were then removed and cells were washed twice with PBS. Next, 100 μL of fresh medium containing H_2O_2 (200 μM) was added and incubated for 24 h followed by addition of 100 μL of caspase-Glo reagent (for measurement of caspases-3/7, -8, and -9, separately). Plates were then incubated at room temperature for 30 min and the luminescence intensity of each well was read using a Spectramax M2 plate reader.

2.8. Statistical analysis

Statistical analyses were performed using GraphPad Prism 6 (GraphPad Software, La Jolla, CA, USA). Data are expressed as the mean value \pm standard deviation (S.D.) obtained from triplicates of experiments. The significance of differences was determined using a two-way analysis of variance

(ANOVA) followed by a post hoc Student-Newman-Keuls multiple comparison test (SNK). $P < 0.05$, $P < 0.01$, or $P < 0.001$ was determined to be significant.

3. Results and Discussion

3.1. Hydrogen peroxide (H_2O_2) induces the production of ROS and cytotoxicity in HaCaT cells

Hydrogen peroxide (H_2O_2) is a common ROS produced in keratinocytes and its toxic effects were examined in human keratinocytes HaCaT cells. Treatment of H_2O_2 (200 and 400 μ M) significantly elevated the production of ROS in HaCaT cells by 4.58-, and 9.01-fold, respectively (Fig. 1A). In addition, H_2O_2 (200, 400, and 800 μ M) significantly induced cytotoxicity by decreasing the viability of HaCaT cells to 70.0, 51.8, and 6.6%, respectively (Fig. 1B). The toxic effects of H_2O_2 in HaCaT cells were confirmed by morphological analyses using crystal violet and Hoechst 33342 staining methods (Fig 1C). The nucleus of cells treated with H_2O_2 (200-800 μ M) had irregular shapes as compared to the cells without H_2O_2 treatment suggesting that treatments of H_2O_2 (>200 μ M) induced oxidative stress and caused cell death in HaCaT cells.

Although excessive accumulation of H_2O_2 is harmful for skin cells, studies have also showed that moderate levels of ROS is important for cellular signaling and proliferation (Ray, Huang, & Tsuji, 2012). Therefore, the effects of H_2O_2 at various concentrations on HaCaT cells were evaluated, first. Our results from the cell viability and staining assays were in agreement with published data (Ray et al., 2012) showing that at lower concentrations (50 and 100 μ M), treatment of H_2O_2 was non-toxic; however, H_2O_2 at 200 μ M or higher concentrations caused significantly cytotoxicity. Therefore, H_2O_2 at 200 μ M, was used as an inducer of oxidative stress and cytotoxicity in HaCaT cells for further experiments.

3.2. PE, PA, and EA reduce H_2O_2 -induced ROS production in HaCaT cells

Prior to the investigation of the protective effects of PE and the pure pomegranate phenolics on HaCaT cells, the non-toxic concentrations of test samples were determined. PE (6.25-100 μ g/mL; Fig. 2A) and its phenolics including PA, EA, and UA (6.25-100 μ M; Fig. 2B-D, respectively) did not induce

significant cytotoxicity in HaCaT cells. Therefore, PE (at 12.5, 25, and 50 $\mu\text{g/mL}$), PA, EA, and UA (at 12.5, 25, and 50 μM) were selected for the evaluation of their protective effects in HaCaT cells. Next, the protective effects of PE and the pomegranate phenolics against oxidative stress in HaCaT cells was evaluated. Treatment of PE (12.5, 25, and 50 $\mu\text{g/mL}$) significantly reduced the production of H_2O_2 -induced ROS in HaCaT cells by 1.36-, 1.07-, and 1.03-fold, respectively, as compared to the H_2O_2 -treated group (Fig. 3A). In addition, PA and EA (12.5, 25, and 50 μM) reduced H_2O_2 -induced ROS production by 1.50-, 1.38-, 1.37-fold and 2.85-, 2.80-, and 2.67-fold, respectively, as compared to the H_2O_2 -treated group (Fig. 3B and C). Although a trend was observed for UA, the reduction of ROS production was not significant at the test concentrations (Fig. 3D).

Our results showed that PE and its phenolics including PA and EA had promising antioxidant effects against H_2O_2 in HaCaT cells. This is in agreement with a previously reported study showing that PA attenuated ROS production in primary human epidermal keratinocytes stimulated by an airborne particulate matter (Seok, Lee, Kim, & Boo, 2018). In addition, EA has also been reported to show protective effects in HaCaT cells against UVA-mediated oxidative stress by regulation of antioxidant genes such as HO-1 and Nrf-2 (Hseu et al., 2012). However, to date, the effects of urolithins, the gut microbial metabolites of ellagitannins, on HaCaT cells have not been reported. In this study, we observed that compared to PA and EA, UA had lower antioxidant effects which is agreement with a previous study reporting that the antioxidant capacities of urolithins were less potent than ellagitannins in a panel of biochemical assays (Ito, 2011). Similar to our observations, a study showed that EA but not UA reduced H_2O_2 -induced oxidative stress in human neuroblastoma SH-SY5Y cells (Gonzalez-Sarrias, Nunez-Sanchez, Tomas-Barberan, & Espin, 2017). However, it should be noted that urolithins have been reported to show cellular antioxidant effects in other cell types including bladder T24 cells and human liver carcinoma HepG2 cells (Qiu et al., 2013; Wang et al., 2015). This may be due to differences in the redox activities of urolithins which could be influenced by different bioassay systems (Kallio et al., 2013). Therefore, further studies are warranted to elucidate the mechanisms of antioxidant effects of urolithins in skin cells.

3.3. PE, PA, and UA reduce H_2O_2 -induced cytotoxicity in HaCaT cells

The protective effects of pomegranate phenolics against H₂O₂-induced toxicity in HaCaT cells were evaluated. Treatment with PE (25 and 50 µg/mL) significantly reduced H₂O₂-induced cytotoxicity by increasing the viability of HaCaT cells by 85.6% and 89.9%, respectively, as compared to the H₂O₂-treated group (Fig. 4A). Treatments of PA (25 and 50 µM) and UA (25 and 50 µM) also significantly inhibited H₂O₂-induced cell death by 86.4% and 94.9% (Fig. 4B), and 90.0% and 90.0%, (Fig. 4D), respectively, as compared to the H₂O₂-treated group. However, EA (12.5-50 µM) did not increase the viability of H₂O₂-treated HaCaT cells (Fig. 4C). Although UA did not show potent antioxidant effects in the aforementioned assay, it protected HaCaT cells against oxidative stress in HaCaT cells. This may possibly be explained since urolithins may exert cytoprotective effects by different mechanisms. For example, urolithins have been reported to regulate cell proliferation by as endocrine-disrupting molecules with estrogenic and/or antiestrogenic activities (Larrosa, González-Sarrías, García-Conesa, Tomás-Barberán, & Espín, 2006). UA has also been reported to increase the viability of neonatal rat cardiomyocytes in a myocardial ischemia/reperfusion injury model through regulation of PI3K/Akt pathway (Tang et al., 2017). In addition, our group reported that urolithins increased the cell viability of differentiated human neuronal SH-SY5Y cells by down-regulating the levels of inflammatory stress and related cytokines (DaSilva et al., 2017). However, the underlying mechanism(s) of the protective effects of urolithins in skin cells in the current study are not clear warranting further investigations.

3.4. PE, PA, and UA show protective effects against H₂O₂-induced apoptosis and necrosis in HaCaT cells

The protective effects of pomegranate phenolics against H₂O₂-induced cytotoxicity were further evaluated by analyses of the apoptotic and necrotic cell population. The treatment of H₂O₂ increased the percentage of apoptotic cells including early- and late-apoptotic cells by 2.65% and 10.7%, respectively, as compared to the H₂O₂-untreated control group (Fig. 5). Treatments of PE (50 µg/mL), PA, and UA (50 µM) significantly decreased the apoptotic cell population by 3.39%, 7.11%, and 8.26%, respectively, as compared to the H₂O₂-treated group (Fig. 5). Interestingly, treatment of EA (50 µM) increased the apoptotic cell populations by 52.9 % as compared to the H₂O₂-treated group (Fig. 5). The anti-necrosis effects of pomegranate phenolics in HaCaT cells were further evaluated by morphological analyses

using Hoechst 33342 and PI staining. Treatment of H₂O₂ significantly increased the number of PI positive cells as compared to the H₂O₂-untreated control cells, suggesting that H₂O₂ induced HaCaT cell necrosis (Fig. 6). The treatment of PE (50 µg/mL) significantly reduced the number of PI positive cells, compared to the H₂O₂-treated cells, indicating that PE attenuated the H₂O₂-induced necrosis in HaCaT cells. The treatment of PA, EA, and UA (50 µM) also reduced the number of PI positive cells as compared to the H₂O₂-treated cells. Among the pomegranate phenolics, UA showed the highest anti-necrotic effects in HaCaT cells. Flow cytometry analyses showed that PE and the pomegranate phenolics had different effects in the H₂O₂-stimulated HaCaT cells. PA and UA showed anti-apoptotic effects in HaCaT cells while EA increased the population of apoptotic cells. This is in agreement with the observation from the CTG assay in which PA and UA, but not EA, increased the viability of H₂O₂-treated cells. This is not surprising since it has been well established that EA shows anti-proliferative effects in several cell lines by modulations of apoptosis-related pathways (Chung et al., 2013; Wang et al., 2016; Zhao et al., 2017). In addition, PE (which contains both PA and EA) showed anti-apoptotic effects suggesting that the pomegranate phenolics may exert cytoprotective effects against H₂O₂-induced oxidative stress in an additive and/or synergistic manner. Notably, apart from PA and EA, our group reported that over seventy phenolic compounds, which may also show antioxidant effects, have also been identified from the PE, a standardized pomegranate extract (Pomella[®]), used in this study (Liu & Seeram, 2018). Thus, it is possible that other compounds present in PE may also contribute to its overall cytoprotective effects in HaCaT cells.

3.5. PE, PA, and UA inhibit Caspase-3 content of HaCaT cells induced by H₂O₂

To further investigate the mechanisms of the anti-apoptotic effects of pomegranate phenolics, their effects on the levels of apoptosis-associated enzymes including caspases -3/7, -8, and -9, were evaluated in HaCaT cells. Treatment of H₂O₂ (200 µM) stimulated HaCaT cells and increased the levels of caspases-3/7 and -8 by 6.1- and 1.2-fold, respectively, as compared to the H₂O₂-untreated control group (Fig. 7A and B). PE (50 µg/mL), PA, and UA (50 µM) significantly reduced the levels of caspases-3/7 by 2.31-, 2.07-, and 2.68-fold, respectively, as compared to the H₂O₂-treated group (Fig. 7A). Although the pomegranate phenolics showed a trend in reducing the levels of caspase-8, only PA (50 µM)

significantly decreased the levels of caspase-8 by 98.2% as compared to the H₂O₂-treated group (Fig. 7B). Treatments of H₂O₂ and the pomegranate phenolics did not affect the level of caspase-9 in HaCaT cells (Fig. 7C). Caspases are a family of cysteine proteases that regulate programmed cell death processes including apoptosis, pyroptosis, and necroptosis (McIlwain, Berger, & Mak, 2015). Down-regulation of caspases activities is a plausible mechanism to prolong the life of skin cells against oxidative stress (He, Huang, Block, Hong, & Chignell, 2005; Yang et al., 2015). Our data showed that PE, PA, and UA decreased the levels of H₂O₂-activated caspases 3/7 in HaCaT cells. This is in agreement with a previous study showing that PE reduced the gene expression of caspase 3 in SKU-1064 human skin fibroblast cells after exposure to UV radiation (Pacheco-Palencia, Noratto, Hingorani, Talcott, & Mertens-Talcott, 2008). In addition, our group has reported that urolithins mitigated H₂O₂-induced apoptosis by reducing the levels of caspases-3/7 and -9 in murine microglia BV-2 and human neuronal SH-SY5Y cells (DaSilva et al., 2017). However, in the current study, PE and its phenolics did not reduce the levels of caspase-9 in HaCaT cells, suggesting that the pomegranate phenolics, especially urolithins, may display anti-apoptotic and -necrotic effects in various cell lines via modulation of different pathways. Further studies are warranted to elucidate the mechanism(s) of pomegranate phenolics on skin cells.

Although it is common that natural products from dietary supplements are used topically for skin health, consumable applications of dietary supplements have also been developed for dermatological and cosmetic purposes (Szyszkowska, Lepecka-Klusek, Kozłowicz, Jazienicka, & Krasowska, 2014). The beneficial effects of oral consumption of PE on skin has also been supported by a human clinical study (Adhami, Khan, & Mukhtar, 2009), however, the underlying mechanisms remained unclear. Overall, our study supports the possibility that pomegranate phenolics may exert protective effects in human HaCaT skin cells by reducing oxidative stress. A limitation of the current study is that the bioavailability of pomegranate phenolics in skin cells and tissue were not explored but this will be pursued in our future studies.

In summary, pomegranate phenolics showed protective effects against H₂O₂-induced oxidative stress and cytotoxicity in human keratinocytes HaCaT cells. Pomegranate phenolics protected keratinocytes by reducing H₂O₂-induced ROS production and cytotoxicity. In addition, pomegranate

phenolics decreased H₂O₂-induced apoptotic cell population and down-regulated the level of caspases-3/7 in HaCaT cells. These results suggest that pomegranate phenolics may be utilized as natural antioxidants for cosmeceutical applications for skin health.

Acknowledgements

Data were acquired from instruments located at the University of Rhode Island in the RI-INBRE core facility obtained from Grant P20GM103430 from the National Center for Research Resources (NCRR), a component of the National Institutes of Health (NIH). C.L. was supported by a teaching assistantship from College of Pharmacy, the University of Rhode Island. H.G. was supported by a funding from China Scholarship Council (201708210229). D.L. was supported by grants from the Department of Education of Guangdong Province (2016KCXTD005; 2017KSYS010). The plant material was kindly provided by Mr Ajay Patel, Verdure Sciences (Noblesville, IN, USA).

Declarations of interest:

none

Ethics statement:

Research did not include any human subjects and animal experiments

References

- Adhami, V. M., Khan, N., & Mukhtar, H. (2009). Cancer chemoprevention by pomegranate: laboratory and clinical evidence. *Nutrition and Cancer*, 61(6), 811-815. doi: 10.1080/01635580903285064
- Ahmed H., A., Subaiea G. M., Eid, A., Li, L., Seeram, N. P., & Zawia, N. H. (2014). Pomegranate extract modulates processing of amyloid- β precursor protein in an aged Alzheimer's disease animal model. *Current Alzheimer Research*, 11(9), 834-843.
- Baroni, A., Buommino, E., De Gregorio, V., Ruocco, E., Ruocco, V., & Wolf, R. (2012). Structure and function of the epidermis related to barrier properties. *Clinics in Dermatology*, 30(3), 257-262. doi: 10.1016/j.clindermatol.2011.08.007
- Blume-Peytavi, U., Kottner, J., Sterry, W., Hodin, M. W., Griffiths, T. W., Watson, R. E., et al. (2016). Age-associated skin conditions and diseases: current perspectives and future options. *Gerontologist*, 56 Suppl 2, S230-242. doi: 10.1093/geront/gnw003
- Chung, Y. C., Lu, L. C., Tsai, M. H., Chen, Y. J., Chen, Y. Y., Yao, S. P., et al. (2013). The inhibitory effect of ellagic acid on cell growth of ovarian carcinoma cells. *Evidence-Based Complementary and Alternative Medicine*, 2013, 306705. doi: 10.1155/2013/306705
- D'Orazio, J., Jarrett, S., Amaro-Ortiz, A., & Scott, T. (2013). UV radiation and the skin. *International Journal of Molecular Sciences*, 14(6), 12222-12248. doi: 10.3390/ijms140612222
- DaSilva, N. A., Nahar, P. P., Ma, H., Eid, A., Wei, Z., Meschwitz, S., et al. (2017). Pomegranate ellagitannin-gut microbial-derived metabolites, urolithins, inhibit neuroinflammation in vitro. *Nutritional Neuroscience*, 1-11. doi: 10.1080/1028415X.2017.1360558
- Farage, M. A., Miller, K. W., Elsner, P., & Maibach, H. I. (2008). Intrinsic and extrinsic factors in skin ageing: a review. *International Journal of Cosmetic Science*, 30(2), 87-95. doi: 10.1111/j.1468-2494.2007.00415.x
- Feingold, K. R. (2007). Thematic review series: skin lipids. The role of epidermal lipids in cutaneous permeability barrier homeostasis. *Journal of Lipid Research*, 48(12), 2531-2546. doi: 10.1194/jlr.R700013-JLR200

- Filip, A., Daicoviciu, D., Clichici, S., Mocan, T., Muresan, A., & Postescu, I. D. (2011). Photoprotective effects of two natural products on ultraviolet B-induced oxidative stress and apoptosis in SKH-1 mouse skin. *Journal of Medicinal Food*, 14(7-8), 761-766. doi: 10.1089/jmf.2010.0142
- Gkogkolou, P., & Bohm, M. (2012). Advanced glycation end products: Key players in skin aging? *Dermatoendocrinology*, 4(3), 259-270. doi: 10.4161/derm.22028
- Gonzalez-Sarrias, A., Nunez-Sanchez, M. A., Tomas-Barberan, F. A., & Espin, J. C. (2017). Neuroprotective effects of bioavailable polyphenol-derived metabolites against oxidative stress-induced cytotoxicity in human neuroblastoma SH-SY5Y cells. *Journal of Agricultural and Food Chemistry*, 65(4), 752-758. doi: 10.1021/acs.jafc.6b04538
- He, Y. Y., Huang, J. L., Block, M. L., Hong, J. S., & Chignell, C. F. (2005). Role of phagocyte oxidase in UVA-induced oxidative stress and apoptosis in keratinocytes. *Journal of Investigative Dermatology*, 125(3), 560-566. doi: 10.1111/j.0022-202X.2005.23851.x
- Hseu, Y. C., Chou, C. W., Senthil Kumar, K. J., Fu, K. T., Wang, H. M., Hsu, L. S., et al. (2012). Ellagic acid protects human keratinocyte (HaCaT) cells against UVA-induced oxidative stress and apoptosis through the upregulation of the HO-1 and Nrf-2 antioxidant genes. *Food and Chemical Toxicology*, 50(5), 1245-1255. doi: 10.1016/j.fct.2012.02.020
- Ito, H. (2011). Metabolites of the ellagitannin geraniin and their antioxidant activities. *Planta Medica*, 77(11), 1110-1115. doi: 10.1055/s-0030-1270749
- Kallio, T., Kallio, J., Jaakkola, M., Mäki, M., Kilpeläinen, P., & Virtanen, V. (2013). Urolithins display both antioxidant and pro-oxidant activities depending on assay system and conditions. *Journal of Agricultural and Food Chemistry*, 61(45), 10720-10729.
- Kasai, K., Yoshimura, M., Koga, T., Arii, M., & Kawasaki, S. (2006). Effects of oral administration of ellagic acid-rich pomegranate extract on ultraviolet-induced pigmentation in the human skin. *Journal of Nutritional Science and Vitaminology*, 52(5), 383-388.
- Khan, N., Syed, D. N., Pal, H. C., Mukhtar, H., & Afaq, F. (2012). Pomegranate fruit extract inhibits UVB-induced inflammation and proliferation by modulating NF-kappaB and MAPK signaling

- pathways in mouse skin. *Photochemistry and Photobiology*, 88(5), 1126-1134. doi: 10.1111/j.1751-1097.2011.01063.x
- Larrosa, M., González-Sarriás, A., García-Conesa, M. T., Tomás-Barberán, F. A., & Espín, J. C. (2006). Urolithins, ellagic acid-derived metabolites produced by human colonic microflora, exhibit estrogenic and antiestrogenic activities. *Journal of Agricultural and Food Chemistry*, 54(5), 1611-1620.
- Lawrence, J., Dickson, F., & Benford, D. (1997). Skin irritant-induced cytotoxicity and prostaglandin E2 release in human skin keratinocyte cultures. *Toxicology in Vitro*, 11(5), 627-631.
- Liu, W., Ma, H., Frost, L., Yuan, T., Dain, J. A., & Seeram, N. P. (2014). Pomegranate phenolics inhibit formation of advanced glycation endproducts by scavenging reactive carbonyl species. *Food & Function*, 5(11), 2996-3004. doi: 10.1039/c4fo00538d
- Liu, Y., & Seeram, N. P. (2018). Liquid chromatography coupled with time-of-flight tandem mass spectrometry for comprehensive phenolic characterization of pomegranate fruit and flower extracts used as ingredients in botanical dietary supplements. *Journal of Separation Science*, 41(15), 3022-3033. doi: 10.1002/jssc.201800480
- Ma, H., DaSilva, N. A., Liu, W., Nahar, P. P., Wei, Z., Liu, Y., et al. (2016). Effects of a standardized phenolic-enriched maple syrup extract on beta-amyloid aggregation, neuroinflammation in microglial and neuronal cells, and beta-amyloid induced neurotoxicity in *Caenorhabditis elegans*. *Neurochemical Research*, 41(11), 2836-2847. doi: 10.1007/s11064-016-1998-6
- Ma, H., Johnson, S. L., Liu, W., DaSilva, N. A., Meschwitz, S., Dain, J. A., et al. (2018). Evaluation of polyphenol anthocyanin-enriched extracts of blackberry, black raspberry, blueberry, cranberry, red raspberry, and strawberry for free radical scavenging, reactive carbonyl species trapping, anti-glycation, anti-beta-amyloid aggregation, and microglial neuroprotective effects. *International Journal of Molecular Sciences*, 19(2). doi: 10.3390/ijms19020461
- McIlwain, D. R., Berger, T., & Mak, T. W. (2015). Caspase functions in cell death and disease. *Cold Spring Harbor Perspectives in Biology*, 7(4). doi: 10.1101/cshperspect.a026716
- Pacheco-Palencia, L. A., Mertens-Talcott, S., & Talcott, S. T. (2008). Chemical composition, antioxidant properties, and thermal stability of a phytochemical enriched oil from Acai

- (*Euterpe oleracea* Mart.). *Journal of Agricultural and Food Chemistry*, 56(12), 4631-4636. doi: 10.1021/jf800161u
- Pacheco-Palencia, L. A., Noratto, G., Hingorani, L., Talcott, S. T., & Mertens-Talcott, S. U. (2008). Protective effects of standardized pomegranate (*Punica granatum* L.) polyphenolic extract in ultraviolet-irradiated human skin fibroblasts. *Journal of Agricultural and Food Chemistry*, 56(18), 8434-8441. doi: 10.1021/jf8005307
- Poljsak, B., Dahmane, R. G., & Godic, A. (2012). Intrinsic skin aging: the role of oxidative stress. *Acta Dermatovenerol Alp Pannonica Adriat*, 21(2), 33-36.
- Qiu, Z., Zhou, B., Jin, L., Yu, H., Liu, L., Liu, Y., et al. (2013). In vitro antioxidant and antiproliferative effects of ellagic acid and its colonic metabolite, urolithins, on human bladder cancer T24 cells. *Food and Chemical Toxicology*, 59, 428-437. doi: 10.1016/j.fct.2013.06.025
- Rahman, I., Biswas, S. K., & Kirkham, P. A. (2006). Regulation of inflammation and redox signaling by dietary polyphenols. *Biochemical Pharmacology*, 72(11), 1439-1452. doi: 10.1016/j.bcp.2006.07.004
- Ray, P. D., Huang, B. W., & Tsuji, Y. (2012). Reactive oxygen species (ROS) homeostasis and redox regulation in cellular signaling. *Cellular Signalling*, 24(5), 981-990. doi: 10.1016/j.cellsig.2012.01.008
- Rinnerthaler, M., Bischof, J., Streubel, M. K., Trost, A., & Richter, K. (2015). Oxidative stress in aging human skin. *Biomolecules*, 5(2), 545-589. doi: 10.3390/biom5020545
- Sengupta, A., Lichti, U. F., Carlson, B. A., Ryscavage, A. O., Gladyshev, V. N., Yuspa, S. H., et al. (2010). Selenoproteins are essential for proper keratinocyte function and skin development. *PLoS One*, 5(8), e12249. doi: 10.1371/journal.pone.0012249
- Seok, J. K., Lee, J. W., Kim, Y. M., & Boo, Y. C. (2018). Punicalagin and (-)-epigallocatechin-3-gallate rescue cell viability and attenuate inflammatory responses of human epidermal keratinocytes exposed to airborne particulate matter PM10. *Skin Pharmacology and Physiology*, 31(3), 134-143. doi: 10.1159/000487400
- Syed, D. N., Malik, A., Hadi, N., Sarfaraz, S., Afaq, F., & Mukhtar, H. (2006). Photochemopreventive effect of pomegranate fruit extract on UVA-mediated activation of cellular pathways in normal

- human epidermal keratinocytes. *Photochemistry and Photobiology*, 82(2), 398-405. doi: 10.1562/2005-06-23-RA-589
- Szyszkowska, B., Lepecka-Klusek, C., Kozłowicz, K., Jazienicka, I., & Krasowska, D. (2014). The influence of selected ingredients of dietary supplements on skin condition. *Advances in Dermatology and Allergology*, 31(3), 174-181. doi: 10.5114/pdia.2014.40919
- Tang, L., Mo, Y., Li, Y., Zhong, Y., He, S., Zhang, Y., et al. (2017). Urolithin A alleviates myocardial ischemia/reperfusion injury via PI3K/Akt pathway. *Biochemical and Biophysical Research Communications*, 486(3), 774-780. doi: 10.1016/j.bbrc.2017.03.119
- Wang, D., Chen, Q., Liu, B., Li, Y., Tan, Y., & Yang, B. (2016). Ellagic acid inhibits proliferation and induces apoptosis in human glioblastoma cells. *Acta Cirurgica Brasleira*, 31(2), 143-149. doi: 10.1590/S0102-865020160020000010
- Wang, S. T., Chang, W. C., Hsu, C., & Su, N. W. (2017). Antimelanogenic effect of urolithin A and urolithin B, the colonic metabolites of ellagic acid, in B16 melanoma cells. *Journal of Agricultural and Food Chemistry*, 65(32), 6870-6876. doi: 10.1021/acs.jafc.7b02442
- Wang, Y., Qiu, Z., Zhou, B., Liu, C., Ruan, J., Yan, Q., et al. (2015). In vitro antiproliferative and antioxidant effects of urolithin A, the colonic metabolite of ellagic acid, on hepatocellular carcinomas HepG2 cells. *Toxicology In Vitro*, 29(5), 1107-1115. doi: 10.1016/j.tiv.2015.04.008
- Yaar, M., & Gilchrist, B. A. (2001). Skin aging: postulated mechanisms and consequent changes in structure and function. *Clinics in Geriatric Medicine*, 17(4), 617-630, v.
- Yang, H., Liu, C., Zhang, Y. Q., Ge, L. T., Chen, J., Jia, X. Q., et al. (2015). Ilexgenin A induces B16-F10 melanoma cell G1/S arrest in vitro and reduces tumor growth in vivo. *International Immunopharmacology*, 24(2), 423-431. doi: 10.1016/j.intimp.2014.12.040
- Yuan, T., Ding, Y., Wan, C., Li, L., Xu, J., Liu, K., et al. (2012). Antidiabetic ellagitannins from pomegranate flowers: inhibition of alpha-glucosidase and lipogenic gene expression. *Organic Letters*, 14(20), 5358-5361. doi: 10.1021/ol302548c
- Yuan, T., Ma, H., Liu, W., Niesen, D. B., Shah, N., Crews, R., et al. (2016). Pomegranate's neuroprotective effects against Alzheimer's disease are mediated by urolithins, its ellagitannin-

- gut microbial derived metabolites. *ACS Chemical Neuroscience*, 7(1), 26-33. doi: 10.1021/acschemneuro.5b00260
- Yuan, T., Wan, C., Ma, H., & Seeram, N. P. (2013). New phenolics from the flowers of *Punica granatum* and their in vitro alpha-glucosidase inhibitory activities. *Planta Medica*, 79(17), 1674-1679. doi: 10.1055/s-0033-1350925
- Zaid, M. A., Afaq, F., Syed, D. N., Dreher, M., & Mukhtar, H. (2007). Inhibition of UVB-mediated oxidative stress and markers of photoaging in immortalized HaCaT keratinocytes by pomegranate polyphenol extract POMx. *Photochemistry and Photobiology*, 83(4), 882-888.
- Zhang, Y. Q., Yang, H., Sun, W. D., Wang, J., Zhang, B. Y., Shen, Y. J., et al. (2018). Ethanol extract of *Ilex hainanensis* Merr. exhibits anti-melanoma activity by induction of G1/S cell-cycle arrest and apoptosis. *Chinese Journal of Integrative Medicine*, 24(1), 47-55. doi: 10.1007/s11655-017-2544-8
- Zhao, J., Li, G., Bo, W., Zhou, Y., Dang, S., Wei, J., et al. (2017). Multiple effects of ellagic acid on human colorectal carcinoma cells identified by gene expression profile analysis. *International Journal of Oncology*, 50(2), 613-621. doi: 10.3892/ijo.2017.3843

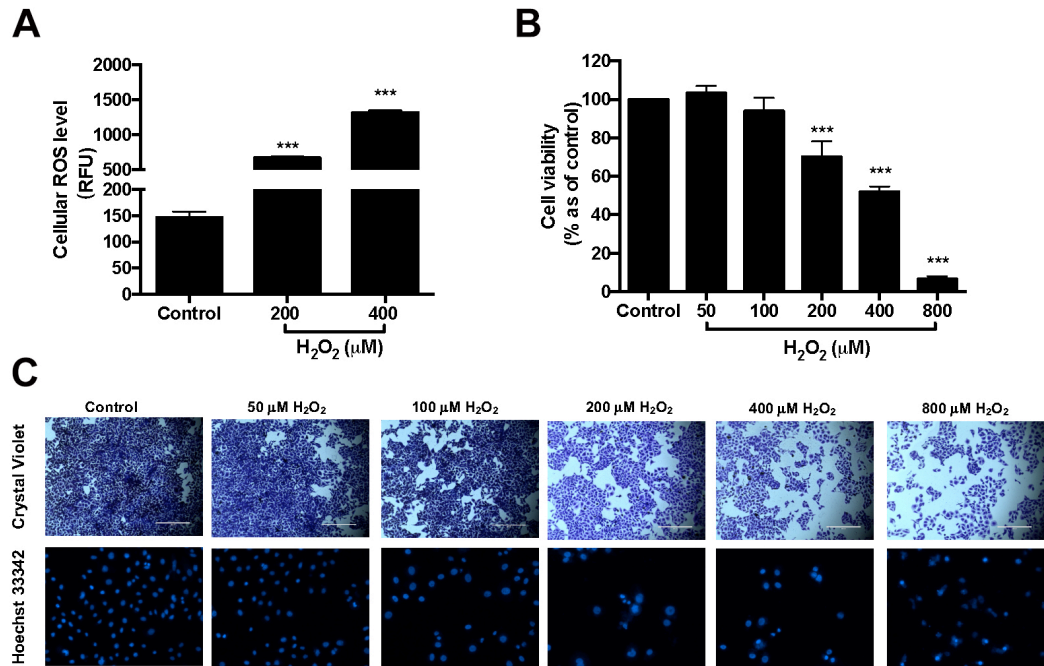


Fig. 1 Effects of H₂O₂ on viability of HaCaT cells and ROS production in HaCaT cells (A). HaCaT cells were incubated with H₂O₂ at concentrations of 200 and 400 μM and then incubated with DMEM containing 20 μM DCFDA. Fluorescence intensity of each well was measured at excitation and emission wavelength of 485 and 525 nm, respectively. HaCaT cells were treated with H₂O₂ at concentrations of 50, 10, 200, 400, and 800 μM. Cell viability was measured by using CTG 2.0 assay (B). Representative images of HaCaT cells exposed to H₂O₂ for 24 h and then stained with crystal violet and Hoechst 33342 (C). Significance was defined as compared with control group: ****P* < 0.001. The values presented are the means ± S.D.

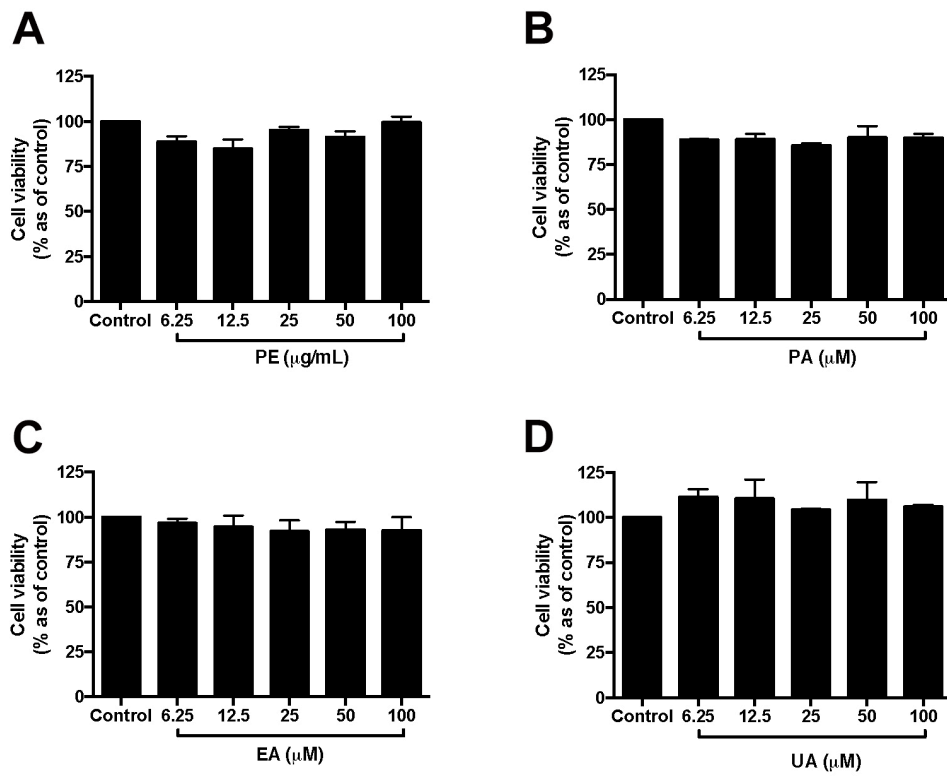


Fig. 2 Effects of PE and pomegranate phenolics on viability of HaCaT cells. HaCaT cells were incubated with PE (**A**), PA (**B**), EA (**C**), and UA (**D**) for 24 h. Cell viability was measured by CTG 2.0 assay. Values are presented as means \pm S.D. from three replicates.

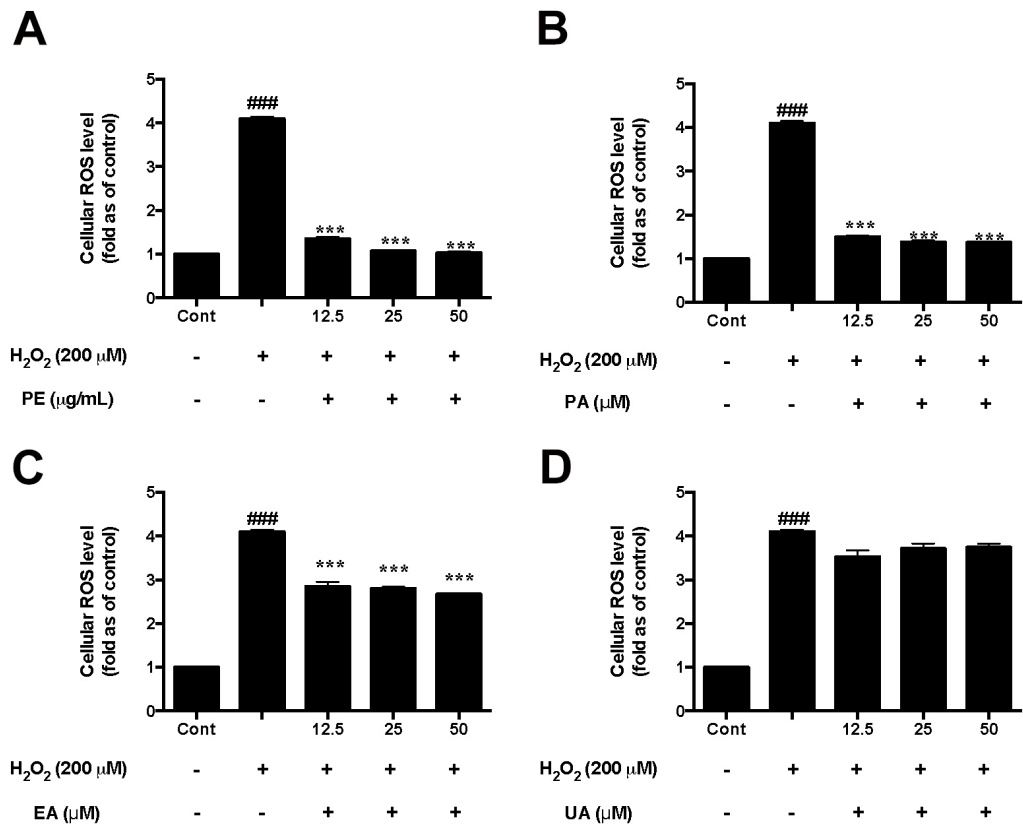


Fig. 3 Effects of PE and pomegranate phenolics on ROS production in HaCaT cells exposed to H₂O₂. HaCaT cells were incubated with PE (**A**), PA (**B**), EA (**C**), and UA (**D**) for 12 h before H₂O₂ induction. Cells were incubated with DMEM containing 20 μM DCFDA after medium removal. Fluorescence intensity of each well was measured at excitation and emission wavelength of 485 and 525 nm, respectively. Significances were defined as compared with control group: ###P < 0.01; compared with the H₂O₂-treated group: ***P < 0.001. Values are presented as means ± S.D. from three replicates.

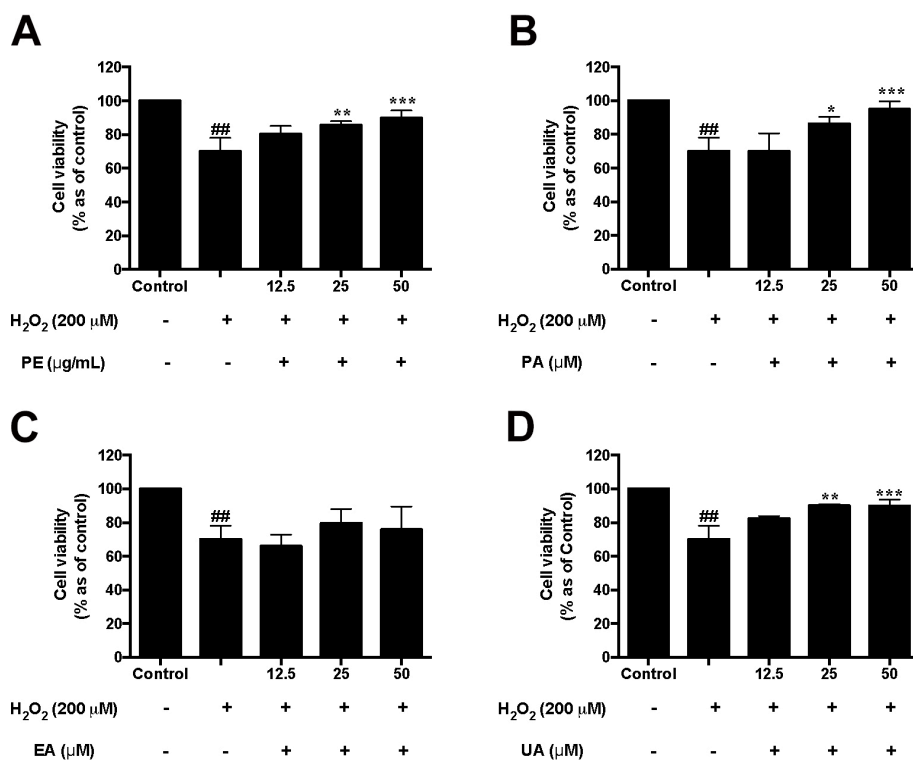


Fig. 4 Effects of PE and pomegranate phenolics on cell viability of HaCaT cells exposed to H₂O₂. HaCaT cells were incubated with PE (**A**), PA (**B**), EA (**C**), and UA (**D**) for 12 h before H₂O₂ induction. Cell viability was measured by using CTG 2.0 assay. Significances were defined as compared with control group: ###P < 0.01; compared with the H₂O₂-treated group: *P < 0.05, **P < 0.01, ***P < 0.001. Values are presented as means ± S.D. from three replicates.

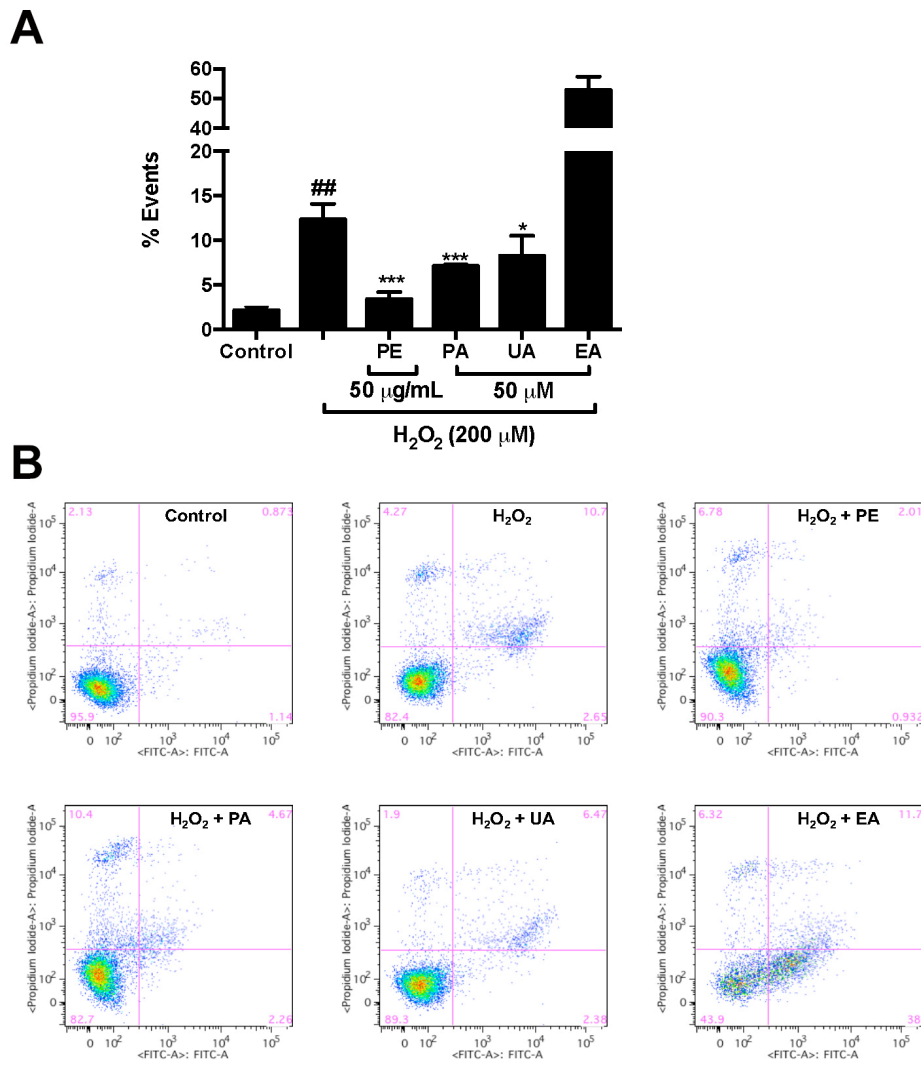


Fig. 5 Effects of PE and pomegranate phenolics on apoptosis of HaCaT cells induced by H₂O₂. The apoptotic cell populations (annexin V+/PI- and annexin V+/PI+) of HaCaT cells with or without treatments of PE, PA, EA, and UA were quantified by gated patterns in double stains (A). HaCaT cells stained with annexin V-FITC/PI and assayed by flow cytometry (B). Significances were defined as compared with control group: ##*P* < 0.001; compared with the H₂O₂-treated group: **P* < 0.05, ****P* < 0.001.

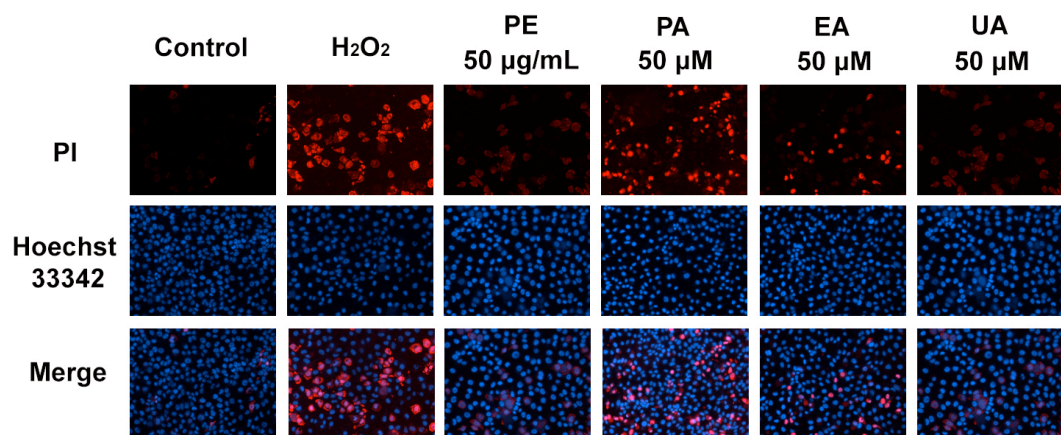


Fig. 6 Effects of PE and pomegranate phenolics on necrosis of HaCaT cells induced by H₂O₂. Fluorescence microscopy shows representative pictures of HaCaT cells treated with PE, PA, EA, and UA. HaCaT cells were stained with Hoechst 33342 and PI.

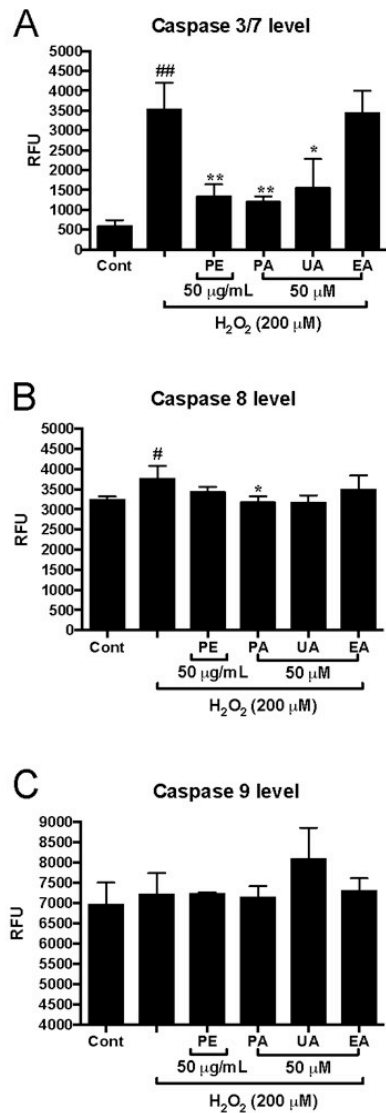


Fig. 7 Effects of PE and pomegranate phenolics on cellular caspase 3/7 (**A**), caspase 8 (**B**) and caspase 9 (**C**) in HaCaT cells exposed to H₂O₂. HaCaT cells were incubated with PE, PA, EA, and UA for 12 h before H₂O₂ induction. Significances were defined as compared with control group: ##*P* < 0.01; compared with H₂O₂-treated group: **P* < 0.05, ***P* < 0.01, ****P* < 0.001. Values are presented as means ± S.D. from three replicates.

CHAPTER 2

MANUSCRIPT 2

Published: 30 April 2020

Food & Function, 2020, 11, 5105-5114

Cytoprotective Effects of A Proprietary Red Maple Leaves Extract and Its Major Polyphenol, Ginnalin A, against Hydrogen Peroxide and Methylglyoxal Induced Oxidative Stress in Human Keratinocytes

Chang Liu^b, Hao Guo^{b,c,d}, Joel A. Dain^e, Yinsheng Wan^d, Xing-Hua Gao^c, Hong-Duo Chen^c, Navindra P. Seeram^{b*}, Hang Ma^{a,b*}

^aSchool of Chemical and Environment Engineering, Wuyi University; International Healthcare Innovation Institute (Jiangmen), Jiangmen 529020, Guangdong, China

^bBioactive Botanical Research Laboratory, Department of Biomedical and Pharmaceutical Sciences, College of Pharmacy, University of Rhode Island, Kingston, RI 02881, USA

^cDepartment of Dermatology, Key Laboratory of Immunodermatology, No.1 Hospital of China Medical University, Shenyang, China

^dDepartment of Biology, Providence College, Providence, RI 02918, USA

^eDepartment of Chemistry, University of Rhode Island, Kingston, RI 02881, USA

**Corresponding authors*

Tel.: +1 401 874 9367; E-mail address: nseeram@uri.edu (N.P.S.)

Tel.: +1 401 874 7654; E-mail address: hang_ma@uri.edu (H.M.)

7 Greenhouse Road, Kingston, RI 02881 USA, The University of Rhode Island

Abstract

Phytochemicals from functional foods are common ingredients in dietary supplements and cosmetic products for anti-skin aging effects due to their antioxidant activities. A proprietary red maple (*Acer rubrum*) leaves extract (Maplifa™) and its major phenolic compound, ginnalin A (GA), have been reported to show antioxidant, anti-melanogenesis, and anti-glycation effects but their protective effects against oxidative stress in human skin cells remain unknown. Herein, we investigated the cytoprotective effects of Maplifa™ and GA against hydrogen peroxide (H₂O₂) and methylglyoxal (MGO)-induced oxidative stress in human keratinocytes (HaCaT cells). H₂O₂ and MGO (both at 400 μM) induced toxicity in HaCaT cells and reduced their viability to 59.2 and 61.6 %, respectively. Treatment of Maplifa™ (50 μg/mL) and GA (50 μM) increased the viability of H₂O₂- and MGO-treated cells by 22.0 and 15.5 %, respectively. Maplifa™ and GA also showed cytoprotective effects by reducing H₂O₂-induced apoptosis in HaCaT cells by 8.0 and 7.2 %, respectively. The anti-apoptotic effect of Maplifa™ was further supported by the decreased levels of apoptosis associated enzymes including caspases-3/7 and -8 in HaCaT cells by 49.5 and 19.0 %, respectively. In addition, Maplifa™ (50 μg/mL) and GA (50 μM) reduced H₂O₂- and MGO-induced reactive oxygen species (ROS) by 84.1 and 56.8 %, respectively. Furthermore, flow cytometry analysis showed that Maplifa™ and GA reduced MGO-induced total cellular ROS production while increasing mitochondria-derived ROS production in HaCaT cells. The cytoprotective effects of Maplifa™ and GA in human keratinocytes support their potential utilization for cosmetic and/or dermatological applications.

Keywords: Red maple (*Acer rubrum*), ginnalin A, keratinocytes, methylglyoxal, antioxidant, skin protection

1. Introduction

Botanical extracts from functional foods are common ingredients found in cosmeceutical products. These botanical ingredients are used for topical applications, for e.g. as bioactives in cosmetics, as well as for consumable products, such as dietary beauty supplements, i.e. as capsules or tinctures.¹ It has been reported that several botanical extracts from functional foods are included in the top ten list of botanical ingredients in anti-aging creams in 2010.¹ Numerous published studies have also reported that phytochemicals in botanical extracts show a wide range of biological activities including antioxidant, anti-microbial, anti-inflammation, and anti-glycation effects,^{2, 3} which contribute to their overall skin beneficial effects.

Skin, the largest organ of the human body, is subjected to exposure of intrinsic oxidative stress from several intra- and extra-cellular biochemical reactions including oxidation and glycation.⁵ Both extrinsic and intrinsic oxidative stress lead to excessive production of cellular reactive oxygen species (ROS), which further lead to the impairment of skin cells by triggering cell survival signaling pathways including cell necrosis and apoptosis.⁴ Another contributing factor for the induction of skin cellular oxidative stress is the process of glycation, a non-enzymatic reaction involving the metabolism of glucose. In the glycolysis pathway, glucose is converted into pyruvate and a group of dicarbonyl compounds, for e.g. glyoxal and methylglyoxal (MGO), which are formed as side products.⁵ These dicarbonyl compounds are highly reactive and can interact with biomacro-molecules including protein, lipids, and DNA, to form a class of complex and heterogeneous compounds known as advanced glycation endproducts (AGEs). Both AGEs and its precursor, MGO, can exacerbate the production of ROS and largely contribute to the occurrence and development of many skin disorders including skin aging and inflammation.⁶ Thus, inhibitors of AGEs and scavengers of reactive dicarbonyl species, especially natural antioxidants, such as several polyphenols from botanical extracts, are considered as promising management strategies for AGEs associated skin complications.^{6, 7}

Our laboratory has had a long interest in investigating the biological effects of phytochemicals in functional foods and botanical extracts. During the course of our studies, using a combination of *in vitro* and *in vivo* assays, we developed an algorithm to screen the anti-aging effects of over thirty botanical extracts, several of which showed promising neuroprotective effects including antioxidant, MGO

scavenging capacity, anti-glycation, and anti-inflammatory activity.⁸ In addition, some of the pure constituents from these botanical extracts, for e.g. punicalagin and ellagic acid from a pomegranate extract (*Punica granatum*; commercially available as Pomella[®]), showed anti-glycation effects and protected human keratinocytes against ROS-induced cytotoxicity.⁹ Our group has also reported on the development of a proprietary phenolic-enriched botanical extract from red maple (*Acer rubrum*) leaves (known as Maplifa[™])¹⁰ as a botanical ingredient for dietary supplement and cosmeceutical applications. Maplifa[™] showed several skin beneficial effects including antioxidant, anti-glycation effects, and anti-melanogenic activity.^{10, 11} However, the protective effects of Maplifa[™] and its major phenolic compound, ginnalin A (GA), against oxidative stress in human keratinocytes remain unexplored. Herein, we aimed to investigate the cytoprotective effects of Maplifa[™] and GA against hydrogen peroxide (H₂O₂) and MGO-induced oxidative stress in human keratinocytes HaCaT cells.

2. Materials and Methods

2.1. Chemicals and reagents

Maplifa[™], a proprietary phenolic-enriched red maple leaves extract, was prepared with protocols developed in our laboratory.¹⁰ The phytochemical composition of Maplifa[™] has been extensively studied by our laboratory with over 100 phenolics identified.¹² Maplifa[™] was standardized to ginnalin A (GA) content (c.a. 45%), which is the major phenolic compound present in the extract.¹⁰ Methylglyoxal (MGO), hydrogen peroxide (H₂O₂), crystal violet powder, Hoechst 33342 staining agent, dimethyl sulfoxide (DMSO), and 2',7'-dichlorofluorescein diacetate (DCFDA) were purchased from Sigma Chemical Co. (St. Louis, MO, USA). MitoTracker[™] Red CMXRos, and Annexin and propidium iodide (PI) staining kits were purchased from Thermo Fisher Scientific (Waltham, MA, USA). MCellTiter-Glo[®] (CTG) 2.0 and caspase-Glo[®] assay kits (caspase- 3/7, -8, and -9) were purchased from Promega (Fitchburg, WI, USA).

2.2. Cell culture and sample preparation

Human keratinocytes (HaCaT cells) were purchased from the American Type Culture Collection (ATCC, Rockville, USA). HaCaT cells were cultured in Dulbecco's modified Eagle's medium (DMEM) (Life Technologies, Gaithersburg, MD, USA) supplemented with 10% fetal bovine serum (FBS; GIBCO[™], Grand Island, NY, USA) at 37 °C in the presence of 5% CO₂. Stock solution of

test samples were prepared in DMSO and diluted with cell culture medium without FBS to desired concentrations (6.25-200 µg/mL for MaplifaTM and 6.25-200 µM for GA). The final percentage of DMSO in the treatments groups was less than 0.2% and HaCaT cells in all of the control groups were treated with medium containing 0.2% of DMSO.

2.3. Measurement of cell viability

The effects of MaplifaTM and GA on the viability of HaCaT cells were determined by the CTG 2.0 assay.¹³ The model for the H₂O₂-induced cell damage was according to our previously reported method with minor modifications.⁹ In brief, HaCaT cells were seeded in 96-well plates at 1×10⁴ cells per well and allowed to attach for 12 h. Media was then removed and cells were incubated with test samples for 12 h, following treatment of H₂O₂ (400 µM) for 24 h. CTG 2.0 reagent was then added in each well and the plate was kept at room temperature for 10 min. Luminescence intensity was recorded using a Spectramax M2 plate reader (Molecular Devices, Sunnyvale, CA, USA). The MGO-induced cell damage model was constructed similarly with minor modifications. HaCaT cells were seeded in 96-well plates at 5×10³ cells per well and allowed to attach for 12 h. After incubation, the cells were treated with test samples for 2 h. The cells were washed with PBS twice and treated with MGO (400 µM) for 24 h, and then cell viability was measured using the CTG 2.0 assay.

2.4. Measurement of reactive oxygen species (ROS)

HaCaT cells were seeded in 96-well plates at 1×10⁴ cells or 5×10³ cells per well for H₂O₂-induced or MGO-induced cell damage model, respectively, for 12 h. Next, cells were treated with test samples for 12 h (in H₂O₂-induced model) or 2 h (in MGO-induced model). Then cell culture media were removed and cells were washed twice with phosphate-buffered saline (PBS). Media containing a fluorescent agent (DCFDA; 20 µM) were added to the cells and incubated for 20 mins. Next, HaCaT cells were washed with PBS to remove excessive exogenous ROS and cells were treated with H₂O₂ or MGO (both at 400 µM) for 1 h or 24 h, respectively. Cellular fluorescence intensity was measured with excitation and emission wavelengths of 485 and 525 nm, respectively, using a Spectramax M2 plate reader (Molecular Devices, Sunnyvale, CA, USA).

2.5. Detection of cell apoptosis

Flow cytometric assays for the measurements of cell apoptosis were conducted as previously

reported.⁹ HaCaT cells were seeded in 6-well plates at 3×10^5 cells per well and allowed to attach for 12 h, followed by the treatment with test samples for 6 h. Cell culture media were then removed, and cells were washed twice with PBS. Next, H_2O_2 (400 μ M) was added to cells and incubated for 24 h, then cells were harvested and stained with binding buffer containing Annexin and PI agents for 15 mins in the dark. Cell suspensions were quantified using flow cytometry and data were analyzed using FlowJo software.

2.6. Measurements of caspases-3/7, -8, and -9

Levels of caspases -3/7, -8, and -9 were measured as previously reported.⁹ HaCaT cells were seeded in 96-well plates at 5×10^3 cells per well and allowed to attach for 12 h, followed by treatment of test samples for 6 h. Media were then removed and cells were washed twice with PBS. Next, H_2O_2 (400 μ M) was added and incubated for 24 h followed by adding caspase-Glo kit reagents. Plates were then incubated at room temperature for 30 min and the luminescence intensity of each well was read using a Spectramax M2 plate reader.

2.7. Detection of total and mitochondria-derived ROS

In the MGO-induced cell damage model, HaCaT cells were seeded in 6-well plates at 3×10^5 cells per well and allowed to attach for 12 h. Cells were then treated with test samples for 2 h and washed twice with PBS, before adding MGO (400 μ M) for 24 h. Cells were then harvested and stained with MitoTracker™ Red agents for 15 mins in dark. Cell suspensions were quantified using flow cytometry (BD FACSCalibur, San Jose, CA, USA) and data were analyzed using FlowJo software (FlowJo, Ashland, OR, USA).

2.8. Statistical analysis

Statistical analyses were performed using GraphPad Prism 6 (GraphPad Software, La Jolla, CA, USA). Data are expressed as the mean value \pm standard deviation (S.D.) obtained from triplicates of experiments. The significance of differences was determined using a two-way analysis of variance (ANOVA) followed by a post hoc Student-Newman–Keuls multiple comparison test (SNK). $P < 0.05$, $P < 0.01$, or $P < 0.001$ was determined as significant.

3. Results and discussion

3.1. Maplifa™ and GA reduced H_2O_2 and MGO-induced cytotoxicity in HaCaT

Prior to evaluating the protective effects of Maplifa™ and GA, their range of non-cytotoxic concentrations in HaCaT cells were determined by the CTG 2.0 cell viability assay. Maplifa™ and GA, at concentrations ranging from 6.25-100 µg/mL and 6.25-100 µM, respectively, did not induce cytotoxicity in HaCaT cells (cell viability >96.0%; Fig. 1). Next, concentrations of 12.5, 25, and 50 µg/mL (for Maplifa™) and 12.5, 25, and 50 µM (for GA) were selected for further evaluation. Hydrogen peroxide (H₂O₂; reactive oxygen species) and methylglyoxal (MGO; reactive carbonyl species) were used as oxidative inducers and their cytotoxic effects were evaluated in HaCaT cells. H₂O₂ (at 400 µM) induced cytotoxicity by decreasing viability of HaCaT cells to 59.2% (Fig. 2A). Similarly, treatment of MGO (400 µM) reduced viability of HaCaT cells to 61.6% (Fig. 2B). Maplifa™ and GA showed cytoprotective effects by increasing the viability of HaCaT cells exposed to H₂O₂ (Fig. 2A and B) and MGO (Fig. 2C and D). Both Maplifa™ (12.5, 25, and 50 µg/mL) and GA (12.5, 25, and 50 µM) increased the viability of H₂O₂ challenged cells by 11.1-21.5% and 13.8-21.0%, respectively. Maplifa™, at the highest test concentration (50 µg/mL), maintained 89.7% viable cells as compared to the control group, while GA at 12.5, 25, and 50 µM, maintained cell viability at 85.9%, 91.7%, and 93.9%, respectively. The ameliorative effect of Maplifa™ and GA in H₂O₂-treated HaCaT cells was further supported by morphological analysis with crystal violet staining methods (Fig. 2E). Exposure to H₂O₂ impaired the integrity of cell nuclei which was shown as deformable shapes of stained nuclei whilst the treatment of Maplifa™ (50 µg/mL) and GA (50 µM) redeemed the normal shape of cell nuclei. Similarly, exposure to MGO (at 400 µM) led to significant morphological changes of HaCaT cells. However, Maplifa™ (50 µg/mL) and GA (50 µM) did not change the shape of cell nuclei as compared to the MGO-treated group.

Hydrogen peroxide, one of the most common form of ROS, has been utilized as an inducer of oxidative stress and cytotoxicity in experimental models.¹⁴ Previously reported studies support that H₂O₂-induced cell death can be ameliorated by dietary hydrolyzable tannins including ellagitannins (e.g. punicalagin) and gallotannins (e.g. penta-*O*-galloyl-β-D-glucose) in human skin cells.^{9, 15} MGO, a byproduct formed during the oxidation of glucose and a precursor of AGEs, is also considered as a detrimental factor for skin cells as it exacerbates oxidative stress induced skin cytotoxicity, which further leads to many diabetes related dermatological complications.⁵ To date, a few studies have shown

that MGO-induced cell death in human keratinocytes can be alleviated by some synthetic compounds,¹⁶
¹⁷ but there have been no prior reports to show that natural maple-derived phenolics exert protective effects in HaCaT cells. It is possible that Maplifa™ and GA counteracted the MGO-induced toxicity in HaCaT cells by their antioxidant capacity. This is supported by our previous report that the inhibitory effects of Maplifa™ and GA against the formation of MGO-induced glycation were attributed to their antioxidant capacity rather than their ability to directly scavenge MGO.¹¹ Therefore, we further evaluated the antioxidant activity of Maplifa™ and GA in the HaCaT cells.

3.2. Maplifa™ and GA reduced H₂O₂ and MGO-induced production of ROS in HaCaT

To further understand the cytoprotective of Maplifa™ and GA in HaCaT cells against cellular oxidative stress, we evaluated whether Maplifa™ and GA can diminish H₂O₂- and MGO-induced production of ROS. HaCaT cells responded to the oxidative stimulation of H₂O₂ by producing cellular ROS by 8.2-fold as compared to the control group. Maplifa™ (at 12.5, 25, and 50 µg/mL) showed cytoprotective effect in the HaCaT cells by reducing the production of H₂O₂-induced ROS by 81.2, 84.1, and 84.1%, respectively. Similarly, treatment of GA (12.5, 25, and 50 µM) effectively reduced the level of ROS in HaCaT cells by 78.8, 82.7, and 86.0%, respectively, compared to the H₂O₂-treated group. In addition, the protective effects of Maplifa™ and GA against MGO-induced oxidative stress in HaCaT cells were evaluated. MGO (400 µM) elevated the production of ROS in HaCaT cells by 2.2-fold as compared to the control group (Fig. 3C and D). Treatment with Maplifa™ (12.5, 25, and 50 µg/mL) alleviated MGO-induced oxidative stress by reducing the level of ROS in HaCaT cells by 41.2, 51.3, and 54.7%, respectively, while treatment with GA (12.5, 25, and 50 µM) also reduced ROS production by 14.2, 52.4, and 56.8%, respectively. This effect was further supported by the morphological analysis of confocal images of cells stained with DCFDA agent (Fig. 3E).

Although our laboratory has reported that GA reduced the production of H₂O₂-induced ROS in murine melanoma B16F10 cells,¹⁰ this is the first study to show GA's antioxidant effects against ROS-induced stress in human keratinocytes. The cytoprotective effects of red maple phenolics including GA have been associated with its modulation of antioxidant related genes and proteins.¹⁹ For instance, GA was reported to have chemopreventive effects mediated by its activation of antioxidant related signaling pathways including [NAD(P)H quinone dehydrogenase 1; (NQO1)], heme oxygenase-1 (HO-1), and

nuclear factor erythroid 2-related factor 2 (Nrf2) in colon cancer cells.²⁰ Notably, the transcription factor, Nrf2, has been reported to play a pivotal role in the protective effects of several phenolic compounds against oxidative stress²¹. In addition, Nrf2 has been reported to regulate the antioxidant effects of phenolic compounds by the mediation of redox-sensitive anti-inflammatory signaling pathways including nuclear factor kappa-light-chain-enhancer of activated B cells (NF- κ B)^{22, 23}. Therefore, it is possible that GA's antioxidant activity is attributed to its mediation of antioxidant and anti-inflammatory transcription factors including Nrf2 and NF- κ B. However, further studies are warranted to confirm this.

3.3. *MaplifaTM and GA alleviated H₂O₂-induced apoptosis in HaCaT cells*

The cytoprotective effects of MaplifaTM and GA in HaCaT cells against H₂O₂-induced apoptosis were evaluated by flow cytometry analysis. The rate of apoptotic cells in the control group was 6.9 %, which was elevated to 21.4 % after exposure to H₂O₂ (400 μ M; Fig. 4). MaplifaTM (50 μ m/mL) and GA (50 μ M) showed anti-apoptosis effects by reducing the population of apoptotic cells by 8.0 and 7.2%, respectively, as compared to the H₂O₂-treated group (Fig. 4B). The population of viable cells in the control group was reduced from 86.8% to 60.8% after exposure to H₂O₂ (400 μ M), and both MaplifaTM (50 μ m/mL) and GA (50 μ M) showed protective effects by increasing the population of viable cells to 82.4 and 78.1%, respectively (Fig. 4C). In contrast to the pro-apoptotic effect induced by the H₂O₂ stimulation, no significant increase of apoptotic cells was observed in the MGO-treated group (Supplementary Materials; Fig. S1), suggesting that the keratinocytes responded to H₂O₂- and MGO-induced oxidative stress via different pathways. It has been observed that MGO can cause apoptosis in HaCaT cells with a longer incubation time (48 h),¹⁶ thus, further studies on the mechanisms of MGO-induced cell death, and whether MaplifaTM and GA can mitigate these detrimental effects were explored.

3.4. *MaplifaTM down-regulated activity of enzymes caspase-3/7 and -8 in HaCaT cells*

The anti-apoptotic effect of MaplifaTM and GA were further investigated by measuring their effects on the level of apoptosis-related enzymes, caspases-3/7, -8, and -9 in HaCaT cells. Stimulation with H₂O₂ significantly increased the level of caspases-3/7 (by 1.92-fold) and -8 (by 19.5%) as compared to the control group, while not affecting caspase 9 (Fig. 5). MaplifaTM counteracted H₂O₂-induced upregulation of caspases-3/7 and -8 level by 49.5 and 19.0%, respectively, while GA only reduced

caspase-3/7 (by 48.1%). No significant changes of caspase-9 were observed in the MaplifaTM and GA treated groups (Fig. 5).

Caspases are checkpoint proteases responsible for the initiation of cell death (apoptosis) and their activation can be triggered by H₂O₂ and other oxidative stress inducers.²⁴ Results from our study show that caspases-3/7 and -8, caspase isoforms which mediate cell death via the extrinsic pathway of apoptosis, were elevated by the stimulation of H₂O₂ in HaCaT cells, and diminished by the treatment of MaplifaTM and GA. This suggested that MaplifaTM and GA may protect HaCaT cells against apoptosis triggered by extracellular ligands binding to cell-surface death receptors.²⁵ This is in agreement with our previously reported study showing that punicalagin, the major polyphenol in a pomegranate fruit extract, protected HaCaT cells from H₂O₂-induced apoptosis through the modulation of caspases-3/7 and -8 level.⁹ Conversely, caspase-9, the initiator of apoptosis that senses endogenous oxidative stress, was not affected by stimulation with H₂O₂ in the HaCaT cells. Since studies have shown that caspase-9 activation is involved in the UV- and ROS-induced apoptosis of human keratinocytes,^{26, 27} further studies are warranted to delineate the signaling pathways of oxidative stress induced apoptosis in human keratinocytes.

3.5. MaplifaTM and GA decreased total ROS production but increased mitochondria-derived ROS production in MGO-stimulated HaCaT cells

It is possible that MaplifaTM and GA protected HaCaT cells against MGO-induced cell death via their antioxidant activity, rather than through anti-apoptotic effects. This is because MGO did not induce apoptosis in HaCaT cells suggesting that ROS may play a critical role in MGO's cytotoxic effects. Although DCFDA is a common chemical probe used for the measurement of ROS as shown in the aforementioned section (Fig. 3), it only provides qualitative information on the production of cellular oxidants in the fluorescent based assay¹⁸. Therefore, we further characterized the antioxidant effects of MaplifaTM and GA on MGO-induced production of both total ROS and mitochondria-derived ROS in HaCaT cells with quantitative flow cytometry assays. The total cellular ROS was measured with fluorescent dye DCFDA and stimulation by MGO (400 μ M) significantly increased fluorescent intensity by 13.5-fold compared to the control group. Treatment of MaplifaTM (50 μ g/mL) and GA (50 μ M) counteracted MGO-induced total ROS production by 31.2 and 23.6%, respectively (Fig. 6). In

addition, MGO increased specific fluorescent intensity for mitochondria-derived ROS by 30.9%, compared to control group. However, Maplifa™ and GA did not prevent MGO-stimulated production of mitochondria-derived ROS (Fig. 6C). In order to confirm this effect, a mitochondria-specific probe, namely, MitoSOX™, was applied to assess the levels of mitochondria-derived ROS in HaCaT cells (Fig. 7). ROS level, generated from mitochondria, increased by 30.9% in the MGO-treated group and was further increased by the treatment of Maplifa™ and GA (by 1.1- and 1.2-fold, respectively). Results from detection by both ROS tracker Green and MitoSOX™ methods confirmed that Maplifa™ and GA enhanced the production of mitochondria-derived ROS in cells stimulated with MGO.

ROS-induced intracellular and extracellular oxidative stress is a key factor for skin cellular damage, which leads to skin cell death and greatly contributes to skin aging process.²⁸ Evidence from extensive studies have demonstrated that antioxidants including many dietary natural products exert skin protective effects by reducing ROS production in skin cells.^{29,30} Our previously reported study was in agreement with this proposition as phenolics from pomegranate extract alleviated H₂O₂-induced cytotoxicity in HaCaT cells through reducing the production of cellular ROS.⁹ Similarly, Maplifa™ and GA reduced the production of MGO-induced total ROS, which may contribute to their overall cytoprotective effects in HaCaT cells. Maplifa™ and GA also increased the levels of specific mitochondria-derived ROS in MGO-treated cells, which seemed contradictory to the results from the measurement of total production of ROS. However, this effect may be justified by the fact that ROS plays complex dual roles in prooxidant and antioxidant pathways. Studies have shown that ROS can also serve as a stress signal that triggers various redox-sensitive signaling pathways, which may lead to protective functions against oxidative stress in microorganism.³¹ For instance, mitochondria produced ROS is crucial for *Caenorhabditis elegans* to maintain normal lifespan and increased ROS production even prolonged their lifespan.^{32,33} Therefore, it is possible that treatment of Maplifa™ and GA may boost mitochondria oxidative phosphorylation, and consequently trigger signaling pathways as a response to simulation by MGO in HaCaT cells. However, further investigations on the mechanisms of Maplifa™ and GA's protective effects against MGO-induced oxidative stress are warranted.

In summary, the cytoprotective effects of Maplifa™ and GA against H₂O₂-and MGO-induced oxidative stress in human keratinocytes were evaluated. Maplifa™ and GA ameliorated H₂O₂-and

MGO-induced cell death and cellular ROS production. Furthermore, the cytoprotective effects of Maplifa™ and GA were attributed to their anti-apoptotic activity by reducing the population of apoptotic cells and downregulating the levels of apoptosis related enzymes including caspases-3/7 and -8 in the H₂O₂-challenged cells. Maplifa™ and GA displayed distinct effects in the MGO-induced oxidative stress model as they diminished the total ROS production whilst increasing the level of mitochondria-derived ROS. Findings from this study support the potential skin beneficial effects of Maplifa™ and GA. To develop Maplifa™ and GA as bioactive ingredients for cosmeceutical and/or dermatological applications, further investigations on their mechanisms of action are warranted.

Acknowledgements

Data were acquired from instruments located at the University of Rhode Island in the RI-INBRE core facility obtained from Grant P20GM103430 from the National Center for Research Resources (NCRR), a component of the National Institutes of Health (NIH). C.L. was supported by a teaching assistantship from College of Pharmacy, the University of Rhode Island.

Declarations of interest:

HM and NPS are co-inventors on a patent application (International Publication Number: WO 2015/154074 A9) on the skin-whitening applications of maple gallotannins. The other authors declare no conflicts of interest.

REFERENCES

1. H. Cronin and Z. D. Draelos, Top 10 botanical ingredients in 2010 anti-aging creams, *J Cosmet Dermatol*, 2010, **9**, 218-225.
2. M. Iriti and F. Faoro, Grape phytochemicals: a bouquet of old and new nutraceuticals for human health, *Med Hypotheses*, 2006, **67**, 833-838.
3. R. H. Liu, Dietary bioactive compounds and their health implications, *Journal of food science*, 2013, **78**, A18-A25.
4. M. A. Farage, K. W. Miller, P. Elsner and H. I. Maibach, Intrinsic and extrinsic factors in skin ageing: a review, *Int J Cosmet Sci*, 2008, **30**, 87-95.
5. S. Radjei, B. Friguet, C. Nizard and I. Petropoulos, Prevention of dicarbonyl-mediated advanced glycation by glyoxalases: implication in skin aging, *Biochem Soc Trans*, 2014, **42**, 518-522.
6. P. Gkogkolou and M. Bohm, Advanced glycation end products: Key players in skin aging?, *Dermatoendocrinol*, 2012, **4**, 259-270.
7. A. Elostá, T. Ghous and N. Ahmed, Natural products as anti-glycation agents: possible therapeutic potential for diabetic complications, *Current diabetes reviews*, 2012, **8**, 92-108.
8. W. Liu, H. Ma, N. A. DaSilva, K. N. Rose, S. L. Johnson, L. Zhang, C. Wan, J. A. Dain and N. P. Seeram, Development of a neuroprotective potential algorithm for medicinal plants, *Neurochem Int*, 2016, **100**, 164-177.
9. C. Liu, H. Guo, N. A. DaSilva, D. Li, K. Zhang, Y. Wan, X.-H. Gao, H.-D. Chen, N. P. Seeram and H. Ma, Pomegranate (*Punica granatum*) phenolics ameliorate hydrogen peroxide-induced oxidative stress and cytotoxicity in human keratinocytes, *Journal of functional foods*, 2019, **54**, 559-567.
10. H. Ma, J. Xu, N. A. DaSilva, L. Wang, Z. Wei, L. Guo, S. L. Johnson, W. Lu, J. Xu, Q. Gu and N. P. Seeram, Cosmetic applications of glucitol-core containing gallotannins from a proprietary phenolic-enriched red maple (*Acer rubrum*) leaves extract: inhibition of melanogenesis via down-regulation of tyrosinase and melanogenic gene expression in B16F10 melanoma cells, *Arch Dermatol Res*, 2017, **309**, 265-274.

11. H. Ma, W. Liu, L. Frost, L. J. Kirschenbaum, J. A. Dain and N. P. Seeram, Glucitol-core containing gallotannins inhibit the formation of advanced glycation end-products mediated by their antioxidant potential, *Food Funct.*, 2016, **7**, 2213-2222.
12. C. Li and N. P. Seeram, Ultra-fast liquid chromatography coupled with electrospray ionization time-of-flight mass spectrometry for the rapid phenolic profiling of red maple (*Acer rubrum*) leaves, *Journal of separation science*, 2018, **41**, 2331-2346.
13. N. A. DaSilva, P. P. Nahar, H. Ma, A. Eid, Z. Wei, S. Meschwitz, N. H. Zawia, A. L. Slitt and N. P. Seeram, Pomegranate ellagitannin-gut microbial-derived metabolites, urolithins, inhibit neuroinflammation in vitro, *Nutr Neurosci*, 2019, **22**, 185-195.
14. J. J. Gille and H. Joenje, Cell culture models for oxidative stress: superoxide and hydrogen peroxide versus normobaric hyperoxia, *Mutat Res*, 1992, **275**, 405-414.
15. B. H. Kim, M. S. Choi, H. G. Lee, S. H. Lee, K. H. Noh, S. Kwon, A. J. Jeong, H. Lee, E. H. Yi, J. Y. Park, J. Lee, E. Y. Joo and S. K. Ye, Photoprotective potential of penta-o-galloyl-beta-dglucose by targeting NF-kappaB and MAPK signaling in UVB radiation-induced human dermal fibroblasts and mouse skin, *Mol Cells*, 2015, **38**, 982-990.
16. C. T. Yang, Y. Zhao, M. Xian, J. H. Li, Q. Dong, H. B. Bai, J. D. Xu and M. F. Zhang, A novel controllable hydrogen sulfide-releasing molecule protects human skin keratinocytes against methylglyoxal-induced injury and dysfunction, *Cell Physiol Biochem*, 2014, **34**, 1304-1317.
17. C. T. Yang, F. H. Meng, L. Chen, X. Li, L. J. Cen, Y. H. Wen, C. C. Li and H. Zhang, Inhibition of methylglyoxal-induced AGEs/RAGE expression contributes to dermal protection by N-Acetyl-L-Cysteine, *Cell Physiol Biochem*, 2017, **41**, 742-754.
18. M. Hardy, J. Zielonka, H. Karoui, A. Sikora, R. Michalski, R. Podsiadly, M. Lopez, J. Vasquez-Vivar, B. Kalyanaraman and O. Ouari, Detection and characterization of reactive oxygen and nitrogen species in biological systems by monitoring species-specific products, *Antioxid Redox Signal*, 2018, **28**, 1416-1432.

19. W. Bi, Y. Gao, J. Shen, C. He, H. Liu, Y. Peng, C. Zhang and P. Xiao, Traditional uses, phytochemistry, and pharmacology of the genus *Acer* (maple): A review, *J Ethnopharmacol*, 2016, **189**, 31-60.
20. W. Bi, C. N. He, X. X. Li, L. Y. Zhou, R. J. Liu, S. Zhang, G. Q. Li, Z. C. Chen and P. F. Zhang, Ginnalin A from Kujin tea (*Acer tataricum* subsp. *ginnala*) exhibits a colorectal cancer chemoprevention effect via activation of the Nrf2/HO-1 signaling pathway, *Food Funct*, 2018, **9**, 2809-2819.
21. R. Valenzuela, P. Illesca, F. Echeverria, A. Espinosa, M. A. Rincon-Cervera, M. Ortiz, M. C. Hernandez-Rodas, A. Valenzuela and L. A. Videla, Molecular adaptations underlying the beneficial effects of hydroxytyrosol in the pathogenic alterations induced by a high-fat diet in mouse liver: PPAR-alpha and Nrf2 activation, and NF-kappaB down-regulation, *Food Funct*, 2017, **8**, 1526-1537.
22. M. C. Hernandez-Rodas, R. Valenzuela, F. Echeverria, M. A. Rincon-Cervera, A. Espinosa, P. Illesca, P. Munoz, A. Corbari, N. Romero, D. Gonzalez-Manan and L. A. Videla, Supplementation with docosahexaenoic acid and extra virgin olive oil prevents liver steatosis induced by a high-fat diet in mice through PPAR-alpha and Nrf2 upregulation with concomitant SREBP-1c and NF-kB downregulation, *Mol Nutr Food Res*, 2017, **61**.
23. F. Echeverria, R. Valenzuela, A. Bustamante, D. Alvarez, M. Ortiz, A. Espinosa, P. Illesca, D. Gonzalez-Manan and L. A. Videla, High-fat diet induces mouse liver steatosis with a concomitant decline in energy metabolism: attenuation by eicosapentaenoic acid (EPA) or hydroxytyrosol (HT) supplementation and the additive effects upon EPA and HT co-administration, *Food Funct*, 2019, **10**, 6170-6183.
24. J. Li and J. Yuan, Caspases in apoptosis and beyond, *Oncogene*, 2008, **27**, 6194-6206.
25. P. Schneider and J. Tschopp, in *Pharmacochemistry Library*, Elsevier, 2000, vol. 31, pp. 281-286.
26. L. A. Sitailo, S. S. Tibudan and M. F. Denning, Activation of caspase-9 is required for UV-induced apoptosis of human keratinocytes, *Journal of Biological Chemistry*, 2002, **277**, 19346-19352.

27. H. R. Rezvani, F. Mazurier, M. Cario-Andre, C. Pain, C. Ged, A. Taieb and H. de Verneuil, Protective effects of catalase overexpression on UVB-induced apoptosis in normal human keratinocytes, *J Biol Chem*, 2006, **281**, 17999-18007.
28. H. Masaki, Role of antioxidants in the skin: anti-aging effects, *J Dermatol Sci*, 2010, **58**, 85-90.
29. L. A. Pacheco-Palencia, G. Noratto, L. Hingorani, S. T. Talcott and S. U. Mertens-Talcott, Protective effects of standardized pomegranate (*Punica granatum* L.) polyphenolic extract in ultraviolet-irradiated human skin fibroblasts, *J Agric Food Chem*, 2008, **56**, 8434-8441.
30. A. Svobodova, J. Psotova and D. Walterova, Natural phenolics in the prevention of UV-induced skin damage. A review, *Biomed Pap Med Fac Univ Palacky Olomouc Czech Repub*, 2003, **147**, 137-145.
31. A. L. Santos, S. Sinha and A. B. Lindner, The good, the bad, and the ugly of ROS: New insights on aging and aging-related diseases from eukaryotic and prokaryotic model organisms, *Oxid Med Cell Longev*, 2018, **2018**, 1941285.
32. R. Doonan, J. J. McElwee, F. Matthijssens, G. A. Walker, K. Houthoofd, P. Back, A. Matscheski, J. R. Vanfleteren and D. Gems, Against the oxidative damage theory of aging: superoxide dismutases protect against oxidative stress but have little or no effect on life span in *Caenorhabditis elegans*, *Genes & development*, 2008, **22**, 3236-3241.
33. C. T. Murphy, S. A. McCarroll, C. I. Bargmann, A. Fraser, R. S. Kamath, J. Ahringer, H. Li and C. Kenyon, Genes that act downstream of DAF-16 to influence the lifespan of *Caenorhabditis elegans*, *Nature*, 2003, **424**, 277-283.

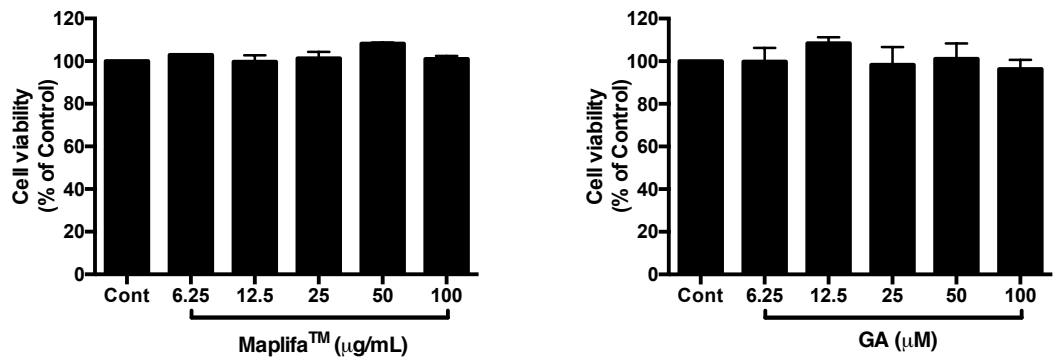


Fig. 1 Effect of Maplifa[™] and GA on viability of HaCaT cells. HaCaT cells were treated with (A) Maplifa[™] (12.5, 25, 50, and 100 µg/mL) or (B) GA (12.5, 25, 50, and 100 µM) for 24 h. Cell viabilities were measured using CTG2.0 assay.

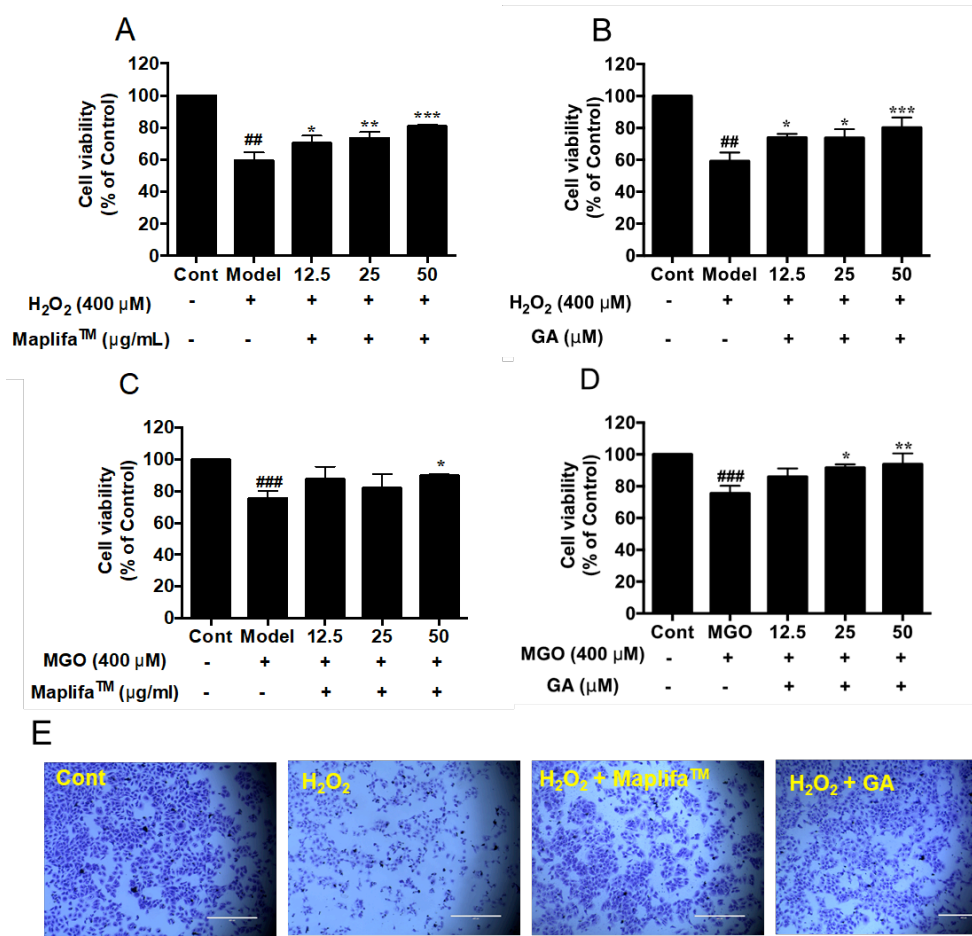


Fig. 2 Effects of Maplifa[™] and GA on the viability of HaCaT cells insulted with H₂O₂ or MGO. (A and C) Maplifa[™] (12.5, 25, and 50 µg/mL) or (B and D) GA (12.5, 25, and 50 µM) was incubated with HaCaT cells for 12 h. Then cells were insulted with H₂O₂ (400 µM) or MGO (400 µM) and further incubated for 24 h. (E) Representative microscopic images of H₂O₂-insulted HaCaT cells treated with Maplifa[™] or GA. HaCaT cells were stained with crystal violet. ^{##}*p* < 0.01 and ^{###}*p* < 0.001 as compared with control group; ^{*}*p* < 0.05, ^{**}*p* < 0.01, and ^{***}*p* < 0.001 as compared with model group.

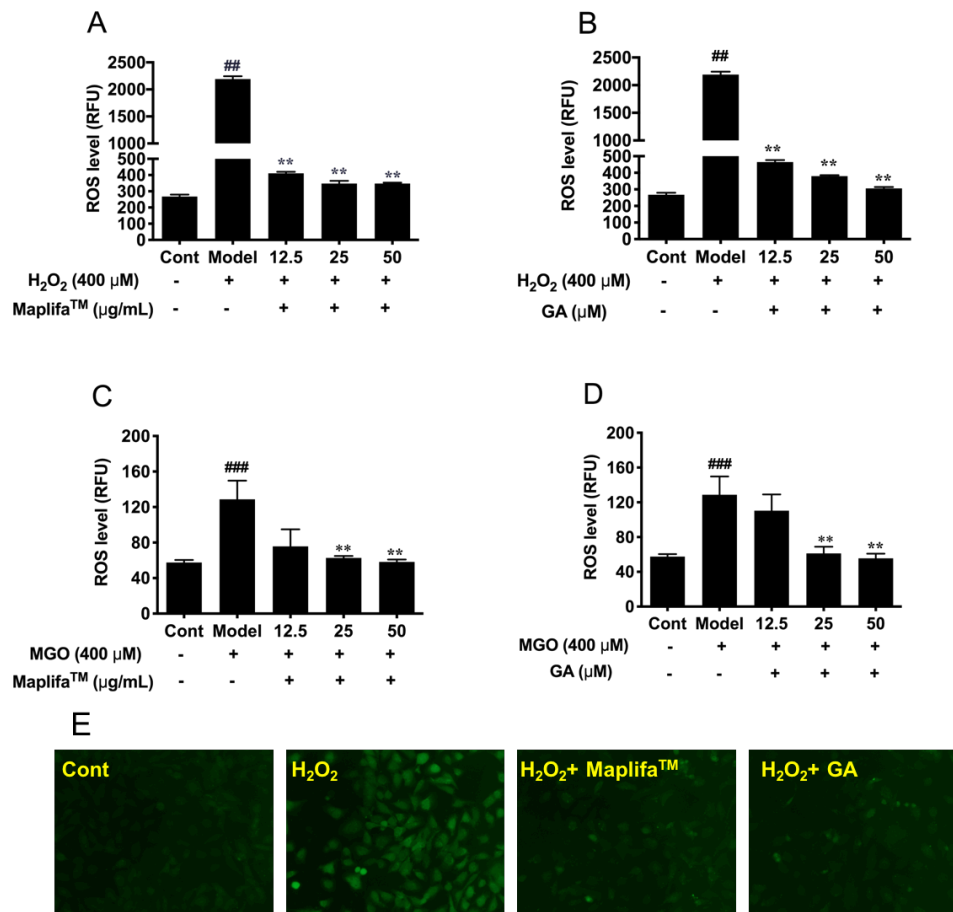


Fig. 3 Effects of Maplifa™ and GA on the H₂O₂- and MGO-induced ROS production. Cells were treated with (A and C) Maplifa™ (12.5, 25, and 50 μg/mL) for 12 h or (B and D) GA (12.5, 25, and 50 μM) for 2 h. Then cells were incubated with DMEM containing DCFDA (20 μM) for 20 mins, followed by exposure of H₂O₂ or MGO (both at 400 μM) for 1 h or 24 h, respectively. ROS level was measured by cellular fluorescence intensity with excitation and emission wavelengths of 485 and 525 nm, respectively. (E) Representative fluorescent images of H₂O₂- and MGO-insulted HaCaT cells treated with Maplifa™ or GA. ^{##}*p* < 0.01 and ^{###}*p* < 0.001 as compared with control group; ^{**}*p* < 0.01 as compared with model group.

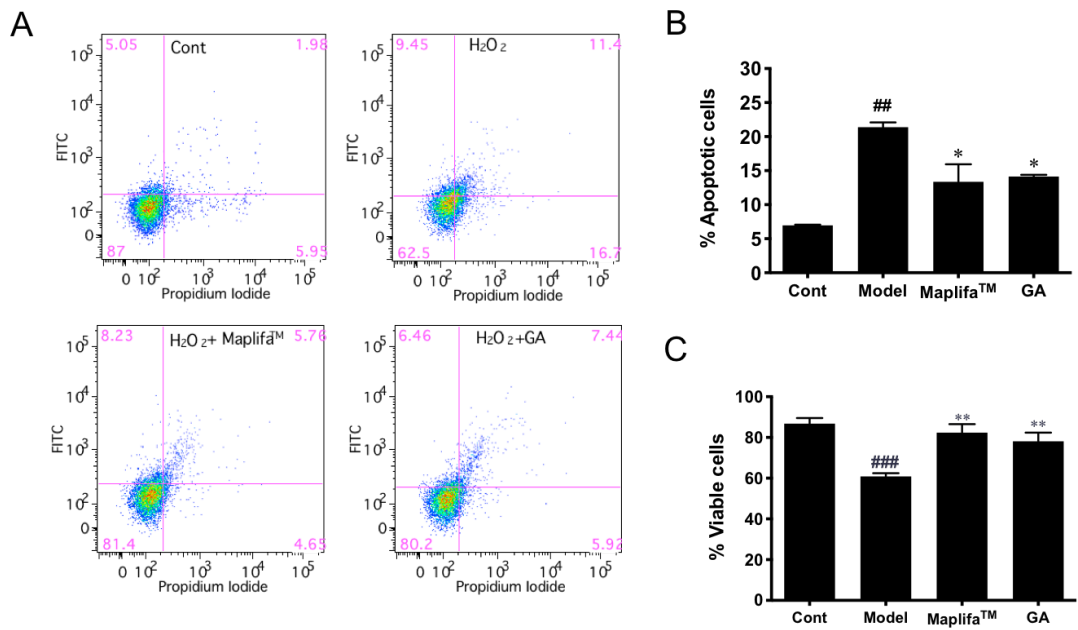


Fig. 4 Effects of Maplifa™ and GA on H₂O₂-induced apoptosis in HaCaT cells. (A) HaCaT cells stained with annexin V-FITC/PI and assayed by flow cytometry. The flow cytometry graphs show the population of cells from one representative values of three separate experiments. (B-C) Graphs showing apoptotic cell populations (annexin V+/PI- and annexin V+/PI+) (B) and viable cell populations (annexin V-/PI-) (C) of HaCaT cells with or without treatments of Maplifa™ and GA were quantified by gated patterns in double stains. ^{##}*p* < 0.01 as compared with control group; ^{*}*p* < 0.05 as compared with model group.

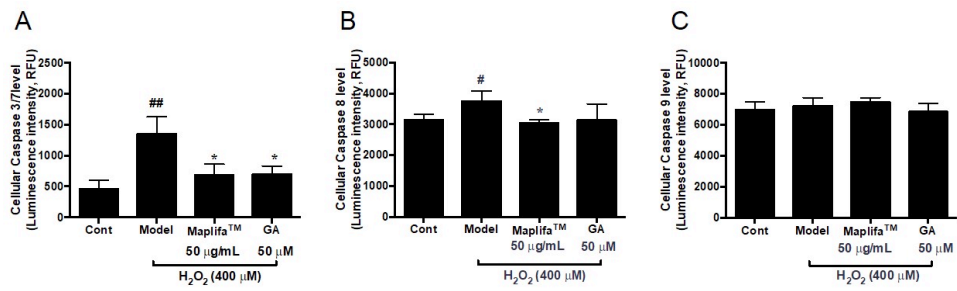


Fig. 5 Effects of MaplifaTM and GA on (A) cellular caspase-3/7, (B) caspase-8, and (C) caspase-9 in HaCaT cells exposed to H₂O₂. HaCaT cells were incubated with MaplifaTM (50 μg/mL) and GA (50 μM) for 12 h before H₂O₂ induction. [#]*p* < 0.05 and ^{##}*p* < 0.01 as compared with control group; ^{*}*p* < 0.05 as compared with model group.

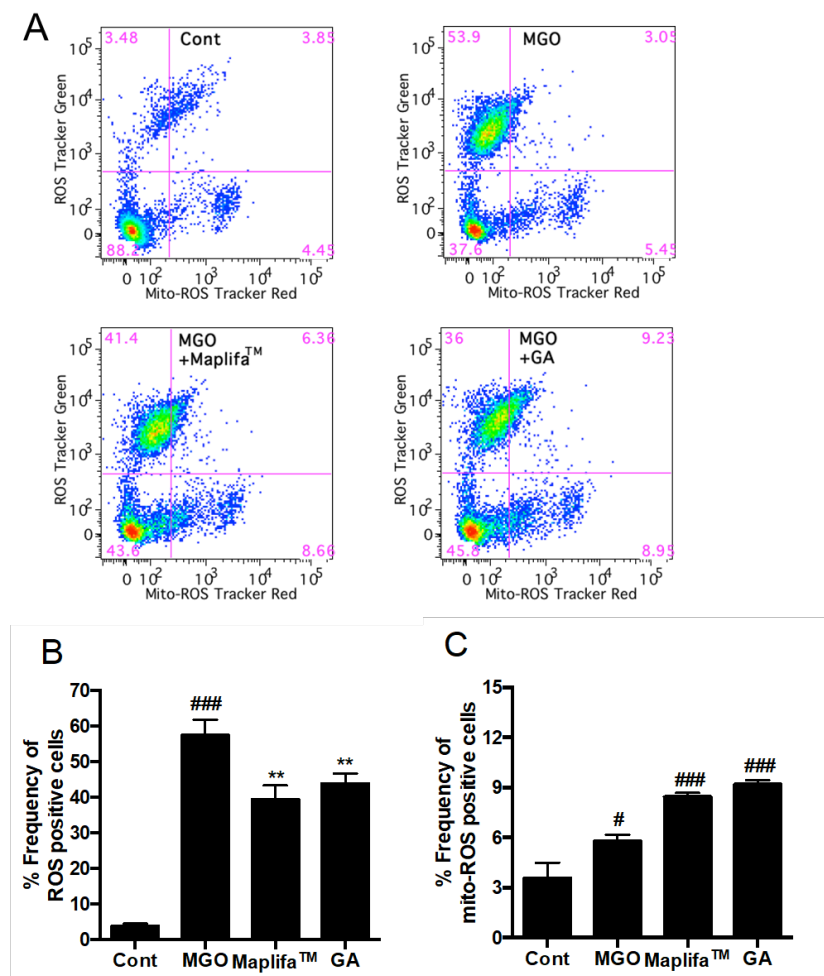


Fig. 6 Effects of Maplifa[™] and GA on MGO-induced production of mitochondria-derived ROS. HaCaT cells were treated with Maplifa[™] (50 µg/mL) or GA (50 µM) for 2 h, followed by exposure of MGO (400 µM) for 24 h. Next, the cells were incubated with 20 µM DCFDA for 20 mins. After the cells were washed, 5 µM MitoSOX[™] reagent working solution was added and incubated for 10 mins and the cells were assayed by flow cytometry (A). The frequency of ROS positive cells (B) and frequency of mitochondria-derived ROS positive cells were quantified (C) with FlowJo. # $p < 0.05$ and ### $p < 0.001$ as compared with control; ** $p < 0.01$ as compared with model group.

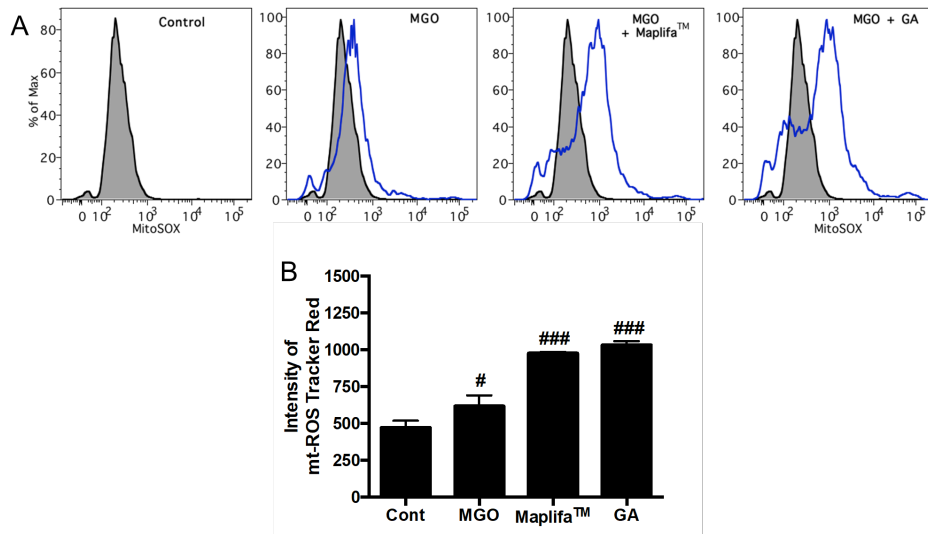


Fig. 7 Effects of Maplifa[™] and GA on MGO-induced production of mitochondria-derived ROS. HaCaT cells were treated with Maplifa[™] (50 µg/mL) or GA (50 µM) for 2 h, followed by exposure of MGO (400 µM) for 24 h. Next, the cells were incubated with 5 µM MitoSOX[™] reagent working solution for 10 mins and assayed by flow cytometry (**A**). Intensity of mitochondria-derived ROS measured by Tracker Red were quantified with FlowJo (**B**). #*p* < 0.05 and ###*p* < 0.001 as compared with control group.

CHAPTER 3

MANUSCRIPT 3

Published: 16 April 2020

DERMATOLOGIC THERAPY, 2020;33: e13426

Phenolic-Enriched Maple Syrup Extract Protects Human Keratinocytes against Hydrogen Peroxide and Methylglyoxal Induced Cytotoxicity

Running title: Protective Effects of MSX on Keratinocytes

Jie Sheng^{1,2,3} M.D., Chang Liu² M.S., Sophia Petrovas², Yinsheng Wan^{3,4} Ph.D., Hong-Duo Chen⁴ M.D., Navindra P. Seeram² Ph.D., Hang Ma² Ph.D.

¹Department of Anesthesiology, The First Hospital of China Medical University, Shenyang, 110001 China

²Bioactive Botanical Research Laboratory, Department of Biomedical and Pharmaceutical Sciences, College of Pharmacy, University of Rhode Island, Kingston, RI 02881, USA

³Department of Biology, Providence College, RI 02881, USA

⁴Department of Dermatology, The First Hospital of China Medical University, Shenyang, 110001, China

Email:

Jie Sheng, M.D., Email: shengjie27@126.com

Chang Liu, M.S., Email: hichang813@uri.edu

Sophia Petrovas, Email: sophiapetro@cox.net

Yin-Sheng Wan, Ph.D., Email: yswan@providence.edu

Hong-Duo Chen, M.D., Email: hongduochen@hotmail.com

Navindra P. Seeram, Ph.D., Email: nseeram@uri.edu

Hang Ma, Ph.D., Email: hang_ma@uri.edu

Co-corresponding authors:

Navindra P. Seeram, Ph.D. Tel: +1-401-874-9367; Email: nseeram@uri.edu

Hang Ma, Ph.D.; Tel: +1-401-874-7654; Email: hang_ma@uri.edu

Avedisian Hall, College of Pharmacy, The University of Rhode Island

7 Greenhouse Road, Kingston, RI 02881, USA

Words count: 4324

For abstract: 199

For the text: 2575

Figure count:3

Table count:0

Conflicting Interest: None

Abstract

Introduction: Reactive carbonyl species including methylglyoxal (MGO) are oxidation metabolites of glucose and precursors of advanced glycation end products (AGEs). They are important mediators of cellular oxidative stress and exacerbate skin complications. Published data supports that certain phenolic compounds can exert cellular protective effects by their antioxidant activity. A phenolic-enriched maple syrup extract (MSX) was previously reported to show protective effects against AGEs- and MGO-induced cytotoxicity in human colon cells but its skin protective effects remain unknown.

Objective: The protective effects of MSX were evaluated against hydrogen peroxide (H₂O₂)- and MGO-induced cytotoxicity in human keratinocytes (HaCaT cells). **Methods:** Cellular viability and antioxidant activity were evaluated by the luminescent cell viability CellTiter-Glo[®] assay and the reactive oxygen species (ROS) assay, respectively. A single-cell gel electrophoresis (Comet assay) was used to measure the strand breaks in the DNA of HaCaT cells. **Results:** MSX (at 50 µg/mL) ameliorated H₂O₂- and MGO-induced cytotoxicity by increasing cell viability by 21.5 and 25.9%, respectively. MSX reduced H₂O₂- and MGO-induced ROS production by 69.4 and 56.6%, respectively. MSX also reduced MGO-induced DNA damage by 47.5%. **Conclusion:** MSX showed protective effects against H₂O₂- and MGO-induced cytotoxicity in HaCaT cells supporting its potential for dermatological and/or cosmeceutical applications.

Key words: Maple syrup extract; phenolics, methylglyoxal; keratinocytes; antioxidant; DNA integrity

1 INTRODUCTION

Skin aging and skin complications associated with many systemic disorders such as diabetes are linked to the accumulation of a group of proteins known as advanced glycation endproducts (AGEs) (Ahmed, 2005; Gkogkolou & Böhm, 2012). The formation of AGEs is a non-enzymatic process in which reducing sugar molecules e.g. glucose, interact with free amino acids of biological macromolecules including protein, DNA, and lipids to form covalent-bond Maillard reaction products. This Maillard reaction leads to the generation of a group of unstable compounds known as Schiff bases (aldehyde- or ketone-like chemicals in which the carbonyl moiety is replaced by an imine or azomethine group), which can further undergo a series of chemical rearrangements to form stable keto-amine adducts known as Amadori products. Both Schiff bases and Amadori products react with amino acids of proteins to form cross-linked protein complexes and undergo multi-step reactions including oxidation, dehydration, and polymerization to form late stage AGEs. During the formation of AGEs, glucose and Amadori products are oxidized to generate highly reactive dicarbonyl chemicals including 3-deoxyglucosone (3-DG), glyoxal (GO), and methylglyoxal (MGO) (Desai & Wu, 2007). These reactive dicarbonyl species (RCS) are regarded as metabolites of sugar molecules and are known to exacerbate the formation of AGEs. As the precursors of AGEs, RCS can induce intracellular oxidative stress and cause damage to human dermal cells including fibroblasts and keratinocytes, which can further lead to accelerated skin aging (Roberts, Wondrak, Laurean, Jacobson, & Jacobson, 2003). Therefore, AGEs inhibitors have immense potential for the management of skin complications including those associated with diabetes mellitus (Ahmed, 2005). Considerable research efforts have been directed towards the development of AGEs inhibitors for the treatment of AGE-mediated skin complications associated with diabetes mellitus (Rahbar, Kumar Yernini, Scott, Gonzales, & Lalezari, 1999). Several synthetic chemicals, including aminoguanidine, are promising AGEs inhibitors but many have failed drug approval due to their adverse effect profile (Abdel-Rahman & Kline Bolton, 2002; Nilsson, 1999). Conversely, natural products, including several food-derived phenolic compounds (e.g. curcumin, epigallocatechin gallate, and flavonoids including kaempferol, luteolin, quercetin, naringenin, and rutin) are generally regarded as safe and have been reported to inhibit AGEs formation (Wu, Huang, Lin, & Yen, 2011; Wu & Yen, 2005). In addition, a growing body of data suggests that these phenolic

AGE-inhibitors can exert protective effects on keratinocytes by reducing cellular oxidative stress (Babu, Sabitha, & Shyamaladevi, 2006; Huang et al., 2007).

Our laboratory has initiated a research program focused on the identification of AGE inhibitors from several medicinal plants and functional foods (foods that provide health benefits in addition to macro- and micronutrients) (Liu et al., 2014, 2017; Liu et al., 2016; Ma et al., 2016; Ma et al., 2018, 2015; Sun et al., 2016; Zhang, Ma, Liu, Yuan, & Seeram, 2015). Among these natural products, we reported that phenolic-enriched extracts of pomegranate fruit (*Punica granatum*) and red maple leaves (*Acer rubrum*) showed potent inhibitory effects against AGEs formation and protected human keratinocytes against oxidative stress induced cytotoxicity (Liu et al., 2014; Ma et al., 2016; Liu et al., 2019). In addition, we also reported that a polyphenol-enriched maple syrup extract (MSX) showed inhibitory activity against AGEs formation and protective effects against AGEs- and MGO-induced cytotoxicity in normal human colon cells (Liu et al., 2017). MSX has also been reported to show a diverse range of biological activities including antioxidant, anti-diabetic, anti-inflammatory and anti-neuroinflammatory effects (Liu et al., 2017; Ma et al., 2016; Nahar, Driscoll, Li, Slitt, & Seeram, 2014; Zhang et al., 2014) but its skin protective effects in human keratinocytes remain unknown. Herein, we evaluated the protective effects of MSX against hydrogen peroxide (H₂O₂)- and MGO-induced cytotoxicity, as well as its antioxidant and cellular DNA protection activities in human keratinocytes (HaCaT cells).

2 MATERIALS AND METHODS

2.1 Materials

A standardized food grade phenolic-enriched maple syrup extract (MSX), which contains over 90% of phenolic compounds (determined by High-performance liquid chromatography, liquid chromatography-mass spectrometry, and nuclear magnetic resonance methods), was prepared in our laboratory as previously reported (Li & Seeram, 2010, 2011; Liu, Ma, & Seeram, 2016; Zhang et al., 2014). Our previous phytochemical characterization studies of MSX led to the isolation and identification of several phenolic sub-classes including lignans, gallic acid derivatives and other phenolic acids, coumarins, and stilbenes (Zhang et al., 2014). However, lignans are the major type of phenolics present in MSX. Other minor constituents in MSX include ash (ca. 2.21%), fiber (ca. 11%),

minerals (ca. 788.6 mg/100g), amino acids (ca. 31.7 mg/100g), organic acids (ca. 796.9 mg/100g), and vitamins (ca. 16670.7 mg/100g) (Zhang et al., 2014). Methylglyoxal (MGO), hydrogen peroxide (H₂O₂), crystal violet staining agent, trypsin solution, dimethyl sulfoxide (DMSO), and 2',7'-dichlorofluorescein diacetate (DCFDA) were purchased from Sigma-Aldrich (St. Louis, MO, USA). Dulbecco's modified Eagle's medium (DMEM) and fetal bovine serum (FBS) were purchased from Gibco BRL (Ground Island, NY, USA). A luminescent cell viability CellTiter-Glo[®] (CTG 2.0 assay) kit was purchased from Promega (Fitchburg, WI, USA). Comet assay kit was purchased from TREVIGEN (Gaithersburg, MD, USA).

2.2 Cell culture and cell viability

Human keratinocytes (HaCaT cells) were obtained from American Type Culture Collection (Manassas, VA, USA). HaCaT cells were maintained in DMEM supplemented with 5% FBS at 37 °C under an atmosphere of 5% CO₂. Cellular viability was assessed using the luminescent cell viability CellTiter-Glo[®] (CTG 2.0 assay). Briefly, HaCaT cells were seeded at 5×10⁴ cells/mL to 50-60% confluency in a 96-well microplate. HaCaT cells were exposed to the test compounds at different concentrations (6.25 – 100 µg/mL) for 24 h. Then the CTG 2.0 agent was added in a 1:1 ratio with existing media and mixed for 5 min on an orbital shaker prior to luminescence measurement using a plate reader (Spectramax M2, Molecular Devices, Sunnyvale, CA, USA).

2.3 Effect of MSX on H₂O₂ or MGO induced cell toxicity

HaCaT cells were seeded at 5×10⁴ cells/mL to 60% confluency in a 96-well microplate. After 12 h incubation, cells were pre-treated with different concentrations of MSX (12.5, 25, and 50 µg/mL) for 2 h. Cells were washed with PBS twice and treated with H₂O₂ (400 µM) or MGO (400 µM) and then cell viability was determined using the CTG 2.0 assay.

2.5 Crystal violet staining

Crystal violet staining solution was prepared by dissolving 5 g of crystal violet powder into 100 mL 20% aqueous ethanol. HaCaT cells seeded at 25×10⁴ cells/mL to 80% confluency in 6-well plates. Cells were fixed with 75% ethanol for 15 min at room temperature and incubated with staining solution for 10 min, followed by washing with PBS for 5 times. Images were captured with a fluorescence microscope cells imaging system (EVOS; Invitrogen, Waltham, MA, USA).

2.6 Reactive oxygen species (ROS) assay

HaCaT cells were seeded at 5×10^4 cells/mL to 50-60% confluency in a 96-well microplate. After 12 h incubation, cells were pre-treated with MSX (12.5, 25, and 50 $\mu\text{g/mL}$) for 2 h and medium was replaced with fresh medium containing DCFDA (20 μM). Then cells were treated with H_2O_2 (400 μM) or MGO (400 μM) for 24 h. The fluorescence signals were read at excitation and emission wavelengths of 485 and 525 nm, respectively, using a plate reader (Spectra Max M2 spectrometer, Molecular Devices, Sunnyvale, CA, USA).

2.7 Comet assay

Comet assay, a single-cell gel electrophoresis that is used to measure the strand breaks in the DNA of HaCaT cells, was performed according to the instructions of the manufacturers (Trevigen, Gaithersburg, MD, USA). Briefly, HaCaT cells were seeded at about 5×10^4 cells/mL to yield 70-90% confluence in a 6-well plate. Cells were pre-treated with MSX (50 $\mu\text{g/mL}$) for 2 h and then washed with PBS twice followed by treatment of H_2O_2 (400 μM) or MGO (400 μM) for 24h. Cells were then collected and combined with melted LMAgarose (a 1% low melting agarose in PBS that is designed for the Comet assay) at a ratio of 1:10 (v/v). Then the respective suspensions were transferred onto comet slides and incubated with cell lysis at 4 °C for 12 h. The slides were immersed into alkaline unwinding solution for 20 min and subjected to electrophoresis in an alkaline electrophoresis solution at 21 volts for 30 min. Slides were fixed in 75% ethanol and stained in diluted SYBR GOLD solution (1:3000). SYBR GOLD is a cyanine dye that exhibits higher binding affinity to nucleic acids including double- or single-stranded DNA. Comet images were captured with EVOS fluorescence microscope and the percentage of tailed cell DNA were analyzed with CASP software program (Końca et al., 1981).

2.8 Statistical analysis

All data was expressed as the mean \pm the standard error of the mean (S.E.M.). The significance of differences was determined using a two-way analysis of variance (ANOVA) followed by a post hoc Student-Newman-Keuls multiple comparison test (SNK). A threshold of p value < 0.05 was considered the cut-off for statistical significance of results.

3 RESULTS AND DISCUSSION

3.1 MSX ameliorates H_2O_2 - and MGO-induced cytotoxicity

Reactive carbonyl species exacerbate cellular oxidative stress and suppress cell viability (Desai & Wu, 2007). Therefore, we first evaluated whether MSX can reduce H₂O₂- and MGO-induced toxicity in HaCaT cells. As shown in Figure 1 A, MSX at concentrations ranging from 6.25 – 100 µg/mL did not affect cell viability of HaCaT cells (viability > 98.0%), and concentrations of 12.5, 25, and 50 µg/mL were selected for further evaluations. Both H₂O₂ and MGO (at 400 µM) significantly induced cytotoxicity by reducing cell viability by 59.2 and 61.7%, respectively. Treatment of MSX (12.5, 25, and 50 µg/mL) increased the viability of cells exposed to H₂O₂ by 11.0, 14.1, and 21.5%, respectively, as compared to the model (H₂O₂-treated) group (Figure 1 B). MSX also reduced MGO-induced cytotoxicity by increasing cell viability by 25.9% at concentration of 50 µg/mL (Figure 1 C). This protective effect was further supported by data obtained from crystal violet staining assay. Treatment of MSX maintained the normal shape of cell nuclei, as compared to H₂O₂ and MGO challenged cells, which had irregular shaped nuclei (Figure 1 D). This finding is in agreement with our previously reported study showing that phenolics from a commercially available standardized pomegranate fruit extract (Pomella[®]) attenuated H₂O₂-induced cytotoxicity in HaCaT cells (Liu et al., 2019).

3.2 MSX reduces H₂O₂- and MGO-induced cellular reactive oxygen species (ROS)

Hydrogen peroxide (H₂O₂) and MGO induce cytotoxicity in HaCaT cells by mediating the production of cellular reactive oxygen species (ROS) (Roberts et al., 2003). Levels of ROS in HaCaT cells were elevated by 8.18- and 2.24-fold when cells were stimulated by H₂O₂ (200 µM) and MGO (400 µM), respectively, as compared to the control group. Treatment of MSX reduced the production of ROS in cells exposed to H₂O₂ and MGO in a concentration dependent manner. MSX (12.5, 25, and 50 µg/mL) reduced H₂O₂- and MGO-induced ROS production by 44.4, 59.0, and 69.4%, and 34.9, 51.3, and 56.6%, respectively, as compared to the model group (Figure 2). This is in agreement with our previously reported studies showing that MSX exerts cytoprotective effects by attenuating cellular ROS in normal human colon CCD-18Co cells (Liu et al., 2017) and murine microglial BV-2 cells (Ma, et al., 2016).

3.3 MSX maintains MGO-induced cellular DNA damage

Reported studies suggested that MGO can bind to nucleotides and induce DNA chain fracture in human skin cells (Roberts et al., 2003). The protective effects of MSX against H₂O₂- and MGO-induced DNA damage were evaluated in the Comet assay. As shown in Figure 3 A, MGO (400 μM) significantly increased the levels of fractured DNA chain in HaCaT cells (by 73.9%) and the treatment of MSX (50 μM) maintained the integrity of DNA structures in HaCaT cells with a lower percentage of tailed DNA (47.5%; Figure 3 A lower panel). Treatment of H₂O₂ (400 μM) did not result in DNA damage in HaCaT cells as shown in the comet assay (Figure 3 B), suggesting that different mechanism(s) are involved in the oxidative stress induced cell damage. This difference was in agreement with our previously reported observation where H₂O₂ induced cell apoptosis (Liu et al., 2019) while MGO did not show apoptotic effects in HaCaT cells (data not shown). Although several synthetic small molecules including penicillamine (Roberts et al., 2003) and N-acetylcysteine (Yang et al., 2014) are reported to show protective effects, to the best of our knowledge, this is the first report showing that a polyphenol-enriched natural product extract protects the integrity of DNA in HaCaT cells from MGO induced damage.

TRANSLATIONAL THERAPEUTIC IMPLICATIONS OF OUR RESEARCH

A growing body of basic pharmacological research support the utilization of several natural polyphenols to combat AGEs-mediated dermatological dysfunctions and skin disorders induced by oxidative stress (Ho & Wang, 2013; Jeanmaire, Danoux, & Pauly, 2001). Several of these polyphenols are found in plant based-diets including in fruits, vegetables, grains, and plant-derived beverages (Khan, Liu, Wang, & Sun, 2020). Therefore, because of their inherent lack of toxicity and natural origin, these polyphenols show great promise for preventive and therapeutic effects against skin aging, skin damage and cutaneous toxicity, including ulcer, burns, and wounds (Działo et al., 2016). Moreover, several clinical studies support the skin protective effects of polyphenols and their dermatological applications (Gianeti, Mercurio, & Maia Campos, 2013; Mirnezami, Jafarimanesh, Rezagholizamenjany, Alimoradian, & Ranjbaran, 2020; Palmer & Kitchin, 2010). The skin protective effects of dietary polyphenols as well as their therapeutic potential for the treatment of skin disorders have been reviewed in several articles (Daniyal et al., 2019; Działo et al., 2016; Svobodová, Psotová, & Walterová, 2003; Zillich, Schweiggert-Weisz, Eisner, & Kerscher, 2015). For instance, the skin protective effects of

honey, a natural sweetener, has been supported by empirical evidence and modern scientific studies (Bogdanov, Jurendic, Sieber, & Gallmann, 2008; Saranraj & Sivasakthi, 2018). Published data suggest that honey is suitable as a remedy for skin conditions including wounds and burns (Burlando & Cornara, 2013; McLoone, Warnock, & Fyfe, 2016). Apart from bioactives including amino acids, vitamins, minerals, and phenolics, some honey, for e.g. Manuka honey, has been reported to contain MGO, which partially contributes to its antimicrobial activity (Alvarez-Suarez, Gasparrini, Forbes-Hernández, Mazzoni, & Giampieri, 2014). To date, the skin protective effects of maple syrup, a plant derived natural sweetener, are unknown. Therefore, we evaluated the cytoprotective effects of a phenolic-enriched maple syrup extract (MSX) on human keratinocytes HaCaT cells against oxidative and glycolytic stress induced cytotoxicity. MSX at non-toxic concentrations (ranging from 6.25 – 100 µg/mL) reduced H₂O₂- and MGO-induced cytotoxicity and production of ROS in HaCaT cells. Results from the Comet assay showed that MSX can protect the integrity of DNA of HaCaT cells from MGO-induced DNA damage. It is possible that the protective effects of MSX in skin cells are involved with several molecular pathways, such as activation of extracellular signal-regulated kinases (ERK) 1/2 phosphorylation, which was observed in our previously reported study (Liu et al., 2017). Further studies on the underlying mechanism(s) of the skin protective effects of MSX are warranted. In summary, the findings from the current study support the protective effects of MSX in keratinocytes and its potential for dermatological and/or cosmeceutical applications.

ACKNOWLEDGMENTS

Data were acquired from instruments located in the RI-INBRE core facility (at the University of Rhode) supported by Grant P20GM103430 from the National Center for Research Resources (NCRR), a component of the National Institutes of Health (NIH).

Conflict of interest

The authors declare no potential conflict of interest.

Abbreviation

MGO: methylglyoxal; AGEs: advanced glycation end products; MSX: maple syrup extract; ROS: reactive oxygen species; RCS: reactive dicarbonyl species; FBS: fetal bovine serum; DCFDA: 2',7'-dichlorofluorescein diacetate; DMEM: Dulbecco's modified Eagle's medium; CTG: CellTiter-Glo[®]

References

- Abdel-Rahman, E., & Kline Bolton, W. (2002). Pimagedine: A novel therapy for diabetic nephropathy. *Expert Opinion on Investigational Drugs*. <https://doi.org/10.1517/13543784.11.4.565>
- Ahmed, N. (2005). Advanced glycation endproducts - Role in pathology of diabetic complications. *Diabetes Research and Clinical Practice*. <https://doi.org/10.1016/j.diabres.2004.09.004>
- Alvarez-Suarez, J., Gasparrini, M., Forbes-Hernández, T., Mazzoni, L., & Giampieri, F. (2014). The composition and biological activity of honey: A focus on Manuka honey. *Foods*. <https://doi.org/10.3390/foods3030420>
- Babu, P. V. A., Sabitha, K. E., & Shyamaladevi, C. S. (2006). Therapeutic effect of green tea extract on advanced glycation and cross-linking of collagen in the aorta of streptozotocin diabetic rats. *Clinical and Experimental Pharmacology and Physiology*. <https://doi.org/10.1111/j.1440-1681.2006.04374.x>
- Bogdanov, S., Jurendic, T., Sieber, R., & Gallmann, P. (2008). Honey for nutrition and health: A review. *Journal of the American College of Nutrition*. <https://doi.org/10.1080/07315724.2008.10719745>
- Burlando, B., & Cornara, L. (2013). Honey in dermatology and skin care: A review. *Journal of Cosmetic Dermatology*. <https://doi.org/10.1111/jocd.12058>
- Daniyal, M., Akram, M., Zainab, R., Munir, N., Shah, S. M. A., Liu, B., ... Jabeen, F. (2019). Progress and prospects in the management of psoriasis and developments in phyto-therapeutic modalities. *Dermatologic Therapy*. <https://doi.org/10.1111/dth.12866>
- Desai, K., & Wu, L. (2007). Methylglyoxal and advanced glycation endproducts: New therapeutic horizons? *Recent Patents on Cardiovascular Drug Discovery*. <https://doi.org/10.2174/157489007780832498>
- Działo, M., Mierziak, J., Korzun, U., Preisner, M., Szopa, J., & Kulma, A. (2016). The potential of plant phenolics in prevention and therapy of skin disorders. *International Journal of Molecular Sciences*. <https://doi.org/10.3390/ijms17020160>
- Gianeti, M. D., Mercurio, D. G., & Maia Campos, P. M. B. G. (2013). The use of green tea extract in cosmetic formulations: Not only an antioxidant active ingredient. *Dermatologic Therapy*. <https://doi.org/10.1111/j.1529-8019.2013.01552.x>
- Gkogkolou, P., & Böhm, M. (2012). Advanced glycation end products: Keyplayers in skin aging? *Dermato-Endocrinology*. <https://doi.org/10.4161/derm.22028>
- Ho, C. T., & Wang, M. (2013). Dietary phenolics as reactive carbonyl scavengers: Potential impact on human health and mechanism of action. *Journal of Traditional and Complementary Medicine*. <https://doi.org/10.4103/2225-4110.114892>

- Huang, C. C., Wu, W. Bin, Fang, J. Y., Chiang, H. S., Chen, S. K., Chen, B. H., ... Hung, C. F. (2007). (-)-Epicatechin-3-gallate, a green tea polyphenol is a potent agent against UVB-induced damage in HaCaT keratinocytes. *Molecules*. <https://doi.org/10.3390/12081845>
- Jeanmaire, C., Danoux, L., & Pauly, G. (2001). Glycation during human dermal intrinsic and actinic ageing: An in vivo and in vitro model study. *British Journal of Dermatology*. <https://doi.org/10.1046/j.1365-2133.2001.04275.x>
- Khan, M., Liu, H., Wang, J., & Sun, B. (2020). Inhibitory effect of phenolic compounds and plant extracts on the formation of advance glycation end products: A comprehensive review. *Food Research International*. <https://doi.org/10.1016/j.foodres.2019.108933>
- Końca, Krzysztof, Anna Lankoff, Anna Banasik, Halina Lisowska, Tomasz Kuszewski, Stanisław Gózdź, Zbigniew Koza, and A. W. (1981). A cross-platform public domain PC image-analysis program for the comet assay. *Profesional Psychology*. https://doi.org/10.1163/_q3_SIM_00374
- Li, L., & Seeram, N. P. (2010). Maple syrup phytochemicals include lignans, coumarins, a stilbene, and other previously unreported antioxidant phenolic compounds. *Journal of Agricultural and Food Chemistry*. <https://doi.org/10.1021/jf1033398>
- Li, L., & Seeram, N. P. (2011). Further investigation into maple syrup yields 3 new lignans, a new phenylpropanoid, and 26 other phytochemicals. In *Journal of Agricultural and Food Chemistry*. <https://doi.org/10.1021/jf2011613>
- Liu, C., Guo, H., DaSilva, N. A., Li, D., Zhang, K., Wan, Y., ... Ma, H. (2019). Pomegranate (*Punica granatum*) phenolics ameliorate hydrogen peroxide-induced oxidative stress and cytotoxicity in human keratinocytes. *Journal of Functional Foods*. <https://doi.org/10.1016/j.jff.2019.02.015>
- Liu, W., Ma, H., Frost, L., Yuan, T., Dain, J. A., & Seeram, N. P. (2014). Pomegranate phenolics inhibit formation of advanced glycation endproducts by scavenging reactive carbonyl species. *Food and Function*, 5(11). <https://doi.org/10.1039/c4fo00538d>
- Liu, W., Wei, Z., Ma, H., Cai, A., Liu, Y., Sun, J., ... Seeram, N. P. (2017). Anti-glycation and anti-oxidative effects of a phenolic-enriched maple syrup extract and its protective effects on normal human colon cells. *Food and Function*, 8(2). <https://doi.org/10.1039/c6fo01360k>
- Liu, W., Ma, H., DaSilva, N. A., Rose, K. N., Johnson, S. L., Zhang, L., ... Seeram, N. P. (2016). Development of a neuroprotective potential algorithm for medicinal plants. *Neurochemistry International*. <https://doi.org/10.1016/j.neuint.2016.09.014>
- Liu, W., Wei, Z., Ma, H., Cai, A., Liu, Y., Sun, J., ... Seeram, N. P. (2017). Anti-glycation and anti-oxidative effects of a phenolic-enriched maple syrup extract and its protective effects on normal human colon cells. *Food and Function*. <https://doi.org/10.1039/c6fo01360k>
- Liu, Y., Ma, H., & Seeram, N. P. (2016). Development and UFLC-MS/MS characterization of a product-specific standard for phenolic quantification of maple-derived foods. *Journal of Agricultural and Food Chemistry*. <https://doi.org/10.1021/acs.jafc.6b01381>
- Ma, H., DaSilva, N. A., Liu, W., Nahar, P. P., Wei, Z., Liu, Y., ... Seeram, N. P. (2016). Effects of a standardized phenolic-enriched maple syrup extract on β -amyloid aggregation, neuroinflammation in microglial and neuronal cells, and β -amyloid induced neurotoxicity in *Caenorhabditis elegans*. *Neurochemical Research*, 41(11). <https://doi.org/10.1007/s11064-016-1998-6>

- Ma, H., Liu, W., Frost, L., Kirschenbaum, L. J., Dain, J. A., & Seeram, N. P. (2016). Glucitol-core containing gallotannins inhibit the formation of advanced glycation end-products mediated by their antioxidant potential. *Food and Function*, 7(5). <https://doi.org/10.1039/c6fo00169f>
- Ma, H., Johnson, S. L., Liu, W., Dasilva, N. A., Meschwitz, S., Dain, J. A., & Seeram, N. P. (2018). Evaluation of polyphenol anthocyanin-enriched extracts of blackberry, black raspberry, blueberry, cranberry, red raspberry, and strawberry for free radical scavenging, reactive carbonyl species trapping, anti-glycation, anti- β -amyloid aggregation, and mic. *International Journal of Molecular Sciences*. <https://doi.org/10.3390/ijms19020461>
- Ma, H., Liu, W., Frost, L., Wang, L., Kong, L., Dain, J. A., & Seeram, N. P. (2015). The hydrolyzable gallotannin, penta-*O*-galloyl-beta-D-glucopyranoside, inhibits the formation of advanced glycation endproducts by protecting protein structure. *Molecular Biosystems*. <https://doi.org/10.1039/c4mb00722k>
- McLoone, P., Warnock, M., & Fyfe, L. (2016). Honey: an immunomodulatory agent for disorders of the skin. *Food and Agricultural Immunology*. <https://doi.org/10.1080/09540105.2015.1104653>
- Mirnezami, M., Jafarimanesh, H., Rezagholizamenjany, M., Alimoradian, A., & Ranjbaran, M. (2020). The effect of silymarin on liver enzymes in patients taking isotretinoin: A randomized clinical trial. *Dermatologic Therapy*. <https://doi.org/10.1111/dth.13236>
- Nahar, P. P., Driscoll, M. V., Li, L., Slitt, A. L., & Seeram, N. P. (2014). Phenolic mediated anti-inflammatory properties of a maple syrup extract in RAW 264.7 murine macrophages. *Journal of Functional Foods*. <https://doi.org/10.1016/j.jff.2013.09.026>
- Nilsson, B. O. (1999). Biological effects of aminoguanidine: An update. *Inflammation Research*. <https://doi.org/10.1007/s000110050495>
- Palmer, D. M., & Kitchin, J. S. (2010). A double-blind, randomized, controlled clinical trial evaluating the efficacy and tolerance of a novel phenolic antioxidant skin care system containing *Coffea arabica* and concentrated fruit and vegetable extracts. *Journal of Drugs in Dermatology*, 9(12):1480-1487
- Rahbar, S., Kumar Yernini, K., Scott, S., Gonzales, N., & Lalezari, I. (1999). Novel inhibitors of advanced glycation endproducts. *Biochemical and Biophysical Research Communications*. <https://doi.org/10.1006/bbrc.1999.1275>
- Roberts, M. J., Wondrak, G. T., Laurean, D. C., Jacobson, M. K., & Jacobson, E. L. (2003). DNA damage by carbonyl stress in human skin cells. *Mutation Research - Fundamental and Molecular Mechanisms of Mutagenesis*. [https://doi.org/10.1016/S0027-5107\(02\)00232-4](https://doi.org/10.1016/S0027-5107(02)00232-4)
- Saranraj, P., & Sivasakthi, S. (2018). Comprehensive review on honey: Biochemical and medicinal properties. *Journal of Academia and Industrial Research*.
- Sun, J., Liu, W., Ma, H., Marais, J. P. J., Khoo, C., Dain, J. A., ... Seeram, N. P. (2016). Effect of cranberry (*Vaccinium macrocarpon*) oligosaccharides on the formation of advanced glycation end-products. *Journal of Berry Research*. <https://doi.org/10.3233/JBR-160126>
- Svobodová, A., Psotová, J., & Walterová, D. (2003). Natural phenolics in the prevention of UV-induced skin damage. A review. *Biomedical Papers*. <https://doi.org/10.5507/bp.2003.019>
- Wu, C. H., Huang, S. M., Lin, J. A., & Yen, G. C. (2011). Inhibition of advanced glycation endproduct formation by foodstuffs. *Food and Function*. <https://doi.org/10.1039/c1fo10026b>

- Wu, C. H., & Yen, G. C. (2005). Inhibitory effect of naturally occurring flavonoids on the formation of advanced glycation endproducts. *Journal of Agricultural and Food Chemistry*.
<https://doi.org/10.1021/jf048550u>
- Yang, C.T., Meng, F.H., Chen, L., Li, X., Cen, L.J., Wen, Y.H., Li, C.C. and Zhang, H. (2014). Inhibition of Methylglyoxal-Induced AGEs/ RAGE Expression Contributes to Dermal Protection by N-Acetyl-L-Cysteine. https://doi.org/10.1163/_q3_SIM_00374
- Zhang, Y., Ma, H., Liu, W., Yuan, T., & Seeram, N. P. (2015). New antiglycative compounds from cumin (*Cuminum cyminum*) spice. *Journal of Agricultural and Food Chemistry*, 63(46).
<https://doi.org/10.1021/acs.jafc.5b04796>
- Zhang, Y., Yuan, T., Li, L., Nahar, P., Slitt, A., & Seeram, N. P. (2014). Chemical compositional, biological, and safety studies of a novel maple syrup derived extract for nutraceutical applications. *Journal of Agricultural and Food Chemistry*. <https://doi.org/10.1021/jf501924y>
- Zillich, O. V., Schweiggert-Weisz, U., Eisner, P., & Kerscher, M. (2015). Polyphenols as active ingredients for cosmetic products. *International Journal of Cosmetic Science*.
<https://doi.org/10.1111/ics.12218>

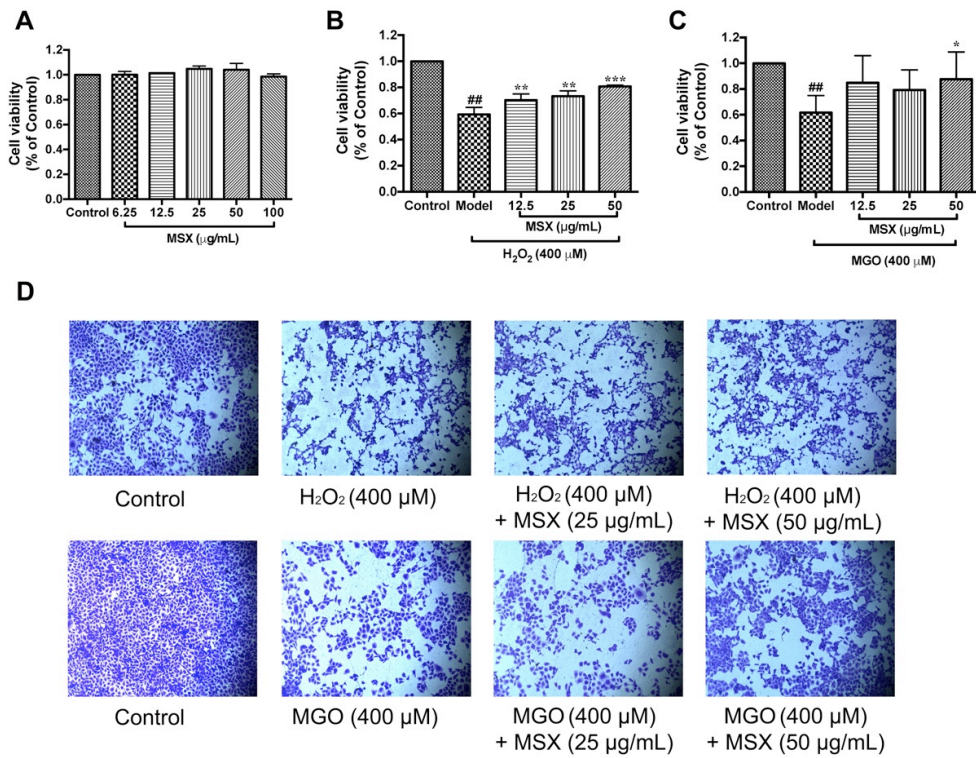


Figure 1 Effects of MSX on the cell viability of H₂O₂ and MGO challenged HaCaT cells. MSX (6.25-100 $\mu\text{g/mL}$) were nontoxic to HaCaT cells, A. HaCaT cells were pretreated with MSX (12.5, 25, and 50 $\mu\text{g/mL}$) for 2 hours, then treated with H₂O₂ (400 μM ; B), or MGO (400 μM , C). Representative images of cells stained with crystal violet reagent. HaCaT cells were pretreated with MSX and then exposed to H₂O₂ or MGO, D. ^{###} Compared to control $P < .01$; *compared to model $P < .05$, **Compared to model $P < .01$, ***compared to model $P < .001$

Figure 2

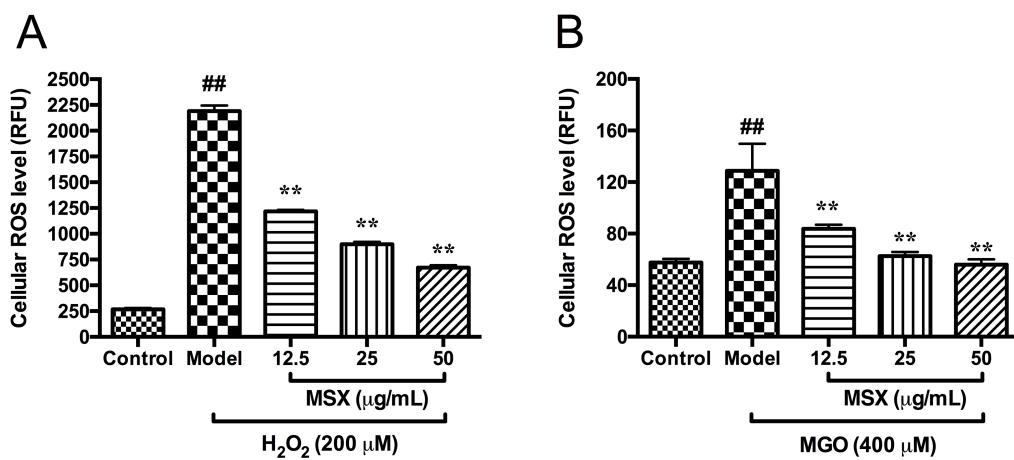


Figure 2 Effects of MSX on the production of ROS in HaCaT cells in the DCFDA assay. HaCaT cells were pretreated with MSX (12.5, 25, and 50 $\mu\text{g/mL}$) for 2 hours and then treated with DCFDA reagent (20 μM) followed by incubation with H_2O_2 (200 μM) for 1 hour, A; or with MGO (400 μM) for 24 hours, B. Levels of cellular ROS were determined by measuring the fluorescent intensity of cells.

^{##}Compared to control $P < .01$; ^{**}compared to model $P < .01$

Figure 3

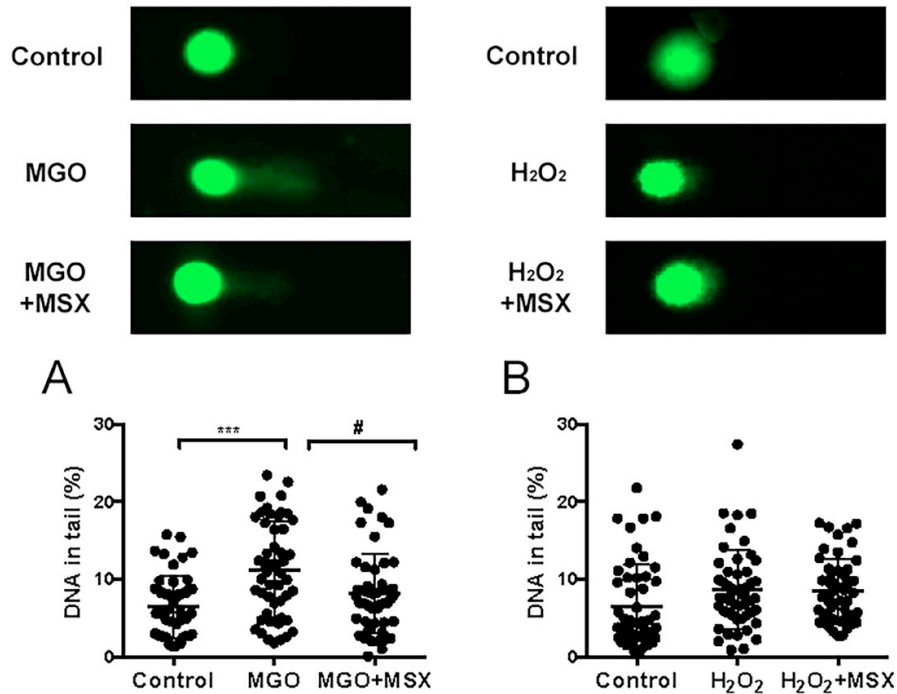


Figure 3 Effects of MSX (50 μ M) on the integrity of DNA in MGO- and H₂O₂-challenged HaCaT cells, A and B. Representative fluorescent images of SYBR GOLD stained comet slides captured by EVOS microscope system. The percentages of tailed DNA were measured from at least fifty randomly selected cells and analyzed with CASP software. ***Compared to control $P < .001$; # compared to model $P < .05$.

CHAPTER 4

MANUSCRIPT 4

Published: 25 September 2020

Journal of Functional Foods, 75 (2020) 104208

Inhibitory effects of skin permeable glucitol-core containing gallotannins from red maple leaves on elastase and their protective effects on human keratinocytes

Chang Liu^b, Yiming Xu^b, Riley D. Kirk^b, Huifang Li^{a,b}, Dongli Li^a, Nicholas A. DaSilva^b, Matthew J. Bertin^b, Navindra P. Seeram^{b*}, Hang Ma^{a,b*}

^a School of Biotechnology and Health Sciences, Wuyi University, International Healthcare Innovation Institute (Jiangmen), Jiangmen 529020, China

^b Department of Biomedical and Pharmaceutical Sciences, College of Pharmacy, University of Rhode Island, Kingston, RI 02881, USA

*Corresponding authors

Tel.: +1 401 874 9367; E-mail address: nseeram@uri.edu (N.P.S.)

Tel.: +1 401 874 7654; E-mail address: hang_ma@uri.edu (H.M.)

7 Greenhouse Rd, Kingston, RI 02881, USA

Department of Biomedical and Pharmaceutical Sciences, College of Pharmacy

University of Rhode Island

ABSTRACT

Glucitol-core containing gallotannins (GCGs) from the red maple (*Acer rubrum*) species have been reported to exhibit skin beneficial activities but their inhibitory effects on elastase remain unclear. Herein, we evaluated a series of GCGs for their anti-elastase activity, skin permeability, and cytoprotective effects in human keratinocytes HaCaT cells. GCGs' anti-elastase effects were enhanced as their number of galloyl groups increased which contributed to the formation of more stable protein-ligand complexes. In addition, GCGs were predicted to have moderate skin permeability with ginnalin A (GA) showing favorable permeability in the PAMPA model and cell uptake assay. Moreover, GA, ginnalin B, and maplexin F (at 50 μ M) alleviated H₂O₂-induced reactive oxygen species in HaCaT cells by 70.8, 92.8, and 84.6%, respectively. In conclusion, red maple GCGs are skin permeable elastase inhibitors with antioxidant activity, which may contribute to their overall skin beneficial effects and support their potential for cosmeceutical applications.

Keywords: red maple; glucitol-core containing gallotannin; ginnalin A; elastase; anti-wrinkle; antioxidant

Abbreviations

AAAPVN: N-Succinyl-Ala-Ala-Ala-p-nitroanilide; CTG: Cell Titer-Glo 2.0 assay; EGCG :
epigallocatechin gallate; GA: ginnalin A; GB: ginnalin B; GC: ginnalin C; GCGs: glucitol-core containing
gallotannins; GLA: gallic acid; GT: gallotannins; HPLC: high-performance liquid chromatography; MF:
maplexin F; MJ: maplexin J; PAMPA: parallel artificial membrane permeability assay; PGG: pentagalloyl
glucose; PYG: pyrogallol; ROS: reactive oxygen species; TA: tannic acid

1 Introduction

Gallotannins (GTs), a class of polyphenols formed by the esterification of gallic acid(s) and a polyol carbohydrate moiety (e.g. glucose), are common phytochemicals used in traditional medicine systems. They have been reported to show numerous pharmacological activities including antioxidant (Zhao et al., 2005), anti-microbial (Engels et al., 2009), anti-cancer (J. Zhang, Li, Kim, Hagerman, & Lü, 2009), anti-diabetic (J. Zhang et al., 2009), and anti-inflammatory (Kiss & Piwowarski, 2016) effects. In addition, pre-clinical studies showed that GTs exert skin protective effects via various mechanisms including prevention of UV-induced skin damage (Svobodová, Psotová, & Walterová, 2003), down-regulation of skin hyperpigmentation (Goenka, Ceccoli, & Simon, 2019), and anti-proliferation of skin cancer cells (Ho, Chen, Lin-Shiau, & Lin, 2002). Due to these potential promising skin beneficial effects, plant extracts containing GTs are widely used as bioactive ingredients in skin care products (Choubey, Varughese, Kumar, & Beniwal, 2015). Our research group has had a long interest in identifying phytochemicals from medicinal plants for their cosmeceutical and dermatological applications (Liu et al., 2020, 2019; Sheng et al., 2020). This led to the discovery of a series of unique GTs, namely, glucitol-core containing gallotannins (GCGs), from the red maple (*Acer rubrum*) species (C. Li & Seeram, 2018; Wan et al., 2012; Yuan, Wan, Liu, & Seeram, 2012; Y. Zhang, Ma, Yuan, & Seeram, 2015). Biological evaluations of these GCGs showed several skin beneficial activities including anti-melanogenic effects in murine melanoma B16F10 cells (Ma et al., 2017) and cytoprotective effects against oxidative stress in human keratinocyte HaCaT cells (Liu et al., 2020). In addition, GCGs have been reported to show inhibitory effects on the formation of advanced glycation endproducts (AGEs) (Ma, Liu, et al., 2016), which are biomarkers that contribute to aging-related skin conditions including sagging and wrinkling (Gkogkolou & Böhm, 2012; Ichihashi, Yagi, Nomoto, & Yonei, 2011).

Apart from AGEs, the formation of skin wrinkles can be exacerbated by the loss of skin elasticity due to hyperactivity of elastase (Imokawa & Ishida, 2015). Pancreatic elastase, also known as elastase 1 (ELA1) or chymotrypsin-like elastase family, member 1 (CELA1), is a serine-type protease expressed in the basal layers of epidermis (Talas, Dunlop, Khalaf, Leigh, & Kelsell, 2000). It catalyzes the reaction of breaking down elastin protein by cleaving peptide bonds on the carboxyl-terminal end of amino acids with an alkyl side chain (Mecham et al., 1997). Elastase, along with metalloproteases and cysteine proteases, are

the major proteases for the degradation of tissue elastin. Elastin is a polymeric protein consisting of tropoelastin monomers that account for 2 to 4% of the total protein content of the skin tissue (Rosenbloom, Abrams, & Mecham, 1993). It is an essential protein for maintaining skin's mechanical structures by resuming the shape of skin after physical stretching or contracting. Declining elastin level in skin tissue can lead to the loss of skin structural integrity and consequently result in the formation of skin wrinkle (Imokawa, 2009). Although elastin is a long-lasting protein with a half-life of over 70 years (Toyama & Hetzer, 2013), its degradation can be exacerbated by both environmental stress (e.g. ultraviolet radiation) and intrinsic factors, such as the overexpression of elastase. Inhibitors of elastase, especially from herbal extracts, have been reported to show ameliorative effects against elastase-associated wrinkle formation (Tsukahara et al., 2006a), and are considered as active anti-wrinkle ingredients for cosmetic products (K. K. Lee, Kim, Cho, & Choi, 1999; Liyanaarachchi, Samarasekera, Mahanama, & Hemalal, 2018). Several tannin-rich plants have been screened for anti-elastase activity (Piwowarski, Kiss, & Kozłowska-Wojciechowska, 2011), however, the inhibitory effects of GTs on elastase remain unclear. Moreover, although GTs are common phytochemicals used in skin care products, their cosmeceutical properties, such as the skin permeability, are not well characterized. Herein, GTs including GCGs (ginnalins A-C and maplexins F-J) previously isolated by our group from red maple leaves, along with two common GTs including pentagalloyl glucose (PGG) and tannic acid (TA), as well as GTs' structural building unit, gallic acid (GLA), and a gut microbial metabolite of GTs, namely, pyrogallol (PYG), were evaluated for their anti-elastase activity. The structure-activity relationship and mechanisms of elastase inhibition of the GCGs were studied. In addition, the skin permeability of GCGs and their protective effects in human keratinocytes HaCaT cells against oxidative stress are reported here.

2 Materials and Methods

2.1. Chemicals

Red maple glucitol-core containing gallotannins (GCGs) including ginnalin A (GA; contains 2 galloyls), ginnalin B (GB; contains 1 galloyl), ginnalin C (GC; contains 1 galloyl), maplexin F (MF; contains 3 galloyls), and maplexin J (MJ; contains 4 galloyls) were isolated from the red maple species or chemically synthesized as previously reported (Ma et al., 2015; Y. Zhang et al., 2015). Pentagalloyl glucose (PGG; contains 5 galloyls) was isolated from *Rhus* species as reported (Ma et al., 2012). Tannic acid (TA; contains

10 galloyls), gallic acid (GLA), pyrogallol (PYG), epigallocatechin gallate (EGCG), elastase from porcine pancreas (EC 254-453-6), elastase substrate (N-Succinyl-Ala-Ala-Ala-p-nitroanilide; AAAPVN), 2',7'-dichlorofluorescein diacetate (DCF-DA), dimethyl sulfoxide (DMSO), and analytical grade methanol and acetonitrile were purchased from Sigma Aldrich (St. Louis, MO, USA). Tris-HCl buffer (pH 8.8) was purchased from Teknova (Hollister, CA, USA).

2.2. Elastase inhibition assay

Test samples were dissolved in DMSO at 10 mg/mL and diluted to desired concentrations with Tris-HCl buffer (pH adjusted to 7.2; DMSO < 5%). A reaction mixture of test sample (30 μ L) and elastase solution (100 μ L; 0.3 U/mL) in Tris-HCl buffer was incubated in a 96-well plate at 37 °C for 10 min. Then substrate AAAPVN (40 μ L; 0.25 mg/mL) was added to each well at timed intervals. The reaction mixture was incubated at room temperature for 5 min and absorbance was recorded at wavelength of 410 nm by a micro-plate reader (SpectraMax M2, Molecular Devices Corp., operated by SoftmaxPro v.4.6 software, Sunnyvale, CA, USA). Control group had buffer solution (30 μ L) in place of the test sample. The elastase inhibitory activity was expressed as inhibition% and was calculated as follows: inhibition% = 100 X [(C₅ - C₀) - (S₅ - S₀)] / (C₅ - C₀), where C₀ is the absorbance of the reagent blank in 0 min, S₀ is the absorbance of the samples in 0 min, C₅ is the absorbance of the reagent blank in 5 min, and S₅ is the absorbance of the samples in 5 min.

2.3. Kinetics of elastase inhibition

The inhibition type of ginnalin A (GA) and maplexins J (MJ) was determined by the Lineweaver–Burk plot using previously reported method (Ma et al., 2015). Briefly, two concentrations around the IC₅₀ value of each sample (dissolved in Tri-HCl buffer; DMSO < 5%) were selected and their inhibition rates on elastase were evaluated with substrate AAAPVN in a range of concentrations from 125 to 1000 μ M.

2.4. Molecular docking

Crystal structure of porcine pancreatic elastase complexed with a potent peptidyl inhibitor was retrieved from Protein Data Bank (PDB ID: 3HGP). The X-ray crystal structure of 3HGP with a resolution of 0.94 Å. UCSF Chimera was applied to remove solvent (water) molecule, non-complexed ions, and ligand. Canonical SMILES files of GLA, GA, MJ, and PGG were acquired from PubChem to generate their chemical structure. The 3D structure of these molecules was constructed using Molecular Operating

Environment (MOE). PDBQT format for both 3HGP and these molecules was prepared using Autodock 4.2 algorithm and Autodock Tools 1.5.6 was used to perform the molecular docking. AutoDock was used to generate the coordinates for each docked conformation along with information on clustering and interaction energies. The estimated free energy of binding was calculated according to the equation. Estimated free energy of binding = [(1) + (2) + (3) - (4)], where (1) is the final intermolecular energy, (2) is the final total internal energy, (3) is the torsional free energy, and (4) is the unbound systems. The ligand-target complex with lowest binding energy was analyzed using Discovery Studio 4.5 (Accelrys Inc., San Diego, CA, USA).

2.5. Skin permeability and stability

GTs' skin permeability was evaluated by computational experiment (SwissADME) using previously reported method (Daina, Michielin, & Zoete, 2017). Simplified molecular input line entry specification (SMILES) files of each compound were generated by ChemDraw (PerkinElmer Inc.; Waltham, MA, USA) and their skin permeability were predicted by SwissADME (<http://www.swissadme.ch/>) with parameters including Log $P_{o/w}$, Log $S_{(ESOL)}$, Log $S_{(Ali)}$ and Log Kp (cm/s, skin permeation). GA, which is the most abundant GCG in red maple plant parts, was selected as a representative GCG for further evaluation of its skin permeability in a biochemical based assay, namely, the parallel artificial membrane permeability assay (PAMPA). Supplies for PAMPA assay including preloaded support plate, deep well plates, and skin plates, as well as PAMPA test reagents including Prisma HT buffer, positive controls (verapamil, piroxicam, progesterone, and atenolol) were obtained from Pion Inc (Billerica, MA, USA). The stability of GA under conditions of basic and acidic environments, ultraviolet (UV) radiation, and heat was measured by HPLC-diode array detector (DAD) analyses using a Hitachi Elite LaChrom system according to published method (Singh et al., 2013). Briefly, GA was incubated in different conditions including basic (pH = 13; 0.1 M HCl), acidic (pH = 1; 0.1 M NaOH), oxidation (3% H₂O₂); UV light, heat (heating chamber at 60 °C) for 1 h and was analyzed by HPLC to determine the degradation. The HPLC-DAD analyses was performed with an Alltima C₁₈ column (250×4.6 mm, 5µm) and a solvent system consist of 0.1% trifluoroacetic acid in water (A)/methanol (B) was used as the mobile phase using a linear gradient as follows: 0-30 min 90-5% A; 30-31 min, 5-90% A; 31-38 min, 5% A with a total run time of 38 min, a flow rate of 0.8 mL/min.

2.6. Cell culture and viability

Human keratinocytes (HaCaT cells) were purchased from the American Type Culture Collection (ATCC, Rockville, USA). The cells were cultured in Dulbecco's modified Eagle's medium (DMEM) (Life Technologies, Gaithersburg, MD, USA) supplemented with 10% fetal bovine serum (FBS; Gibico, Grand Island, NY, USA) at 37 °C with 5% CO₂. Test compounds were prepared in DMSO (10 mM) and diluted to desired concentrations with cell culture medium. The viability of HaCaT cells treated with test compounds (at 10, 100, and 1000 μM) were determined with the Cell Titer-Glo 2.0 assay (CTG; Promega Corp, Madison, WI, USA) CTG 2.0 with previously reported method (Ma, DaSilva, et al., 2016). By measuring luminescence intensity using a Spectramax M2 plate reader (Molecular Devices, Sunnyvale, CA, USA).

2.7. Measurement of reactive oxygen species (ROS)

Levels of cellular oxidative stress were evaluated by reactive oxygen species (ROS) assay with DC-FDA agent as previously reported (Liu et al., 2019). Briefly, HaCaT cells were seeded in 96-well plate and allowed to grow for 12 h following incubation with test compounds for 12 h. Cells were then washed with phosphate-buffered saline (PBS) and incubated with a fluorescent agent (DCF-DA; 20 μM) in culture medium for 20 min. Next, cells were treated with H₂O₂ (400 μM) for 1 h and cellular ROS levels were determined by measuring fluorescence intensity with excitation and emission wavelength of 485 and 525 nm, respectively, using a Spectramax M2 plate reader (Molecular Devices, Sunnyvale, CA, USA). Morphological evaluation of cells stained with DCF-DA agent was analyzed by confocal images captured with a fluorescence microscope cells imaging system (EVOS; Invitrogen, Waltham, MA, USA).

2.8. Sample preparation for cell uptake assay

Cellular uptake of GA by HaCaT cells were evaluated with high-performance liquid chromatography with a diode-array detector (HPLC-DAD) method using reported method with modifications (Hsu, Weng, Lin, & Chien, 2007). Briefly, HaCaT cells were seeded in 9 mm petri dishes for 12 h to reach a confluency of 80% and GA (at 50 μM) was added and incubated with cells for 2 h. Next, cell culture medium (1.5 mL) was carefully collected at 1, 2, 4, 8, and 24 hours and centrifuged at 12000 g/min for 10 min to obtain supernatant. The supernatant was then freeze dried for HPLC analysis for extracellular GA level. For intracellular level of GA, cells were treated with GA (at 50 μM) for 24 h and then washed with cold PBS (2x) to remove remaining extracellular GA. Cells were then collected in culture medium (2 mL) and centrifuged at 12000 g/min for 10 min to obtain cell pellets. Cell pellets were suspended in PBS buffer and

placed in a freezer (at -80°C) for 15 mins followed by thawing at 37°C for 5 min for three cycles. Then the cell lysate was centrifuged at 12000 g/min for 10 mins at 4°C and freeze dried for HPLC analysis.

2.9. Statistical analysis

Statistical analyses were performed using GraphPad Prism 8 (GraphPad Software, La Jolla, CA, USA). Data were expressed as the mean value \pm standard deviation (SD). The significance of differences was determined using a two-way analysis of variance (ANOVA) followed by a post hoc Student-Newman-Keuls multiple comparison test (SNK). $P < 0.05$, $P < 0.01$, or $P < 0.001$ was determined to be significant.

3 Results

3.1. GTs inhibit elastase enzyme activity

The structures of GTs including GCGs are varied in the number of galloyl groups attached to a polyol carbohydrate (e.g. glucose or glucitol; Figure 1). A trend of enhanced inhibitory effect on elastase activity was observed when the number of galloyl groups on GTs increased. GCGs with 1 galloyl [ginnalin B (GB) and ginnalin C (GC)] or 2 galloyls (GA) showed inhibitory effects at concentrations of 31.25-1000 μ M with a range of inhibition rate from 7.5-68.6, 2.5-19.4, and 5.7-59.5%, respectively. GCGs including maplexins F and J (MF and MJ, with 3 and 4 galloyls, respectively) showed enhanced inhibitory effects with inhibition rates of 38.6-86.3 and 28.4-87.9%, at concentrations from 1.25-1000 μ M, respectively. The inhibitory effect of pentagalloyl glucose (PGG; 5 galloyls) was comparable to MJ with an inhibition rate of 80.3% at 1000 μ M. Tannic acid (TA), a large GT with 10 galloyls, had the most potent inhibitory effect with inhibition rates ranging from 70.2-98.8%, at concentrations of 31.25-1000 μ M, respectively. In addition, gallic acid (GLA), which contains 1 galloyl group without any attachment to a sugar core, along with a gut microbial metabolite of GTs, namely, pyrogallol (PYG), showed weak inhibitory effects on elastase. PYG (at 31.25-1000 μ M) had inhibition rates of 6.6-38.2%, respectively, whilst GLA showed a minimum inhibitory activity (inhibition $<$ 15% at 31.5 μ M). The structure-activity relationship of GTs on elastase inhibition was further analyzed by comparing their IC_{50} values (Table 1). Moderate elastase inhibitors including GB and GA had an IC_{50} values of 617.4 and 810.6 μ M, respectively. The IC_{50} values of GTs with 3-5 galloyls (MF, MJ, and PGG) ranged from 237.5 to 262.3 μ M, respectively. TA with 10 galloyls had the strongest inhibitory effect with an IC_{50} value of 16.1 μ M, which was 10-fold stronger than the positive control epigallocatechin gallate with 1 galloyl group (EGCG; IC_{50} = 160.7 μ M). In addition,

another positive control, namely, oleanolic acid (a pentacyclic triterpenoid which does not contain any galloyl groups), had similar anti-elastase activity with an IC_{50} value of 163.1 μ M, which was in agreement with published data (K. K. Lee, Cho, Park, & Choi, 2001). GLA, GC, and PYG had weak inhibitory activities with IC_{50} values greater than 1000 μ M. Furthermore, two GCGs including GA (the most abundant GCG in the red maple plant used as a representative compound) and MJ (a red maple GCG with the most potent anti-elastase activity) were selected to further study the mechanism of inhibitory effects on elastase by determining their enzyme inhibition mode with kinetic assay. Lines generated in the Lineweaver-Burk plot intersected at the X-axis, suggesting that GA and MJ were noncompetitive inhibitors of elastase (Figure 2). Therefore, GA and MJ may inhibit the activity of elastase by binding to the allosteric site of enzyme protein.

3.2. GTs bind to elastase protein

Molecular docking was conducted to study the interactions between elastase enzyme and red maple GCGs including GA and MJ, along with GLA and PGG. An X-ray crystal structure of elastase from protein data bank (PDB ID: 3HGP) was used for docking (Figure 3A). Estimated free energy of binding of test compounds and elastase was predicted (Figure 3B). GA and MJ had an estimated free binding energy of -4.86 and -1.62 Kcal/mol, respectively, while GLA and PGG showed binding energy of -3.53 and -0.11 Kcal/mol, respectively. In addition, molecular interactions between elastase and test compounds were explored. GLA, as the structural basic unit of GCGs, was able to interact with elastase enzyme primarily by forming hydrogen bonds between its hydroxyl groups and protein residues including GLY-A:184, ASN-A:132, THR-A:162, and ASN-A:133. A pi-sigma bond between the benzyl ring of GLA and protein residue VAL-A:163 was formed to enhance the ligand-protein interactions (Figure 3C). Further binding analysis showed that hydroxyl bonds on the galloyl group at 2-position of GA formed conventional hydrogen bonds with the THR-A:41 residue of elastase enzyme (Figure 3D). Similarly, two hydrogen bonds were formed between hydroxyl groups of galloyl moiety (at 6-position of GA) and elastase's ASP-A:97 and ARG-A:217A residues. Additionally, the stabilization of the GA-elastase complex was facilitated by forming pi-cation and pi-sulfur bonds with residues ARG61 and CYS42, respectively, as well as by van der Waals force with protein residues including ALA-A:99A, ASP-A:98, GLA-A:192, and GLY-A193. Similar molecular interactions were observed between MJ and elastase enzyme (Figure 3E). For instance,

hydrogen bonds were formed between hydroxyl groups at two galloyl moieties (positions 4 and 6) of MJ and protein residues ALA-A:152, LEU-A:151, GLU-A:70, and TRP-A:38 (Figure 3E). A pi-alkyl bonds was also formed between benzyl ring of MJ (at position 6) and residue LUE-A:73. Given that MJ has two more galloyl groups than GA, it formed additional van der Waals bonds (VAL-A:67, GLN-A:34, HIS-A:40, ALA-A:39, GLN-A:150, GLN-A:153, SER-A:36A, SER-A:37, ARG-A:65A, and TYR-A:82) to stabilize the ligand-protein complex. Furthermore, the binding mode of GCGs to elastase was compared to that of PGG. Although similar hydrogen bonds were formed between hydroxyl groups of PGG and amino acid residues of elastase enzyme (at residues ANS-A:204 and GLY-A:127), PGG also had additional hydrogen bonds formed between its carbonyl groups and protein residues ASN-A:132 and ILE-A:129, as well as its glucose core and residue ALA-A:131 (Figure 3F). Although MJ and PGG share some structural similarities, they had different torsional energy (7.46 v.s. 9.25, respectively) which was the major contributor that led to their distinctive overall binding energy. This may account for the observation that although MJ has 1 less galloyl group compared to PGG, they both had comparable inhibitory effects on elastase.

3.4. Red maple GCGs are skin permeable

To further evaluate red maple GCGs' potential for cosmeceutical applications, their permeability on skin barrier was first predicted *in silico*. The skin permeability coefficient (Log K_p; cm/s) of test compounds were obtained by SwissADME computational model with a multiple linear regression of factors correlated with physicochemical properties including molecular weight, Log P_{o/w}, molecular size, and lipophilicity (Figure 4A). Based on Log K_p prediction, the more negative the coefficient value, the less skin permeable is the compound. GLA and PYG, as the 'structure building scaffold' and metabolite of GTs, respectively, had moderate Log K_p (-6.84 and -6.7 cm/s, respectively), whilst large GTs including PGG and TA were unlikely to be able to penetrate skin barrier. GCGs and EGCG (the positive control in the elastase inhibition assay) had comparable Log K_p (ranging from -9.25 to -9.56, vs -8.27 cm/s), which are less permeable when compared to some known skin permeable drugs (Chen, Chen, Huang, & Chang, 2018). Notably, EGCG has been reported to show desirable skin penetration and retention for cosmetic applications with *ex vivo* assays using fresh human skin model and static Franz diffusion assay (Dal Belo, Gaspar, Maia Campos, & Marty, 2009). Therefore, we further evaluated the skin penetration and skin cell uptake capacity of GA, the most abundant GCG in red maple leaves extract, with experimental methods including parallel artificial

membrane permeability assay (PAMPA) and a cell uptake assay. In the PAMPA assay, GA's skin permeability was evaluated based on its experimental $-\text{Log } P_e$ values, and compared to several drugs including atenolol ($-\text{Log } P_e$ value = 9.87), verapamil ($-\text{Log } P_e$ value = 4.86), and progesterone ($-\text{Log } P_e$ value = 4.22) were used as controls (at pH = 7.4) representing high, medium, and low skin permeability, respectively. GA had $-\text{Log } P_e$ values of 4.64 and 4.76 at pHs 6.5 and 7.4, respectively, suggesting that it has a moderate skin permeability (Figure 4B and C). In addition, GA was evaluated for its cell uptake capacity in HaCaT cells (Figure 4B and C). HPLC analysis showed that GA (at 100 $\mu\text{g}/\text{mL}$) was detectable in human keratinocyte HaCaT cells after a treatment period up to 4 h (Figure 4D). To evaluate whether GA was stable in the conditions of biological evaluation systems used herein, we performed forced degradation assay using HPLC-DAD analyses (Figure S3 in the Supplementary Material). GA was stable in conditions including acidic environment (in 0.1 M HCl), oxidation (in 3% H_2O_2), UV radiation, and heat at 60 °C with degradation percentages of 2.4, 2.7, 2.8, and 2.9%, respectively (Figure 4E). GA was less stable in the basic condition (0.1 M NaOH) with a degradation percentage of 35.2%.

3.3. Red maple GCGs protect human keratinocytes against oxidative stress

To further study the skin protective effects of GCGs for their potential cosmeceutical applications, cellular assays were used to evaluate GTs' antioxidant effects in human keratinocytes HaCaT cells. First, cytotoxic effects of all GTs at concentrations of 10, 100, and 1000 μM in HaCaT cells were assessed (Figure 5). Red maple GCGs including GB, GC, GA, and MF were nontoxic to HaCaT cells and the median inhibition concentrations (IC_{50}) values were 247.1, >1000, 730.2, 429.1 μM , respectively. In addition, apart from TA, other GTs, GLA, and PRG showed minimum toxicity to HaCaT cells at low concentration (10 μM). Cytotoxic effects of GTs in HaCaT cells were observed at higher concentrations. IC_{50} values of large GTs (with 4 or more galloyls) including MJ, PGG, and TA were 16.7, 70.1, and 9.8 μM , respectively. The antioxidant effects of GTs were evaluated at nontoxic concentrations (10 and 50 μM) against H_2O_2 induced generation of ROS in HaCaT cells. The level of ROS was elevated when cells were exposed to H_2O_2 (400 μM ; as the model group). Red maple GCGs including GA, MF, and MJ (at 10 and 50 μM) ameliorated H_2O_2 -induced oxidative stress by reducing ROS level to 47.1-92.8 %, 58.4-84.6 %, and 16.4-35.4 %, respectively (Figure 6A). In addition, GA showed protective effects by reducing H_2O_2 -induced ROS generation by 47.1 and 92.8 %, respectively (at 10 and 50 μM). The cytoprotective effects of red maple

GCGs were supported by the morphologic analysis of cells stained with a fluorescent probe DCFDA. Microscope images showed that the treatment of red maple GCGs reduced the fluorescent intensity of cells stained with DC-FDA (Figure 6B). Other GTs did not significantly reduce H₂O₂-induced ROS generation in HaCaT cells.

4. Discussion

We showed that GTs including GCGs from red maple leaves inhibited the activity of elastase and their anti-elastase effect appeared to be correlated with the number of galloyl moieties in their chemical structure with a higher number of galloyls in the GTs resulting in more potent inhibition of elastase. This structure-activity relationship (SAR) is in agreement with our previously reported SAR studies of GCGs on anti- α -glucosidase (Ma et al., 2015), anti-tyrosinase (Ma et al., 2017), anti-glycation (Ma, Liu, et al., 2016), and anti-proliferative activities (González-Sarriás, Ma, Edmonds, & Seeram, 2013; González-Sarriás, Yuan, & Seeram, 2012). For instance, GCGs with 1 galloyl (e.g. GB and GC) only had a moderate inhibitory effect on the formation of AGEs, whilst GCGs with multi-galloyls (e.g. GA, MF, MJ) showed more potent anti-glycation activity. A similar SAR effect was observed in the evaluation of GCGs' anti-tyrosinase effect, in which GA, MF, and MJ (with 2-4 galloyls) showed more potent inhibitory effects as compared to GB and GC (both containing 1 galloyl). Apart from these enzymatic assays, this SAR effect has also been observed in cell-based models in which GCGs with 2 or more galloyls had superior anti-proliferative effects against the growth of tumorigenic cells as compared to single-galloyl GCGs (González-Sarriás et al., 2013, 2012). In the current study, mechanistic investigation with molecular docking of the elastase-ligand complex suggested that enhanced inhibitory effects of GCGs including GA and MJ may be attributed to their capacity to form stronger molecular forces to stabilize the enzyme-ligand complex leading to inhibition of elastase. Taken together, our data suggest that GCGs were able to bind to specific binding site on elastase enzyme and inhibited the activity of elastase in specific mode (i.e. noncompetitive inhibition for GA and MJ). This is in contrast to the non-specific protein precipitating effects generally known for tannins, which is supportive for developing GCGs as potential elastase inhibitors for cosmeceutical applications. In addition, the SAR analyses revealed that TA, the largest GT (MW = 1701.19 g/mol) evaluated in this study, was the most potent elastase inhibitor with an IC₅₀ value superior to other GTs (16.1 vs. 237.5-617.4 μ M). However, several potential safety concerns regarding TA's development for cosmeceutical applications

remain to be addressed. First, TA may cause skin irritation, redness, and pain according to its material safety data sheets (MSDS). In addition, toxicity of oral administration of TA has been reported in toxicological studies with animal models (Boyd, 1965; Ma, Liu, et al., 2016; Rayudu, Kadirvel, Vohra, & Kratzer, 1970). Conversely, our group has recently reported that consumption of a red maple leaves extract containing high level of GCGs at an oral dosage of 8 g/kg/body weight did not induce acute toxicity in mouse (L. Li et al., 2020). Therefore, the development of a GCGs enriched proprietary red maple leaves extract, namely, Maplifa[®], as a potential bioactive ingredient for cosmeceutical applications shows promise. In addition, Maplifa[®] showed anti-elastase activity (inhibited elastase by 6.55 to 86.75%, at concentrations from 62.5 to 1000 µg/mL; Figure S1 in the Supplementary Material) and skin permeability (with -Log Pe value of 4.2 and 4.1 at pH of 7.4 and 6.5, respectively in the PAMPA assay; Figure S2 in the Supplementary Materials). However, further safety evaluations including chronic and skin-specific toxicity studies on these GCGs with in vivo models are warranted.

Elastase inhibitors are considered as a viable option to protect elastin from degradation and reduce formation of skin wrinkle. For instance, N-phenethylphosphonyl-L-leucyl-L-tryptophane (NPLT), a chemically synthesized small molecule, was reported to show potent inhibitory effect on skin fibroblast elastase and suppress wrinkle formation in hairless mice skin tissue received UV irradiation (Tsuji, Moriwaki, Suzuki, Takema, & Imokawa, 2007). In addition, further investigation showed that some herbal extracts including ginger (*Zingiber officinale*) had similar inhibitory activity, as compared to NPLT, on fibroblast-derived elastase and were able to reduce UV-B irradiation induced wrinkle formation in hairless mouse model (Tsukahara et al., 2006b). Although GCGs showed inhibitory effect on elastase, it is still unknown whether they can inhibit the formation of skin wrinkle, which is included in our future planned studies of GCGs and Maplifa[®] for their skin protective effects.

Elastase inhibitors may require the capacity to penetrate skin barrier to reach to the inner layers of skin tissue for desirable biological effects. Therefore, in the cosmetic industry, skin permeability is a critical factor to consider for the development of elastase inhibitors as topical skin care products. In fact, the interpretation of skin permeability of natural products-based elastase inhibitors is hindered by several challenges including 1) complexity of skin tissue due to its highly ordered intercellular lipid matrix of the stratum corneum, and, 2) broad range of structural diversity of natural products. Herein, we further

predicted the skin permeability of GCGs, along with EGCG (a known elastase inhibitor), with in silico algorithm SwissADME. Skin permeability related physico-chemical parameters including lipophilicity ($\text{Log } P_{o/w}$), water solubility ($\text{Log } S_{\text{ESOL}}$), and skin permeability coefficient ($\text{Log } K_p$) were compared between the GCGs and EGCG. EGCG, which has been reported as a skin penetrable natural product (Dal Belo et al., 2009; Shetty et al., 2017), had similar skin permeability coefficient as compared to GCGs including GA, GB, GC, MF, and MJ ($\text{Log } K_p = -8.27$ vs. -9.56 to -8.87 , respectively; Figure 4A). Notably, the size of GTs including PGG and TA are too large to penetrate skin barrier as predicted by SwissADME, which makes them less suitable for further cosmeceutical development. Similar studies have been previously reported to show the physico-chemical properties of gallic acid derivatives by quantitative structure–activity relationship (QSAR) modeling and in silico ADMET analysis (Yadav, Khan, & Negi, 2012). These gallic acid derivatives varied in numbers of methylated groups on the galloyl group and different linear side chains. They showed favorable skin permeability with a $\text{Log } K_p$ ranging from -3.39 to -0.48 cm/s, as compared to the standard range for 95% of known drugs with $\text{Log } K_p$ from -8.0 to -1.0 cm/s. Given that the $\text{Log } K_p$ values of GCGs are close to -8.0 cm/s, which is on the edge of skin permeable parameter, we further evaluated the skin penetration capacity of GA, the most abundant and representative GCG in Maplifa[®], with biochemical based assays. Data obtained from PAMPA assay showed that GA is skin penetrable (Figure 4A), which is in agreement with the prediction from the aforementioned SwissADME analysis. In addition, GA was stable in various conditions including acidic environment, UV radiation, and heat, suggesting that GA did not release degradation products (e.g. gallic acid) in the bioassays, which is supportive for its further development as a potential cosmeceutical ingredient. It is notable that PYG, a gut microbial metabolite of gallic acid and GTs, showed the most favorable skin penetration ability from the SwissADME prediction. This pattern has also been observed from our previously reported study, in which gut microbial metabolites of polyphenols, namely, equol (from metabolism of isoflavone daidzein), enterodiol, and enterolactone (from metabolism of lignans including secoisolariciresinol) were more membrane permeable as compared to their parent compounds (Johnson et al., 2019). In addition, polyphenol gut microbial metabolites including equol, enterodiol, and enterolactone showed promising anti-neuroinflammatory effect (Johnson et al., 2019). Although PYG only showed weaker inhibitory effect on elastase activity as compared to GTs, it is possible that being a bioavailable

metabolite of GTs, it may exert other skin protective effect. Therefore, GTs, GLA, and PYG were further assessed for their cytoprotective effect in human keratinocyte HaCaT cells.

Prior to the evaluation of their cytoprotective effect, GTs, along with GLA and PYG, were assayed to determine their non-toxic range of concentrations to HaCaT cells. TA showed considerable cytotoxicity as it significantly decreased the viability of HaCaT cells (by 46.9 %) at the lowest test concentration (10 μ M). Conversely, GCGs were not only non-toxic to HaCaT cells (at concentration of 10 μ M with cell viability greater than 97.2 %), but were also able to exert cytoprotective effect against H₂O₂-induced oxidative stress. This is in agreement with our previously reported study showing that Maplifa[®] and its major polyphenol, GA, alleviated oxidative stress induced toxicity in HaCaT cells (Liu et al., 2020). Therefore, it is possible that other GCGs (e.g. ginnalins B and C, and maplexins) in Maplifa[®] share a similar mechanism of antioxidant activity as GA. For instance, other GCGs may be able to alleviate H₂O₂-induced oxidative stress in HaCaT cells by modulating the total ROS production and mitochondria-derived ROS production (Liu et al., 2020). However, further studies are warranted to confirm this. Additionally, other research groups have also reported skin beneficial effects of GCGs. For instance, GA was reported to protect human keratinocyte (HEK001 cells) from tumor necrosis factor-related apoptosis-inducing ligand (TRAIL)-induced apoptosis via the mediation of reactive oxygen/nitrogen species (C. S. Lee et al., 2011). Moreover, it was reported that GCGs including maplexin E (ME) and MF were able to protect ceramide by the inhibition of its degradation enzyme (namely, ceramidase) (Kamori et al., 2016). ME and MF also increased the production of ceramide, which is a critical component of the stratum corneum that maintains skin tissue integrity (Kamori et al., 2016). In addition, GCGs including GB showed protective effect on human epidermal keratinocytes PHK16-0b cells via the modulation of cell proliferation/differentiation and upregulation of gene notch homolog 1 (NOTCH1), which is a key biomarker of keratinocyte differentiation (Kato et al., 2019). Therefore, the findings from our current study, along with data from studies reported by other groups, support that GCGs showed skin protective effects and have the potential to be further developed as bioactive ingredients for skin care products. Nevertheless, further studies are warranted to evaluate whether GCGs are able to show skin beneficial effects, such as the prevention of skin wrinkle formation, using in vivo models.

In summary, a collection of GTs including GCGs, PGG, and TA, along with their structure basic unit, GLA, and GTs' gut microbial metabolite, PYG, showed inhibitory effects on the activity of elastase. The inhibition capacity of GTs on elastase was enhanced when the number of galloyl moieties increased. This SAR observation was supported by mechanistic studies with molecular docking. In addition, GCGs could penetrate skin barrier based on in silico modeling, and GA showed favorable skin permeability in the PAMPA assay and stability. Moreover, some GCGs showed cytoprotective effects against oxidative stress induced toxicity in human keratinocytes HaCaT cells at non-toxic concentrations. Overall, the findings from this study add to the growing body of evidence supporting the skin beneficial effects of GCGs from red maple and their potential utilization as bioactive cosmeceuticals for skin care products.

Acknowledgements

Data were acquired from instruments located at the University of Rhode Island in the RI-INBRE core facility obtained from Grant # P20GM103430 from the National Center for Research Resources (NCRR), a component of the National Institutes of Health (NIH). H.L. was supported by funding from the Department of Education of Guangdong Province (2017KSYS010 and 2019KZDZX2003) and Jiangmen Program for Innovative Research Team (No: 2018630100180019806).

Conflict of interest

HM and NPS are co-inventors on a patent (Patent No.: US 10,155,738 B2) issued to the Rhode Island Board of Education on methods of skin-whitening using a gallotannin, which has been licensed to Verdure Sciences (Noblesville, IN, USA). The other authors declare no conflicts of interest.

REFERENCE

- Boyd, E. M. (1965). The Acute Toxicity of Tannic Acid Administered Intragastrically. *Canadian Medical Association Journal*, 92(25), 1292. Retrieved from /pmc/articles/PMC1928430/?report=abstract
- Chen, C. P., Chen, C. C., Huang, C. W., & Chang, Y. C. (2018). Evaluating molecular properties involved in transport of small molecules in stratum corneum: A quantitative structure-activity relationship for skin permeability. *Molecules*, 23(4). <https://doi.org/10.3390/molecules23040911>
- Choubey, S., Varughese, L. R. ache., Kumar, V., & Beniwal, V. (2015). Medicinal importance of gallic acid and its ester derivatives: a patent review. *Pharmaceutical Patent Analyst*, Vol. 4, pp. 305–315. <https://doi.org/10.4155/ppa.15.14>

- Daina, A., Michielin, O., & Zoete, V. (2017). SwissADME: A free web tool to evaluate pharmacokinetics, drug-likeness and medicinal chemistry friendliness of small molecules. *Scientific Reports*, 7. <https://doi.org/10.1038/srep42717>
- Dal Belo, S. E., Gaspar, L. R., Maia Campos, P. M. B. G., & Marty, J. P. (2009). Skin penetration of epigallocatechin-3-gallate and quercetin from green tea and Ginkgo biloba extracts vehiculated in cosmetic formulations. *Skin Pharmacology and Physiology*, 22(6), 299–304. <https://doi.org/10.1159/000241299>
- Engels, C., Knödler, M., Zhao, Y. Y., Carle, R., Gänzle, M. G., & Schieber, A. (2009). Antimicrobial activity of gallotannins isolated from mango (*Mangifera indica* L.) kernels. *Journal of Agricultural and Food Chemistry*, 57(17), 7712–7718. <https://doi.org/10.1021/jf901621m>
- Gkogkolou, P., & Böhm, M. (2012, July). Advanced glycation end products: Keyplayers in skin aging? *Dermato-Endocrinology*, Vol. 4. <https://doi.org/10.4161/derm.22028>
- Goenka, S., Ceccoli, J., & Simon, S. R. (2019). Anti-melanogenic activity of ellagitannin casuarictin in B16F10 mouse melanoma cells. *Natural Product Research*. <https://doi.org/10.1080/14786419.2019.1636242>
- González-Sarrías, A., Ma, H., Edmonds, M. E., & Seeram, N. P. (2013). Maple polyphenols, ginnalins A-C, induce S- and G2/M-cell cycle arrest in colon and breast cancer cells mediated by decreasing cyclins A and D1 levels. *Food Chemistry*, 136(2), 636–642. <https://doi.org/10.1016/j.foodchem.2012.08.023>
- González-Sarrías, A., Yuan, T., & Seeram, N. P. (2012). Cytotoxicity and structure activity relationship studies of maplexins A-I, gallotannins from red maple (*Acer rubrum*). *Food and Chemical Toxicology*, 50(5), 1369–1376. <https://doi.org/10.1016/j.fct.2012.02.031>
- Ho, L. L., Chen, W. J., Lin-Shiau, S. Y., & Lin, J. K. (2002). Penta-O-galloyl- β -D-glucose inhibits the invasion of mouse melanoma by suppressing metalloproteinase-9 through down-regulation of activator protein-1. *European Journal of Pharmacology*, 453(2–3), 149–158. [https://doi.org/10.1016/S0014-2999\(02\)02340-3](https://doi.org/10.1016/S0014-2999(02)02340-3)
- Hsu, Y. C., Weng, H. C., Lin, S. R., & Chien, Y. W. (2007). Curcuminoids - Cellular uptake by human primary colon cancer cells as quantitated by a sensitive Hplc assay and its relation with the inhibition of proliferation and apoptosis. *Journal of Agricultural and Food Chemistry*, 55(20), 8213–8222.

<https://doi.org/10.1021/jf070684v>

- Ichihashi, M., Yagi, M., Nomoto, K., & Yonei, Y. (2011). Glycation Stress and Photo-Aging in Skin. *Anti-Aging Medicine*, 8(3), 23–29. <https://doi.org/10.3793/jaam.8.23>
- Imokawa, G. (2009). Mechanism of UVB-induced wrinkling of the skin: Paracrine cytokine linkage between keratinocytes and fibroblasts leading to the stimulation of elastase. *Journal of Investigative Dermatology Symposium Proceedings*, 14(1), 36–43. <https://doi.org/10.1038/jidsymp.2009.11>
- Imokawa, G., & Ishida, K. (2015). Biological mechanisms underlying the ultraviolet radiation-induced formation of skin wrinkling and sagging I: Reduced skin elasticity, highly associated with enhanced dermal elastase activity, triggers wrinkling and sagging. *International Journal of Molecular Sciences*, 16(4), 7753–7775. <https://doi.org/10.3390/ijms16047753>
- Johnson, S. L., Kirk, R. D., Dasilva, N. A., Ma, H., Seeram, N. P., & Bertin, M. J. (2019). Polyphenol microbial metabolites exhibit gut and blood–brain barrier permeability and protect murine microglia against lps-induced inflammation. *Metabolites*, 9(4). <https://doi.org/10.3390/metabo9040078>
- Kamori, A., Kato, A., Miyawaki, S., Koyama, J., Nash, R. J., Fleet, G. W. J., ... Adachi, I. (2016). Dual action of acertannins as potential regulators of intracellular ceramide levels. *Tetrahedron Asymmetry*, 27(22–23), 1177–1185. <https://doi.org/10.1016/j.tetasy.2016.09.006>
- Kato, A., Koyama, J., Shinzawa, K., Imaeda, S., Adachi, I., Nash, R. J., ... Ishikawa, F. (2019). Ginnalin B induces differentiation markers and modulates the proliferation/differentiation balance via the upregulation of NOTCH1 in human epidermal keratinocytes. *Bioorganic and Medicinal Chemistry*, 27(11), 2172–2180. <https://doi.org/10.1016/j.bmc.2019.04.008>
- Kiss, A. K., & Piwowarski, J. P. (2016). Ellagitannins, Gallotannins and their Metabolites- The Contribution to the Anti-Inflammatory Effect of Food Products and Medicinal Plants. *Current Medicinal Chemistry*, 25(37), 4946–4967. <https://doi.org/10.2174/0929867323666160919111559>
- Lee, C. S., Jang, E. R., Kim, Y. J., Seo, S. J., Choi, S. E., & Lee, M. W. (2011). Polyphenol acertannin prevents TRAIL-induced apoptosis in human keratinocytes by suppressing apoptosis-related protein activation. *Chemico-Biological Interactions*, 189(1–2), 52–59. <https://doi.org/10.1016/j.cbi.2010.10.009>
- Lee, K. K., Cho, J. J., Park, E. J., & Choi, J. D. (2001). Anti-elastase and anti-hyaluronidase of phenolic

- substance from Areca catechu as a new anti-ageing agent. *International Journal of Cosmetic Science*, 23(6), 341–346. <https://doi.org/10.1046/j.0412-5463.2001.00102.x>
- Lee, K. K., Kim, J. H., Cho, J. J., & Choi, J. D. (1999). Inhibitory effects of 150 plant extracts on elastase activity, and their anti-inflammatory effects. *International Journal of Cosmetic Science*, 21(2), 71–82. <https://doi.org/10.1046/j.1467-2494.1999.181638.x>
- Li, C., & Seeram, N. P. (2018). Ultra-fast liquid chromatography coupled with electrospray ionization time-of-flight mass spectrometry for the rapid phenolic profiling of red maple (*Acer rubrum*) leaves. *Journal of Separation Science*, 41(11), 2331–2346. <https://doi.org/10.1002/jssc.201800037>
- Li, L., Ma, H., Liu, T., Ding, Z., Liu, W., Gu, Q., ... Xu, J. (2020). Glucitol-core containing gallotannins-enriched red maple (*Acer rubrum*) leaves extract alleviated obesity via modulating short-chain fatty acid production in high-fat diet-fed mice. *Journal of Functional Foods*, 70, 103970. <https://doi.org/10.1016/j.jff.2020.103970>
- Liu, C., Guo, H., Dain, J. A., Wan, Y., Gao, X. H., Chen, H. D., ... Ma, H. (2020). Cytoprotective effects of a proprietary red maple leaf extract and its major polyphenol, ginnalin A, against hydrogen peroxide and methylglyoxal induced oxidative stress in human keratinocytes. *Food & Function*, 11(6), 5105–5114. <https://doi.org/10.1039/d0fo00359j>
- Liu, C., Guo, H., DaSilva, N. A., Li, D., Zhang, K., Wan, Y., ... Ma, H. (2019). Pomegranate (*Punica granatum*) phenolics ameliorate hydrogen peroxide-induced oxidative stress and cytotoxicity in human keratinocytes. *Journal of Functional Foods*, 54, 559–567. <https://doi.org/10.1016/j.jff.2019.02.015>
- Liyanarachchi, G. D., Samarasekera, J. K. R. R., Mahanama, K. R. R., & Hemalal, K. D. P. (2018). Tyrosinase, elastase, hyaluronidase, inhibitory and antioxidant activity of Sri Lankan medicinal plants for novel cosmeceuticals. *Industrial Crops and Products*, 111, 597–605. <https://doi.org/10.1016/j.indcrop.2017.11.019>
- Ma, H., DaSilva, N. A., Liu, W., Nahar, P. P., Wei, Z., Liu, Y., ... Seeram, N. P. (2016). Effects of a Standardized Phenolic-Enriched Maple Syrup Extract on β -Amyloid Aggregation, Neuroinflammation in Microglial and Neuronal Cells, and β -Amyloid Induced Neurotoxicity in *Caenorhabditis elegans*. *Neurochemical Research*. <https://doi.org/10.1007/s11064-016-1998-6>

- Ma, H., Liu, W., Frost, L., Kirschenbaum, L. J., Dain, J. A., & Seeram, N. P. (2016). Glucitol-core containing gallotannins inhibit the formation of advanced glycation end-products mediated by their antioxidant potential. *Food and Function*, 7(5), 2213–2222. <https://doi.org/10.1039/c6fo00169f>
- Ma, H., Wang, L., Niesen, D. B., Cai, A., Cho, B. P., Tan, W., ... Seeram, N. P. (2015). Structure activity related, mechanistic, and modeling studies of gallotannins containing a glucitol-core and α -glucosidase. *RSC Advances*, 5(130), 107904–107915. <https://doi.org/10.1039/c5ra19014b>
- Ma, H., Xu, J., DaSilva, N. A., Wang, L., Wei, Z., Guo, L., ... Seeram, N. P. (2017). Cosmetic applications of glucitol-core containing gallotannins from a proprietary phenolic-enriched red maple (*Acer rubrum*) leaves extract: inhibition of melanogenesis via down-regulation of tyrosinase and melanogenic gene expression in B16F10 melanoma ce. *Archives of Dermatological Research*, 309(4), 265–274. <https://doi.org/10.1007/s00403-017-1728-1>
- Ma, H., Yuan, T., González-Sarrias, A., Li, L., Edmonds, M. E., & Seeram, N. P. (2012). New galloyl derivative from winged sumac (*Rhus copallinum*) fruit. *Natural Product Communications*, 7(1), 45–46. <https://doi.org/10.1177/1934578X1200700116>
- Mecham, R. P., Broekelmann, T. J., Fliszar, C. J., Shapiro, S. D., Welgus, H. G., & Senior, R. M. (1997). Elastin degradation by matrix metalloproteinases: Cleavage site specificity and mechanisms of elastolysis. *Journal of Biological Chemistry*, 272(29), 18071–18076. <https://doi.org/10.1074/jbc.272.29.18071>
- Piowowski, J. P., Kiss, A. K., & Kozłowska-Wojciechowska, M. (2011). Anti-hyaluronidase and anti-elastase activity screening of tannin-rich plant materials used in traditional Polish medicine for external treatment of diseases with inflammatory background. *Journal of Ethnopharmacology*, 137(1), 937–941. <https://doi.org/10.1016/j.jep.2011.05.039>
- Rayudu, G. V., Kadirvel, R., Vohra, P., & Kratzer, F. H. (1970). Toxicity of tannic acid and its metabolites for chickens. *Poultry Science*, 49(4), 957–960. <https://doi.org/10.3382/ps.0490957>
- Rosenbloom, J., Abrams, W. R., & Mecham, R. (1993). Extracellular matrix 4: The elastic fiber. *The FASEB Journal*, 7(13), 1208–1218. <https://doi.org/10.1096/fasebj.7.13.8405806>
- Sheng, J., Liu, C., Petrovas, S., Wan, Y., Chen, H. D., Seeram, N. P., & Ma, H. (2020). Phenolic-enriched maple syrup extract protects human keratinocytes against hydrogen peroxide and methylglyoxal

- induced cytotoxicity. *Dermatologic Therapy*, 33(3). <https://doi.org/10.1111/dth.13426>
- Shetty, P. K., Manikkath, J., Tupally, K., Kokil, G., Hegde, A. R., Raut, S. Y., ... Mutalik, S. (2017). Skin Delivery of EGCG and Silibinin: Potential of Peptide Dendrimers for Enhanced Skin Permeation and Deposition. *AAPS PharmSciTech*, 18(6), 2346–2357. <https://doi.org/10.1208/s12249-017-0718-0>
- Singh, S., Junwal, M., Modhe, G., Tiwari, H., Kurmi, M., Parashar, N., & Sidduri, P. (2013, September 1). Forced degradation studies to assess the stability of drugs and products. *TrAC - Trends in Analytical Chemistry*, Vol. 49, pp. 71–88. <https://doi.org/10.1016/j.trac.2013.05.006>
- Svobodová, A., Psotová, J., & Walterová, D. (2003). Natural phenolics in the prevention of UV-induced skin damage. A review. *Biomedical Papers of the Medical Faculty of the University Palacký, Olomouc, Czechoslovakia*, Vol. 147, pp. 137–145. <https://doi.org/10.5507/bp.2003.019>
- Talas, U., Dunlop, J., Khalaf, S., Leigh, I. M., & Kellsell, D. P. (2000). Human elastase 1: Evidence for expression in the skin and the identification of a frequent frameshift polymorphism. *Journal of Investigative Dermatology*, 114(1), 165–170. <https://doi.org/10.1046/j.1523-1747.2000.00825.x>
- Toyama, B. H., & Hetzer, M. W. (2013, January). Protein homeostasis: Live long, won't prosper. *Nature Reviews Molecular Cell Biology*, Vol. 14, pp. 55–61. <https://doi.org/10.1038/nrm3496>
- Tsuji, N., Moriwaki, S., Suzuki, Y., Takema, Y., & Imokawa, G. (2007). The Role of Elastases Secreted by Fibroblasts in Wrinkle Formation: Implication Through Selective Inhibition of Elastase Activity¶. *Photochemistry and Photobiology*, 74(2), 283–290. [https://doi.org/10.1562/0031-8655\(2001\)0740283troesb2.0.co2](https://doi.org/10.1562/0031-8655(2001)0740283troesb2.0.co2)
- Tsukahara, K., Nakagawa, H., Moriwaki, S., Takema, Y., Fujimura, T., & Imokawa, G. (2006a). Inhibition of ultraviolet-B-induced wrinkle formation by an elastase-inhibiting herbal extract: Implication for the mechanism underlying elastase-associated wrinkles. *International Journal of Dermatology*, 45(4), 460–468. <https://doi.org/10.1111/j.1365-4632.2006.02557.x>
- Tsukahara, K., Nakagawa, H., Moriwaki, S., Takema, Y., Fujimura, T., & Imokawa, G. (2006b). Inhibition of ultraviolet-B-induced wrinkle formation by an elastase-inhibiting herbal extract: Implication for the mechanism underlying elastase-associated wrinkles. *International Journal of Dermatology*, 45(4), 460–468. <https://doi.org/10.1111/j.1365-4632.2006.02557.x>
- Wan, C., Yuan, T., Li, L., Kandhi, V., Cech, N. B., Xie, M., & Seeram, N. P. (2012). Maplexins, new α -

- glucosidase inhibitors from red maple (*Acer rubrum*) stems. *Bioorganic and Medicinal Chemistry Letters*, 22(1), 597–600. <https://doi.org/10.1016/j.bmcl.2011.10.073>
- Yadav, D. K., Khan, F., & Negi, A. S. (2012). Pharmacophore modeling, molecular docking, QSAR, and in silico ADMET studies of gallic acid derivatives for immunomodulatory activity. *Journal of Molecular Modeling*, 18(6), 2513–2525. <https://doi.org/10.1007/s00894-011-1265-3>
- Yuan, T., Wan, C., Liu, K., & Seeram, N. P. (2012). New maplexins F-I and phenolic glycosides from red maple (*Acer rubrum*) bark. *Tetrahedron*, 68(4), 959–964. <https://doi.org/10.1016/j.tet.2011.11.062>
- Zhang, J., Li, L., Kim, S. H., Hagerman, A. E., & Lü, J. (2009). Anti-cancer, anti-diabetic and other pharmacologic and biological activities of penta-galloyl-glucose. *Pharmaceutical Research*. <https://doi.org/10.1007/s11095-009-9932-0>
- Zhang, Y., Ma, H., Yuan, T., & Seeram, N. P. (2015). Red maple (*acer rubrum*) aerial parts as a source of bioactive phenolics. *Natural Product Communications*, 10(8), 1409–1412. <https://doi.org/10.1177/1934578X1501000824>
- Zhao, X., Sun, H., Hou, A., Zhao, Q., Wei, T., & Xin, W. (2005). Antioxidant properties of two gallotannins isolated from the leaves of *Pistacia weinmannifolia*. *Biochimica et Biophysica Acta - General Subjects*, 1725(1), 103–110. <https://doi.org/10.1016/j.bbagen.2005.04.015>

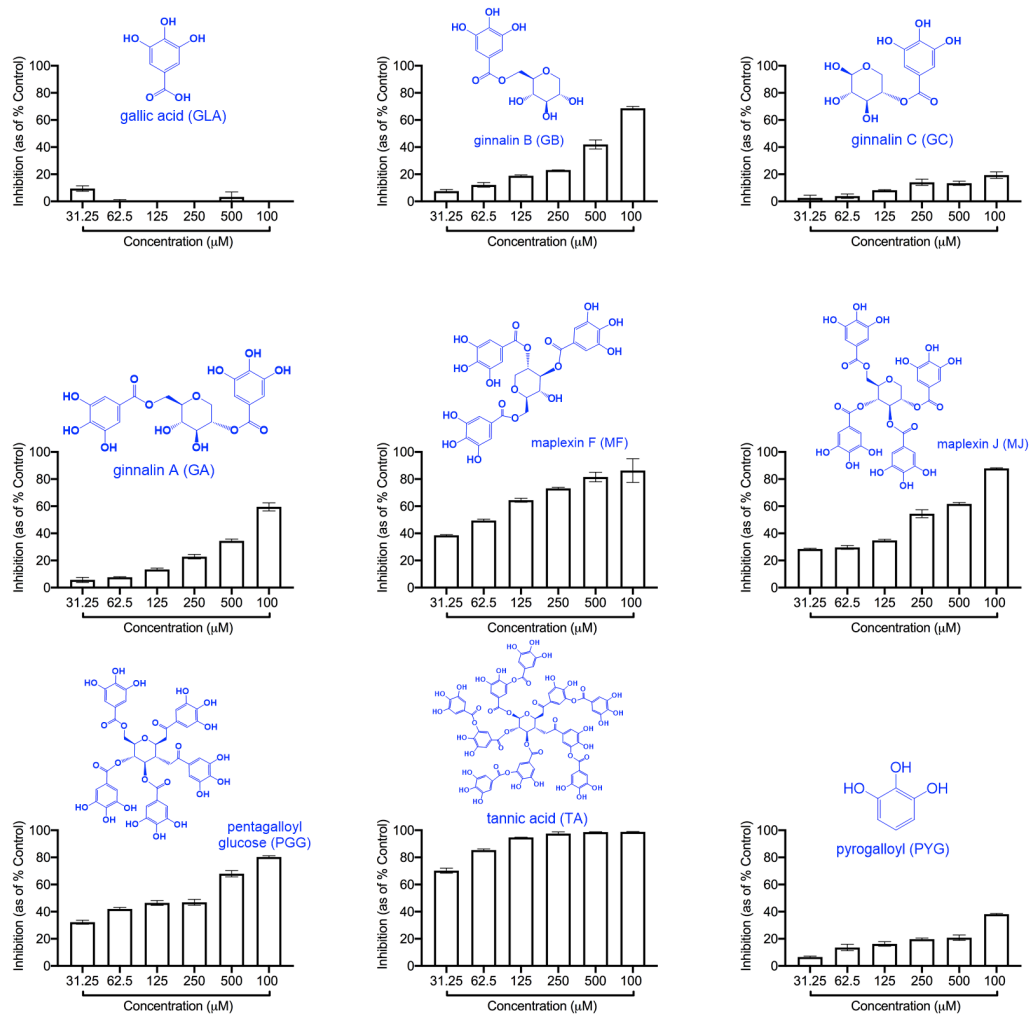


Figure 1. Chemical structures of GTs including GCGs (ginnalins A-C and maplexins F-J), pentagalloyl glucose (PGG), and tannic acid (TA), as well as their structural building moiety gallic acid (GLA) and microbial metabolite pyrogallol (PYG), as well as their inhibitory effects on elastase enzyme. Inhibition values are shown as mean \pm standard deviation (SD) from three independent experiments.

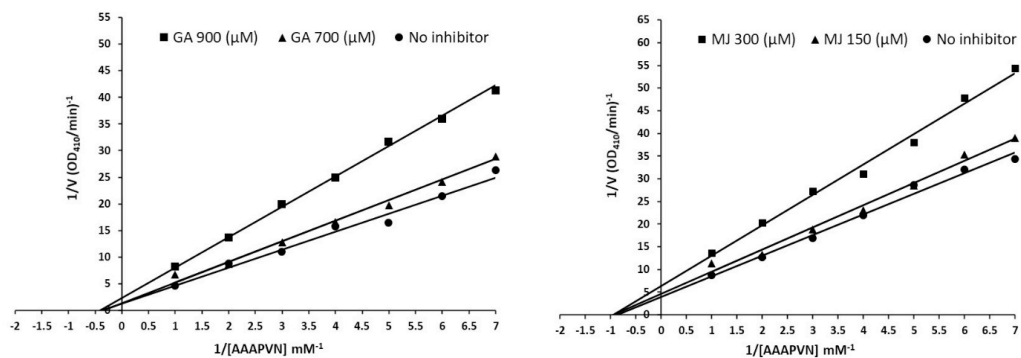


Figure 2. Kinetic assay to determine the inhibition mode of GCGs including GA and MJ on elastase enzyme by plotting the Lineweaver–Burk plots. GA and MJ at two concentrations (ranging from 150-900 μM; close to their IC₅₀ value) were incubated with elastase and substrate AAAPVN (1–1000 μM) at 37 °C for 30 min.

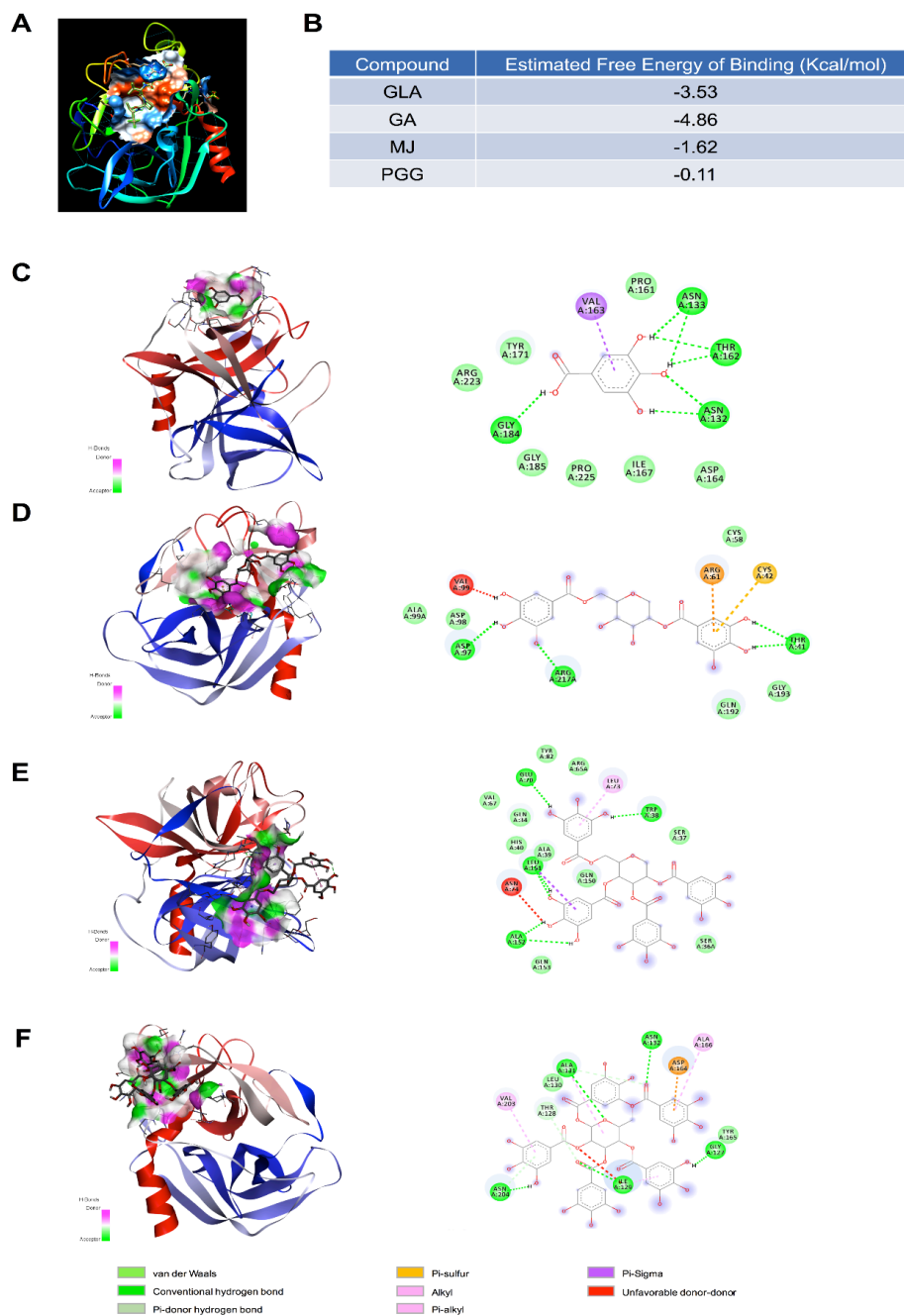


Figure 3. Molecular docking of elastase protein (A) and ligands including GLA, GA, MJ, and PGG. The free binding energy between protein and ligand was estimated (B). Top potential ligand binding sites for GLA (C), GA (D), MJ (E), and PGG (F) and the binding molecular forces were obtained via Site Finder module with MOE.

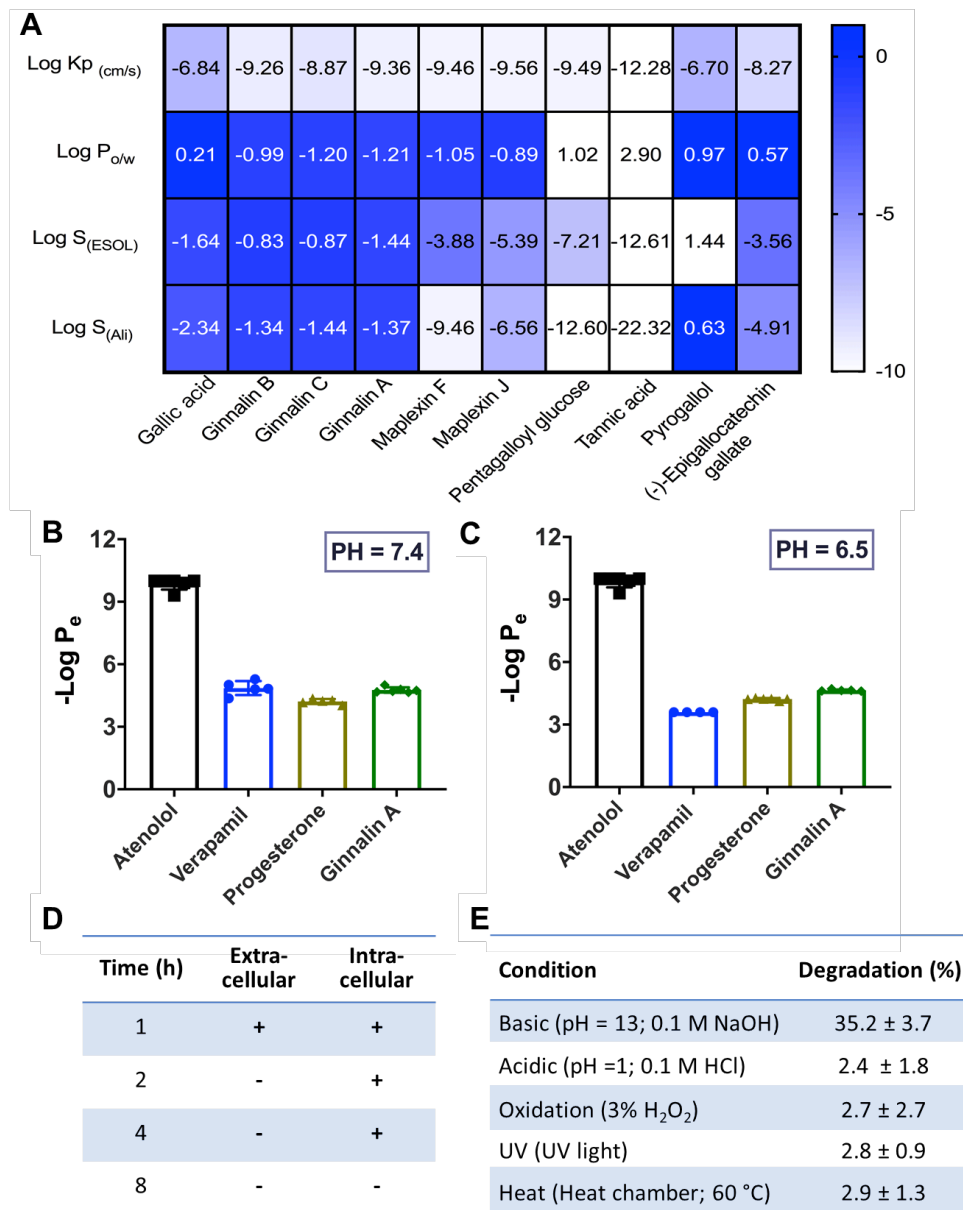


Figure 4. Skin permeability of GTs predicted by the SwissADME tool based on their physico-chemical properties including Log K_p, Log P_{o/w}, Log S(ESOL), and Log S(Ali) (A). The skin permeability of GA verified by biochemical experimental assays including PAMPA (B and C) and cellular uptake assay with human keratinocyte HaCaT cells (D). Degradation of GA in various conditions (E).

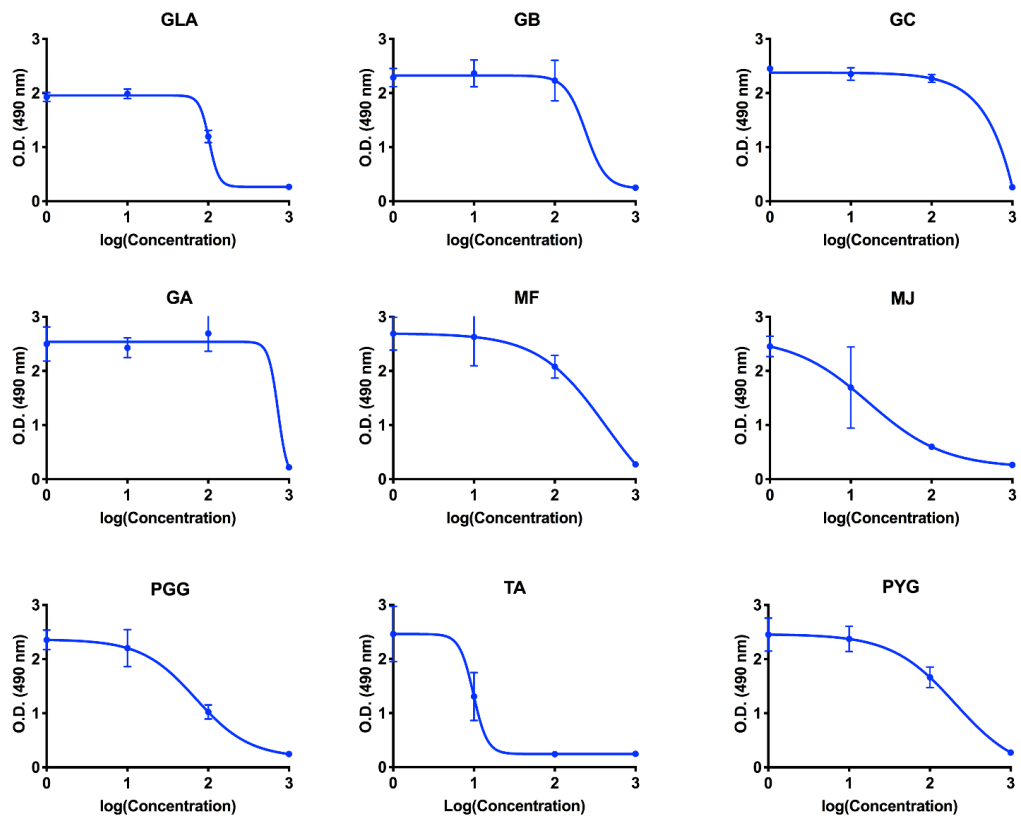


Figure 5. Cytotoxicity of GTs (at concentrations of 10, 1000, and 10000 μ M) including GA, GB, GC, MF, MJ, PGG, and TA, along with their chemical structure unit, GLA, and gut microbial metabolite, PYG, was evaluated in human keratinocytes HaCaT cells by the MTS assay.

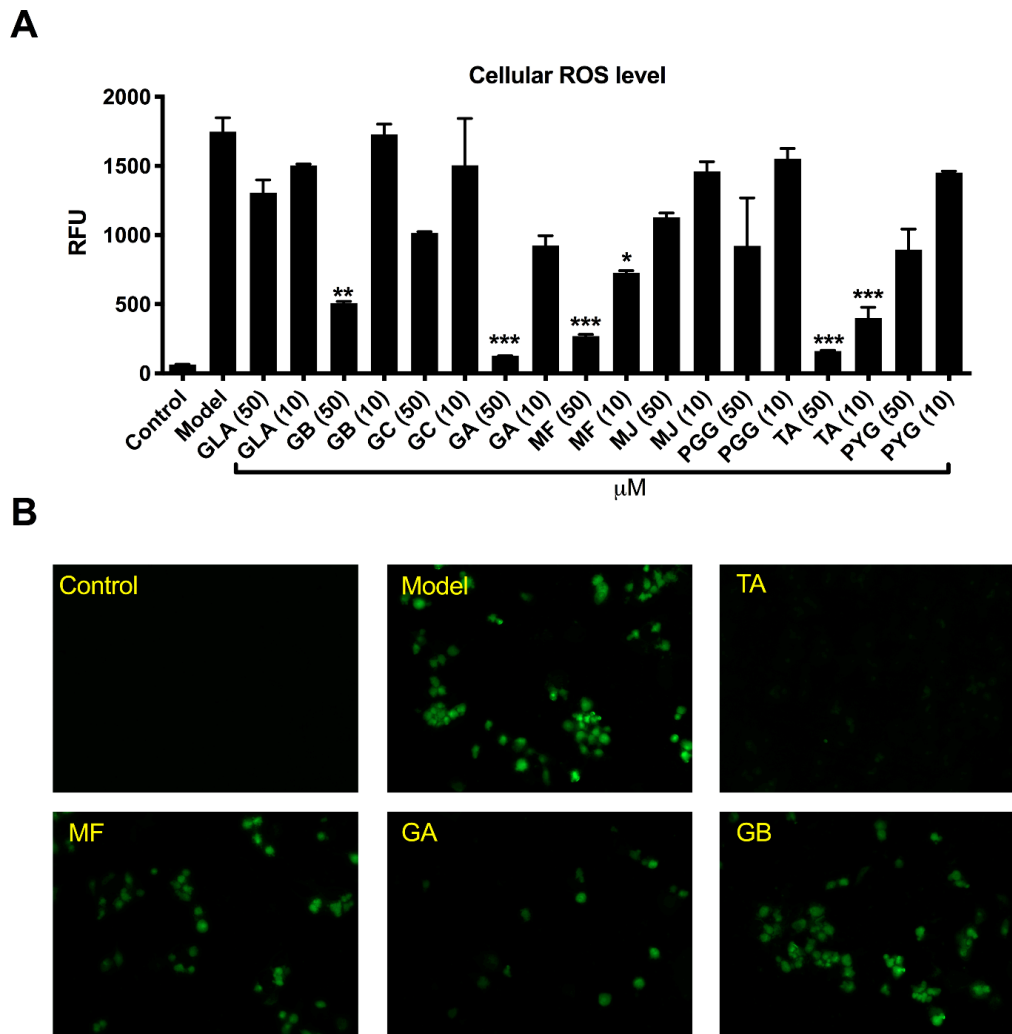


Figure 6. Cytoprotective effects of red maple GTs against H_2O_2 -induced oxidative stress in HaCaT cells. Cells were treated with GTs (10 and 50 $\mu\text{g/mL}$) for 2 h and then incubated with DMEM containing DCFDA (20 μM) for 20 min, followed by exposure of H_2O_2 (400 μM) for 1 h. The ROS level was measured by cellular fluorescence intensity with excitation and emission wavelengths of 485 and 525 nm, respectively (A). Representative fluorescent images of H_2O_2 -exposed HaCaT cells treated with GCGs (B). * $p < 0.05$; ** $p < 0.01$; *** $p < 0.001$ as compared with the model group.

Table 1. Inhibitory effects of GTs on elastase activity.

Compound	# of galloyl group	IC ₅₀ (μM) ^a
gallic acid (GLA)	1	n.d. ^b
ginnalin B (GB)	1	617.4 ± 4.9
ginnalin C (GC)	1	n.d. ^b
ginnalin A (GA)	2	810.6 ± 7.2
maplexin F (MF)	3	250.8 ± 3.2
maplexin J (MJ)	4	237.5 ± 3.9
pentagalloyl glucose (PGG)	5	262.3 ± 4.7
tannic acid (TA)	10	16.1 ± 1.4
pyrogallol (PYG)	0	n.d. ^b
epigallocatechin gallate (EGCG) ^c	1	160.7 ± 3.8
oleanolic acid ^c	0	163.1 ± 2.5

^aIC₅₀ values are shown as mean ± S.D. from three replicates of experiments.

^bn.d.= not determined as the IC₅₀ values are greater than 1000 μM.

^cServed as a positive control.

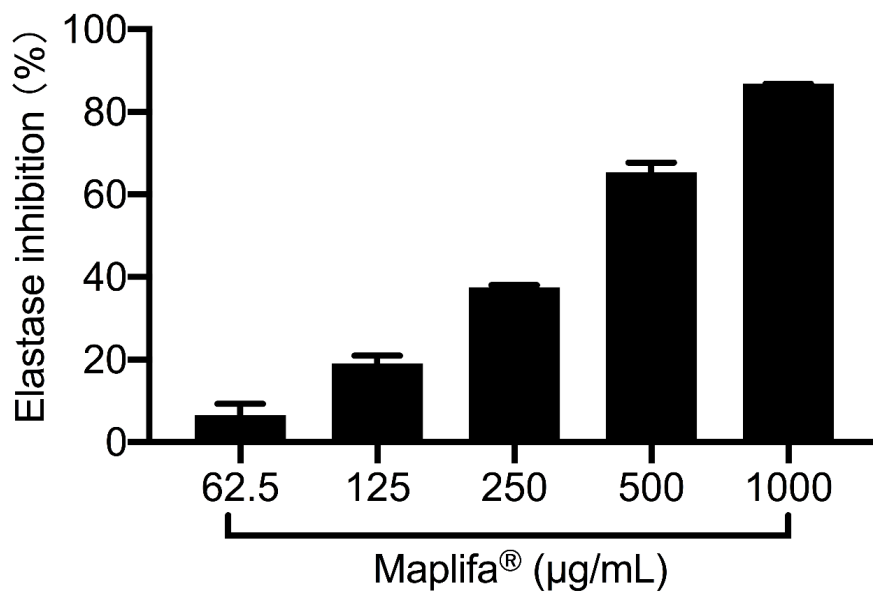


Figure S1. Inhibitory effects of Maplifa[®] on elastase enzyme. Inhibition values are shown as mean \pm standard deviation (SD) from three independent experiments.

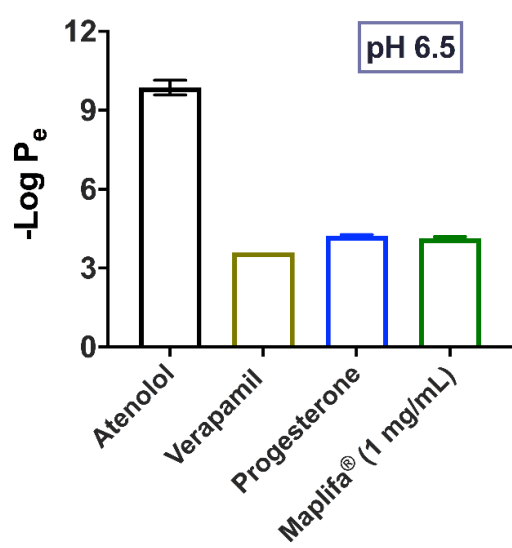
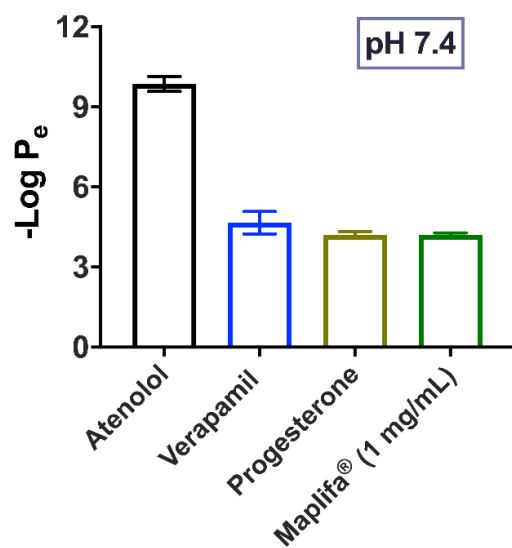


Figure S2. Evaluation of the skin permeability of Maplifa® by the PAMPA assay.

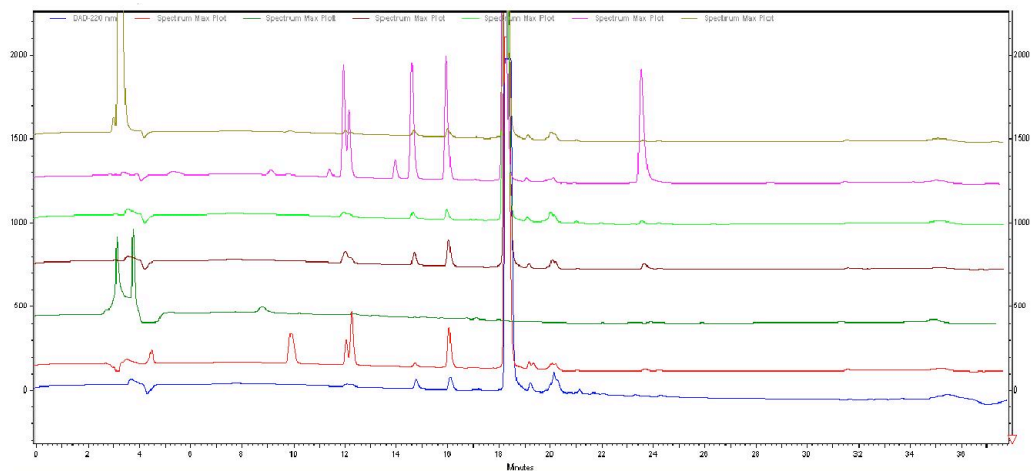


Figure S3. HPLC-DAD profiles of GA in various conditions including basic and acidic environment, UV radiation and heat.

CHAPTER 5

MANUSCRIPT 5

Published: 6 May 2020

Journal of Natural Products, 2020, 83, 6, 2025-2029

**Inhibitory Effect of Cannabidiol on the Activation of NLRP3 Inflammasome is Associated with Its
Modulation of P2X7 Receptor in Human Monocytes**

Chang Liu[†], Hang Ma^{†,*}, Angela L. Slitt^{†,*}, Navindra P. Seeram^{†,*}

[†]Department of Biomedical and Pharmaceutical Sciences, College of Pharmacy, University of Rhode Island,
Kingston, RI 02881, USA

**Authors to whom correspondence should be addressed*

Hang Ma, Phone: +1(401)-874-7654; Email: hang_ma@uri.edu

Angela L. Slitt, Phone: +1(401)-874-7654; Email: angela_slitt@uri.edu

Navindra P. Seeram, +1(401)-874-9367; Email: nseeram@uri.edu

7 Greenhouse Rd, Kingston, RI 02881, USA; Department of Biomedical and Pharmaceutical Sciences,
College of Pharmacy, University of Rhode Island

ABSTRACT: Cannabidiol (CBD), a phytocannabinoid, has been reported to have anti-inflammatory effects associated with NLRP3 inflammasome activation, but its mechanism of anti-inflammasome action remain unclear. Herein, we report CBD's effect on NLRP3 inflammasome activation and its modulation of P2X7, an inflammasome activation-related receptor, in human THP-1 monocytes. CBD (0.1, 1 and 10 μ M) exerted anti-inflammasome activity in LPS-nigericin stimulated THP-1 monocytes by reducing media IL-1 β concentration (by 63.9, 64.1, and 83.1%, respectively), which was similar to the known NLRP3 inflammasome inhibitors, oridonin and MCC950 (16.9 vs. 20.8 and 17.4% respectively; at 10 μ M). CBD (10 μ M) decreased nigericin-alone and nigericin-lipopolysaccharide induced potassium efflux by 13.7 and 13.0 %, respectively in THP-1 monocytes, strongly suggesting P2X7 receptor modulation. Computational docking data supported the potential for CBD binding to the P2X7 receptor via interaction with GluA 72 and VAL 173 residues. Overall, the observed CBD suppressive effect on NLRP3 inflammasome activation in THP-1 monocytes was associated with decreased potassium efflux, as well as *in silico* prediction of P2X7 receptor binding. CBD inhibitory effects on the NLRP3 inflammasome may contribute to the overall anti-inflammatory effects reported for this phytocannabinoid.

KEYWORDS: cannabidiol (CBD), anti-inflammation, NLRP3 inflammasome, P2X7 receptor, THP-1 monocytes, molecular docking

INTRODUCTION

Inflammation is an immune response to harmful stimuli and can be mediated by several biological pathways including the activation of inflammasomes, intracellular proteins complexes which serve as signaling platforms to regulate the production of pro-inflammatory cytokines interleukin-1 β (IL-1 β).¹ One of the most characterized and clinically implicated inflammasome protein complex is known as the NLRP3 inflammasome, which contains members of the nucleotide-binding oligomerization domain-like receptor (NLR) and pyrin domain containing receptor 3.² Activation of NLRP3 inflammasome can be triggered in macrophages by inflammatory stimuli in two steps: 1) stimulation by multiprotein complex assemblies, known as pathogen-associated molecular patterns (PAMPs) including lipopolysaccharide (LPS), to synthesize and mature pro-inflammatory cytokine IL-1 β ;³ 2) a secondary stimulation by stimulus nigericin to induce the assembly and activation of inflammasome complex.⁴ As a response to detrimental stimuli, activation of inflammasomes leads various forms of inflammatory cell death including pyroptosis and necroptosis, and further leads to numerous auto-inflammatory or autoimmune diseases.⁵ Activation of the NLRP3 inflammasome has been linked to a group of purinergic type 2 receptors including the P2X7 receptor, a ligand-gated ion channel modulating intracellular K⁺ efflux.⁶ It has been reported that nigericin, an activator of NLRP3 inflammasome, can bind to P2X7 and increase the permeability of plasma membrane for K⁺ flux, which further facilitates the secretion of IL-1 β .⁶ Therefore, P2X7 receptor has attracted interest as a potential therapeutic target and growing research efforts have been directed towards investigating small molecules as anti-inflammatory agents through the blockade of P2X7.⁷

Cannabidiol (CBD) is a phytocannabinoid with several reported beneficial pharmacological effects including antioxidant, anti-diabetic, anti-cancer and anti-inflammatory effects.⁸ Published studies have reported that CBD ameliorated several inflammatory associated diseases including diabetes and diabetic complications, hypertension, ischemia-reperfusion injury, and neurodegenerative diseases through modulation of key pro-inflammatory transcription factors including NF- κ B, iNOS, and TNF α .^{9,10} Recently, published data suggest that the anti-inflammatory effects of CBD are associated with the regulation of inflammasome activation.^{11,12} For instance, CBD was reported to show hepatoprotective effects against nonalcoholic steatohepatitis in a mice model.¹² Further in vitro studies in murine RAW264.7 macrophages demonstrated that CBD's anti-hepatitis effect was involved with the NLRP3 inflammasome pathway.¹²

However, the effects of CBD on the activation of NLRP3 inflammasome in human THP-1 monocytes and its mechanisms of action remain unclear. Herein, the inhibitory effects of CBD on inflammasome activation were evaluated and compared to the known NLRP3 inflammasome inhibitors, namely, oridonin (a diterpenoid from *Rabdosia rubescens*)¹³ and MCC950 (a synthetic inhibitor; see **Chart 1** for the chemical structures of CBD, oridonin, and MCC950).¹⁴ In addition, CBD's effects on the modulation of the P2X7 receptor, as a function of intracellular K⁺ flux, in human THP-1 monocytes were investigated.

RESULTS AND DISCUSSION

CBD inhibited LPS-induced IL-1 β secretion in THP-1 monocytes

Prior to the evaluation of the anti-inflammasome activity of CBD, its effects on the viability of THP-1 monocytes with and without the presence of lipopolysaccharide (LPS) were assessed. Treatment of CBD (0.1, 1, 10, and 100 μ M) did not induce significant cytotoxicity in THP-1 monocytes as it maintained cell viability at 96.5, 97.6, 103.1, and 99.9%, respectively, as compared to the control group (Supporting Information). Similarly, in the presence of LPS (100 ng/mL), no signs of cytotoxicity were observed with the treatment of CBD (0.1 - 100 μ M; cell viability > 97%; Supporting Information). Next, the anti-inflammatory effects of CBD in THP-1 monocytes were evaluated. Stimulation by LPS significantly increased the concentration of IL-1 β and TNF- α in THP-1 monocytes by 38.7-fold (from 1.3 - 51.2 pg/mL) and 93.1-fold (from 6.9 - 647.2 pg/mL), respectively, compared to the control group. Treatment of CBD (0.1, 1, and 10 μ M) decreased the LPS-induced secretion of IL-1 β to 41.2, 43.5, and 32.9 pg/mL, respectively, while not affecting the level of TNF- α (Figure 1).

It has been reported that CBD can modulate inflammatory responses by both up- and down-regulation of inflammatory cytokines in murine RAW264.7 macrophages. Treatment of hemp oil containing CBD (10.6 μ M) significantly increased several inflammatory cytokines including IL-1 α , IL-6, IL-27, and TNF- α in murine RAW264.7 macrophages.¹⁵ Conversely, CBD (25 μ M) showed anti-inflammatory activity by effectively reducing LPS-induced production of the pro-inflammatory cytokine, TNF- α , in RAW264.7 macrophages.¹⁶ In the current study, CBD reduced the level of the pro-inflammatory cytokine, IL-1 β , while not affecting TNF- α in LPS stimulated THP-1 monocytes, supporting its anti-inflammatory effect. The selective inhibitory effect on IL-1 β by CBD (0.1 - 10 μ M) suggested that this effect could be associated with the activation of the NLRP3 inflammasome, a multiprotein complex that is

responsible for the cleavage and production of IL-1 β . Therefore, CBD's inflammasome-specific inhibitory effects were further evaluated in human monocytes.

CBD inhibited LPS-nigericin induced activation of NLRP3 inflammasome

Specific inhibition of NLRP3 inflammasome activation by CBD was evaluated by measuring LPS-nigericin induced IL-1 β in THP-1 monocytes. Stimulation by LPS and nigericin significantly induced the production of IL-1 β as compared to the LPS-alone treated group (492.1 vs. 51.2 pg/mL). Stimulation by LPS-nigericin also increased the concentration of TNF- α as compared to the LPS-alone treated group (957.6 vs. 647.2 pg/mL), indicating that the stimulation by LPS-nigericin activated the NLRP3 inflammasome (Figure 2). CBD (0.1, 1, and 10 μ M) reduced the concentration of IL-1 β to 177.5, 176.9, and 83.0 pg/mL, respectively, as compared to the LPS-nigericin treated group (Figure 2A). At equivalent concentrations of 10 μ M, CBD showed similar inhibitory activity to the known NLRP3 inflammasome inhibitors, oridonin and MCC950 (16.9 vs. 20.8 and 17.4 %, respectively; Figure 3A). As expected, CBD, oridonin, and MCC950 (all at 10 μ M) did not inhibit the LPS-nigericin induced elevation of TNF- α (661.9, 777.2, and 957.6 vs 957.6 pg/mL, respectively; Figure 2B), suggesting that CBD, similar to oridonin and MCC950, was a specific inhibitor of NLRP3 inflammasome activation.

Previously reported studies have shown that the anti-inflammatory effects of CBD may be attributed to its ability of deactivating the NLRP3 inflammasome.^{11,12} CBD was shown to suppress the expression of several inflammasome-related genes in human gingival mesenchymal stem cells.¹¹ This effect was supported by western blot analysis showing that CBD was able to suppress the expression of proteins including NALP3, IL-18, and CASP1 in the same cell line. However, the level of inflammasome-specific pro-inflammatory cytokines, such as IL-1 β , was not examined. It was also reported that CBD showed hepatoprotective and anti-inflammatory effects by regulation of NF κ B and NLRP3 inflammasome pathways in murine RAW264.7 macrophages.¹² However, solely using murine RAW264.7 macrophages to evaluate CBD's anti-inflammasome activity is insufficient to delineate its inhibitory effects since these cells do not release mature IL-1 β nor do they express apoptotic proteins with a caspase-activating recruiting domain,¹⁷ which are critical factors for the activation of NLRP3 inflammasome. Therefore, the utilization of human THP-1 monocytes has been adopted by other researcher to investigate anti-inflammasome

activity.¹⁸ This is the first report to show that CBD, similar to the known NLRP3 inflammasome inhibitors, oridonin and MCC950, selectively reduced the secretion of IL-1 β in human THP-1 monocytes.

CBD alleviated LPS and nigericin stimulated increase of intracellular potassium but did not affect intracellular calcium in THP-1 monocytes

The anti-inflammasome activity of CBD was further evaluated by assessment of its effects on P2X7 receptor, a ligand-gated cation channel, which modulates the level of intracellular potassium (K⁺) in THP-1 monocytes. Stimulation by nigericin, a K⁺/H⁺ ionophore, led to the formation of cell membrane pore and increased K⁺ efflux in THP-1 monocytes as the intensity of fluorescent dye Green-2 increased as shown by cell flow cytometry. Incubation of THP-1 monocytes with nigericin (1, 5, and 10 μ M) led to increased release of intracellular K⁺ by 18.9, 14.0, and 17.9 %, respectively, as compared to the control group (Figure 3). This effect was alleviated by the treatment of CBD (10 μ M) by reducing nigericin (1, 5, and 10 μ M)-induced K⁺ efflux by 11.0, 9.1, and 13.7 %, respectively.

Inflammatory stimuli, such as LPS, can potentiate nigericin induced cell membrane pore formation, which increases the cell membrane permeabilization for K⁺ efflux.¹⁹ To verify the modulatory effects of CBD on the P2X7 receptor, LPS (100 ng/mL) was co-incubated with nigericin in THP-1 monocytes, followed by CBD treatment. The level of intracellular K⁺ in THP-1 monocytes was determined by measuring the fluorescent intensity of Green-2 dye with flow cytometry. Stimulation by LPS-nigericin increased intracellular K⁺ by 27.5 % as compared to the control group and CBD (1 and 10 μ M) alleviated LPS-nigericin induced intracellular K⁺ efflux by 9.2 and 13.3 %, respectively (Figure 4).

In addition, the effect of CBD on intracellular calcium (Ca⁺) was evaluated with flow cytometry. Stimulation by nigericin (10 μ M) effectively increased the permeability of cell membrane as it increased the cell uptake of fluorescent dye Fluo-3 and intracellular Ca⁺ in THP-1 monocytes by 84.3% comparing to the control group. However, a modulatory effect of CBD (1, 10, and 100 μ M) on intracellular Ca⁺ in THP-1 monocytes was not observed (Supporting Information). CBD's anti-inflammatory effects have been reported to be linked to its up-regulation of intracellular Ca⁺ in RBL-2H3 mast cells leading to cell activation via yet-to-be identified receptors.²⁰ Therefore, further studies on whether CBD's modulation of cellular ion channels in various cell lines can contribute to its anti-inflammasome effects are warranted.

CBD and nigericin interacted with P2X7 receptor

Molecular modeling was used to study the interactions between CBD and the P2X7 receptor to predict possible binding sites. The most favorable binding pocket was identified by comparing the calculated free binding energy in different binding modes. As depicted in Figures 5A and B, the most suitable binding site of CBD was at the upper body, between the head and left flipper of the P2X7 receptor, with the lowest free binding energy of -6.62 kcal/mol. CBD was able to bind to the P2X7 receptor by forming hydrogen bond between its hydroxyl group and residue Glu 172 and the stabilization of the CBD-P2X7 complex may be facilitated by forming a pi-sigma covalent bond between the aromatic ring of CBD and residue VAL 173 of the receptor (Figure 5C).

In summary, the anti-inflammasome activity of CBD and its modulatory effects on the P2X7 receptor in human THP-1 monocytes were investigated. CBD is a specific inhibitor for the activation of NLRP3 inflammasome and showed similar inhibitory potency as the known NLRP3 inflammasome inhibitors, oridonin and MCC950 (at 10 μ M). Findings from this study suggest that the anti-inflammasome effect of CBD was associated with its modulation of the P2X7 receptor in THP-1 monocytes. Additional studies of CBD on cellular signaling pathways involved with the modulation of P2X7 receptor are warranted to further elucidate the mechanisms of its anti-inflammasome activity.

MATERIAL AND METHODS

Chemical and reagents

Cannabidiol (CBD) was purchased from Sigma Chemical Co. (St. Louis, MO, USA). CellTiter-Glo[®] (CTG) 2.0 assay kit was purchased from Promega (Fitchburg, WI, USA). Dimethyl sulfoxide (DMSO), nigericin, phorbol 12-myristate 13-acetate (PMA), and phosphate-buffered saline (PBS) were purchased from Sigma Chemical Co. (St. Louis, MO, USA).

Cell culture and differentiation

Human THP-1 monocytes were purchased from the American Type Culture Collection (ATCC, Rockville, USA). The cells were cultured in Roswell Park Memorial Institute (RPMI) 1640 Medium supplied with 10% fetal bovine serum (FBS) (Gibco, Life Technologies, Gaithersburg, MD, USA) and 1% P/S solution (100 U/ml

penicillin, 100 µg/ml streptomycin (Gibco, Life Technologies, Grand Island, NY, USA). THP-1 monocytes were differentiated by incubation with phorbol 12-myristate 13-acetate (PMA; 25 nM) for 48 hours. After that, PMA was removed and cells were cultured with PMA free medium for another 24 hours.

Cell viability assay

Cytotoxicity of CBD in THP-1 monocytes was measured by using a CTG 2.0 assay.²¹ Briefly, differentiated THP-1 monocytes were seeded into a 96-well plate at 1×10^4 cells per well and incubated with PMA free complete medium for 24 hours. Cells were then treated with CBD at concentrations of 0.1, 1, 10, and 100 µM with the presence or absence of LPS (100 ng/mL) for 24 hours. CTG 2.0 reagent (100 µL) was then added in each well and incubated for 10 min at room temperature. Luminescence intensity was measured using a Spectramax M2 microplate reader (Molecular Devices, Sunnyvale, CA, USA).

Measurement of IL-1 β and TNF- α

THP-1 monocytes were seeded at a density of 5×10^4 cells per well in 48-well plate and differentiated with PMA (25 ng/mL). For the evaluation of LPS-induced cytokines secretion, CBD at concentrations of 0.1, 1, 10, and 100 µM were incubated with cells for 1 hour followed by adding LPS (100 ng/mL). After incubation of 24 hours, the cell culture supernatant was collected for the measurement of IL-1 β and TNF- α . The in vitro anti-inflammasome activity of CBD was evaluated by measuring the concentrations of LPS- and nigericin-induced cytokines with previously reported method.²² THP-1 monocytes were treated with LPS (100 ng/mL) for 4 hours, followed by treatment of CBD (0.1, 1, 10, and 100 µM) for 1 hour. Then, nigericin (10 µM) was incubated with the cells for 1 hour and the cell culture supernatant was collected. The levels of IL-1 β and TNF- α were determined using specific ELISA kits (BioLegend, San Diego, CA, USA).

Intercellular potassium and calcium measurement

THP-1 monocytes were seeded at a density of 5×10^6 cells per well in 6-well plates. The differentiated THP-1 monocytes were incubated with CBD (10 µM) for 30 mins prior to incubating with nigericin (10 µM) for 30 mins. To measure the intracellular potassium or calcium, fluorescent dye Green-2 or Fluo-3 (Abcam; Cambridge, MA, USA) was added into each well and incubated for 30 mins, followed by washing with PBS. Level of intercellular potassium in THP-1 monocytes was measured by flow cytometric assay.²³

Molecular Docking

The 3D structural coordinates of CBD were obtained from the human metabolome database (www.HMDB.ca). Biovia Discovery Studio Visualizer 4.5 was used to convert to the PDB file format. The structural coordinates of P2X7 receptor were retrieved in PDB format from the RCSB protein data bank (www.rcsb.org; PDB ID: 5U1L). AutodockTools 1.5.6 was used to perform molecular docking with Autodock 4.2 algorithm.

Statistical analysis

Statistical analysis was performed using GraphPad Prism 6 (GraphPad Software, La Jolla, CA, USA). Data were shown as mean \pm standard deviation (S.D). One-way analysis of variance with multiple comparisons and Student-Newman-Keuls (SNK) test were performed. A *p*-value that less than 0.05 was defined as a statistical significance between the two groups.

ASSOCIATED CONTENT

Supporting Information

Data for the effects of CBD on the viability of THP-1 monocytes and the intracellular calcium in THP-1 are available free of charge via the Internet at <http://pubs.acs.org>.

AUTHOR INFORMATION

Corresponding Authors

* Tel/Fax: 401-874-9367/5787; E-mail: hang_ma@uri.edu (H. Ma)

* Tel/Fax: 401-874-5020/5787; Email: angela_slitt@uri.edu (A. L. Slitt)

* Tel/Fax: 401-874-9367/5787; Email: nseeram@uri.edu (N. P. Seeram)

ORCID

Hang Ma: 0000-0001-7565-6889

Navindra P. Seeram: 0000-0001-7064-2904

Notes

The authors declare no competing financial interest.

ACKNOWLEDGMENTS

Data were acquired from instruments located at the University of Rhode Island in the RI-INBRE core facility obtained from Grant P20GM103430 from the National Center for Research Resources (NCRR), a component of the National Institutes of Health (NIH).

REFERENCE

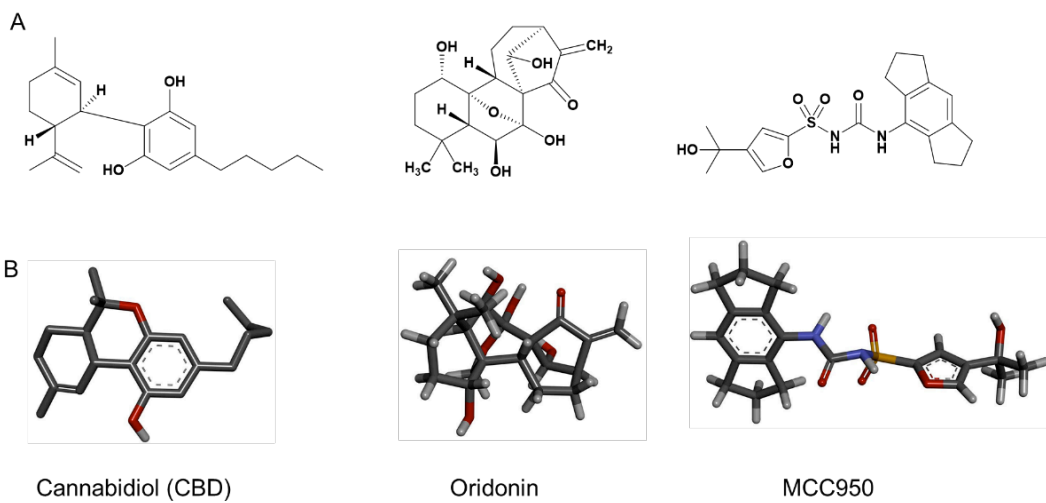
- (1) Guo, H.; Callaway, J. B.; Ting, J. P. Y. Inflammasomes: Mechanism of action, role in disease, and therapeutics. *Nature Medicine*. 2015. <https://doi.org/10.1038/nm.3893>.
- (2) Davis, B. K.; Wen, H.; Ting, J. P.-Y. The inflammasome NLRs in immunity, inflammation, and associated diseases. *Annu. Rev. Immunol.* **2011**. <https://doi.org/10.1146/annurev-immunol-031210-101405>.
- (3) Bauernfeind, F. G.; Horvath, G.; Stutz, A.; Alnemri, E. S.; MacDonald, K.; Speert, D.; Fernandes-Alnemri, T.; Wu, J.; Monks, B. G.; Fitzgerald, K. A.; et al. Cutting edge: NF-KB activating pattern recognition and cytokine receptors license NLRP3 inflammasome activation by regulating NLRP3 expression. *J. Immunol.* **2009**. <https://doi.org/10.4049/jimmunol.0901363>.
- (4) Muñoz-Planillo, R.; Kuffa, P.; Martínez-Colón, G.; Smith, B. L.; Rajendiran, T. M.; Núñez, G. K+ Efflux is the common trigger of NLRP3 inflammasome activation by bacterial toxins and particulate matter. *Immunity* **2013**. <https://doi.org/10.1016/j.immuni.2013.05.016>.
- (5) Schroder, K.; Tschopp, J. The inflammasomes. *Cell*. 2010. <https://doi.org/10.1016/j.cell.2010.01.040>.
- (6) Di Virgilio, F. Liaisons dangereuses: P2X7 and the inflammasome. *Trends in Pharmacological Sciences*. 2007. <https://doi.org/10.1016/j.tips.2007.07.002>.
- (7) Bartlett, R.; Stokes, L.; Sluyter, R. The P2x7 Receptor channel: recent developments and the use of P2x7 antagonists in models of disease. *Pharmacol. Rev.* **2014**. <https://doi.org/10.1124/pr.113.008003>.
- (8) Mechoulam, R.; Parker, L. A.; Gallily, R. Cannabidiol: An overview of some pharmacological Aspects. *J. Clin. Pharmacol.* **2002**. <https://doi.org/10.1002/j.1552-4604.2002.tb05998.x>.
- (9) Burstein, S. Cannabidiol (CBD) and its analogs: A review of their effects on inflammation. *Bioorganic and Medicinal Chemistry*. 2015. <https://doi.org/10.1016/j.bmc.2015.01.059>.
- (10) Booz, G. W. Cannabidiol as an emergent therapeutic strategy for lessening the impact of inflammation on oxidative stress. *Free Radical Biology and Medicine*. 2011. <https://doi.org/10.1016/j.freeradbiomed.2011.01.007>.
- (11) Libro, R.; Scionti, D.; Diomede, F.; Marchisio, M.; Grassi, G.; Pollastro, F.; Piattelli, A.; Bramanti,

- P.; Mazzon, E.; Trubiani, O. Cannabidiol modulates the immunophenotype and inhibits the activation of the inflammasome in human gingival mesenchymal stem cells. *Front. Physiol.* **2016**. <https://doi.org/10.3389/fphys.2016.00559>.
- (12) Huang, Y.; Wan, T.; Pang, N.; Zhou, Y.; Jiang, X.; Li, B.; Gu, Y.; Huang, Y.; Ye, X.; Lian, H.; et al. Cannabidiol protects livers against nonalcoholic steatohepatitis induced by high-fat high cholesterol diet via regulating NF-KB and NLRP3 inflammasome pathway. *J. Cell. Physiol.* **2019**. <https://doi.org/10.1002/jcp.28728>.
- (13) He, H.; Jiang, H.; Chen, Y.; Ye, J.; Wang, A.; Wang, C.; Liu, Q.; Liang, G.; Deng, X.; Jiang, W.; et al. Oridonin is a covalent NLRP3 inhibitor with strong anti-Inflammasome activity. *Nat. Commun.* **2018**. <https://doi.org/10.1038/s41467-018-04947-6>.
- (14) Perera, A. P.; Fernando, R.; Shinde, T.; Gundamaraju, R.; Southam, B.; Sohal, S. S.; Robertson, A. A. B.; Schroder, K.; Kunde, D.; Eri, R. MCC950, a specific small molecule inhibitor of NLRP3 inflammasome attenuates colonic inflammation in spontaneous colitis mice. *Sci. Rep.* **2018**. <https://doi.org/10.1038/s41598-018-26775-w>.
- (15) Muthumalage, T.; Rahman, I. Cannabidiol differentially regulates basal and LPS-induced inflammatory responses in macrophages, lung epithelial cells, and fibroblasts. *Toxicol. Appl. Pharmacol.* **2019**. <https://doi.org/10.1016/j.taap.2019.114713>.
- (16) Ben-Shabat, S.; Hanuš, L. O.; Katzavian, G.; Gallily, R. New cannabidiol derivatives: synthesis, binding to cannabinoid receptor, and evaluation of their antiinflammatory activity. *J. Med. Chem.* **2006**. <https://doi.org/10.1021/jm050709m>.
- (17) Pelegrin, P.; Barroso-Gutierrez, C.; Surprenant, A. P2X 7 receptor differentially couples to distinct release pathways for IL-1 β in mouse macrophage . *J. Immunol.* **2008**. <https://doi.org/10.4049/jimmunol.180.11.7147>.
- (18) Chanput, W.; Mes, J. J.; Wichers, H. J. THP-1 cell line: An in vitro cell model for immune modulation approach. *International Immunopharmacology.* **2014**. <https://doi.org/10.1016/j.intimp.2014.08.002>.
- (19) Clark, A. K.; Staniland, A. A.; Marchand, F.; Kaan, T. K. Y.; McMahon, S. B.; Malcangio, M. P2X7-dependent release of interleukin-1 β and nociception in the spinal cord following

- lipopolysaccharide. *J. Neurosci.* **2010**. <https://doi.org/10.1523/JNEUROSCI.3295-09.2010>.
- (20) Giudice, E. Del; Rinaldi, L.; Passarotto, M.; Facchinetti, F.; D'Arrigo, A.; Guiotto, A.; Carbonare, M. D.; Battistin, L.; Leon, A. Cannabidiol, unlike synthetic cannabinoids, triggers activation of RBL-2H3 mast cells. *J. Leukoc. Biol.* **2007**. <https://doi.org/10.1189/jlb.1206738>.
- (21) Liu, C.; Guo, H.; DaSilva, N. A.; Li, D.; Zhang, K.; Wan, Y.; Gao, X. H.; Chen, H. D.; Seeram, N. P.; Ma, H. Pomegranate (*Punica granatum*) phenolics ameliorate hydrogen peroxide-induced oxidative stress and cytotoxicity in human keratinocytes. *J. Funct. Foods* **2019**. <https://doi.org/10.1016/j.jff.2019.02.015>.
- (22) Shi, Y.; Wang, H.; Zheng, M.; Xu, W.; Yang, Y.; Shi, F. Ginsenoside Rg3 suppresses the NLRP3 inflammasome activation through inhibition of its assembly. *FASEB J.* **2020**. <https://doi.org/10.1096/fj.201901537R>
- (23) Sekar, P.; Huang, D. Y.; Chang, S. F.; Lin, W. W. Coordinate effects of P2X7 and extracellular acidification in microglial cells. *Oncotarget* **2018**. <https://doi.org/10.18632/oncotarget.24331>.

Chart 1. Chemical structure of CBD, oridonin, and MCC950 (A); Chemical structures shown in 3D model

(B).



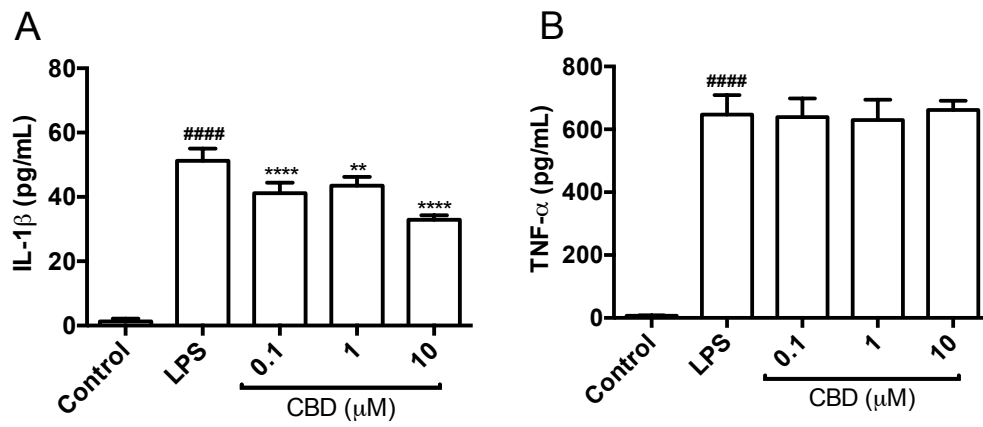


Figure 1. Effects of CBD on the LPS-induced secretion of cytokines IL-1 β (A) and TNF- α (B) in THP-1 monocytes. Cells were treated with CBD (0.1, 1, and 10 μ M) and incubated for 1 hour. LPS (100 ng/mL) was incubated for 24 hours and the supernatant was collected. The concentration of IL-1 β and TNF- α were determined using ELISA kits.

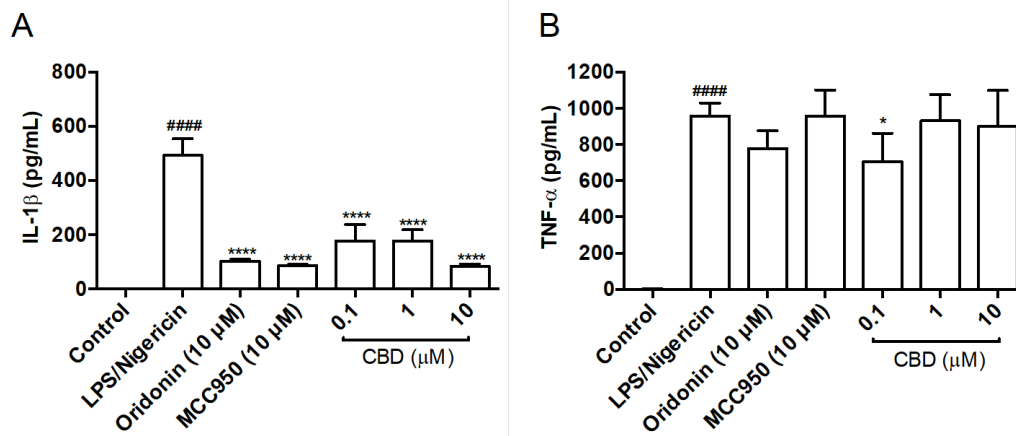


Figure 2. CBD's specific inhibition of NLRP3 inflammasome. LPS (100 ng/mL) was added to THP-1 monocytes for 4 hours followed by the treatment of CBD (0.1, 1, and 10 μ M), oridonin (10 μ M), or MCC950 (10 μ M) for 1 hour. Nigericin (10 μ M) was then added and incubated for 1 hour. Supernatant was collected and measured for the level of IL-1 β (A) and TNF- α (B) using ELISA kits.

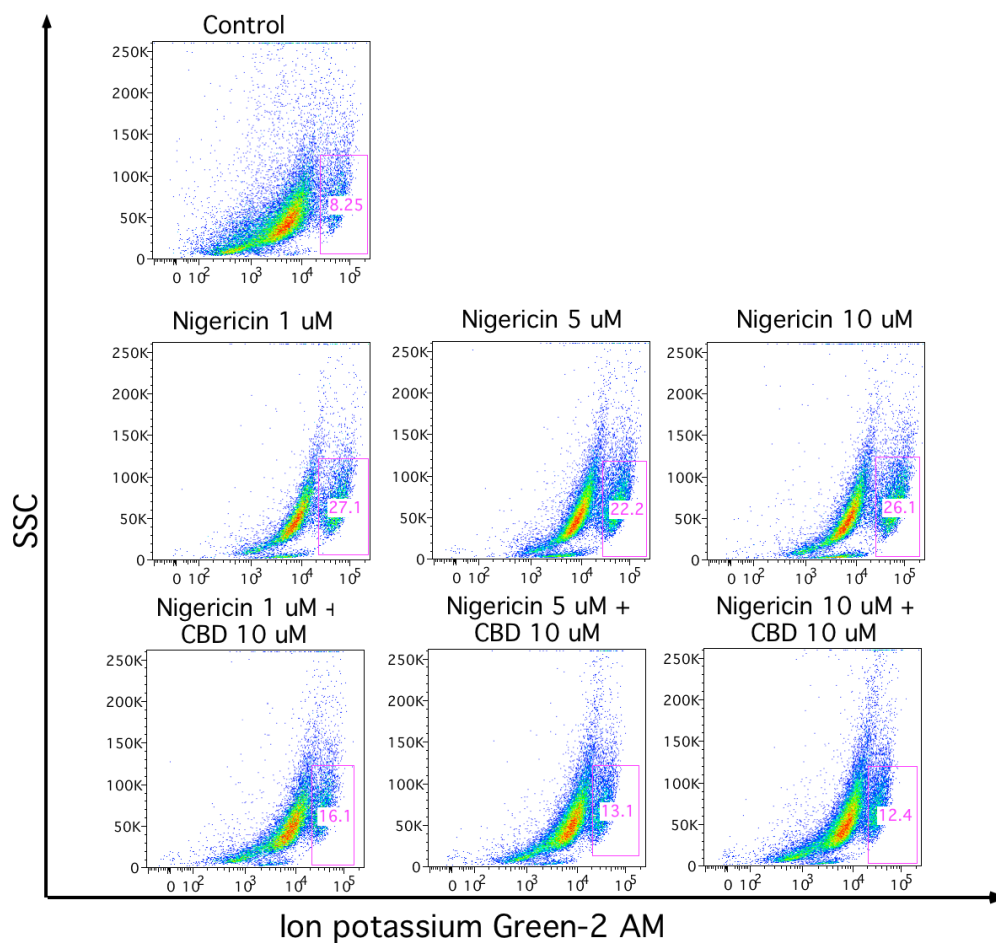


Figure 3. Effects of CBD and nigericin on intracellular potassium in THP-1 monocytes. Nigericin (1, 5, and 10 μ M) was added to THP-1 monocytes for 30 mins followed by the treatment of CBD (10 μ M) for 30 mins. The cells were stained with ion potassium Green-2 AM dye and the fluorescent intensity was measured by flow cytometry.

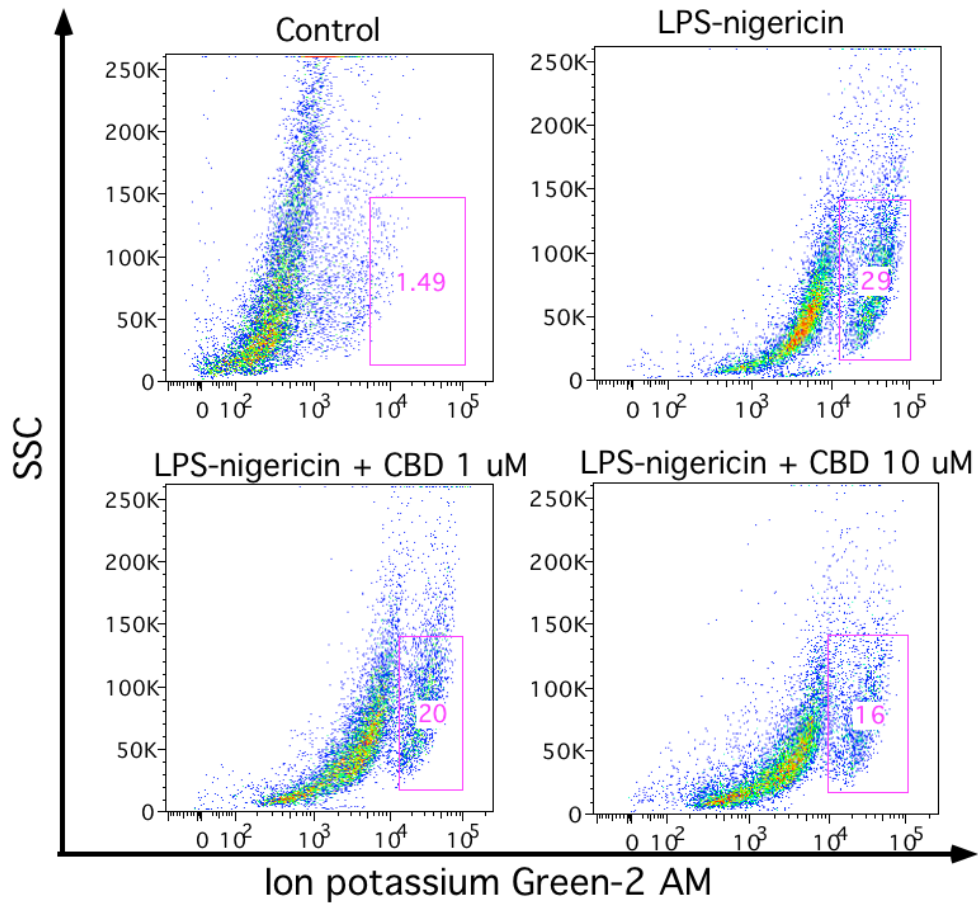


Figure 4. Effects of CBD on LPS-nigericin stimulated intracellular potassium in THP-1 monocytes. LPS (100 ng/mL) was added to THP-1 monocytes for 4 hours followed by the treatment of CBD (1 and 10 μ M) for 1 hour. Nigericin (10 μ M) was then added and incubated for 1 hour. The cells were stained with ion potassium Green-2 AM dye and the fluorescent intensity was measured by flow cytometry.

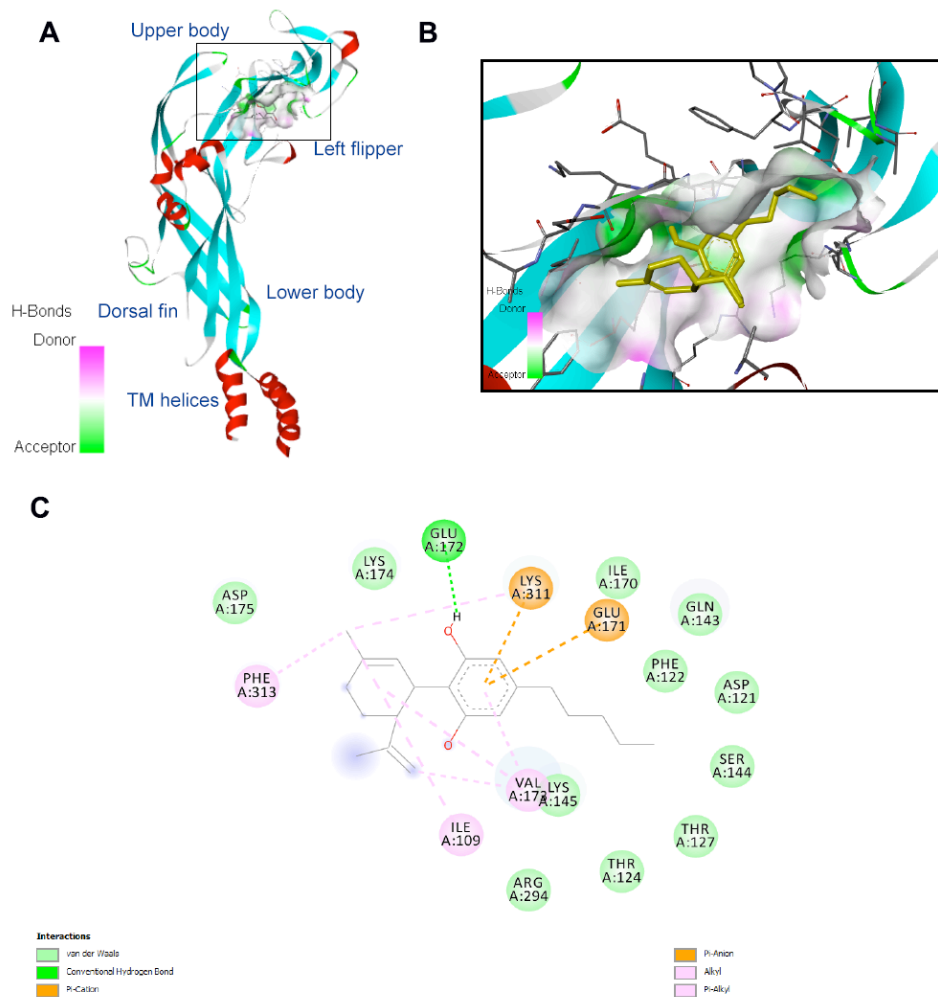


Figure 5. Interactions between CBD and the P2X7 receptor predicted by molecular docking. CBD binds to the P2X7 receptor at a site located at the head and left flipper of the P2X7 receptor's upper body (A). Enlarged view of CBD at the binding site in the P2X7 receptor (B). Illustration of types of interaction between CBD and the P2X7 receptor.

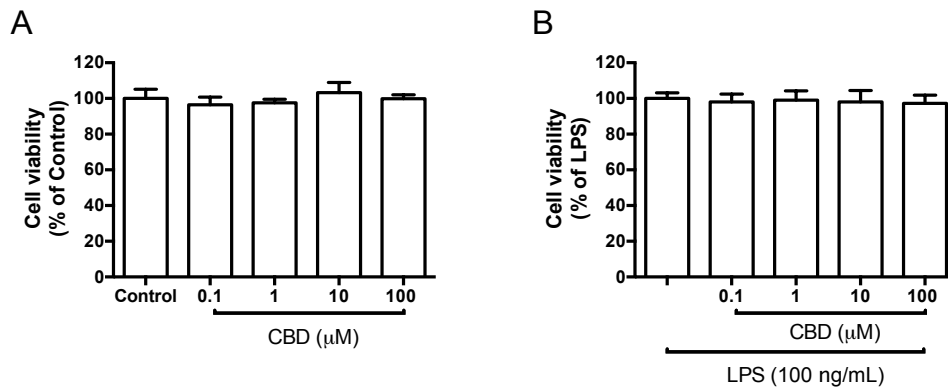


Figure S1. CBD did not affect on the viability of THP-1 monocytes treated with (A) or without LPS (B). Monocytes were treated with CBD (0.1, 1, 10, and 100 μM) for 24 hours with or without the stimulation by LPS (100 ng/mL). Cell viability was determined using a CTG 2.0 assay.

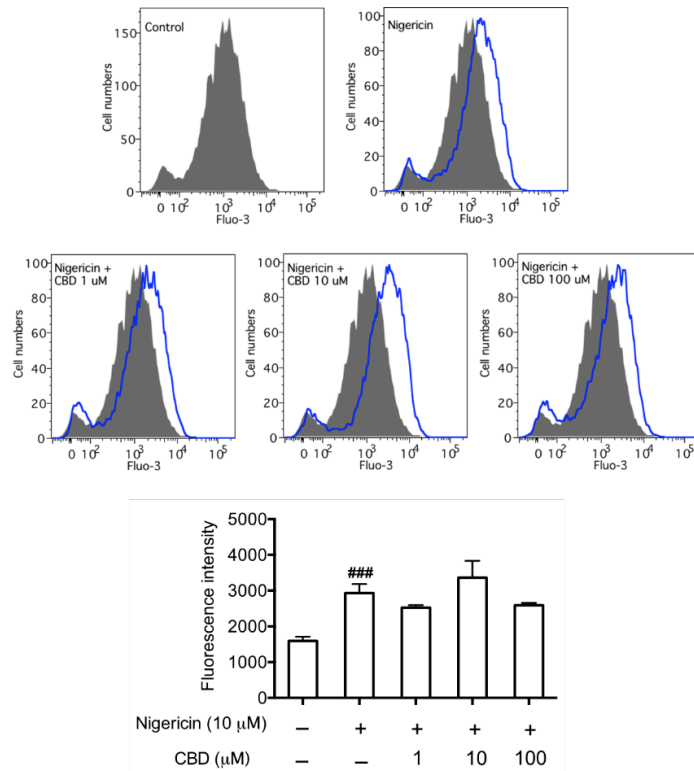


Figure S2. CBD did not affect intracellular calcium in THP-1 monocytes induced by LPS-nigericin. LPS (100 ng/mL) was added to THP-1 monocytes for 4 hours followed by the treatment of CBD (1, 10, and 100 μM) for 1 hour. Nigericin (10 μM) was then added and incubated for 1 hour. The cells were stained with ion calcium Fluo-3 dye and the fluorescent intensity was measured by flow cytometry.

CHAPTER 6

MANUSCRIPT 6

Published: 1 July 2020

Cannabis and Cannabinoid Research Ahead of Print

<https://doi.org/10.1089/can.2020.0025>

A Network Pharmacology Approach to Identify Potential Molecular Targets for Cannabidiol's Anti-Inflammatory Activity

Hang Ma^{1*}, Feng Xu^{1,2}, Chang Liu¹, Navindra P. Seeram^{1*}

¹Bioactive Botanical Research Laboratory, Department of Biomedical and Pharmaceutical Sciences, College of Pharmacy, University of Rhode Island, Kingston, RI 02881, USA

²College of Pharmacy, Guizhou University of Traditional Chinese Medicine, Guiyang 553001, People's Republic of China

*Corresponding authors

Tel.: +1 401 874 7654; E-mail address: hang_ma@uri.edu (H.M.)

Tel.: +1 401 874 9367; E-mail address: nseeram@uri.edu (N.P.S.)

Bioactive Botanical Research Laboratory, Department of Biomedical and Pharmaceutical Sciences, College of Pharmacy, University of Rhode Island

7 Greenhouse Road, Kingston, RI 02881, USA

Abstract

Introduction: Published pre-clinical and clinical studies support the anti-inflammatory activity of cannabidiol (CBD) but the molecular targets (e.g. genes and proteins) that are involved in its mechanisms of action remain unclear. Herein, a network-based pharmacology analysis was performed to aid in the identification of potential molecular targets for CBD's anti-inflammatory activity.

Materials and Methods: Target genes and proteins were obtained from several online databases including Swiss target prediction, Online Mendelian Inheritance in Man, and the DrugBank database. A compound-target-disease network was constructed with Cytoscape tool and a network of protein-protein interactions was established with the Search Tool for the Retrieval of Interacting Genes/Proteins database. Lead proteins identified from the compound-target-disease network were further studied for their interactions with CBD by computational docking. In addition, biological pathways involved in CBD's anti-inflammatory activity were identified with the gene ontology enrichment and the Kyoto Encyclopedia of Genes and Genomes analysis.

Results: A panel of proteins including cellular tumor antigen p53, NF-kappa-B essential modulator, TNF receptor, transcription factor p65, NF-kappa-B p105, NF-kappa-B inhibitor alpha, inhibitor of nuclear factor kappa-B kinase subunit alpha, and epidermal growth factor receptor were identified as lead targets involved in CBD's anti-inflammatory activity. This finding was further supported by molecular docking which showed interactions between the lead proteins and CBD. In addition, several signaling pathways including tumor necrosis factor, toll-like receptor, mitogen-activated protein kinases, nuclear factor kappa-light-chain-enhancer of activated B cells, and nucleotide-binding oligomerization domain-like receptors were identified as key regulators in the mediation of CBD's anti-inflammatory activity.

Conclusion: A network-based pharmacology analysis identified potential molecular targets and signaling pathways for CBD's anti-inflammatory activity. Findings from this study add to the growing body of data supporting the utilization of CBD as a promising anti-inflammatory natural product.

Keywords: cannabidiol (CBD); anti-inflammation; network pharmacology; NFκB; target identification; drug-diseases network

Abbreviations used:

AGEs = advance glycation endproducts

ALS = amyotrophic lateral sclerosis

CASP8 = cysteine-aspartic acid protease-8

CBD = cannabidiol

CDS = cytosolic DNA-sensing

CLRs = C-type lectin receptors

DAVID = Database for Annotation,

Visualization and Integrated Discovery

EGFR = epidermal growth factor receptor

GO = Gene Ontology

IBD = inflammatory bowel disease

IKK- $\alpha/\beta/\gamma$ = inhibitors of nuclear factor kappa-B
kinase subunit alpha/beta/gamma

IL-1 = interleukin-1

I κ B α = NF-kappa-B inhibitor alpha

KEGG = Kyoto encyclopedia of genes and
genomes

MAPK = mitogen-activated protein kinase

NAFLD = nonalcoholic fatty liver diseases

NF κ B = nuclear factor kappa-light-chain-
enhancer of activated B cells

NF κ B p105 = nuclear factor NF-kappa-B p105
subunit

NF κ B p65 = transcription factor p65

NLRs = nucleotide-binding oligomerization
domain-like receptors

PPI = protein-protein interaction

RAGE = receptor for advanced glycation
endproducts

RLRs = retinoic acid-inducible gene-I-like
receptors

STAT3 = signal transducer and activator of
transcription 3

STRING = search tool for the retrieval of
interacting genes/proteins

TCR = T-cell receptor

TLR = toll-like receptor

TNFRSF1A = tumor necrosis factor receptor
superfamily member 1A

TNF α = tumor necrosis factor alpha

Introduction

Inflammation is a vital immune response to combat harmful stimuli, irritants, cell damage, and tissue injury.¹ These stimuli trigger a series of physiological consequences including increased blood flow, dilation of capillary blood vessels, and impaired vascular permeability, which can further lead to numerous cell and tissue dysfunctions. Inflammation mediated pathological progressions are regulated by complex immune systems involving different immune cells and various signaling pathways.² Among these various regulatory mechanisms, one of the most studied signaling pathway is the signal transduction of nuclear factor kappa-light-chain-enhancer of activated B cells (NFκB).³ NFκB is a complex of proteins with five family members including NF-κB1 (subunit p50), NF-κB2 (subunit p100), RelA (subunit p65), RelB, and c-Rel. These proteins are usually formed in dimers (e.g. p50-p65 dimer) to enable a wide range of biological functions and mediate the inflammation processes, such as coordinating the expression of multiple inflammatory genes. NFκB is considered as a central mediator for inflammation responses. NF-κB can be collectively regulated by its upstream signal transduction cascade including inhibitors of nuclear factor kappa-B kinase subunit alpha, beta, and gamma (also known as IKK- $\alpha/\beta/\gamma$), which are associated with the propagation of cellular response to inflammation.³ Activation of the NFκB pathway also leads to a cascade of downstream signaling including the expressions of several proinflammatory cytokines including IL-1 β and tumor necrosis factor alpha (TNF- α). The NFκB pathway in the inflammation process is an example showing that the regulation of inflammation is orchestrated by complex mechanisms involving multiple genes, proteins, and signaling pathways. Therefore, identification of molecular targets for the development of anti-inflammatory agents as therapeutics for inflammatory mediated diseases remains a challenge.

A promising preventive and/or therapeutic strategy against inflammatory mediated disorders is immunomodulation by natural products from medicinal plants.⁴ Cannabis (*Cannabis sativa*) has been widely used in empirical and traditional remedies for various inflammation related ailments.^{5,6} Notably, the anti-inflammatory activity and related molecular targets of a major phytocannabinoid in Cannabis, namely, cannabidiol (CBD), is supported by several reported studies. For instance, CBD showed anti-neuroinflammatory effects in murine microglial cells through the downregulation of the NF-κB

pathway and upregulation of transcription factors including signal transducer and activator of transcription 3 (STAT3).⁷ CBD's anti-inflammatory effects in microglial cells are also supported by other studies, which showed that CBD's anti-inflammatory activity was associated with its modulation of downstream transcriptional events including the regulation of gene expression and transcription.^{8,9} Additionally, functional subsets of genes and genes networks, such as molecular and cellular functions, of CBD's anti-inflammatory effects, were identified by bioinformatic analysis tools including Ingenuity Pathway Analysis, Database for Annotation, Visualization and Integrated Discovery (DAVID) bioinformatics resources, and Kyoto Encyclopedia of Genes and Genomes (KEGG) analysis.^{8,9} These findings suggest that CBD's anti-inflammatory activity is mediated by a complex combination of multiple molecular targets, rather than certain individual proteins.

In addition to experimental 'omic' methods, computational modeling of biological pathways and molecular interactions has been developed as a 'network' approach for a broad view of the interactions between ligands and their multiple-targets.^{10,11} The network-based pharmacology approach has been used to predict molecular targets including genes and proteins, protein-protein interactions, and signaling pathways for drug candidates.¹⁰ A computational pharmacology network analysis has been reported to aid in the identification of CBD's pharmacological targets.¹² This network analysis utilized a combination of chemogenomics-knowledgebase network analysis and integrated in silico modeling for the identification of three human neuro-related rhodopsin-like G-protein-coupled receptors as CBD's molecular targets. However, to date, a network analysis approach has not been utilized for the prediction of potential molecular targets that are related to CBD's anti-inflammatory activity. Herein, the aims of the current study are to: 1) identify putative genes and proteins that contribute to CBD's anti-inflammatory activity; 2) explore the interactions between CBD and inflammation-related proteins; 3) analyze signaling pathways that are involved in CBD's anti-inflammatory activity.

Materials and methods

Target Prediction

Potential targets for CBD's anti-inflammatory effects were obtained from several online databases including the Swiss Target Prediction database (<http://www.swisstargetprediction.ch/>), the Online

Mendelian Inheritance in Man (OMIM, <http://www.omim.org/>), and the DrugBank database (<https://www.drugbank.ca/>). Human target connexins were obtained from the interactive protein database (DIP; <http://dip.doe-mbi.ucla.edu>). All of the tested targets were transformed into the UniProt database in the protein ID format using the Retrieve/ID mapping tool (<http://www.uniprot.org/>).

Construction of Network and Topology Analysis

To elucidate the relationship between CBD and its anti-inflammatory targets, CBD and target genes and enriched pathways were imported into Cytoscape 3.6.1 software (<http://www.cytoscape.org/>) to build a "component-target-disease" network. Then the topological parameters of the network analysis were calculated to identify key nodes. Among the topologic parameters, closeness centrality (a measure of how close a molecule is to other nodes)¹³ and betweenness centrality (the number of nonredundant shortest paths traveling through a node in the network)¹⁴ were used as crucial factors to describe the most influential nodes in the network. Thus, the nodes of degree and betweenness centrality that are two times higher than the median value of the total nodes, and the nodes of closeness centrality are higher than the median value of the total nodes were selected as the hubs for the anti-inflammatory activity.

Molecular Docking

The 3D structural coordinates of CBD were obtained from the human metabolome database (www.HMDB.ca) and the PDB files were generated with Biovia Discovery Studio Visualizer 4.5. The structural coordinates of target proteins were retrieved in PDB format from the RCSB protein data bank (www.rcsb.org). Chimera 1.11.2 was applied to delete the solvent and ligands from the target proteins. AutodockTools 1.5.6 was used to perform molecular docking with Autodock 4.2 algorithm. Biovia Discovery Studio Visualizer 4.5 was applied to analyze the interactions between CBD and target proteins. Binding energies of CBD and its target proteins were obtained from parameters including intermolecular energy (1), internal energy (2), torsional free energy (3), and unbound system's energy (4). The total binding energy was calculated as energy of binding = [(1) + (2) + (3) - (4)].

PPI Network and Cluster Analysis

The hub targets from the aforementioned screening process were further imported into the Search Tool for the Retrieval of Interacting Genes/Proteins (STRING) database (<http://string-db.org/>) database to explore the interactions between the known and predicted proteins. The topological parameters of mean

and maximum degrees of freedom in PPI network were analyzed with Cytoscape 3.6.1 software, and then the network was analyzed with the MCODE plug-in for cluster analysis.

Enrichment Analysis for Target Proteins

The plug-in ClueGO in Cytoscape 3.6.1 software was used to perform the Gene Ontology (GO) including cell component, molecular function, and biological process enrichment and the Kyoto Encyclopedia of Genes and Genomes (KEGG) pathway annotation. The localization of the biological and molecular functions of the proteins was identified based on high confidence with a *P* value (< 0.01) calculated by the two-side hypergeometric test method.

Results and discussion

Protein Targets and Topological Parameters

Potential targets for CBD's anti-inflammatory activity were obtained from several databases. CBD's protein targets were identified through the Swiss Target Prediction database and inflammation related genes and protein targets were obtained through the OMIM and DrugBank databases. An interactive network of CBD's anti-inflammatory activity was constructed through network pharmacological analysis (Fig. 1). The red triangle represents CBD and the circles are proteins for pharmacological targets of CBD (in yellow), inflammation (in violet), and protein-protein interaction (in cyan-blue). The yellow rectangles represent proteins targets that are directly involved with CBD and inflammation pathways. Through the analysis of this "compound-target-disease" interactive network, 100 protein targets are affected by CBD and 570 protein targets are affected by inflammation. Among these protein targets, 20 proteins are common targets shared by CBD and inflammation-related pathways (as shown in yellow triangles; Fig. 1). Analysis of the topological parameters of all nodes in the network showed that the median of degree, betweenness centrality, and closeness centrality values are 1, 0, and 0.19641626, respectively. The thresholds of topological parameters were setup as degree value (> 2), betweenness centrality (> 0), and closeness centrality values (> 0.19641626) and a total of 44 potential targets for CBD's anti-inflammatory activity were obtained (Supplementary Table S1). Targets with degree value greater than 10 are listed in Table 1. The protein target with the highest degree was cellular tumor antigen p53 (p53; 58 degree), followed by NF-kappa-B essential modulator (as known as inhibitor of NFκB kinase subunit gamma; IKK-γ), TNF receptor-associated factor 6

(TRAF6), transcription factor subunit p65 (NF κ B p65), nuclear factor NF-kappa-B p105 subunit (NF κ B p105), NF-kappa-B inhibitor alpha (I κ B α), inhibitor of nuclear factor kappa-B kinase subunit alpha (IKK α), and epidermal growth factor receptor (EGFR) with comparable degrees (21, 20, 19, 19, 18, 18, and 17, respectively).

Notably, several proteins among the identified CBD's anti-inflammatory targets, namely, I κ B α , IKK α , IKK β , and IKK γ are the key regulators of the upstream NF κ B signal cascade.³ NF κ B is in the inactivated state when I κ B α masks the nuclear localization signals of NF- κ B and sequesters NF κ B in the cytoplasm. Phosphorylation of I κ B α proteins by I κ B kinase including IKK α , IKK β , and IKK γ lead to the activation of NF κ B via allowing it to enter into the cell nucleus from the cytoplasm. Therefore, given that I κ B and I κ B kinase are the top predicted protein targets, it is possible that CBD's anti-inflammatory effects are primarily associated with the NF κ B signal cascade. This is in agreement with in vitro experimental data from several previously reported studies. In these studies, CBD showed anti-inflammatory effects by the inhibition of NF κ B pathways in BV-2 microglial cells,⁷ PC12 neuronal cells,¹⁵ and RAW264.7 murine macrophage cells.¹⁶ To further validate the prediction of CBD's target proteins, computational docking was performed to evaluate the interactions between CBD and lead target proteins (top 16 proteins in Table 1).

Computational Docking Analysis

Computational docking revealed the interactions between CBD and the lead target proteins (top 16 from the protein targets analysis in Table 1). CBD can fit into the binding pocket of the target proteins and interact with protein amino acid residues by forming interactions including van der Waals force, conventional hydrogen bonding, carbon hydrogen bonding, pi-donor hydrogen bonding, and pi-sigma, pi-alkyl, pi-anion, amide-pi stacked, and pi-sulfur forces (Fig. 2). In addition, the binding affinities between CBD and lead target proteins were ranked by their predicted free energy of binding and inhibition constant (Table 2). Proteins IKK β and mitogen-activated protein kinase (MAPK) 14 had the lowest binding energy (-7.99 and -7.35 kcal/mol, respectively) and inhibition constant (1.4 and 4.1 μ M, respectively). Comparably, p53, which had the highest degree in the 'compound-target-disease' network, also had a third ranked low binding energy and inhibition constant (-6.08 kcal/mol and 35.0 μ M, respectively).

The utilization of computational docking as a complementary approach to validate the prediction of target proteins for CBD's neurophysiological effects has been reported.¹² In addition, molecular docking has also been used to evaluate the interactions between lupenone, a natural anti-inflammatory agent, and its predicted target proteins.¹⁷ In the current study, data from the computational docking study supported the prediction of CBD's anti-inflammatory target proteins. Four of the top 6 proteins including p53, TRAF6, p65, and I κ B α , with lower binding affinity, matched within the top 6 lead target proteins predicted in Table 1. Additionally, findings from computational docking are supported by reported experimental studies. For instance, CBD had the second lowest free binding energy and inhibition constant with protein mitogen-activated protein kinase 14 (MAPK 14, also known as p38- α), which is a protein known as a mediator for cellular responses to external proinflammatory signals.¹⁸ Animal experimental studies have reported that CBD exerted anti-inflammatory effects by the regulation of p38- α pathway in mouse models of type I diabetic cardiomyopathy¹⁹ and alcohol-induced steatosis.¹⁶ Nevertheless, further biological investigations are warranted to validate other predicted target proteins for CBD's anti-inflammatory activity.

Protein-Protein Interaction (PPI) Network Analysis and Cluster Analysis of Hub targets

The identified potential targets were imported into the STRING database. A protein-protein interaction (PPI) network of protein targets for CBD's inflammation activity was obtained with 44 nodes (target protein; shown as circles) and 288 edges (PPI; shown as lines; Fig. 3). In addition, the clustering of the target interaction network was further analyzed by the Cytoscape software MCODE plug-in to obtain two sub-networks (Fig. 4 A and B), which represent possible independent pathways that contributed to the overall anti-inflammatory effects of CBD. In this PPI network, target proteins including STAT3, RAC-alpha serine/threonine-protein kinase (also known as AKT1), tumor necrosis factor receptor superfamily member 1A (TNFRSF1A), and cysteine-aspartic acid protease-8 (CASP8) had greater number of degrees (as shown in a darker color) suggesting that they may play a pivotal role in the anti-inflammatory effects of CBD. This is in agreement with reported experimental studies. For instance, CBD was reported to exert anti-inflammatory effects by the down-regulation of the pro-inflammatory STAT1 pathway and the activation of anti-inflammatory STAT3 pathway in murine microglial BV-2 cells.⁷ In addition, CBD's anti-inflammatory effects were reported to be associated

with the up-regulation of AKT phosphorylation in a mouse model of experimental autoimmune encephalomyelitis.²⁰ However, further studies are needed to elucidate the roles of other pathways in the predicted PPI network.

Enrichment analysis for GO biological processes and KEGG signaling pathway analysis

A panel of 44 potential targets was analyzed by the ClueGO plug-in for systematical analysis of the enrichment of biological functions and biological processes. There were 155 biological processes that were enriched (P value ≤ 0.01) and they were related to cellular response to the interleukin-1 (IL-1) and IL1-mediated signaling pathways (Table 3). For the molecular functions, 11 biological processes (P value ≤ 0.01) were related to histone deacetylase binding and enhancer binding (Table 3). For the cell components, 5 biological processes (P value ≤ 0.01) were strongly related to I κ B kinase complex and CD40 receptor complex (Table 3). In addition, KEGG analysis revealed that a total of 71 pathways related to CBD's anti-inflammatory activity were found to be enriched with the protein targets (P value ≤ 0.01 ; shown in Fig. 5). The KEGG analysis of CBD's anti-inflammatory activity revealed several related signaling pathways including TNF, toll-like receptor (TLR), retinoic acid-inducible gene-I-like receptors (RLRs), MAPK, C-type lectin receptors (CLRs), IL-17, NF κ B, T-cell receptor (TCR), cytosolic DNA-sensing (CDS), adipocytokine, nucleotide-binding oligomerization domain-like receptors (NLRs), neurotrophin, B cell receptor, chemokine, and advance glycation endproducts (AGE)-receptor for AGE (RAGE). Notably, some of these signaling pathways are known to be associated with a specific anti-inflammation mechanism, namely, the inflammasome pathway, which is responsible for the maturation and secretion of pro-inflammatory cytokines IL-1 β .²¹ Our group has previously reported that the inhibitory effect of CBD on NLRP3 inflammasome activation is associated with its modulation of a purinergic receptor, namely, P2X7 receptor, which regulates several signaling pathways to release proinflammatory cytokines.²² Published studies have also reported that the activation of signaling pathways including TLR,²³ TCR,²⁴ NLRs,²⁵ and RAGE²⁶ are closely related to the regulation of inflammasome activation. Therefore, multiple signaling pathways may be involved in CBD's anti-inflammasome activity, which contribute to CBD's overall anti-inflammatory activity. Additionally, the drug-target association network also suggested that CBD had significant correlations with several inflammatory mediated diseases including hepatitis B and C, herpesviruses infection,

various type of cancers (e.g. lung cancer, pancreatic cancer, prostate cancer, bladder cancer, myeloid leukemia, colorectal cancer, and melanoma), nonalcoholic fatty liver diseases (NAFLD), inflammatory bowel disease (IBD), and amyotrophic lateral sclerosis (ALS) (Fig. 5). These findings are supported by several pre-clinical investigations of CBD as interventions for the aforementioned inflammatory diseases including hepatitis,²⁷ viral infections,²⁸ cancers,^{29,30} liver diseases,³¹ IBD,^{32,33} and ALS.³⁴ Further experimental studies using ‘-omic’ approaches (e.g. genomics, proteomics, and metabolomics) with in vitro and in vivo models are warranted to verify the biological effects of predicted protein targets.³⁵ Several challenges still remain before CBD’s therapeutic applications for inflammatory mediated diseases can be fully explored, due to: 1) only limited data from clinical trials are available,³⁶⁻³⁹ 2) CBD may exert anti-inflammatory activity via multiple pharmacological targets (e.g. the endocannabinoid system);^{40,41} 3) further mechanistic studies of CBD’s pharmacological effects are warranted. It should be noted that the current study solely focused on the analysis of CBD’s network for anti-inflammatory effects. However, there are numerous other phytochemicals, including over a hundred phytocannabinoids, such as tetrahydrocannabinol (THC), present in cannabis extracts. Similar to CBD, these phytochemicals (phytocannabinoids and non-phytocannabinoids), may also be involved in the modulation of the pharmacological targets identified herein, and contribute to the overall anti-inflammatory effects of cannabis extracts. Therefore, it is possible that CBD and other phytochemicals including THC in cannabis extracts, exert pharmacological effects in a complementary, additive, and/or synergistic manner, but further studies are warranted to confirm this.

In summary, a network based pharmacological analysis was utilized to predict the potential molecular targets for CBD’s anti-inflammatory activity which revealed the NFκB cascade as one of its primary anti-inflammatory mechanism of action. In addition, target proteins including p53, IκBα, IKKs, and MAP kinases, as well as signaling pathways including STAT3, AKT1, TNF, TLR, RLRs, and MAPK were linked to CBD’s anti-inflammatory activity. These molecular targets may contribute to CBD’s overall anti-inflammatory activity and its potential therapeutic applications for several inflammatory mediated diseases. Although further biological experiments are warranted to validate these molecular targets, our findings add to the growing body of data supporting the utilization of CBD as a promising anti-inflammatory natural product.

Author Disclosure Statement

N.P.S serves on the Advisory Board of Alluvion Brands, LLC (Warwick, RI, USA) as a consultant for the biological evaluations of phytocannabinoids. Alluvion Brands did not influence the design of this study nor had any financial contributions to this work. The other authors declare no conflicts of interest.

REFERENCE

1. Grivennikov SI, Greten FR, Karin M. Immunity, Inflammation, and Cancer. *Cell*. 2010;140(6):883-899. doi:10.1016/j.cell.2010.01.025
2. Mantovani A. Molecular Pathways Linking Inflammation and Cancer. *Curr Mol Med*. 2010;10(4):369-373. doi:10.2174/156652410791316968
3. Liu T, Zhang L, Joo D, Sun SC. NF- κ B signaling in inflammation. *Signal Transduct Target Ther*. 2017;2. doi:10.1038/sigtrans
4. Arulsevan P, Fard MT, Tan WS, et al. Role of Antioxidants and Natural Products in Inflammation. *Oxid Med Cell Longev*. 2016;2016. doi:10.1155/2016/5276130
5. Ryz NR, Remillard DJ, Russo EB. Cannabis Roots: A Traditional Therapy with Future Potential for Treating Inflammation and Pain. *Cannabis Cannabinoid Res*. 2017;2(1):210-216. doi:10.1089/can.2017.0028
6. Zlas J, Stark H, Seligman J, et al. Early medical use of cannabis [5]. *Nature*. 1993;363(6426):215. doi:10.1038/363215a0
7. Kozela E, Pietr M, Juknat A, Rimmerman N, Levy R, Vogel Z. Cannabinoids Δ^9 -tetrahydrocannabinol and cannabidiol differentially inhibit the lipopolysaccharide-activated NF- κ B and interferon- β /STAT proinflammatory pathways in BV-2 microglial cells. *J Biol Chem*. 2010;285(3):1616-1626. doi:10.1074/jbc.M109.069294
8. Juknat A, Pietr M, Kozela E, et al. Differential transcriptional profiles mediated by exposure to the cannabinoids cannabidiol and Δ^9 -tetrahydrocannabinol in BV-2 microglial cells. *Br J Pharmacol*. 2012;165(8):2512-2528. doi:10.1111/j.1476-5381.2011.01461.x
9. Juknat A, Rimmerman N, Levy R, Vogel Z, Kozela E. Cannabidiol affects the expression of genes involved in zinc homeostasis in BV-2 microglial cells. In: *Neurochemistry International*. 61, 2012:923-930. doi:10.1016/j.neuint.2011.12.002

10. Zhao S, Iyengar R. Systems Pharmacology: Network Analysis to Identify Multiscale Mechanisms of Drug Action. *Annu Rev Pharmacol Toxicol.* 2012;52(1):505-521. doi:10.1146/annurev-pharmtox-010611-134520
11. Berger SI, Iyengar R. Network analyses in systems pharmacology. *Bioinformatics.* 2009. doi:10.1093/bioinformatics/btp465
12. Bian Y min, He X bing, Jing Y kang, Wang L rong, Wang J mei, Xie XQ. Computational systems pharmacology analysis of cannabidiol: a combination of chemogenomics-knowledgebase network analysis and integrated in silico modeling and simulation. *Acta Pharmacol Sin.* 2019;40(3):374-386. doi:10.1038/s41401-018-0071-1
13. Berger SI, Iyengar R. Network analyses in systems pharmacology. *Bioinformatics.* 2009;25(19):2466-2472. doi:10.1093/bioinformatics/btp465
14. Hopkins AL. Network pharmacology: The next paradigm in drug discovery. *Nat Chem Biol.* 2008;4(11):682-690. doi:10.1038/nchembio.118
15. Esposito G, De Filippis D, Maiuri MC, De Stefano D, Carnuccio R, Iuvone T. Cannabidiol inhibits inducible nitric oxide synthase protein expression and nitric oxide production in β -amyloid stimulated PC12 neurons through p38 MAP kinase and NF- κ B involvement. *Neurosci Lett.* 2006;399(1-2):91-95. doi:10.1016/j.neulet.2006.01.047
16. Huang Y, Wan T, Pang N, et al. Cannabidiol protects livers against nonalcoholic steatohepatitis induced by high-fat high cholesterol diet via regulating NF- κ B and NLRP3 inflammasome pathway. *J Cell Physiol.* 2019;234(11):21224-21234. doi:10.1002/jcp.28728
17. Xu F, Yang L, Huang X, Liang Y, Wang X, Wu H. Lupenone is a good anti-inflammatory compound based on the network pharmacology. *Mol Divers.* 2020;24(1):21-30. doi:10.1007/s11030-019-09928-5
18. She H, He Y, Zhao Y, Mao Z. Release the autophagy brake on inflammation: The MAPK14/p38 α -ULK1 pedal. *Autophagy.* 2018;14(6):1097-1098. doi:10.1080/15548627.2018.1446626
19. Rajesh M, Mukhopadhyay P, Btkai S, et al. Cannabidiol attenuates cardiac dysfunction, oxidative stress, fibrosis, and inflammatory and cell death signaling pathways in diabetic

- cardiomyopathy. *J Am Coll Cardiol*. 2010;56(25):2115-2125. doi:10.1016/j.jacc.2010.07.033
20. Giacoppo S, Pollastro F, Grassi G, Bramanti P, Mazzon E. Target regulation of PI3K/Akt/mTOR pathway by cannabidiol in treatment of experimental multiple sclerosis. *Fitoterapia*. 2017;116:77-84. doi:10.1016/j.fitote.2016.11.010
 21. Schroder K, Tschopp J. The Inflammasomes. *Cell*. 2010. doi:10.1016/j.cell.2010.01.040
 22. Liu C, Ma H, L. Slitt A, P. Seeram N. Inhibitory effect of cannabidiol on the activation of NLRP3 inflammasome is associated with its modulation of the P2X7 receptor in human monocytes. *J Nat Prod*. 2020;0(0). doi:10.1021/acs.jnatprod.0c00138
 23. Hanamsagar R, Hanke ML, Kielian T. Toll-like receptor (TLR) and inflammasome actions in the central nervous system. *Trends Immunol*. 2012;33(7):333-342. doi:10.1016/j.it.2012.03.001
 24. Dostert C, Ludigs K, Guarda G. Innate and adaptive effects of inflammasomes on T cell responses. *Curr Opin Immunol*. 2013;25(3):359-365. doi:10.1016/j.coi.2013.02.008
 25. Mason DR, Beck PL, Muruve DA. Nucleotide-binding oligomerization domain-like receptors and inflammasomes in the pathogenesis of non-microbial inflammation and diseases. *J Innate Immun*. 2011;4(1):16-30. doi:10.1159/000334247
 26. Kang R, Chen R, Xie M, et al. The Receptor for Advanced Glycation End Products Activates the AIM2 Inflammasome in Acute Pancreatitis. *J Immunol*. 2016;196(10):4331-4337. doi:10.4049/jimmunol.1502340
 27. Hegde VL, Nagarkatti PS, Nagarkatti M. Role of Myeloid-derived suppressor cells in amelioration of experimental autoimmune hepatitis following activation of TRPV1 receptors by cannabidiol. *PLoS One*. 2011;6(4). doi:10.1371/journal.pone.0018281
 28. Reiss CS. Cannabinoids and viral infections. *Pharmaceuticals*. 2010. doi:10.3390/ph3061873
 29. Ramer R, Hinz B. Cannabinoids as Anticancer Drugs. In: *Advances in Pharmacology*. ; 2017. doi:10.1016/bs.apha.2017.04.002
 30. Massi P, Solinas M, Cinquina V, Parolaro D. Cannabidiol as potential anticancer drug. *Br J Clin Pharmacol*. 2013;75(2):303-312. doi:10.1111/j.1365-2125.2012.04298.x
 31. Patsenker E, Stickel F. Cannabinoids in liver diseases. *Clin Liver Dis*. 2016;7(2):21-25. doi:10.1002/cld.527

32. Naftali T, Mechulam R, Lev LB, Konikoff FM. Cannabis for inflammatory bowel disease. *Dig Dis*. 2014;32(4):468-474. doi:10.1159/000358155
33. Esposito G, De Filippis D, Cirillo C, et al. Cannabidiol in inflammatory bowel diseases: A brief overview. *Phyther Res*. 2013. doi:10.1002/ptr.4781
34. Elliott DM, Singh N, Nagarkatti M, Nagarkatti PS. Cannabidiol attenuates experimental autoimmune encephalomyelitis model of multiple sclerosis through induction of myeloid-derived suppressor cells. *Front Immunol*. 2018;9. doi:10.3389/fimmu.2018.01782
35. Horgan RP, Kenny LC. ‘Omic’ technologies: genomics, transcriptomics, proteomics and metabolomics. *Obstet Gynaecol*. 2011;13(3):189-195. doi:10.1576/toag.13.3.189.27672
36. Samanta D. Cannabidiol: A review of clinical efficacy and safety in epilepsy. *Pediatr Neurol*. 2019;96:24-29. doi:10.1016/j.pediatrneurol.2019.03.014
37. Hill KP, Palastro MD, Johnson B, Ditre JW. Cannabis and pain: A clinical review. *Cannabis Cannabinoid Res*. 2017;2(1):96-104. doi:10.1089/can.2017.0017
38. Iseger TA, Bossong MG. A systematic review of the antipsychotic properties of cannabidiol in humans. *Schizophr Res*. 2015;162(1-3):153-161. doi:10.1016/j.schres.2015.01.033
39. Pisanti S, Malfitano AM, Ciaglia E, et al. Cannabidiol: State of the art and new challenges for therapeutic applications. *Pharmacol Ther*. 2017;175:133-150. doi:10.1016/j.pharmthera.2017.02.041
40. Talevi A. Multi-target pharmacology: Possibilities and limitations of the “skeleton key approach” from a medicinal chemist perspective. *Front Pharmacol*. 2015;6(SEP). doi:10.3389/fphar.2015.00205
41. Kaur R, R. Ambwani S, Singh S. Endocannabinoid system: A multi-facet therapeutic target. *Curr Clin Pharmacol*. 2016;11(2):110-117. doi:10.2174/1574884711666160418105339

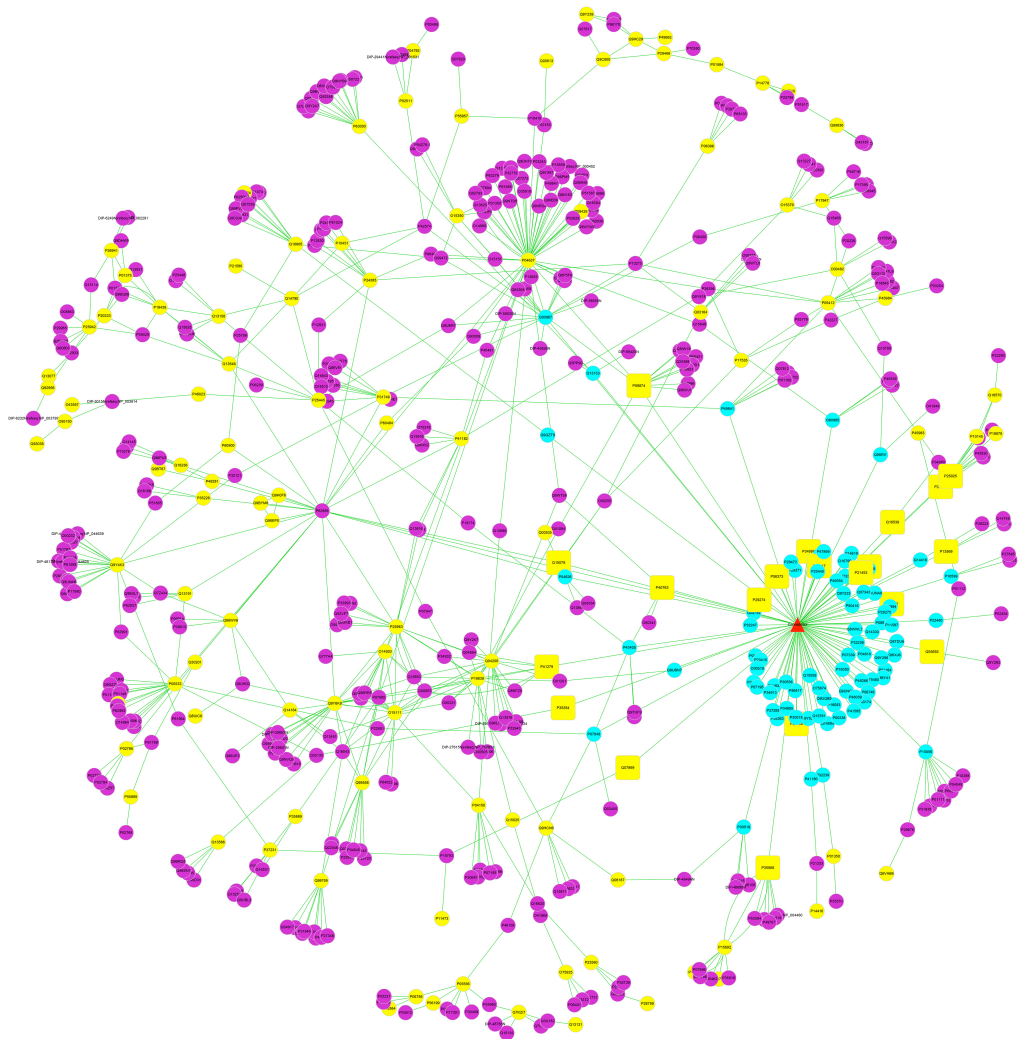


Fig. 1 Cannabidiol-target-inflammation network created by software Cytoscape

(<http://www.cytoscape.org>). All target proteins are represented by their UniProt IDs. Red triangle: CBD; yellow circles: CBD's pharmacological target proteins; violet circle: proteins related to inflammation; cyan-blue circle: protein-protein interaction; yellow rectangles: proteins targets that are directly involved with CBD and inflammation pathways.

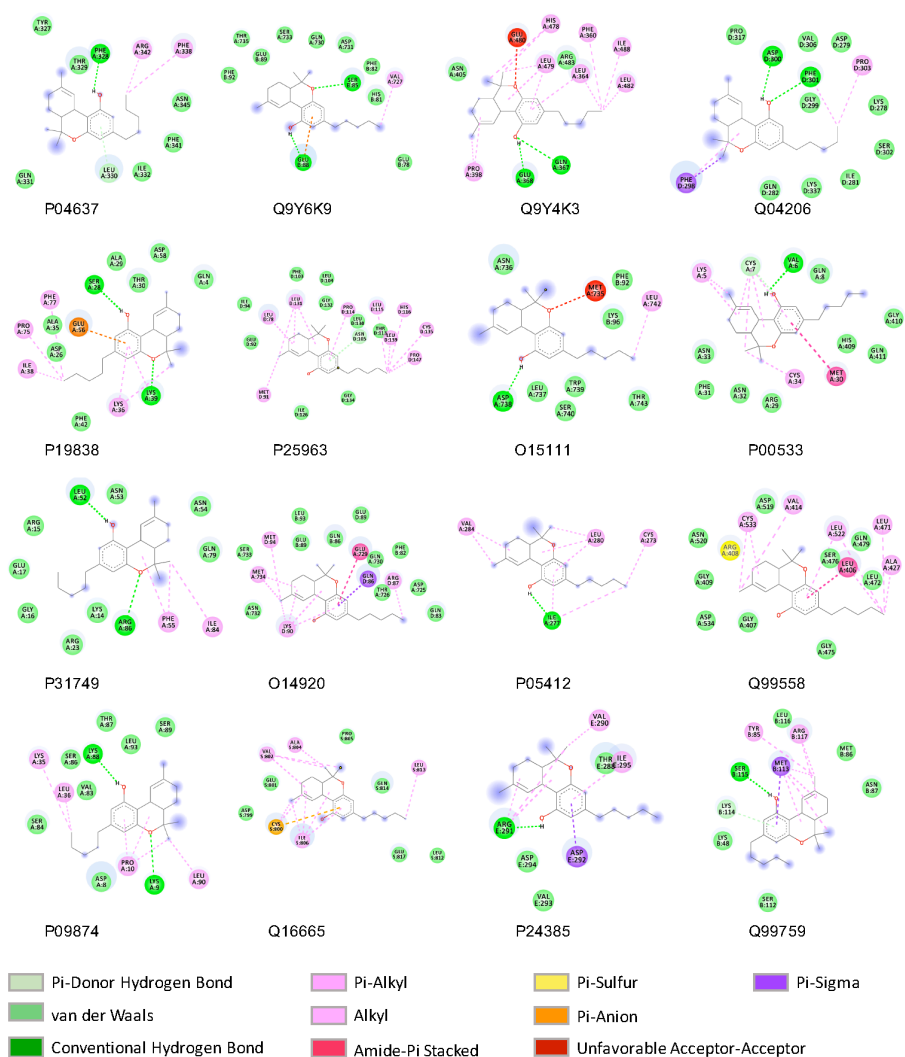


Fig. 2 Computational docking for interactions between CBD and potential target proteins for CBD's anti-inflammatory activity.

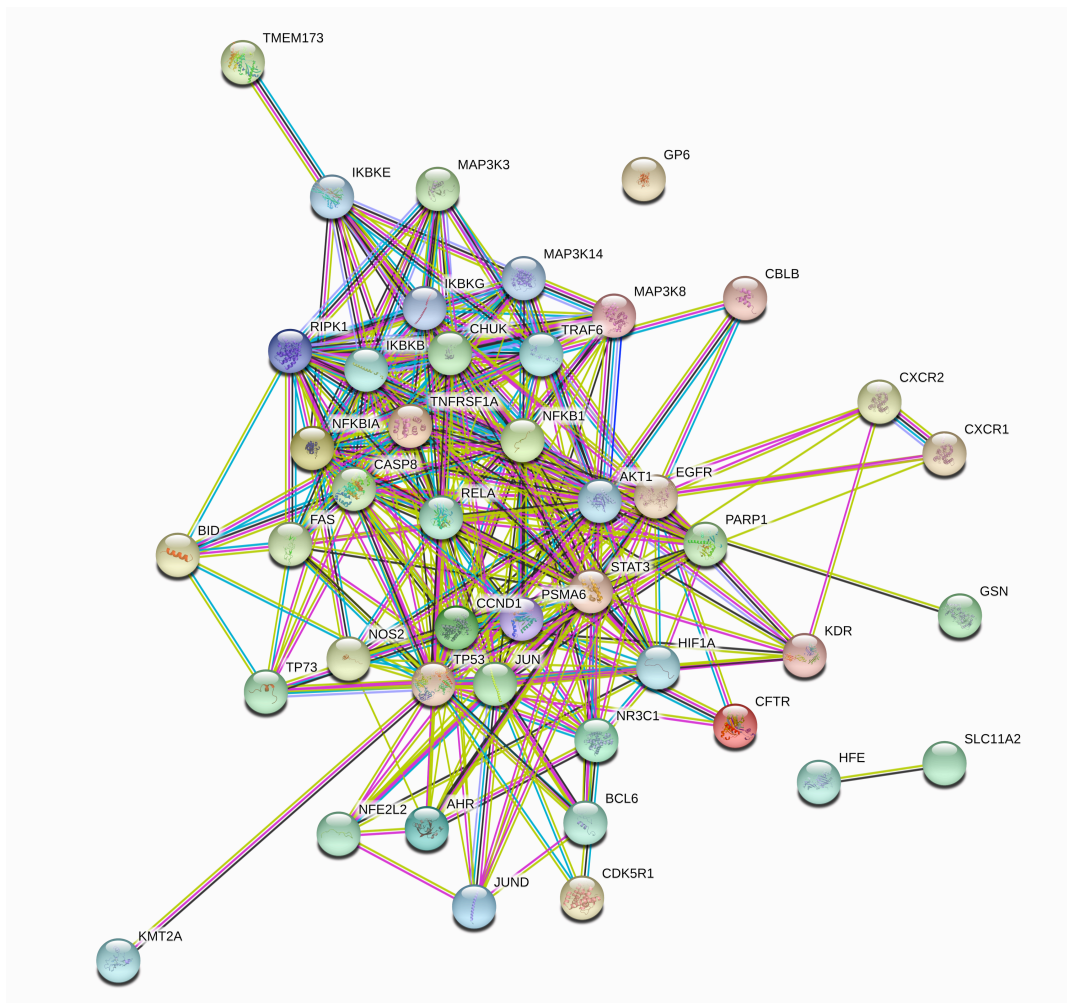


Fig. 3 Interaction network (created by software Cytoscape) of potential target proteins for CBD's anti-inflammatory activity.

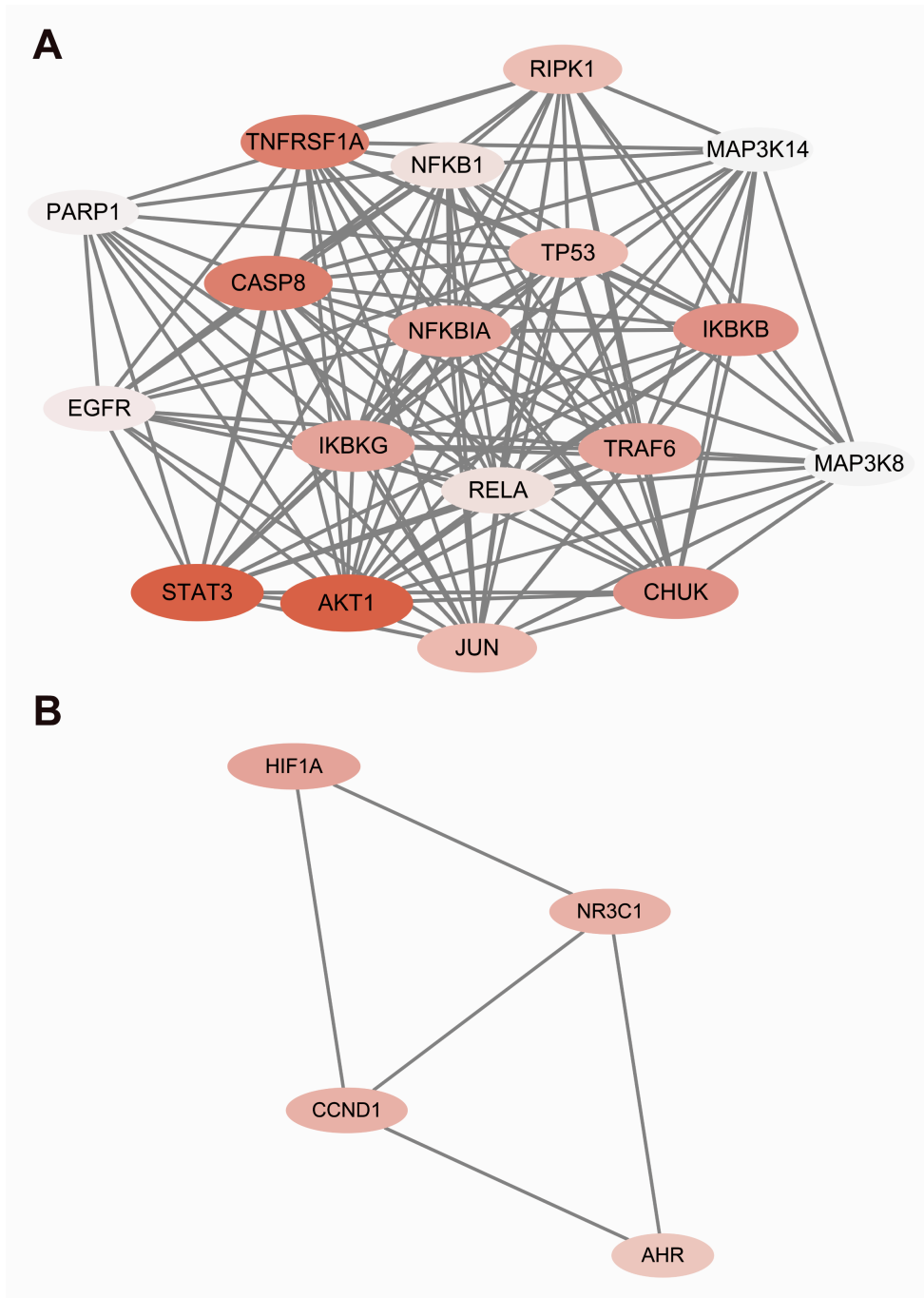


Fig. 4 Interaction network (created by software Cytoscape) of protein core subnetwork of target proteins for CBD's anti-inflammatory activity. Darker color indicates greater number of degrees.

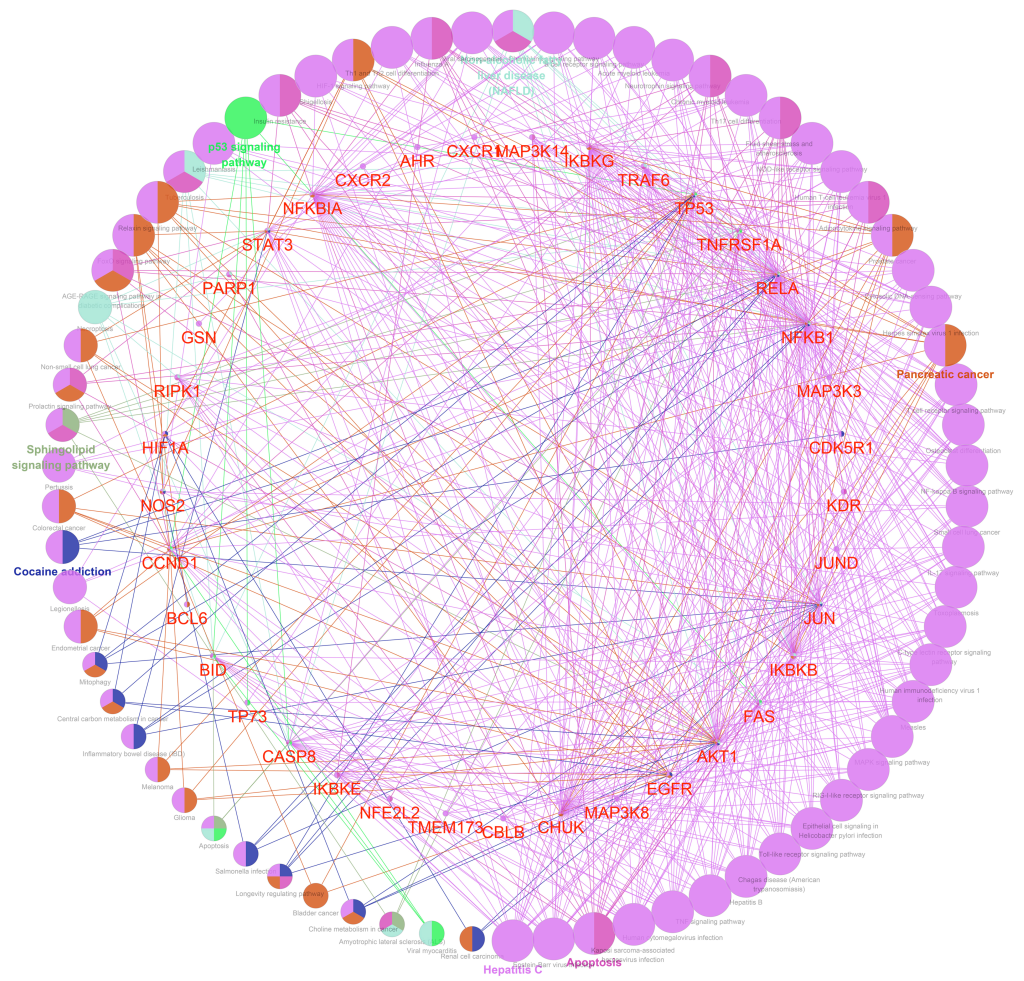


Fig. 5 Network diagram (created by software Cytoscape) of putative signaling pathways that are involved in CBD's anti-inflammatory activity and related diseases. Colors of nodes reflect the enrichment of biological function and classification of diseases associated with inflammation.

TABLES

Table 1. Topological parameters of potential targets for CBD’s anti-inflammatory activity in the “Compound-Target-Disease” network.

UniProt ID	Protein Name	betweenness centrality	closeness centrality	Degree
P04637	Cellular tumor antigen p53	0.3046	0.3012	58
Q9Y6K9	NF-kappa-B essential modulator	0.0648	0.2502	21
Q9Y4K3	TNF receptor-associated factor 6	0.0643	0.2377	20
Q04206	Transcription factor p65	0.0323	0.2513	19
P19838	Nuclear factor NF-kappa-B p105 subunit	0.0472	0.2468	19
P25963	NF-kappa-B inhibitor alpha	0.0426	0.2471	18
O15111	Inhibitor of nuclear factor kappa-B kinase subunit alpha	0.0196	0.2340	18
P00533	Epidermal growth factor receptor	0.0591	0.2427	17
P31749	RAC-alpha serine/threonine-protein kinase	0.0457	0.2653	13
O14920	Inhibitor of nuclear factor kappa-B kinase subunit beta	0.0241	0.2456	13
P05412	Transcription factor AP-1	0.0404	0.2321	13
Q99558	Mitogen-activated protein kinase 14	0.0246	0.2300	13
P09874	Poly [ADP-ribose] polymerase 1	0.1020	0.2864	12
Q16665	Hypoxia-inducible factor 1-alpha	0.0332	0.2254	12
P24385	G1/S-specific cyclin-D1	0.0347	0.2441	10
Q99759	Mitogen-activated protein kinase 3	0.0279	0.1993	10

Table 2. Interactions between CBD and target proteins. Free energy of binding and inhibition constant predicted by computational docking.

UniProt-PBD ID	Protein Name	Free Energy of Binding (kcal/mol)	Inhibition Constant (K _i ; μM)
O14920-3BRT	Inhibitor of nuclear factor kappa-B kinase subunit β	-7.99	1.4
Q99558-4IDT	Mitogen-activated protein kinase 14	-7.35	4.1
P04637-1AIE	Cellular tumor antigen p53	-6.08	35.0
P25963-1IKN	NF-kappa-B inhibitor alpha	-5.82	53.7
Q9Y4K3-1IB6	TNF receptor-associated factor 6	-5.74	62.3
Q04206-1NFI	Transcription factor p65	-5.66	71.5
P00533-1MOX	Epidermal growth factor receptor	-5.64	73.9
Q9Y6K9-3BRV	NF-kappa-B essential modulator	-5.36	117.8
P31749-1UNQ	RAC-alpha serine/threonine-protein kinase	-5.34	121.0
Q99579-2O2V	Mitogen-activated protein kinase 3	-5.34	122.6
P09874-2COK	Poly [ADP-ribose] polymerase 1	-4.88	264.4
Q16665-1H2K	Hypoxia-inducible factor 1-alpha	-4.41	581.3
O15111-3BRT	Inhibitor of nuclear factor kappa-B kinase subunit α	-4.32	686.9
P19838-IMDI	Nuclear factor kappa-B p105 subunit	-4.23	799.9
P24385- 5VZU	G1/S-specific cyclin-D1	-3.44	3010
P05412-1JUN	Transcription factor AP-1	-3.41	3180

Table 3. The functional analysis of identified compound-related targets by gene ontology (GO) analysis and KEGG signaling pathway analysis.

Ontology Source	GOID	GO Term	Term P Value Corrected with Bonferroni step down
GO_BiologicalProcess	GO:0070498	interleukin-1-mediated signaling pathway	2.56E-13
GO_BiologicalProcess	GO:0071347	cellular response to interleukin-1	7.48E-12
GO_BiologicalProcess	GO:0043123	positive regulation of I-kappaB kinase/NF-kappaB signaling	1.83E-11
GO_BiologicalProcess	GO:0070555	response to interleukin-1	4.43E-11
GO_BiologicalProcess	GO:0009612	response to mechanical stimulus	1.57E-09
GO_BiologicalProcess	GO:0033209	tumor necrosis factor-mediated signaling pathway	6.06E-09
GO_BiologicalProcess	GO:0038061	NIK/NF-kappaB signaling	6.28E-09
GO_BiologicalProcess	GO:1902895	positive regulation of pri-miRNA transcription by RNA polymerase II	3.38E-08
GO_BiologicalProcess	GO:0035666	TRIF-dependent toll-like receptor signaling pathway	6.22E-08
GO_BiologicalProcess	GO:0038095	Fc-epsilon receptor signaling pathway	8.02E-08
GO_MolecularFunction	GO:0042826	histone deacetylase binding	2.81E-06
GO_MolecularFunction	GO:0035326	enhancer binding	1E-05
GO_MolecularFunction	GO:0000980	RNA polymerase II distal enhancer sequence-specific DNA binding	3.95E-05
GO_MolecularFunction	GO:0051879	Hsp90 protein binding	0.000357
GO_MolecularFunction	GO:0097110	scaffold protein binding	0.000576
GO_MolecularFunction	GO:0032813	tumor necrosis factor receptor superfamily binding	0.00121
GO_MolecularFunction	GO:0033613	activating transcription factor binding	0.001913
GO_MolecularFunction	GO:0005123	death receptor binding	0.001915
GO_MolecularFunction	GO:0051059	NF-kappaB binding	0.002589
GO_MolecularFunction	GO:0001102	RNA polymerase II activating transcription factor binding	0.002872
GO_CellularComponent	GO:0035631	CD40 receptor complex	0.000252
GO_CellularComponent	GO:0008385	IkappaB kinase complex	0.000297
GO_CellularComponent	GO:1902554	serine/threonine protein kinase complex	0.000316
GO_CellularComponent	GO:0031264	death-inducing signaling complex	0.000402
GO_CellularComponent	GO:0045178	basal part of cell	0.001531

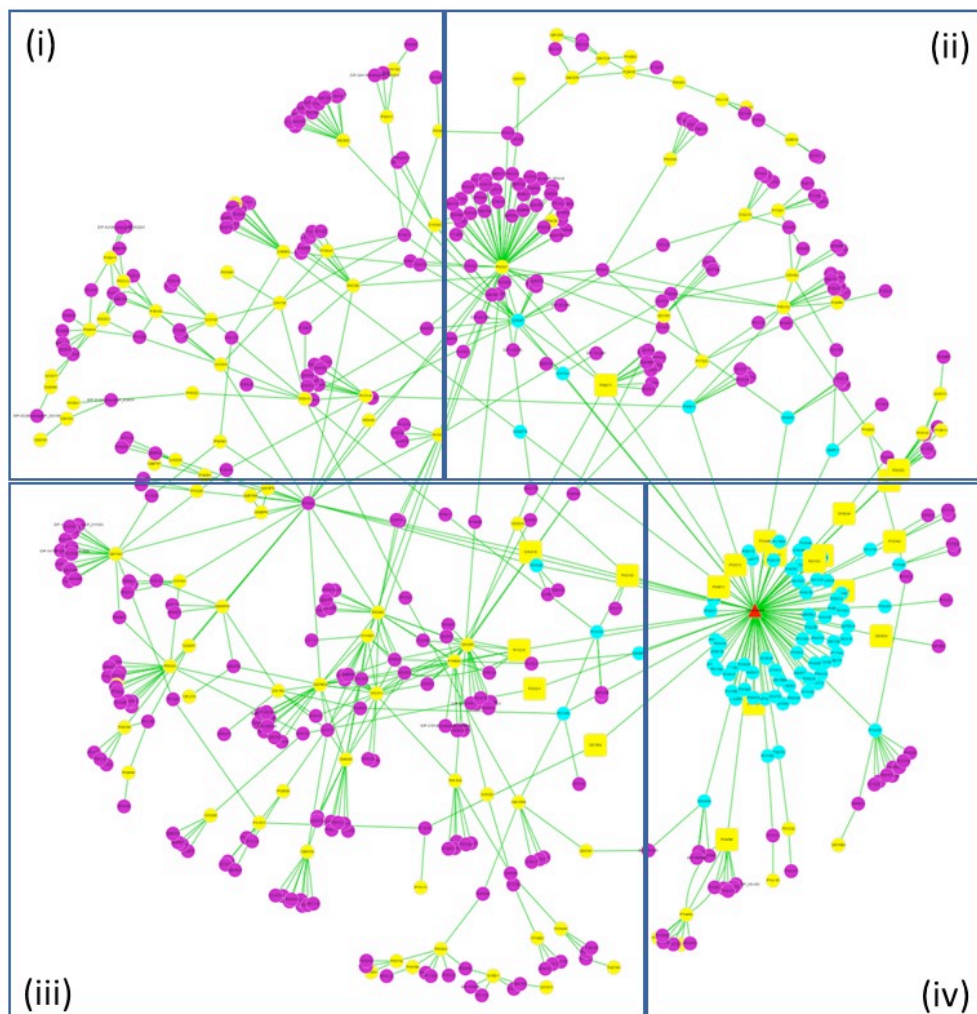


Figure S1. Divided view of Figure 1 'cannabidiol-target-inflammation network'.

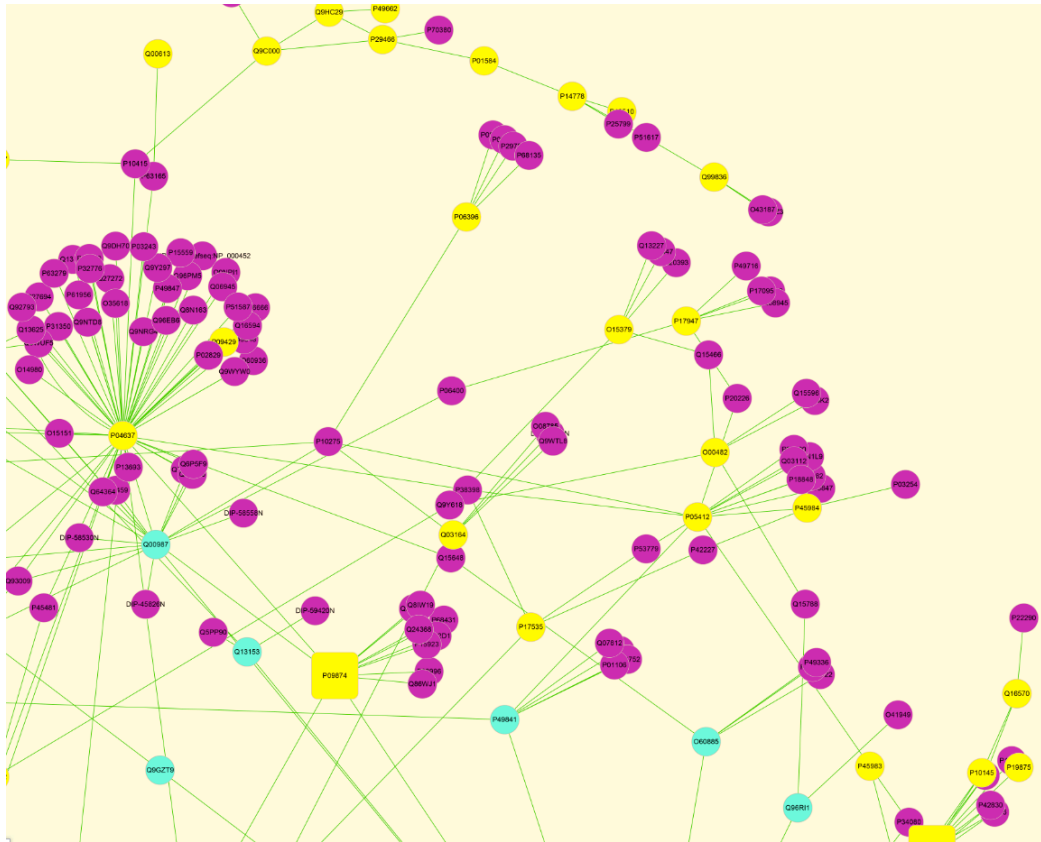


Figure S3. Enlarged view (ii) of Figure 1 ‘cannabidiol-target-inflammation network’.

Table S1 Total Analysis of Topological Parameters of Potential Targets in “Compound-Target-Disease” Network

UniProt ID	Protein Name	betweenness centrality	closeness centrality	Degree
P04637	Cellular tumor antigen p53	0.304623	0.301269	58
Q9Y6K9	NF-kappa-B essential modulator	0.064826	0.250219	21
Q9Y4K3	TNF receptor-associated factor 6	0.064373	0.237797	20
Q04206	Transcription factor p65	0.032397	0.251323	19
P19838	Nuclear factor NF-kappa-B p105 subunit	0.047215	0.24686	19
P25963	NF-kappa-B inhibitor alpha	0.042616	0.247181	18
O15111	Inhibitor of nuclear factor kappa-B kinase subunit alpha	0.0196	0.234086	18
P00533	Epidermal growth factor receptor	0.059172	0.24276	17
P31749	RAC-alpha serine/threonine-protein kinase	0.045702	0.265363	13
O14920	Inhibitor of nuclear factor kappa-B kinase subunit beta	0.024162	0.24569	13
P05412	Transcription factor AP-1	0.040425	0.232179	13
Q99558	Mitogen-activated protein kinase kinase kinase 14	0.024606	0.230024	13
P09874	Poly [ADP-ribose] polymerase 1	0.102009	0.286432	12
Q16665	Hypoxia-inducible factor 1-alpha	0.033271	0.225475	12
P24385	G1/S-specific cyclin-D1	0.034723	0.244111	10
Q99759	Mitogen-activated protein kinase kinase kinase 3	0.027914	0.19937	10
P35968	Vascular endothelial growth factor receptor 2	0.041569	0.240709	9
P25445	Tumor necrosis factor receptor superfamily member 6	0.045595	0.233415	9
P19438	Tumor necrosis factor receptor superfamily member 1A	0.028184	0.200704	9
P41182	B-cell lymphoma 6 protein	0.035707	0.236025	8
P04150	Glucocorticoid receptor	0.038264	0.19979	8
P41279	Mitogen-activated protein kinase kinase kinase 8	0.059232	0.255262	7
Q13546	Receptor-interacting serine/threonine-protein kinase 1	0.092458	0.247181	7
P25025	C-X-C chemokine receptor type 2	0.01742	0.239899	7
O15350	Tumor protein p73	0.008025	0.230676	7
Q9HCN6	Platelet glycoprotein VI	0.075039	0.208715	7
Q86WV6	Stimulator of interferon genes protein	0.014639	0.237006	6
Q14790	Caspase-8	0.011827	0.2194	6
P25024	C-X-C chemokine receptor type 1	0.010408	0.239496	5
Q13191	E3 ubiquitin-protein ligase CBL-B	0.010508	0.238095	5
Q14164	Inhibitor of nuclear factor kappa-B kinase subunit epsilon	0.00502	0.209482	5
Q03164	Histone-lysine N-methyltransferase 2A	0.011844	0.206972	5
P06396	Gelsolin	0.013998	0.20014	5
P40763	Signal transducer and activator of transcription 3	0.005449	0.25266	4
Q16236	Nuclear factor erythroid 2-related factor 2	0.010508	0.233511	4
P17535	Transcription factor jun-D	0.00414	0.198468	4
Q15078	Cyclin-dependent kinase 5 activator 1	0.040275	0.283865	3
P13569	Cystic fibrosis transmembrane conductance regulator	0.007011	0.238693	3
Continued				
P60900	Proteasome subunit alpha type-6	0.006862	0.235343	3
Q30201	Hereditary hemochromatosis protein	0.024302	0.234279	3
P35228	Nitric oxide synthase, inducible	0.007011	0.23332	3
P49281	Natural resistance-associated macrophage protein 2	0.007011	0.23332	3
P55957	BH3-interacting domain death agonist	0.004674	0.209945	3
P35869	Aryl hydrocarbon receptor	0.007011	0.198399	3

CHAPTER 7

MANUSCRIPT 7

To be submitted to

Journal of Natural Products

***In vitro, in silico, and in vivo* evaluation of the inhibitory effects of punicalagin, the major pomegranate (*Punica granatum*) polyphenol, on NLRP3 inflammasome activation**

Chang Liu, Hang Ma,* Angela L. Slitt,* and Navindra P. Seeram*

Department of Biomedical and Pharmaceutical Sciences, College of Pharmacy, University of Rhode

Island, Kingston, RI 02881, USA

**Authors to whom correspondence should be addressed*

Hang Ma, Phone: +1(401)-874-7654; Email: hang_ma@uri.edu

Angela L. Slitt, Phone: +1(401)-874-5020; Email: angela_slitt@uri.edu

Navindra P. Seeram, +1(401)-874-9367; Email: nseeram@uri.edu

7 Greenhouse Rd, Kingston, RI 02881, USA; Department of Biomedical and Pharmaceutical Sciences,
College of Pharmacy, University of Rhode Island

Abstract

Punicalagin (PA), the major polyphenol in pomegranate (*Punica granatum*), has been reported to show anti-inflammatory effects but its inhibitory effects on the inflammasome remain unclear. Herein, we evaluated PA's effects on the inhibition of the NLRP3 inflammasome and inflammasome activation-related receptor (P2X7) using *in vitro*, *in silico*, and *in vivo* models. PA inhibited the NLRP3 inflammasome by reducing IL- β in lipopolysaccharide (LPS) and nigericin stimulated human monocyte THP-1 cells. PA's inhibitory effects on the NLRP3 inflammasome were supported by its down-regulation of the levels of cellular caspase-1, pyroptosis, mRNA and protein expression of IL- β , caspase-1, and NLRP3. In addition, surface plasma resonance assay and molecular docking analysis showed that PA binds to the P2X7 receptor and interacts with the amino acids of the P2X7 protein. *In vivo* studies using two different mouse models of peritonitis (stimulated by either LPS or monosodium urate) showed that PA (50 mg/kg i.p.) exerted anti-inflammatory effects by reducing the levels of cytokines including IL-1 β and TNF- α . The current data suggest that PA's anti-inflammatory effects on the NLRP3 inflammasome may contribute toward the overall anti-inflammatory effects reported for the pomegranate fruit.

KEYWORDS: Pomegranate (*Punica granatum*), polyphenol, Punicalagin, inflammation, NLRP3 inflammasome, P2X7

INTRODUCTION

Inflammation is a complex physiological response to invading pathogens and tissue injury. It is characterized by several physiopathological manifestations including vasodilatation, plasma extravasations, cell migration, and activation of coagulation cascades (Goldstein, Snyderman, & Gallin, 1992). Inflammation is closely associated with numerous diseases including atherosclerosis, Alzheimer's disease, Parkinson's disease, rheumatoid arthritis, and cancers (Davis, Wen, & Ting, 2011; Kotas & Medzhitov, 2015; Libby, 2012; Saitel & Olefsky, 2017). Studies have revealed that inflammation can be exacerbated by the activation of a series of intracellular proteins complexes detecting pathogenic microorganisms and sterile stressors known as the inflammasome (Davis et al., 2011; Petrilli, Papin, & Tschopp, 2005). The inflammasome consists of several important components including the nucleotide-binding domain, leucine rich repeat containing proteins (also known as NOD-like receptors, NLRs) and AIM2-like receptors (ALRs) (Gross, Thomas, Guarda, & Tschopp, 2011; Petrilli et al., 2005). NLRP3, an NLR-subset inflammasome, has been recognized for its crucial role in host defense against pathogens, which is involved in a wide variety of acute and chronic inflammation-driven diseases (Jin & Flavell, 2010; Schroder, Zhou, & Tschopp, 2010). Upon sensing various stimuli, inflammasome complexes are formed by binding to pro-caspase-1 homotypically via its own caspase activation and recruitment domain (CARD) or via an adaptor protein, namely, apoptosis-associated speck-like protein containing CARD (ASC) (Latz, Xiao, & Stutz, 2013). One of the most potent activators of the NLRP3 inflammasome is extracellular ATP acting at the purinergic P2X7 receptor (Franceschini et al., 2015). Upon activation, NLRP3 inflammasome complexes mediate proteolytic cleavage and release of the pro-inflammatory cytokines, IL-1 β and IL-18, which further induce a wide variety of pathological events linked to inflammation (Man, Karki, & Kanneganti, 2017). For example, NLRP3 activation initiates an inflammation related programmed cell death, known as pyroptosis, which contributes to numerous diseases including cardiovascular diseases, immune disorders, infectious diseases and cancers (Ma et al., 2018; Man et al., 2017). Therefore, the NLRP3 inflammasome is considered as a potential therapeutic target for inflammation-related diseases (Shen et al., 2018). Several NLRP3 inflammasome inhibitors have been reported to show beneficial effects for NLRP3-related diseases in animal models (Shao, Xu, Han, Su, & Liu, 2015). For instance, MCC950 is a

synthetic selective inhibitor of NLRP3 and has been reported to show anti-inflammatory activities in a LPS-induced mouse peritonitis model and experimental autoimmune encephalomyelitis (Coll et al., 2015). In addition, CY-09, another synthetic inhibitor of NLRP3, has been shown to specifically inhibit NLRP3 inflammasome both *in vitro* and *in vivo* (Lamkanfi & Dixit, 2017). Another promising NLRP3 inflammasome inhibitor is OLT1177, which is being studied in a phase II clinical trial for arthritis therapy (Klück et al., 2019; Marchetti et al., 2018). However, while most of these aforementioned NLRP3 inflammasome inhibitors are synthetic in origin, there is paucity of data on NLRP3 inflammasome inhibitors from natural products.

Our laboratory has been involved in a comprehensive research program to investigate the phytochemical composition and biological effects of several botanicals including the pomegranate (*Punica granatum*) fruit (Pantuck et al., 2006; N. P. Seeram, S. M. Henning, Y. Zhang, M. Suchard, Z. Li, & D. Heber, 2006) (DaSilva et al., 2019; Yongqiang Liu & Navindra P Seeram, 2018; Loren, Seeram, Schulman, & Holtzman, 2005; Tao Yuan et al., 2012; Tao Yuan, Wan, Ma, & Seeram, 2013). For instance, we reported that a pomegranate fruit extract shows potential protective effect against Alzheimer's disease in an aged animal model due to its anti-neuroinflammatory and anti-glycation effects (Ahmed, Subaiea, Eid, Li, Seeram, & Zawia, 2014; T. Yuan et al., 2016). The pomegranate fruit is known to be a rich source of polyphenols among which punicalagin (PA) is the predominant phytochemical (Adams, Zhang, Seeram, Heber, & Chen, 2010; Y. Liu & N. P. Seeram, 2018). Published studies have shown that PA exerts anti-inflammatory effects against inflammatory bowel disease, diarrhea, and ulcers (Shah, Parikh, Patel, Patel, Joshi, & Gandhi, 2016; Xu et al., 2017). However, it is not clear whether the anti-inflammatory effects of PA are associated with its inactivation of the NLRP3 inflammasome. Herein, we evaluated the inhibitory effects of PA on the activation of NLRP3 and its NLRP3 anti-inflammatory activity using a combination of *in vitro*, *in silico* and *in vivo* (two separate animal models of peritonitis induced by LPS and monosodium urate) models.

RESULTS AND DISCUSSION

PA inhibits IL-1 β secretion in LPS-nigericin treated THP-1 monocytes.

We determined the levels of inflammasome-dependent cytokine IL-1 β and inflammasome-independent cytokine TNF- α in human THP-1 monocytes. PA exhibited inhibitory effects on IL-1 β secretion, but had no effects on TNF- α production (Fig. 1A). We next sought to investigate the inhibitory effects of PA at the doses of 0.01-100 μ M on NLRP3 inflammasome activation using :1) pre-treatment of PA followed by LPS-induced inflammation (i.e. PA exposure for 1 h followed by LPS for 4 h), and, 2) LPS-induced inflammation followed by PA exposure (i.e. LPS exposure for 4 h followed by PA for 1 h). Interestingly, pre-treatment with PA before LPS-induced inflammation inhibited IL-1 β secretion and also suppressed TNF- α secretion (Fig. 1B). However, treatment with PA after LPS-induced inflammation specifically suppressed IL-1 β secretion but had no effects on TNF- α production (Fig. 1B). To confirm whether PA could block NLRP3 activation, we compared it to a known broad-spectrum natural product inhibitor of NLRP3 inflammasome, namely, oridonin, in the NLRP3 activation assay. Oridonin reduced the concentration of extracellular IL-1 β to 187.6 pg/mL as compared to the LPS-nigericin treated group (833.3 pg/mL). At equivalent concentrations of 10 μ M, PA reduced the concentration of extracellular IL-1 β levels to 331.7 pg/mL (Fig. 1C). In addition, PA showed stronger inhibitory activity to cellular IL-1 β levels than oridonin (719.5 pg/mL vs 2785.5 pg/mL; Fig. 1D), suggesting that PA was a specific inhibitor of NLRP3 inflammasome activation.

PA specifically inhibited NLRP3 inflammasome activation in LPS-nigericin treated THP-1 monocytes.

Next, we studied the mechanism of how PA blocked NLRP3 activation by assessment of its effects on NLRP3 inflammasome components. Caspase-1, known as IL-1 β -converting enzyme, is responsible for the processing of inactive pro-IL-1 β to active IL-1 β . Stimulation by LPS/nigericin, leads to the increase of active-cellular and active-extracellular caspase-1 to 1.53- and 1.42-fold, respectively, as compared to the control group (Fig. 2A and B). These effects were alleviated by treatment with PA (10 μ M) by reducing the amount of active-cellular and active-extracellular caspase-1 to 55.1% and 62.0 %, respectively. In addition to the processing of IL-1 β , caspase-1 also triggers pyroptosis, an inflammasome activation-induced cell death, in the macrophages in response to LPS/nigericin. To verify the modulatory effects of PA on caspase-1 activation-mediated cell pyroptosis, we measured the levels of lactate dehydrogenase (LDH), termed as a biomarker of cell pyroptosis. Stimulation by

LPS/nigericin led to an increase of LDH by 4.56-fold as compared to the control group, and PA (10 μ M) alleviated the release of LDH by 64.2% (Fig. 2C).

In addition, the effects of PA on the mRNA and protein levels of IL-1 β , Caspase-1, and NLRP3 were evaluated with qRT-PCR and Western blotting, respectively. Stimulation by LPS/nigericin leads to increased mRNA levels of il-1 β , caspase-1, and nlrp3 by 633.0-, 1.50-, and 2.07-fold, respectively, as compared to the control group. Treatment with PA (10 μ M) decreased the mRNA levels of il-1 β , caspase-1, and nlrp3 to 223.2-, 0.54-, and 1.10-fold, respectively (Fig. 2D-F). This effect was supported by Western blot analysis showing that PA (10 μ M) suppressed the expression of proteins including Caspase-1, NLRP3 in the LPS-nigericin treated THP-1 monocytes (Fig. 2G).

PA inhibited LPS-nigericin-induced mitochondrial damage and mito-ROS production in LPS-nigericin treated THP-1 monocytes.

Mitochondrial damage and mito-ROS production are known as the upstream signaling events of NLRP3 activation. We further evaluated the activities of PA on mitochondrial damage and mito-ROS production in the LPS-nigericin treated THP-1 cells by flow cytometry and confocal microscopy. The levels of mito-derived ROS in THP-1 cells were assessed by using a mitochondria-specific probe, namely, MitoSOXTM. Stimulation by LPS/nigericin leads to increased mito-ROS by 10.9-fold, as compared to the control group. Treatment with PA (10 μ M) decreased the mito-ROS by 43.5% as compared to the LPS-nigericin treated THP-1 cells (Fig. 3A and B). Results from confocal microscopy also confirmed the inhibitory effects of PA (10 μ M) on LPS-nigericin induced mito-ROS production (Fig. 3C). In addition to mito-ROS production, we also evaluated the mitochondrial damage using mito-Tracker red probe. As expected, stimulation by LPS-nigericin caused mitochondrial damage, whereas treatment with PA (10 μ M) alleviated the effects on mitochondrial damage (Fig. 3D).

PA interacted with the P2X7 Receptor.

Activation of the NLRP3 inflammasome has been linked to a purinergic type 2 receptor called P2X7, a ligand-gated ion channel modulating intracellular K⁺ efflux and Ca⁺ influx. Nigericin binds to P2X7 and increases the permeability of the plasma membrane, which further facilitates the secretion of IL-1 β . We

then investigated the interactions between PA and P2X7 receptor to predict their possible binding sites. We calculated the free binding energy in different binding modes to find the most suitable binding pocket. As shown in Fig 4A, the most suitable binding site of PA was at the upper body, between the head and left flipper of the P2X7 receptor, with the lowest free binding energy of -4.61 kcal/mol. We next analyzed the binding parameters between PA and P2X7 receptor using surface plasma resonance (SPR) assay. PA at five concentrations (3.9, 7.8, 15.6, 31.2, and 62.5 μ M) were used to observe PA-associated affinity with the P2X7 receptor. The K_D , calculated using BiaEvolution software, was 4.24×10^6 (M^{-1}) (Fig. 4B). As shown in Fig. 4C, PA was able to bind to the P2X7 receptor by forming hydrogen bonds between its hydroxyl group and residues including LYS145 and ILE147. In addition, hydrogen bonds were also formed between its carbonyl groups and residues including GLN116 and SER165. The stabilization of the PA-P2X7 complex may be facilitated by Pi-Pi T shaped and Pi-Alkyl bonds between the aromatic ring of PA and residue TRP167 (Fig. 4C).

PA affected the levels of inflammasome-panel genes in LPS-nigericin treated THP-1 monocytes.

To further elucidate the effects of PA on inflammasome-related genes, the inflammasome panel genes were assessed with Geneplex assay. We first examined the expressions of inflammasomes including NLRP1, AIM2, NLRP3, NLRP4, NLRC5, NLRP5, NLRP6, and NLRP9 (Fig. 5B). Stimulation by LPS/nigericin led to increased AIM2 and NLRP3 by 6.27- and 1.51-fold, respectively, as compared to the control group. Treatment with PA (10 μ M) decreased AIM2 and NLRP3 to 3.70- and 1.11-fold, respectively, as compared to the control group (Fig. 5A and B). Next, we explored the expressions of inflammasome signaling-related genes (Fig. 5C). Stimulation by LPS/nigericin led to increased CCL-2, PSTPIP1, TNF, CASP5, IKK β , P2X7R, and BRIC3 by 20.8-, 85.4-, 72.04-, 70.5-, 9.9-, 9.7-, and 77.36-fold, respectively, as compared to the control group. Treatment with PA (10 μ M) decreased the CCL-2, PSTPIP1, TNF, CASP5, and BRIC3 to 14.2-, 59.5, 50.4, 42.9, and 60.0-fold, respectively, as compared to the control group (Fig. 5A and C).

PA suppresses NLRP3-dependent inflammation in vivo

We next examined whether PA could inhibit NLRP3 inflammasome activation *in vivo*. Previous studies have shown that the induction of IL-1 β by intraperitoneal (i.p.) injection of LPS and MSU are NLRP3 inflammasome dependent (Coll et al., 2015; Latz, Xiao, & Stutz, 2013). Therefore, these two inflammasome inducers were delivered to animals in separate experiments to induce IL-1 β (Fig. 6A).

Mice were pre-treated with PA (50 mg/kg) one hour before i.p. injection of LPS and were assessed two hours later. Pre-treatment with PA reduced serum concentrations of IL-1 β and TNF- α , indicating the anti-inflammatory effects of PA *in vivo* (Fig. 6B and C). In addition, pre-treatment with PA reduced peritoneal concentrations of IL-1 β , while it did not considerably decrease the amount of TNF- α , indicating that PA was able to specifically inhibit NLRP3 inflammasome activation in the peritoneal cavity (Fig. 6D and E).

In the second experiment, mice were pre-treated with PA (50 mg/kg) before i.p. injection of MSU and were assessed six hours later. As expected, serum concentrations of IL-1 β and TNF- α were significantly increased in the MSU-induced peritonitis mouse model. Treatment with PA (50 mg/kg) significantly alleviated MSU-induced IL-1 β production, while it did not considerably decrease the amount of TNF- α (Fig. 6F and G), indicating that PA was able to specifically inhibit serum IL-1 β in the MSU-induced peritonitis mouse model. These results indicated that PA prevents acute inflammation via inhibition of NLRP3 inflammasome.

Conclusion

In summary, we evaluated the anti-inflammasome activity of PA and its mechanisms of action using *in vitro*, *in silico*, and *in vivo* models. PA inhibited the expression of NLRP3 and its downstream components including caspase-1 and IL-1 β indicating that PA is a specific inhibitor for the activation of the NLRP3 inflammasome (*in vitro* and *in vivo*). The underlying mechanisms of PA on the regulation of NLRP3 inflammasome were associated with its modulatory effects on the P2X7 receptor. In addition, PA exerted anti-inflammatory effects in two separate mouse models of peritonitis by specifically inhibiting peritoneal IL-1 β induced by LPS and serum IL-1 β induced by MSU. PA's inhibitory effects on the NLRP3 inflammasome may contribute to the anti-inflammatory effects reported for this

polyphenol and, overall, for the whole pomegranate fruit, supporting the further investigation of this natural product for the potential management of inflammation-related diseases.

EXPERIMENTAL SECTION

Reagents

Monosodium urate (MSU), phorbol 12-myristate 13-acetate (PMA), dimethyl sulfoxide (DMSO), lipopolysaccharides (LPS; from *Escherichia coli* O55:B5), nigericin, and oridonin were purchased from Sigma Chemical Co. (St. Louis, MO, USA). MitoSOX and MitoTracker™ Red was purchased from Thermo Fisher Scientific (Waltham, MA, USA). Punicalagin (PA) was previously isolated and identified by our laboratory from pomegranate fruit extract (Jean-Gilles et al., 2013; Navindra P Seeram, Susanne M Henning, Yanjun Zhang, Marc Suchard, Zhaoping Li, & David Heber, 2006). Oridonin was purchased from Cayman Chemical Co. (Ann Arbor, MI, USA).

Cell Culture and Differentiation

Human monocyte THP-1 cells were purchased from the American Type Culture Collection (ATCC, Rockville, MD, USA). Cells were cultured in Roswell Park Memorial Institute (RPMI) 1640 medium supplied with 10% fetal bovine serum (FBS) (Gibco, Life Technologies; Gaithersburg, MD, USA) and 1% penicillin/streptomycin solution (100 U/mL penicillin and 100 µg/mL streptomycin; from Gibco, Life Technologies; Grand Island, NY, USA). THP-1 monocytes were differentiated using PMA using our previously reported method (Liu, Ma, Slitt, & Seeram). In brief, cells were cultured in medium containing PMA (25 nM) for 48 h. PMA was then removed and cells were cultured in PMA free medium for 24 h.

Inflammasome Activation Assay

NLRP3 Inflammasome activation assay was according to our previously reported method (Liu, Ma, Slitt, & Seeram). THP-1 monocytes were seeded at a density of 5×10^4 cells per well in a 48-well plate and differentiated with PMA (25 ng/mL). Differentiated THP-1 monocytes were treated with LPS (100 ng/mL) for 4 h, followed by treatment with compound (10 µM) for 1 h. Then, nigericin (10 µM) was incubated with the cells for 1 h, and the cell culture supernatant was collected. The levels of IL-1β and

TNF- α were determined using specific ELISA kits (BioLegend, San Diego, CA, USA). LDH and caspase-1 were determined by using commercial kits from Promega (Fitchburg, WI, USA).

Western Blotting

The harvested cells were homogenized in an ice-cold RIPA buffer containing protease inhibitor. Protein concentration was determined by Bicinchoninic Acid (BCA) protein assay kit (Thermo Fisher, Waltham, MA, USA). Equal amounts of the protein were separated by 10% precast polyacrylamide gel (BIO-RAD, Hercules, CA, USA), transferred to polyvinylidene fluoride (PVDF) membranes, and probed with the primary antibodies against human caspase-1 (D7F10) (1 : 1,000), human NLRP3 (D2P5E) (1 : 1,000), or human β -Actin (13E5) (1: 1,000) overnight at 4 °C, followed by appropriate horseradish peroxidase (HRP)-linked secondary antibodies for 2 hours at room temperature. The immuno-reactive proteins were detected with Pierce ECL Western blotting substrate (Cytiva, Marlborough, MA, USA) and visualized by ChemiDoc MP imaging system. The expression levels of β -actin were used to normalize the expression of target genes.

Animals

Male C57BL/6J mice (4-6 weeks old) were purchased from The Jackson Laboratory. All mice were housed in a room under a 12 h light/dark cycle and fed under experimental conditions with a temperature of 22–24 °C and humidity of 50 \pm 5%. All animal experiments protocols were approved by the Animal Care Committee of the University of Rhode Island.

LPS and MSU-Induced Peritonitis

After one week acclimation, C57BL/6 mice were injected intraperitoneally (i.p.) with 50 mg/kg PA (dissolved in vehicle containing 90% PBS and 10% DMSO) or vehicle control (DMSO/PBS) 1 h before i.p. injection of 10 mg/kg LPS or PBS. After for 2 h mice were sacrificed and 5 ml ice-cold PBS were used to wash the peritoneal cavities. In the model of MSU-induced peritonitis, C57BL/6 mice were injected intraperitoneally (i.p.) with MSU crystals (1 mg dissolved in 0.5 mL of PBS). Before injection of MSU, PA (50 mg/kg; dissolved in vehicle solvent containing 90% PBS and 10% DMSO) were injected intraperitoneally. After 6 h, the mice were killed and the blood was collected and serum was isolated. IL-1 β and TNF- α levels in serum or peritoneal lavage fluid were measured by specific ELISAs.

qRT-PCR

RNA was extracted from the cells using RNAqueous®-Micro Kit (Thermo Fisher, Waltham, MA, USA) according to the manufacturer's instruction. SuperScript® IV Reverse Transcriptase was used to RT reaction and TaqMan® Fast Advanced Master Mix was used to quantitative analysis. To analyze the accuracy of the PCR reaction, the melt curves were used. To evaluate the expressions of genes, $2^{-\Delta\Delta Ct}$ values were calculated. The mRNA expression values of nlrp3, il1 β , and caspase1 were normalized to that of GAPDH. The primer sequences for nlrp3 (Hs00918082), il1 β (Hs01555410), caspase1 (Hs00354836), and house-keeping GAPDH (Hs02786624) were designed and synthesized by Applied Biosystems (Foster City, CA, United States).

Flow cytometry

THP-1 cells were seeded and differentiated in 6-well plates at 0.5×10^6 cells for 48 h. The cells were treated then with LPS (100 ng/mL) for 4 h, followed by treatment with PA (10 μ M) for 1 h. Then, nigericin (10 μ M) was incubated with the cells for 1 h. The cells were then harvested and suspended in 500 μ L of FACS buffer containing 5 μ M Mito-SOX followed by incubation in the dark for 15 min. Then the cells were measured by flow cytometry (BD FACSCalibur, San Jose, CA, USA) and data were analyzed using software FlowJo (LLC, Ashland, Oregon, USA).

Confocal microscopy

THP-1 cells were seeded in 3 mm petri dish at 0.5×10^6 cells. The differentiated THP-1 cells were treated then with LPS (100 ng/mL) for 4 h, followed by treatment with PA (10 μ M) for 1 h. Then, nigericin (10 μ M) was incubated with the cells for 1 h. Hoechst 33342 staining buffer (300 μ L) was added to the cells and incubated for 30 min in darkness. Next, Mito-Tracker Red or MitoSOX staining buffer was added to the cells and incubated for 30 min in darkness. Cells were then subjected to Nikon Eclipse Ti2 inverted confocal microscope (Nikon, Minato City, Tokyo, Japan).

Geneplex assay

Gene expression analysis was conducted on RNA samples using a custom QuantiGene Luminex xMAP gene expression panel (Thermo Fisher, Waltham, MA, USA). The multiplex assay was performed according to the manufacturer's protocols and mean fluorescence intensity (MFI) was quantified using a Bio-rad Bio-plex 200 instrument (Hercules, CA, USA). The expression of transcripts involved in

inflammasome activation were measured in THP-1 cells using a customized QuantiGene panel. The genes were included *PYCARD*, *MEFV*, *PSTPIP1*, *NLRX1*, *RAGE*, *NLRP9*, *P2X7R*, *NLRP4*, *NLRC5*, *NLRP3*, *NLRP5*, *AIM2*, *CASP1*, *CASP5*, *HSP90AA1*, *IKBKB*, *NFKB1*, *TNF*, *CASP4*, *CXCL1*, *TXNIP*, *MYD88*, *BIRC3*, *CCL2*, and *NLRP6*.

Surface Plasmon Resonance

Human P2RX7/P2X7 Protein (Recombinant His-T7) was purchased from LSBio (Seattle, WA, USA). SPR binding measurements were conducted on a Biacore T200 instrument (GE Healthcare; Marlborough, MA, USA). All experiments were performed at 25 °C using carboxymethylated CM 5 chips. Immobilization of P2X7R protein on the surface of the chip was performed by injection of protein solution (20 µg/mL) in sodium acetate buffer (10 mM; pH 4.5) for 20 min at a flow rate of 2 µL/min. Approximately 7800 RU of P2X7R protein was immobilized on the flow cell 2. The flow cell 1 without any modification was used as a reference to adjust the system baseline. PA was prepared at concentrations of 3.9, 7.8, 15.6, 31.2, and 62.5 µM.

Molecular Docking

The structures of punicalagin were obtained from the human metabolome database (www.HMDB.ca). Molecular Operating Environment (MOE) was applied to build the 3D structure of punicalagin. The structural coordinates of the P2X7 receptor with a resolution of 3.40 Å were retrieved in PDB format from the RCSB protein data bank (www.rcsb.org; PDB ID: 5U1L). Chimera 11.3 was applied to delete the water molecules, solvent, non-complexed ions, and ligand of 5U1L. AutodockTools 1.5.6 was used to perform molecular docking with the Autodock 4.2 algorithm. Discovery Studio 4.5 (Accelrys Inc., San Diego, CA, USA) was applied to analyze the interactive residues.

Statistical analyses

Data are presented as average values ± standard deviation (SD) from multiple individual experiments each carried out in triplicate or as mean ± SD. Non-linear regression analysis of inhibitor vs. normalized response (variable slope) was performed using Graphpad Prism8 (GraphPad Software, La Jolla, CA, USA). One-way analysis of variance with multiple comparisons and Student-Newman-Keuls test were performed. A *p*-value less than 0.05 was defined as statistical significance between the two groups.

ASSOCIATED CONTENT
Supporting Information

None

ACKNOWLEDGEMENT

Data were acquired from instruments located at the University of Rhode Island in the RI-INBRE core facility obtained from Grant P20GM103430 from the National Center for Research Resources (NCRR), a component of the National Institutes of Health (NIH).

References

- Adams, L. S., Zhang, Y., Seeram, N. P., Heber, D., & Chen, S. (2010). Pomegranate ellagitannin-derived compounds exhibit antiproliferative and antiaromatase activity in breast cancer cells in vitro. *Cancer Prev Res (Phila)*, 3(1), 108-113. <https://doi.org/10.1158/1940-6207.CAPR-08-0225>.
- Ahmed, A. H., Subaiea, G. M., Eid, A., Li, L., Seeram, N. P., & Zawia, N. H. (2014). Pomegranate extract modulates processing of amyloid-beta precursor protein in an aged Alzheimer's disease animal model. *Curr Alzheimer Res*, 11(9), 834-843. <https://www.ncbi.nlm.nih.gov/pubmed/25274111>.
- Coll, R. C., Robertson, A. A., Chae, J. J., Higgins, S. C., Muñoz-Planillo, R., Inerra, M. C., . . . Stutz, A. (2015). A small-molecule inhibitor of the NLRP3 inflammasome for the treatment of inflammatory diseases. *Nature medicine*, 21(3), 248-255.
- DaSilva, N. A., Nahar, P. P., Ma, H., Eid, A., Wei, Z., Meschwitz, S., . . . Seeram, N. P. (2019). Pomegranate ellagitannin-gut microbial-derived metabolites, urolithins, inhibit neuroinflammation in vitro. *Nutr Neurosci*, 22(3), 185-195. <https://doi.org/10.1080/1028415X.2017.1360558>.
- Davis, B. K., Wen, H., & Ting, J. P.-Y. (2011). The inflammasome NLRs in immunity, inflammation, and associated diseases. *Annual review of immunology*, 29, 707-735.

- Franceschini, A., Capece, M., Chiozzi, P., Falzoni, S., Sanz, J. M., Sarti, A. C., . . . Di Virgilio, F. (2015). The P2X7 receptor directly interacts with the NLRP3 inflammasome scaffold protein. *The FASEB Journal*, *29*(6), 2450-2461.
- Goldstein, I. M., Snyderman, R., & Gallin, J. I. (1992). *Inflammation: basic principles and clinical correlates*: Raven Press.
- Gross, O., Thomas, C. J., Guarda, G., & Tschopp, J. (2011). The inflammasome: an integrated view. *Immunological reviews*, *243*(1), 136-151.
- Jean-Gilles, D., Li, L., Vaidyanathan, V., King, R., Cho, B., Worthen, D. R., . . . Seeram, N. P. (2013). Inhibitory effects of polyphenol punicalagin on type-II collagen degradation in vitro and inflammation in vivo. *Chemico-biological interactions*, *205*(2), 90-99.
- Jin, C., & Flavell, R. A. (2010). Molecular mechanism of NLRP3 inflammasome activation. *Journal of clinical immunology*, *30*(5), 628-631.
- Klück, V., Janssen, M., Jansen, T., Tengesdal, I., Schraa, K., Skouras, D., . . . Joosten, L. (2019). P159/O30 OLT1177™, an oral NLRP3 inflammasome inhibitor, inhibits acute joint inflammation and circulating IL 1 β during gout flares in humans. BMJ Publishing Group Ltd.
- Kotas, M. E., & Medzhitov, R. (2015). Homeostasis, inflammation, and disease susceptibility. *Cell*, *160*(5), 816-827.
- Lamkanfi, M., & Dixit, V. M. (2017). A new lead to NLRP3 inhibition. *The Journal of Experimental Medicine*, *214*(11), 3147.
- Latz, E., Xiao, T. S., & Stutz, A. (2013). Activation and regulation of the inflammasomes. *Nature Reviews Immunology*, *13*(6), 397-411.
- Libby, P. (2012). Inflammation in atherosclerosis. *Arteriosclerosis, thrombosis, and vascular biology*, *32*(9), 2045-2051.
- Liu, C., Ma, H., Slitt, A. L., & Seeram, N. P. Inhibitory Effect of Cannabidiol on the Activation of NLRP3 Inflammasome Is Associated with Its Modulation of the P2X7 Receptor in Human Monocytes. *Journal of Natural Products*.
- Liu, Y., & Seeram, N. P. (2018). Liquid chromatography coupled with time-of-flight tandem mass spectrometry for comprehensive phenolic characterization of pomegranate fruit and flower

extracts used as ingredients in botanical dietary supplements. *J Sep Sci*, 41(15), 3022-3033.

<https://doi.org/10.1002/jssc.201800480>.

Liu, Y., & Seeram, N. P. (2018). Liquid chromatography coupled with time - of - flight tandem mass spectrometry for comprehensive phenolic characterization of pomegranate fruit and flower extracts used as ingredients in botanical dietary supplements. *Journal of separation science*, 41(15), 3022-3033.

Loren, D. J., Seeram, N. P., Schulman, R. N., & Holtzman, D. M. (2005). Maternal dietary supplementation with pomegranate juice is neuroprotective in an animal model of neonatal hypoxic-ischemic brain injury. *Pediatr Res*, 57(6), 858-864.
<https://doi.org/10.1203/01.PDR.0000157722.07810.15>.

Ma, Y., Jiang, J., Gao, Y., Shi, T., Zhu, X., Zhang, K., . . . Xue, B. (2018). Research progress of the relationship between pyroptosis and disease. *American journal of translational research*, 10(7), 2213.

Man, S. M., Karki, R., & Kanneganti, T. D. (2017). Molecular mechanisms and functions of pyroptosis, inflammatory caspases and inflammasomes in infectious diseases. *Immunological reviews*, 277(1), 61-75.

Marchetti, C., Swartzwelter, B., Gamboni, F., Neff, C. P., Richter, K., Azam, T., . . . D'Alessandro, A. (2018). OLT1177, a β -sulfonyl nitrile compound, safe in humans, inhibits the NLRP3 inflammasome and reverses the metabolic cost of inflammation. *Proceedings of the National Academy of Sciences*, 115(7), E1530-E1539.

Pantuck, A. J., Leppert, J. T., Zomorodian, N., Aronson, W., Hong, J., Barnard, R. J., . . . Belldegrun, A. (2006). Phase II study of pomegranate juice for men with rising prostate-specific antigen following surgery or radiation for prostate cancer. *Clin Cancer Res*, 12(13), 4018-4026.
<https://doi.org/10.1158/1078-0432.CCR-05-2290>.

Petrilli, V., Papin, S., & Tschopp, J. (2005). The inflammasome. *Current Biology*, 15(15), R581.

Saltiel, A. R., & Olefsky, J. M. (2017). Inflammatory mechanisms linking obesity and metabolic disease. *The Journal of clinical investigation*, 127(1), 1-4.

- Schroder, K., Zhou, R., & Tschopp, J. (2010). The NLRP3 inflammasome: a sensor for metabolic danger? *Science*, *327*(5963), 296-300.
- Seeram, N. P., Henning, S. M., Zhang, Y., Suchard, M., Li, Z., & Heber, D. (2006). Pomegranate juice ellagitannin metabolites are present in human plasma and some persist in urine for up to 48 hours. *J Nutr*, *136*(10), 2481-2485. <https://doi.org/10.1093/jn/136.10.2481>.
- Seeram, N. P., Henning, S. M., Zhang, Y., Suchard, M., Li, Z., & Heber, D. (2006). Pomegranate juice ellagitannin metabolites are present in human plasma and some persist in urine for up to 48 hours. *The Journal of nutrition*, *136*(10), 2481-2485.
- Shah, T. A., Parikh, M., Patel, K. V., Patel, K. G., Joshi, C. G., & Gandhi, T. R. (2016). Evaluation of the effect of Punica granatum juice and punicalagin on NFκB modulation in inflammatory bowel disease. *Molecular and cellular biochemistry*, *419*(1-2), 65-74.
- Shao, B.-Z., Xu, Z.-Q., Han, B.-Z., Su, D.-F., & Liu, C. (2015). NLRP3 inflammasome and its inhibitors: a review. *Frontiers in pharmacology*, *6*, 262.
- Shen, H.-H., Yang, Y.-X., Meng, X., Luo, X.-Y., Li, X.-M., Shuai, Z.-W., . . . Pan, H.-F. (2018). NLRP3: a promising therapeutic target for autoimmune diseases. *Autoimmunity reviews*, *17*(7), 694-702.
- Xu, Y., Shi, C., Wu, Q., Zheng, Z., Liu, P., Li, G., . . . Xia, X. (2017). Antimicrobial activity of punicalagin against Staphylococcus aureus and its effect on biofilm formation. *Foodborne pathogens and disease*, *14*(5), 282-287.
- Yuan, T., Ding, Y., Wan, C., Li, L., Xu, J., Liu, K., . . . Seeram, N. P. (2012). Antidiabetic ellagitannins from pomegranate flowers: Inhibition of α-glucosidase and lipogenic gene expression. *Organic letters*, *14*(20), 5358-5361.
- Yuan, T., Ma, H., Liu, W., Niesen, D. B., Shah, N., Crews, R., . . . Seeram, N. P. (2016). Pomegranate's Neuroprotective Effects against Alzheimer's Disease Are Mediated by Urolithins, Its Ellagitannin-Gut Microbial Derived Metabolites. *ACS Chem Neurosci*, *7*(1), 26-33. <https://doi.org/10.1021/acschemneuro.5b00260>.

Yuan, T., Wan, C., Ma, H., & Seeram, N. P. (2013). New phenolics from the flowers of *Punica granatum* and their in vitro α -glucosidase inhibitory activities. *Planta medica*, 79(17), 1674-1679.

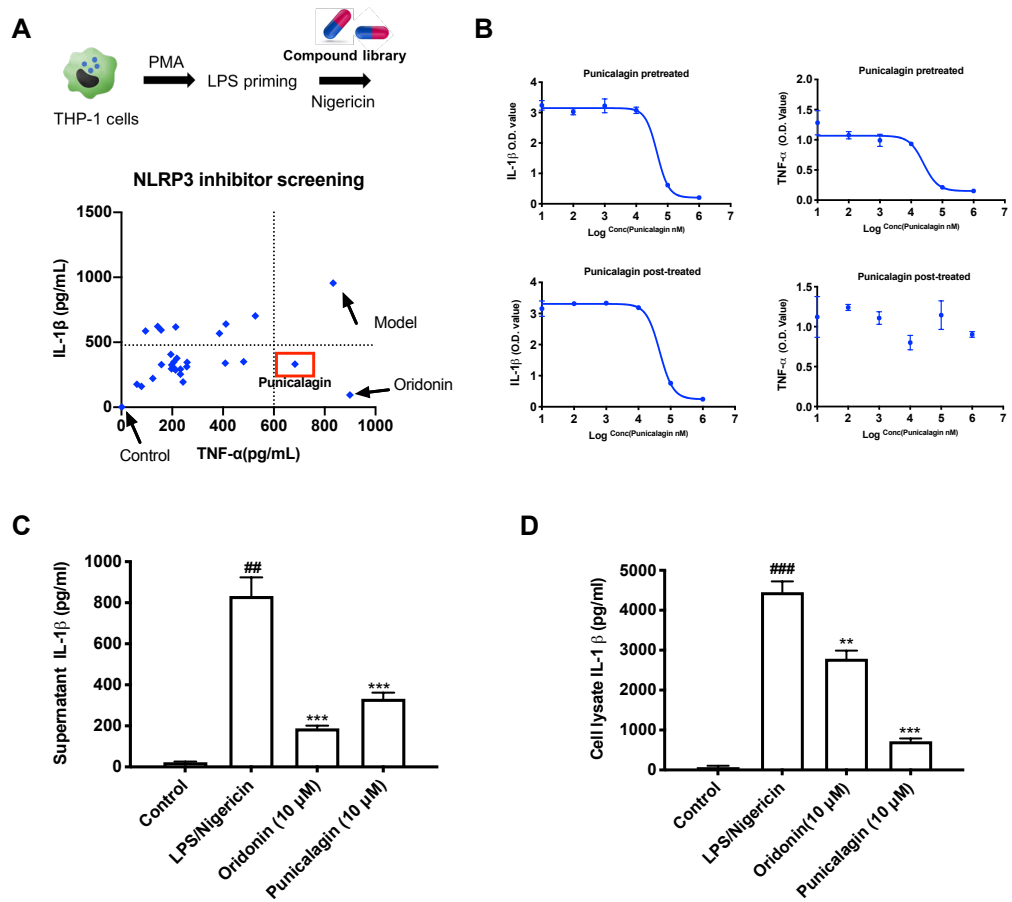


Figure 1. (A) Cytokines IL-1 β and TNF- α changes in LPS-primed (100 ng/mL, 4 h) THP-1 cells after incubation of compound library followed by induction of nigericin (10 μ M, 1 h). Each dot indicates one test compound. Compound that specific reduced IL-1 β not TNF- α was recognized as possible NLRP3 inflammasome inhibitor. Oridinin was used as a positive control. Baseline for IL-1 β and TNF- α were 478ng/mL and 600 pg/mL, respectively. (B) Analysis of IL-1 β and TNF- α release in the PA-pretreated or treated LPS-primed THP-1 cells followed by the induction of nigericin. IL-1 β release in the supernatant (C) and cell lysate (D) from the PA-treated LPS-primed THP-1 cells followed by the induction of nigericin.

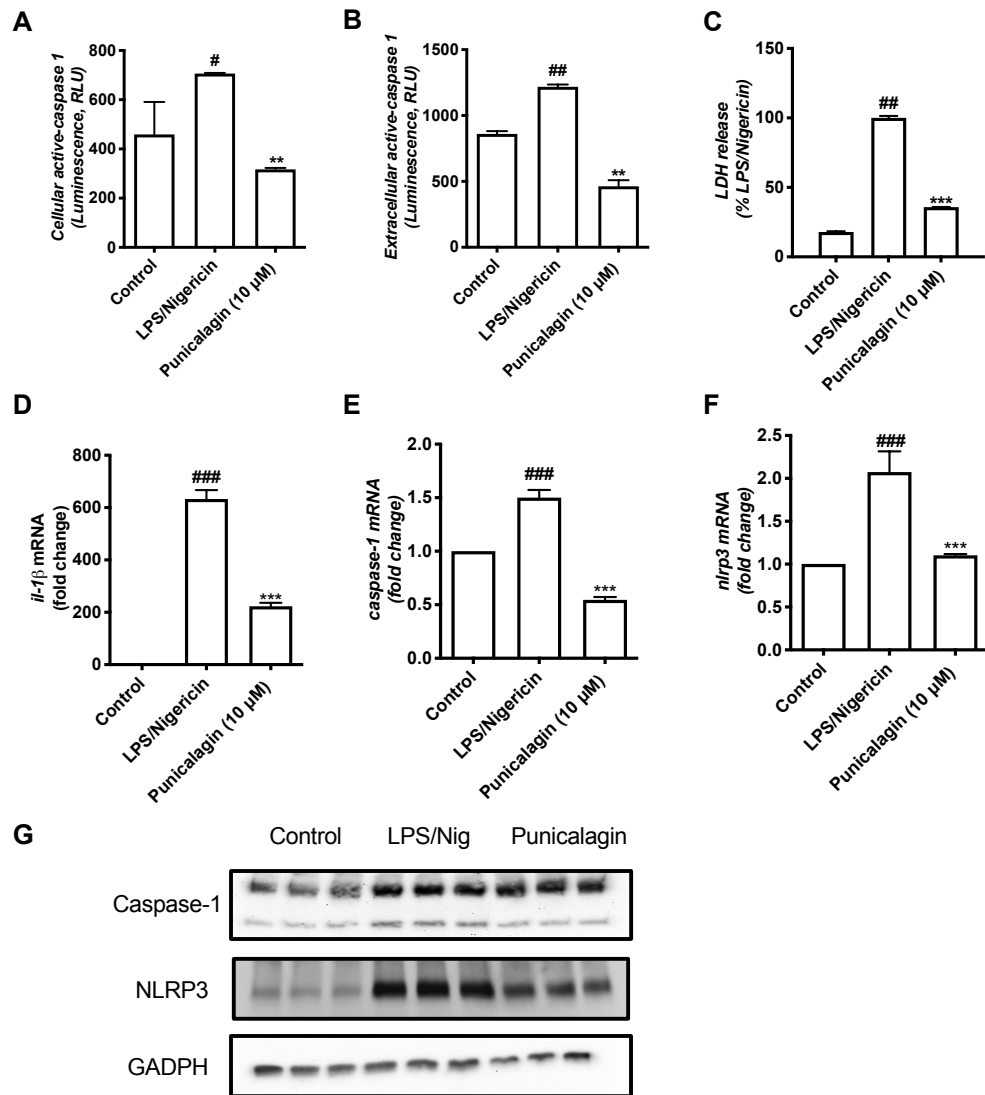


Figure 2. Analysis of cellular active-caspase 1 (A) and extracellular active caspase-1 (B) in the PA-treated LPS-primed (100 ng/mL, 4 h) THP-1 cells followed by the induction of Nigericin (10 μM, 1 h). (C) LDH release in the PA-treated LPS-primed (100 ng/mL, 4 h) THP-1 cells followed by the induction of nigericin (10 μM, 1 h). THP-1 cells were stimulated and treated with PA as indicated, mRNA levels of *il-1β* (D), *caspase-1* (E), and *nlrp3* (F) and protein levels of caspase-1, and *nlrp3* (G) were determined using qRT-PCR and western blotting, respectively.

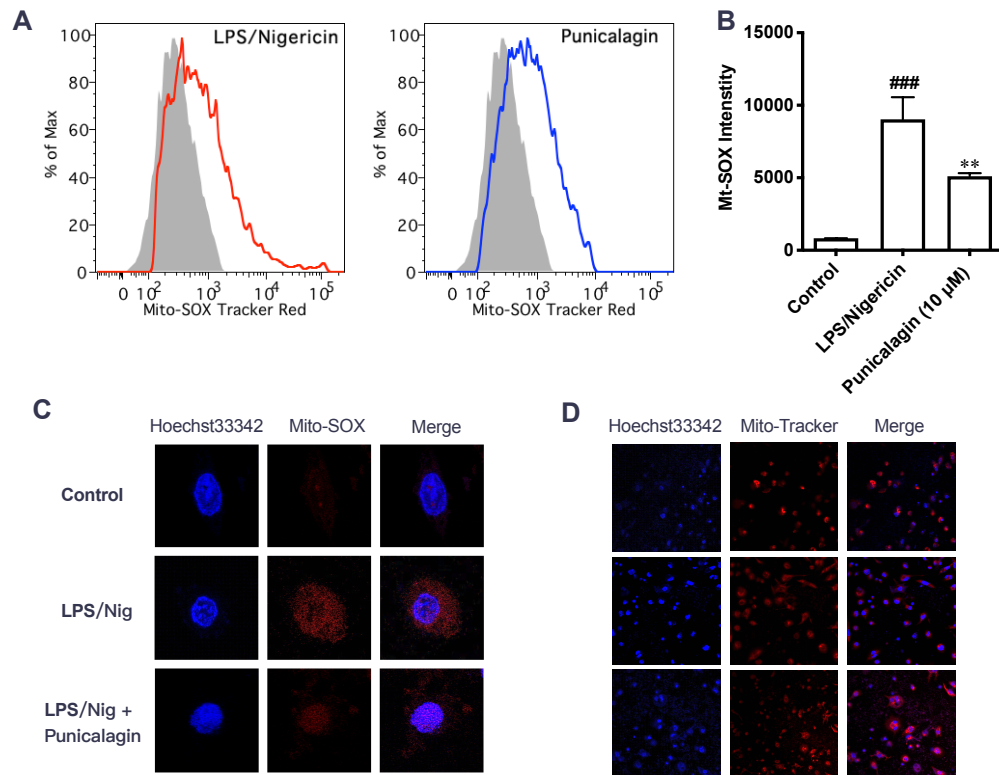


Figure 3. (A-C) THP-1 cells were stimulated and treated with PA as indicated, mito-SOX intensity was determined using Flow cytometry and confocal microscopy, respectively. The results were qualified by FlowJo. (D) Mito-Tracker staining was apply to analyze cellular mitochondrial distribution in the PA-treated LPS-primed (100 ng/mL, 4 h) THP-1 cells followed by the induction of nigericin (10 μ M, 1 h).

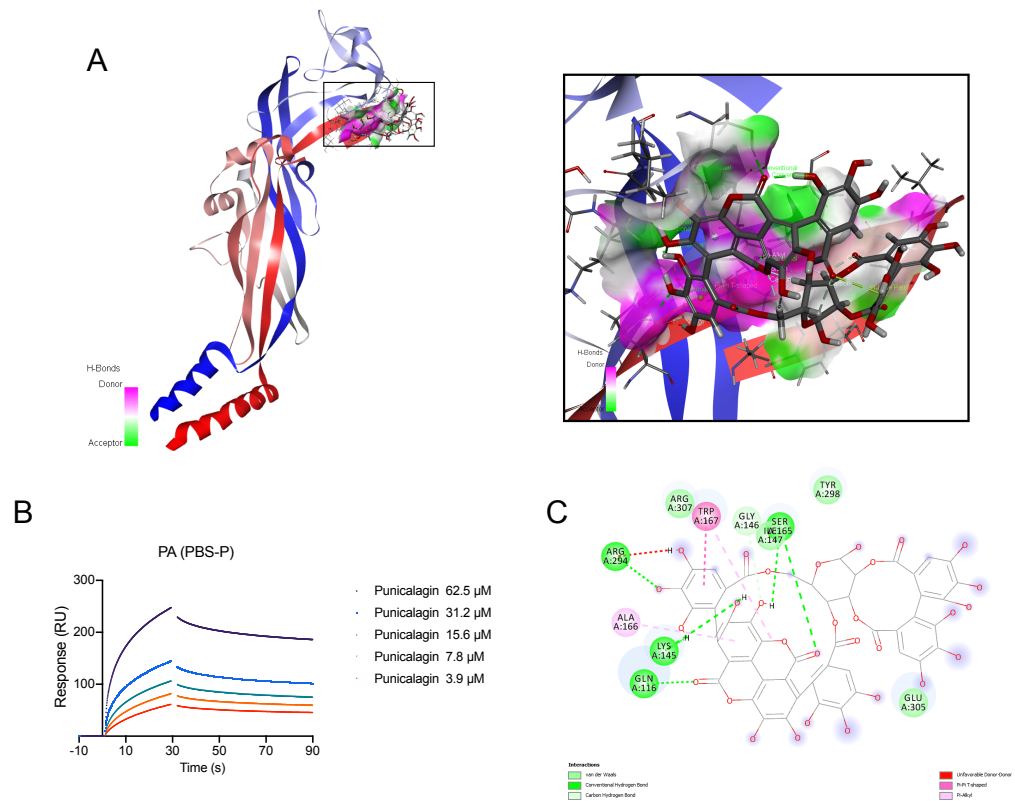


Figure 4. Interactions between PA and the P2X7 receptor predicted by molecular docking. (A) PA binds to the P2X7 receptor at a site located at the head and left flipper of the P2X7 receptor's upper body and enlarged view of PA showed at the binding site in the P2X7 receptor. (B) Surface plasmon resonance (SPR) analysis of PA interaction with P2X7. (C) Illustration of types of interactions between CBD and the P2X7 receptor.

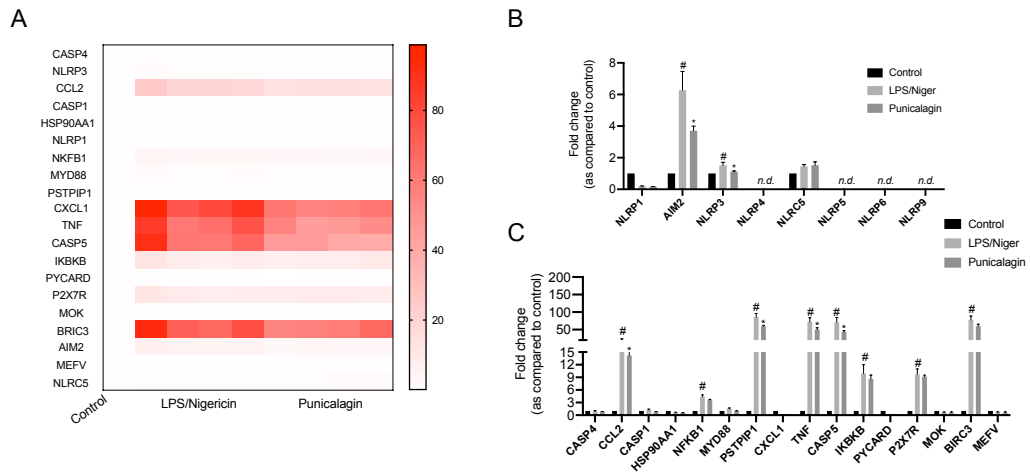


Figure 5. (A-C) Effects of PA on the genes involved in the inflammasome activation. Differentiated THP-1 cells were induced by LPS (100 ng/mL, 4 h) followed by the incubation with PA for 1 hour. Nigericin (10 μ M) was added and incubated for another 1 hour. The cells were lysed and the genes included *PYCARD*, *MEFV*, *PSTPIP1*, *NLRX1*, *RAGE*, *NLRP9*, *P2X7R*, *NLRP4*, *NLRC5*, *NLRP3*, *NLRP5*, *AIM2*, *CASP1*, *CASP5*, *HSP90AA1*, *IKKB*, *NFKB1*, *TNF*, *CASP4*, *CXCL1*, *TXNIP*, *MYD88*, *BIRC3*, *CCL2*, and *NLRP6* were measured using Geneplex assay.

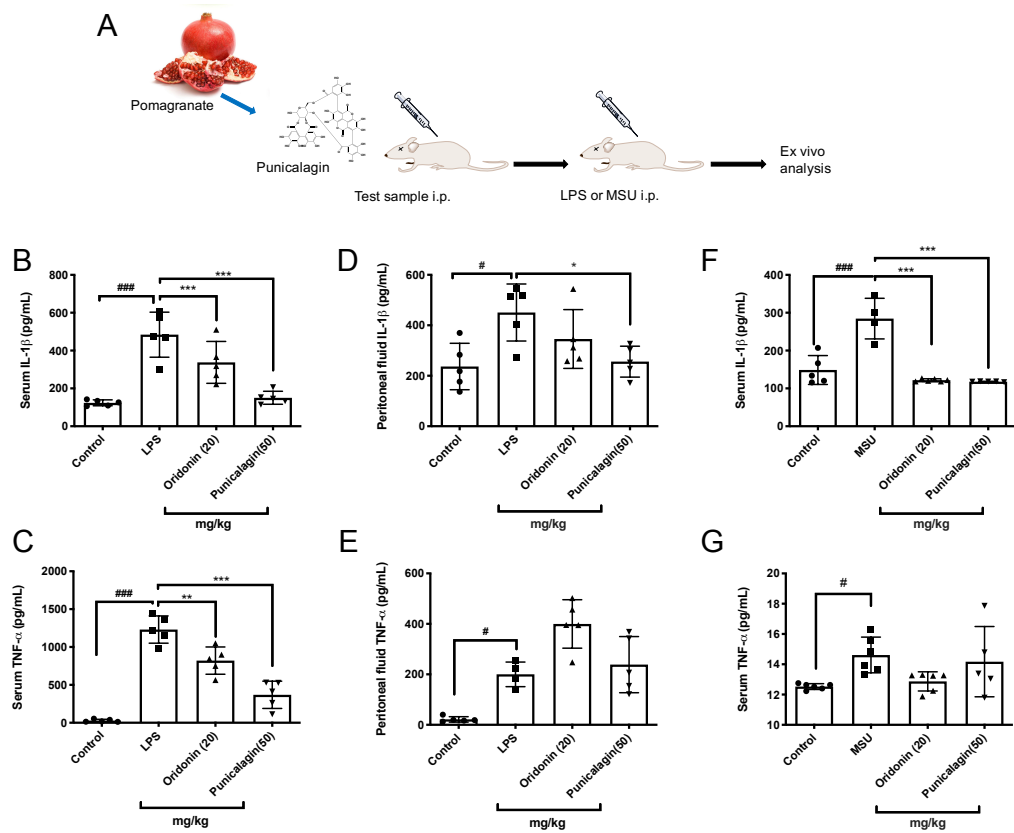


Figure 6. (A) The mice were intraperitoneally injected with PA (50 mg/kg) or oridonin (20 mg/kg). Next, the mice were intraperitoneally injected with LPS (10 mg/kg) or MSU (1 mg/mouse). The serum and peritoneal fluid were collected and IL-1 β and TNF- α in the serum or peritoneal cavity were determined. Treatment of PA inhibited serum IL-1 β (B) and TNF- α (C) and peritoneal fluid IL-1 β (D) but didn't affect peritoneal fluid TNF- α (E). Besides, treatment of PA also inhibited serum IL-1 β (F) but didn't affect serum TNF- α (G).